STUDIES IN THE VAPOUR PHASE GROWTH OF III-V COMPOUNDS WITH SPECIFIC REFERENCE TO GALLIUM ARSENIDE

A thesis submitted for the degree of

Doctor of Philosophy in the

University of London

by

RODNEY HOLLANDS MOSS, B.Sc., M.Phil., Grad. R.I.C.

Department of Electrical Engineering,
Imperial College of Science and Technology
LONDON
SW7 2BT

November 1974

ABSTRACT

This thesis is concerned with the vapour phase growth of group III-V compounds and gallium arsenide in particular. A brief review of the current vapour phase methods is presented.

A general, one-dimensional, theoretical model, describing transport in the gas phase is discussed and its application to sublimation, dissociative sublimation and chemical vapour transport is presented in a logical sequence.

A novel capsule method of vapour phase crystal growth of gallium arsenide is described and its application to the growth of thin epitaxial layers discussed. The value of the method for purifying bulk quantities of gallium arsenide and its potentiality as a method of growing large single crystals is demonstrated.

The morphology of epitaxial layers was studied and the influence of impurities on the morphology is discussed. The observed growth rates are compared with those predicted by the theoretical model.

The need for accurate thermodynamic data was highlighted by the application of the transport model. A new modified entrainment method for measuring vapour pressures and heterogeneous equilibria involving reactive gases was devised and is described in detail. The method was used to study the evaporation of water and lead and also the reactions involved in the gallium-water, gallium-hydrogen chloride and gallium arsenide-hydrogen chloride systems and the results are discussed.

Finally the achievements of the work and the potential of the theory and experimental methods are considered.

To

my wife, Pauline.

ACKNOWLEDGEMENTS

It is a pleasure to express my sincere appreciation of all the advice, guidance and help given to me by Dr. E.A.D. White (my director of studies) and Dr. M.M. Faktor (my supervisor) throughout the period of my studies. I also would like to acknowledge, the helpful and vigorous discussions of my colleagues and co-authors of the appended papers, which contributed much to the structure and thinking of the thesis.

I am grateful to Dr. D.H. Newman for the cathodoluminescence measurements reported in chapter 6 and for his helpful interpretation of the results. I also value the technical assistance of my colleagues and for the help given by the Post Office Research Department Services Division in reproducing this thesis.

I would like to thank the Directorate of the Post Office Research Department for making available such excellent facilities for pursuing this research and to the Director of Research for providing a post-graduate collaborative award and granting permission to use the information contained in this thesis.

Finally, personal thanks are due to my wife whose patience and encouragement has been a constant help during this period of study.

CONTENTS

CHAPTER 1

INTRODUCTION

CHAPTER 1

INTRODUCTION

Crystals occur in nature and have been admired and treasured by man for many centuries[1]. Initially the visible shape and symmetry of particular materials lead to their classification as crystals. However, a crystal may be more generally defined as a substance which consists of a regular, three dimensional arrangement of identical arrays of atoms or molecules (unit cells). Crystals are therefore distinct from other solids where the ordering of atoms is only over a short distance, e.g. glasses and plastics. Although crystallisation of solids from aqueous solution was used as a purification method in the 16th century and compounds such as alum, sugar, saltpetre, etc. were found to crystallise into easily recognisable forms[2], naturally occurring crystals remained the main source of supply for many years. Experiments to prepare crystals increased in number, particularly at the end of the 19th and beginning of the 20th centuries. The invention of the transistor and related electronic devices later in the 20th century provided a large impetus for finding methods of obtaining single crystal materials of high intrinsic purity and crystal perfection[3]. The commercial interest in crystal growth caused a large increase in empirical experimentation, while less effort was made to obtain an understanding of the processes occurring.

There are three main approaches to growing crystals, although within each group there are numerous varieties of methods.

(i) Growth from the vapour phase.

(ii) Growth from solutions.

(iii) Growth from melts.

There are other methods which are less extensively used, e.g. molecular beam techniques[4] and crystal growth in solids[5]. This thesis is concerned with the first approach - vapour phase crystal growth and in particular the growth of III-V compounds. The other methods of crystal growth are well described in various books and reviews[2,5,6-8].

Crystal growth from the gas phase requires that the general reaction

$$\text{Gas (disordered)} \longrightarrow \text{Crystal (ordered)}$$

takes place, i.e. all the necessary constituents of the solid phase must be present in the gas phase. This general reaction may be conveniently divided into two types of gas phase growth, (i) cases where the constituents are volatile at the temperature of the experiment, i.e. sublimation or dissociative sublimation and (ii) those where the constituents are reacted with a third species in order to produce volatile species - chemical vapour transport[9].

Vapour phase crystal growth covers a vast field and a multitude of papers and books concerned with various aspects of it have been published.

The subject is an interdisciplinary one and has been approached from a variety of scientific standpoints, e.g. solid state physics, crystallography, physical chemistry, chemical engineering and metallurgy.

It would be impossible to cover the subject fully in a thesis such as this, therefore it was decided to concentrate on some aspects of a typical system. Gallium arsenide was studied in particular, but many of the processes and principles discussed, are of general applicability to other vapour phase crystal growth systems. The thesis covers three aspects:

(a) Experiments in the vapour phase crystal growth of gallium arsenide

(b) Determination of thermodynamic parameters of the processes occurring in crystal growth

(c) Theoretical approaches to understanding vapour phase growth, which have been formulated during the course of the experimental work.

Before giving a more detailed explanation of these three aspects, it will be helpful to give the historical context of the work reported here. The experimental work was carried out entirely at the Post Office Research Department and formed part of an investigation into the vapour phase growth of gallium arsenide. Prior to this, the author was engaged in a similar study of cadmium sulphide and much of the background and understanding of vapour phase crystal growth stems from this earlier work. Cadmium sulphide

was grown by dissociative sublimation[10,11], gallium arsenide by chemical vapour transport[9,12]. The latter method was considered as an extension and development of vapour transport by dissociative sublimation by the addition of a third species to produce the volatile components. Where it is helpful, reference has been made to cadmium sulphide, particularly in chapter 3 where an understanding of the theory of chemical vapour transport is greatly assisted by considering dissociative sublimation first.

The reasons for choosing the particular aspects considered in thesis are given below, along with a brief introductory outline of each chapter. The choice of gallium arsenide though determined largely by the interests of the Post Office, is convenient for studying chemical vapour transport, since it is typical of other III-V compounds. Furthermore, gallium arsenide is a compound which is becoming increasingly important[13] both on its own and as an alloy with other group III-V compounds, e.g. gallium phosphide[14] and aluminium arsenide[15]. Many devices have been made from it, e.g. IMPATT diodes[16] (Impact-ionisation avalanche and transit time diodes), Gunn diodes[17], light-emitting diodes (LED)[18], lasers[19] and other devices[20].

In chapter 2 a brief review of gallium arsenide crystal growth is presented as well as some general basic information concerning gallium arsenide. The discussion of methods of vapour phase crystal growth has been confined to those relating specifically to gallium arsenide, more general reviews are available[6,158]. In view of the size of the field of crystal growth, certain aspects for which comprehensive reviews are available, have been omitted; subjects included in this category are: crystal defects[21], growth mechanisms[22], non-stoichiometry[23-25] and nucleation[22,26,27]. Chapter 2 concludes with a brief account of methods of obtaining thermodynamic data related to vapour phase crystal growth.

Chapter 3 concerns the theory of vapour transport in crystal growth systems. As a result of the study of cadmium sulphide, preliminary ideas for a theoretical model of vapour phase growth were formulated. These ideas were subsequently improved and developed by my colleagues at the Post Office and the results have been published[28-33]. Using their

results, the theory of transport in the gas phase is presented, starting with the fundamental concepts as illustrated by simple sublimation, then progressing to dissociative sublimation and finally to chemical vapour transport[12].

The movement of gaseous species in a transport system is obviously of fundamental importance, the changes in the partial pressures of the various species due to growth and the steady state conditions that ensue can be calculated. The theoretical model has been employed to calculate the growth rates for the system used to grow gallium arsenide, by assuming equilibrium with the gas phase at the source material and at the growing crystal. The growth rates thus obtained are maximum growth rates for given experimental conditions. If surface kinetics, such as reaction at the surface, determine the growth rate rather than the transport of the reactants through the gas phase, then the observed growth rate will be correspondingly reduced from the predicted value. The model is useful in providing a foundation to understanding vapour phase crystal growth and can be used to assess the importance of surface effects in a particular system, providing the thermodynamic parameters are known.

In chapter 4 a modified entrainment method for obtaining thermodynamic parameters is given. Many crystal growth systems operate under conditions where equilibrium between the solid and the gas is closely approached. The thermodynamics of phase changes and reaction equilibria is therefore very important in crystal growth. Thermodynamics is concerned with macroscopic changes and processes in materials and does not depend on the mechanism or kinetics of the process. In a field such as crystal growth where mechanisms and theories of growth are still not fully understood and are subjects of much speculation, to have a firm reference point which is based on experimentally observed data is invaluable. Equilibrium thermodynamics cannot supply information on mechanisms or rates of growth but it defines the driving forces for crystal growth, i.e. it can show whether a reaction process is possible but not how that process will occur or the time taken to do it.

Experimentally determined data (e.g. enthalpy and entropy changes in a process) may be used for calculating the partial pressures of the reaction species in the gas phase and enable optimum conditions for transport to be determined. Estimated data are helpful in finding the right range of operating conditions but only precisely determined values

can give the necessary accuracy for calculating partial pressures and uncoupling sequential processes. For this reason a substantial part of this thesis is concerned with the measurement of the thermodynamic parameters for the crystal growth systems investigated.

Determination of thermodynamic parameters by the method described uses the theory presented in chapter 3. The success of the method and the accuracy of the results obtained for materials used to calibrate the system, confirms the theoretical model presented for crystal growth. Preprints of four papers, accepted for publication[159], on the method are included at the end of this thesis. Chapter 4 is composed of a brief account of the method and results obtained, reference being made to the appended papers for the full mathematical analysis and discussion of the results.

Chapter 5 consists of a description of the experimental work on the crystal growth of gallium arsenide. In order to obtain material suitable for electronic devices e.g. lasers, IMPATT diodes etc. it is necessary to be able to produce flat, defect free layers, controlling both the dopant distribution and layer thickness. A new method of transporting gallium arsenide in a capsule is described and it was used to produce thin epitaxial layers and for transporting bulk quantities of gallium arsenide. The method is compared with the more conventional flow system[34,35] for producing epitaxial layers, the gallium arsenide-hydrogen chloride chemical transport system being used in both cases.

Discussion of the results of the crystal growth experiments is given in chapter 6. The results are considered both from a morphological point of view and in the light of the theoretical model presented in the thesis. Special mention is made of the bulk crystal growth experiments which showed the feasability of using the new capsule method for purification of gallium arsenide.

The final chapter summarises the achievements of the work and indicates possible future lines of research.

CHAPTER 2

REVIEW

CHAPTER 2

REVIEW

2.1 Introduction

Group III-V compounds form a class of intermetallic semiconducting compounds having the formula $A^{III}\ B^{V}$ and considerable interest has been taken in them since the discovery of their semiconducting properties by Welker in 1952[36]. Their technological importance has arisen from the fact that they present a wider selection of energy band gaps and carrier mobilities than the group IV elements, germanium and silicon[13,37]. Of all the III-V compounds, gallium arsenide has been studied the most as has the technology of manufacturing devices from it. It can be regarded as a typical example of a III-V compound and subsequent discussion is confined largely to this compound.

2.2 Properties of Gallium Arsenide

Gallium arsenide is a dark grey substance which crystallizes in the zinc blende (sphalerite) structure[38]. The zinc blende structure (figure 2.1) is in the cubic crystal class and consists of two interpenetrating cubic close-packed lattices and displaced with respect to each other by $\frac{1}{4}$ of the body diagonal. The bonding in gallium arsenide is mixed covalent and ionic bonding, in common with other III-V compounds[39,40].

Gallium arsenide melts at 1237°C, at which temperature, its dissociation pressure is 0.9 atm[41], the vapour consisting, almost entirely of arsenic. It is for this reason that a dissociative sublimation technique for crystal growth cannot be used and a transporting agent is required to produce a volatile gallium species. Comprehensive reviews of the physical and electronic properties of gallium arsenide are available[13,40,42,43] and therefore these subjects will not be pursued any further.

2.3 Crystal Growth of Gallium Arsenide

Gallium arsenide has been successfully grown from the melt, from solution and from the vapour phase[44]. Large single crystals of gallium arsenide are usually produced from the melt, using either the directional (gradient) freeze[45] or Czochralski methods[46]. However, high temperatures (1250°C) are required and contamination from the boats or crucibles containing the gallium arsenide occurs, thus limiting the purity obtainable by these methods[13]. Purer material can be grown from solution or from the vapour phase where

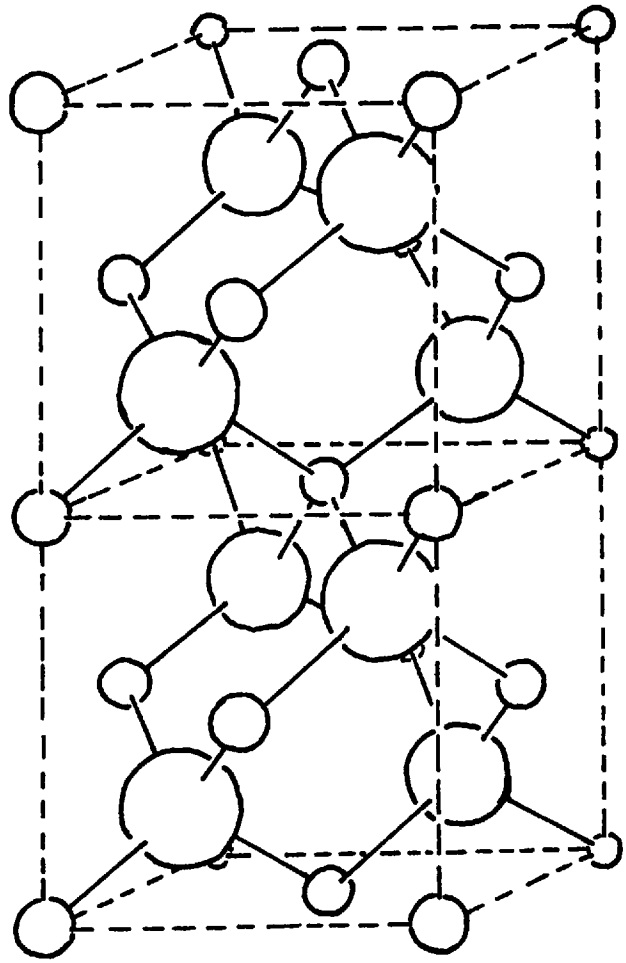

FIG.2.1. THE ZINC BLENDE (SPHALERITE) STRUCTURE

operating temperatures are lower (700°-850°C), such methods are normally confined to producing thin epitaxial layers on a substrate. If the layers are grown from solution then the process is called liquid phase epitaxy (LPE) and if growth is from the vapour - vapour phase epitaxy (VPE). In the case of LPE there are three basic methods employed, each having numerous modifications. The first method was proposed by Nelson[47] in which a saturated solution of gallium arsenide in gallium was tipped onto a slice of gallium arsenide (at 700-800°C) and the whole system cooled at a steady rate. To terminate growth, the solution was tipped off the slice. Although this method has been successfully applied by many people, it is limited in that extension to produce several layers involves repeating the whole experiment for each layer required.

The second method overcomes the limitation of the Nelson technique, being suitable for multilayer growth, it is referred to as the sliding boat method[48]. A series of saturated solutions of gallium arsenide in gallium, having different dopants in each, are held in separate compartments of a graphite boat. They are in turn brought into contact with the substrate, while the whole boat is cooled at a steady rate. The amount deposited from each melt is determined by the cooling rate and the length of time that the melt is in contact with the substrate. A modification of this method uses a rotational motion of the compartments over the substrate[49,50].

The third method consists of dipping a substrate into a crucible containing a saturated solution of gallium arsenide in gallium and then cooling the whole system in order to deposit gallium arsenide from the solution onto the substrate[51]. This method has been successfully applied to other materials besides gallium arsenide, e.g. garnets grown from lead oxide-boric oxide fluxes[52]. The localised cooling (and consequent super-saturation) caused by dipping a cold substrate into a saturated solution of gallium arsenide has also been employed to grow thin epitaxial layers[53].

Methods involving, for example, horizontal rotation of a cylindrical crucible[54] or a system of hydraulic pistons[55] to bring the solution into contact with the substrate have been used, but not as extensively as the three main methods outlined above.

Vapour phase methods for growing epitaxial layers of gallium arsenide have been used extensively. The VPE methods described here are those based on chemical vapour transport systems. The layers obtained by VPE are generally flatter and more uniform than those obtained by LPE. VPE methods can be divided into two types: closed capsule and open flow methods. The closed capsule technique was first used to grow crystals of gallium arsenide by Antell and Effer[56]. Iodine was used as a transporting agent and small crystals were obtained at temperatures around 1070°C. Gallium arsenide films have been produced using iodine transport in closed capsules[57,58] and also using hydrogen chloride instead of iodine[59]. Although this method has produced smooth epitaxial layers[57], it is limited in that only single layers can be produced and control of the growth process and doping levels is difficult. The more favoured approach is the open flow method, which was demonstrated by Antell and Effer[60]. In this method, an inert carrier gas with a transporting agent is passed over source material at high temperature (800-900°C); gallium arsenide is then deposited at a lower temperature further along the reaction tube.

There are several variations of the open flow method and it is probably best to mention each type, although the constructional details of particular apparatus will not be given. Gallium arsenide can be used as the source material[61-63] and hydrogen chloride gas in hydrogen passed over it. The hydrogen chloride reacts with the gallium arsenide to form gallium monochloride and arsenic:

$$GaAs + HCl \rightarrow GaCl + \frac{1}{4}As_4 + \frac{1}{2}H_2$$

At a lower temperature region of the furnace the equilibrium is moved to the left and gallium arsenide is deposited on a substrate.

Elemental arsenic and gallium have been used instead of gallium arsenide source material[64-66].

Because of the difficulties of purifying hydrogen chloride gas, arsenic trichloride is frequently used as a source of hydrogen chloride[62] according to the reaction:

$$2\ AsCl_3 + 3\ H_2 \rightarrow \frac{1}{2}\ As_4 + 6\ HCl$$

Hydrogen is passed through a bubbler containing arsenic trichloride at room temperature and the above reaction takes place when the gases enter the furnace. By using arsenic trichloride as a source of hydrogen chloride, the need for an additional arsenic

source (either as the element or as gallium arsenide) is removed. The most commonly used system at present for producing high purity gallium arsenide therefore involves the use of a gallium source with arsenic trichloride and hydrogen as the only other materials. The arsenic dissolves in the gallium forming a crust of gallium arsenide on the surface, the hydrogen chloride reacting with this crust and transporting it along the furnace tube, - where at a lower temperature, deposition takes place. Typical operating temperatures for this system are 800°C for the gallium source and 750°C for the substrate. This system was first used by Knight et al[67] and has been used by many others since[68-72].

Tietjen and Amick[73] devised a system which can be used for growing both gallium arsenide and other III-V and mixed III-V compounds. The group III metal is reacted with hydrogen chloride to form the volatile metal halide, while the group V element, arsenic or phosphorus, is introduced as arsine (AsH_3) or phosphine (PH_3). The required III-V compound is deposited on a substrate at ~ 750°C, the gaseous reactants having been mixed at ~ 850°C. The main advantage of this system is its versatility in allowing the ratio of the group III to group V species in the gas stream to be varied and indeed to produce mixed III-V compounds e.g. $GaAs_xP_{1-x}$, $Ga_xIn_{1-x}As$ etc.[74].

The halide transport systems of the types described above are by far the most widely used chemical vapour transport systems for the epitaxial growth of gallium arsenide. Two other systems have been used, one employs water as a transporting agent[75-78] and the other uses alkyl gallium compounds and arsine[79-81]. In the water transport process the reaction occurring was assumed to be

$$4\ GaAs_{(s)} + 2\ H_2O_{(g)} \rightarrow 2\ Ga_2O_{(g)} + As_{4(g)} + 2\ H_{2(g)}$$

It is shown later in the thesis that GaOH is also present in significant amounts. Gallium arsenide was reacted at temperatures around 1100°C and growth occurred ~ 50°C lower[77]. Smooth layers have been obtained by this method, however, diffusion of dopants between layers is a problem owing to the high temperatures used.

The second system which has been investigated more recently, introduces the gallium as an alkyl gallium compound, e.g. gallium trimethyl or gallium triethyl, this is then reacted with arsine (or phosphine) to produce the epitaxial layers[79-81].

In the preceding review, no mention has been made of controlling the electrical properties of the material produced. As the specifications for devices become more stringent, so the control of the growth process has to be more precise and particularly in the control of impurities; care in cleaning equipment and handling of material is therefore of utmost importance. In addition to excluding unwanted impurities, it is necessary to be able to introduce controlled amounts of particular "impurities" (dopants) to give the material the required electrical properties. In chemical vapour transport systems, there are two basic approaches: one is to introduce the dopant as a volatile species through a separate gas inlet[74] e.g. sulphur as hydrogen sulphide; the second is to use a doped source material and transport the dopant along with the gallium arsenide[82].

Most chemical vapour transport systems are made from fused silica and silicon contamination in gallium arsenide grown in such systems is well established[83-86]. In order to minimise such contamination it is desirable to operate at as low a temperature as possible.

The two principal methods of obtaining epitaxial layers of gallium arsenide, LPE and VPE have been described above. The choice of method is dependant largely on the required material and comparison of the two approaches has been given by Minden[18]. Alternative methods of growth are not reviewed here, but have been discussed by Jain and Sharma[87].

2.4 Methods of Obtaining Thermodynamic Data

There are a variety of methods which have been used to determine the thermodynamic data (enthalpy and entropy changes) of reactions[88,89]. The earliest methods of determining vapour pressure were static methods, where a sample of material was enclosed in an isothermal chamber and the partial pressure measured using e.g. a manometer or the absorption of light by the vapour species. For high temperature processes, favoured approaches are the effusion and entrainment methods. Each of these will be considered in a little more detail since they form the background to the modified entrainment method described in this thesis.

The Knudsen effusion method[90,91] relies on the measurement of the rate of effusion a vapour through a small orifice, from a container where the vapour is at its saturation pressure.

From kinetic theory the rate (W) at which a gas would strike a surface of area A is given by

$$W = AP(M/2\pi RT)^{\frac{1}{2}} \qquad (2.1)$$

where P is the pressure of the vapour of molecular weight M, T is the temperature and R is the universal gas constant. This rate is equivalent to the loss of molecules through a hole of the same area, providing that all molecules reaching the hole pass straight through and are lost from the container. This condition applies when the mean free path of the molecules is large compared with the diameter of the hole and the wall of the cell is infinitely thin. If the mean free path is small compared to the hole size, then intermolecular collisions become important and streaming of the gas occurs through the hole. If the wall thickness is significant, then collisions of molecules with the wall occur giving a lower rate of effusion. This may be taken into account by applying a correction factor[92], then

$$W = kAP(M/2\pi RT)^{\frac{1}{2}} \qquad (2.2)$$

where k is the Clausing correction factor.

In determining equilibrium vapour pressures, the solid (or liquid) is introduced into a cell having a small orifice of known dimensions. The cell is then heated in vacuo to a particular temperature and the rate of weight loss from the cell measured. The orifice is designed to cause a negligible disturbance of the equilibrium between the condensed phase and its vapour, i.e. the rate of loss through the orifice is small compared with the rate of equilibration. In practice the orifice size is reduced until the calculated pressure in the cell is independent of the area of the orifice. For materials where there is a large surface limitation to vaporisation, the Knudsen method is unsuitable for determining equilibrium vapour pressures, e.g. in the case of arsenic[93], the vapour consists of mainly tetrameric molecules (up to 800°C) and there is a kinetic limitation in forming tetrameric molecules at the solid-gas interface.

In order to calculate the vapour pressure from the weight loss measurements, it can be seen from equation (2.2) that the molecular weight (M) of the effusing species must be known. If more than one vapour species is present, then the relative proportions of each must be known, therefore, to overcome this limitation of the Knudsen method, some workers

have used it in conjunction with mass spectroscopic techniques[94] whereby the molecular weights and relative proportions can be determined independently. An alternative method frequently used is the torsion effusion method first used by Volmer[95], in which a cell having two orifices on opposite sides and at opposite ends is suspended from a fibre of known torsion constant. The effusing molecules give rise to a torque on the fibre, and the angular displacement (β) of the cell is measured. The pressure (p) is calculated from the equation

$$p = (2D\beta)/q_1A_1 + q_2A_2 \qquad (2.3)$$

where D is the torsion constant, q_1 and q_2 are the distances of the two, opposed orifices of areas A_1 and A_2 from axis of suspension. Equation (2.3) is independent of the molecular weight of the effusing species. Information on the molecular complexity of the gas can be obtained by simultaneously measuring the weight loss from the torsion cell and the angular displacement. Using equation (2.3) and substituting for p in equation (2.2) we obtain

$$M = \frac{\pi RT}{2}\left[\frac{W(q_1A_1 + q_2A_2)}{kAD\beta\ .}\right]^2 \qquad (2.4)$$

A further way of obtaining the vapour density was devised by Margrave[96]. A cell was arranged so that when suspended from a microbalance, the force exerted by the effusing molecules gave an apparent weight increase to the cell. If the apparent weight increase was ΔW, then

$$p = 2\ .\ \Delta W\ .\ g/\pi a^2 \quad \text{dynes cm}^{-2} \qquad (2.5)$$

where a is the orifice radius and g is the gravitational constant.

The method has been further developed by Freeman et al.[97] using a cell which could be turned through 90°. In one position the vapour effused in a vertical direction giving an apparent weight increase to the cell and in the other position, the effusion was horizontal giving a true measure of the weight of the cell.

The effusion methods described above have been applied to many systems and have been reviewed and discussed by several workers[88,89,98,99].

The entrainment method (also called transpiration or transportation method) is suitable for studying reaction equilibria involving gases as well as measuring vapour or dissociation pressures[88,89,100]. A stream of gas which may be inert or reactive is passed over a condensed sample at a rate sufficiently low for equilibrium to be established. The products of the reaction or the vapour of sample are collected downstream and analysed. From a knowledge of the number of moles of each gaseous constituent, the total pressure in the system and the temperature of the sample, the partial pressures of the various gases at given temperatures can be calculated, e.g. for vapour pressure measurement

$$p = \frac{n_v}{n_v + n_c} P \qquad (2.6)$$

Where p is the vapour pressure of the sample, P is the total pressure, n_v and n_c are the number of moles of the vapour and carrier gas respectively.

Although the method is simple and flexible, there are limitations and care has to be exercised in interpreting results[100]. The problems arise because the gas is flowed past the sample; if the gas flow-rate is too small, then diffusion of the species out of the uniform temperature zone, where the sample is situated, becomes significant and gives rise to measurements which are too high. At the other extreme if the gas is flowed too fast, then equilibrium is not established because of poor gas mixing above the sample and/or surface kinetics at the surface of the sample limiting the evaporation or reaction rate. In systems where hydrogen is used, thermal diffusion can also cause significant errors[101] by unmixing of the gas.

In practice, if the measured weight loss rate is plotted as a function of the flowrate, there is sometimes a range where the weight loss rate is independent of the flowrate and this is taken to correspond to the equilibrium values of the partial pressure of the species[100]. This assumption may be justified in some cases, but in all systems equilibrium is only established at the surface of the condensed phase and there is a region in which diffusion of reactants to and products from the surface occurs. The region over which this diffusion occurs is not usually well defined and although turbulent mixing of the gas can reduce the boundary layer above the sample, there will always be some composition change in the gas normal to the sample surface and this is an eventual

limitation of the method. In the modified entrainment method presented in chapter 4, the region over which diffusion occurs is limited to a well defined region of known geometry. The limitations of the normal entrainment method are discussed in further detail in the review by Merten and Bell[100].

CHAPTER 3

THEORY OF VAPOUR TRANSPORT

CHAPTER 3

THEORY OF VAPOUR TRANSPORT

3.1 Introduction

In crystal growth from the vapour phase, the growth process may be considered, for conceptual convenience, as two consecutive stages:

(1) Transport of the material to the growth interface.

(2) Deposition of the material at the growth interface.

In some cases, e.g. sublimation, there is a preliminary stage, that of transfer of solid material (the source) into the vapour phase.

Stage 2 may be subdivided into various processes: adsorption of molecules at the interface, migration of adsorbed molecules across the surface, incorporation of molecules into the crystal. Also with chemical vapour transport there is reaction at the interface and the removal of the transporting agent from the growing crystal.

In this chapter the transport of material to the growth interface (Stage 1) will be considered. The theoretical treatment given here is that presented by Faktor et al[28-33]. The fundamental principles of the theory will be described, first by considering transport by sublimation of a single component in the presence of an inert gas, then treatment will be applied to dissociative sublimation and finally to chemical vapour transport.

3.2 Sublimation

Consider the condensation of a vapour, A. As the vapour condenses, a movement of gas occurs due to the change in volume accompanying the phase change. The flux (J) of material (amount transported per unit area in unit time) is proportional to the velocity (u) of the vapour arising from the condensation.

$$J = \frac{uP}{RT}$$

If an inert gas (Z) is present in the system then the wind produced by the movement of the condensible vapour, A, will cause an accumulation of Z at the interface where condensation is occurring. Partial pressure gradients are thus set up in the system and diffusion according to Fick's law will also occur.

For a one dimensional system the fluxes of each component are given by

$$J_A = \frac{uP_A}{RT} - \frac{D}{RT}\frac{dP_A}{dx} \tag{3.1a}$$

$$J_Z = \frac{uP_Z}{RT} - \frac{D}{RT}\frac{dP_Z}{dx} = 0 \tag{3.1b}$$

There is no nett flow of the inert gas ($J_Z = 0$) and J_A is constant along x since there is no accumulation of either species at any point along x once steady state conditions obtain. There is no total pressure gradient of any significance unless the tube diameter becomes small (< 1 mm). From Poiseuille's viscous flow equation, it can be readily shown that to produce a flow velocity of 1 cm sec^{-1} in a tube 1 cm diameter requires a pressure gradient of $\sim 10^{-8}$ atm cm^{-1}. The total pressure (P_T) can therefore be considered constant along x. It follows then that

$$\frac{dP_A}{dx} = -\frac{dP_Z}{dx} \tag{3.2}$$

Summing (3.1a) and (3.1b) gives

$$J_A = \frac{u\,(P_A + P_Z)}{RT} = \frac{uP_T}{RT} \tag{3.3}$$

Substituting this expression for J_A in (3.1a) gives

$$u = \frac{-D}{P_T - P_A} \cdot \frac{dP_A}{dx} \tag{3.4}$$

The experimental basis of equation (3.4) was established by Stefan[102] who measured the evaporation rates of water and ether from partly filled pipes.

In applying these concepts to crystal growth experiments, consider a one dimensional crystal growth system with the growing crystal at $x = 0$ and a source of material at $x = l$ (Figure 3.1). The source can be either evaporating material or simply a vapour from a pipe.

Equation (3.4) may be integrated and by substituting for u using equation (3.3) we obtain

$$ln\left\{\frac{P_T - P_A^{(l)}}{P_T - P_A^{(o)}}\right\} = -J_A\left(\frac{RTl}{DP_T}\right) \tag{3.5}$$

The transport rate, J_A, can be calculated if P_T, $P_A^{(o)}$ and $P_A^{(l)}$ are known. For

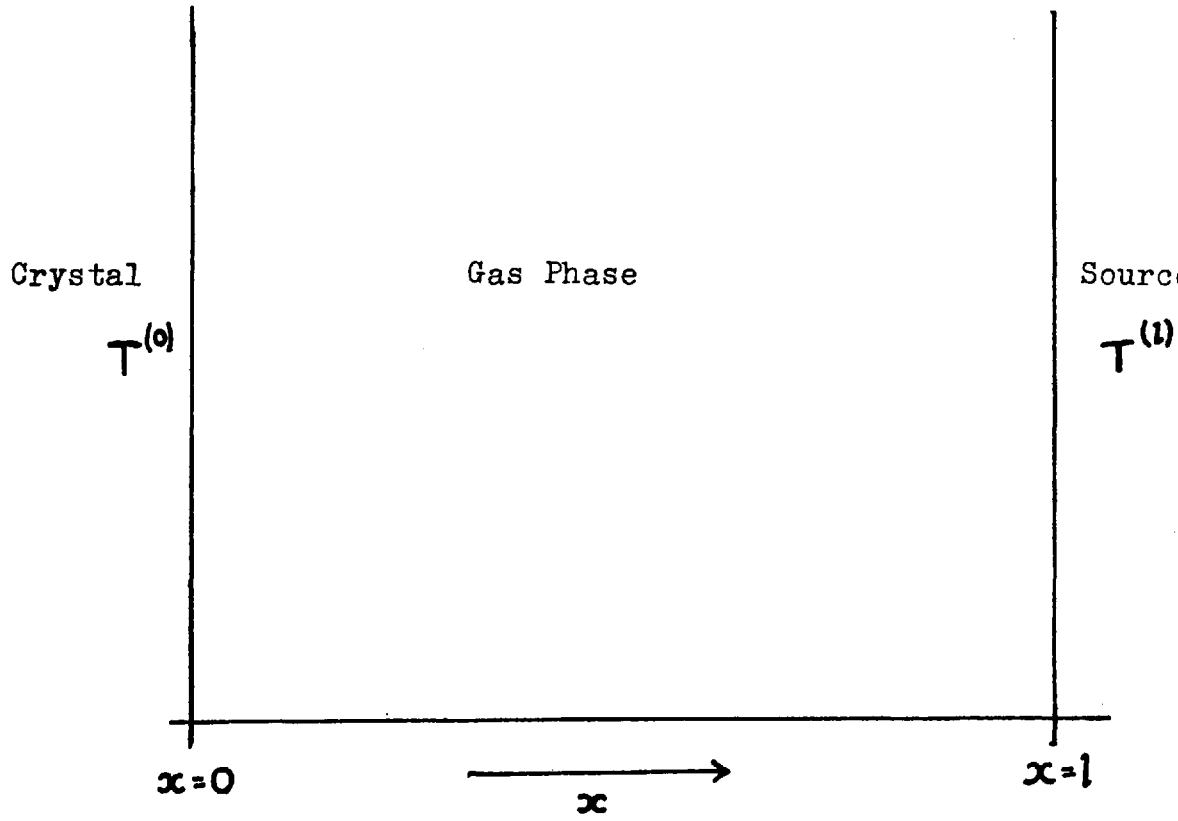

FIG.3.1 ONE DIMENSIONAL MODEL FOR GAS TRANSPORT

convenience, the thermodynamic parameters for evaporation can be used to calculate these pressures. This may only be done if equilibrium between the solid and vapour is closely approached.

The equilibrium vapour pressure of the material (A) is given by

$$P_A = \exp\left\{\frac{-\Delta H}{RT} + \frac{\Delta S}{R}\right\} \tag{3.6}$$

where ΔH and ΔS are the enthalpy and entropy changes for vaporisation. Substituting for P_A in equation (3.5) gives

$$J_A = \left(\frac{DP_T}{RTl}\right) ln \left\{\frac{P_T - \exp\left[\frac{-\Delta H}{RT^{(o)}} + \frac{\Delta S}{R}\right]}{P_T - \exp\left[\frac{-\Delta H}{RT^{(l)}} + \frac{\Delta S}{R}\right]}\right\} \tag{3.7}$$

For small values of ΔT, $(= T^{(l)} - T^{(o)})$, it can be shown that the growth rate is a linear function of ΔT. (The full derivation is given in Appendix 1).

$$J_A \simeq \left(\frac{DP_T}{R^2T^3}\right)\left(\frac{\Delta H}{l}\right)\frac{P_A^{(l)}}{P_g^{(l)}} \cdot \Delta T \tag{3.8}$$

For large values of ΔT, the growth rate assymptotes to a value

$$J_{A_{assymptote}} = \left(\frac{DP_T}{RTl}\right) ln \left\{1 - \frac{P_A^{(l)}}{P_g^{(l)}}\right\} \tag{3.9}$$

A plot of J_A versus ΔT is given in Figure 3.2. The plot of growth rate as a function of temperature difference may be considered as consisting of three distinct regions: an initial linear portion, an intermediate region and a final saturation region.

The linear region occurs at small values of ΔT where the growth rate is directly proportional to ΔH. If a different compound were used with a larger enthalpy change on evaporation, then the gradient of the initial portion would be steeper, other conditions remaining the same.

The saturation region occurs at large values of ΔT. In this region the growth rate is independent of ΔH, in direct contrast to the linear region. In the saturation region, increase of ΔT has virtually no effect on the growth rate. It is to be noted also that

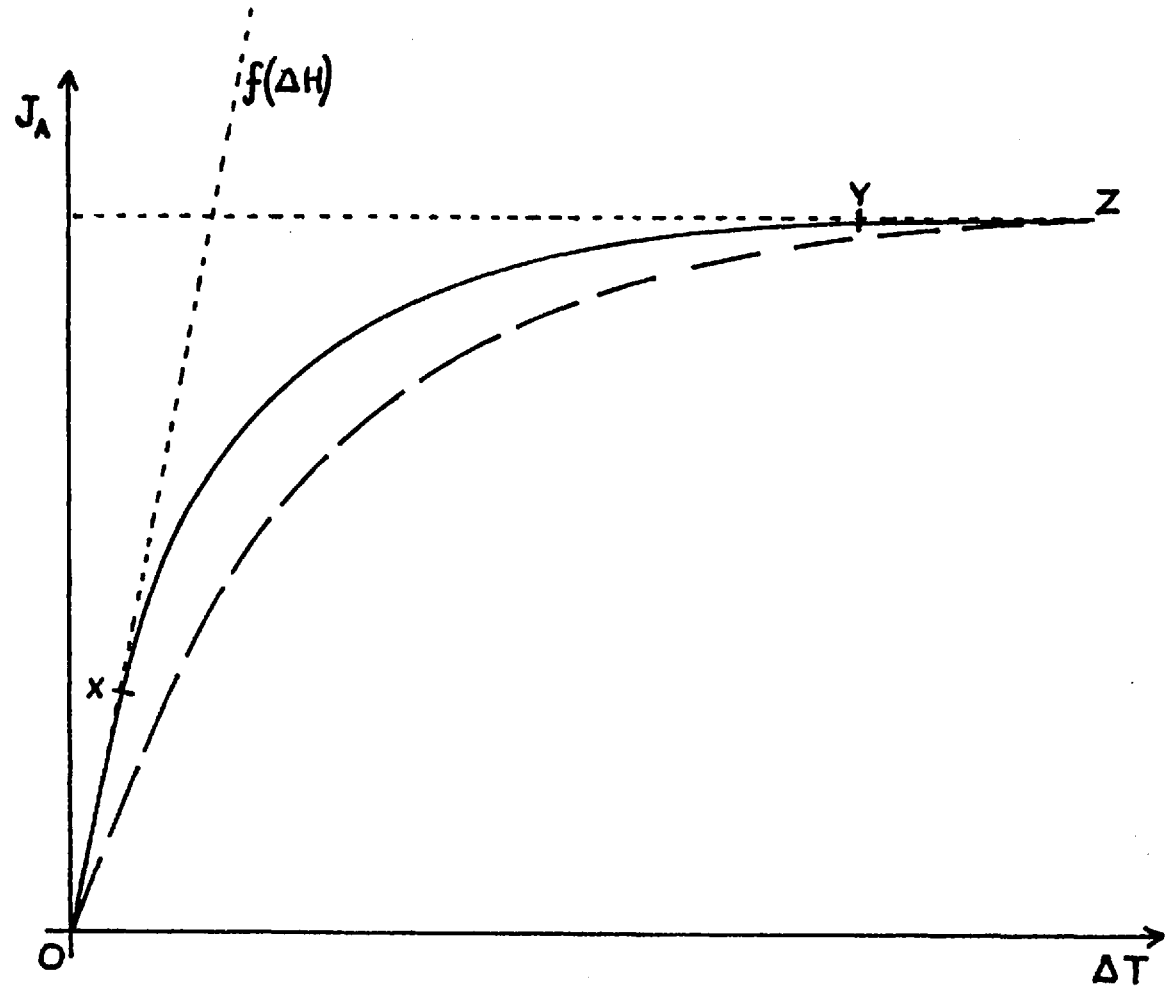

FIG.3.2. PLOT OF GROWTH RATE VERSUS TEMPERATURE DIFFERENCE FOR SUBLIMATION.

——————— THEORETICAL GROWTH RATE

——— ——— — GROWTH RATE IN THE PRESENCE OF A KINETIC BARRIER AT THE SURFACE.

O – X LINEAR REGION

X – Y INTERMEDIATE REGION

Y – Z SATURATION REGION

J_A in this region is only a weak function of $P_A^{(l)}$ whereas in the linear region J_A is strongly dependent on $P_A^{(l)}$.

The intermediate region occurs between the two extreme regions mentioned above. Although in this region, the growth rate is a function of ΔH, it is not directly proportional to it.

In the absence of a full analysis including surface barriers to growth it is possible to test for kinetic barriers at the surface by looking for deviations from the theoretical growth rate. The dotted line in Figure 3.2 gives the type of result expected, if kinetic barriers are present. From Figure 3.2 it can be seen that maximum deviation from the theoretical growth rate (in absence of kinetic barriers to growth) occurs in the intermediate region. If one is looking for kinetic effects then it is necessary to work in the intermediate region, i.e. not to use small values of ΔT nor very large values of ΔT.

It is also possible to calculate the partial pressures of the species as a function of x by imposing different boundary conditions during the integration of equation (3.4). If we integrate from $x = x$ to $x = l$, we obtain $P_A^{(x)}$ in terms of $P_A^{(l)}$.

$$P_A^{(x)} = \left[P_A^{(l)} - P_T\right] \exp\left\{\frac{JRT}{DP_T}(x - l) + P_T\right\} \tag{3.10}$$

If we integrate from $x = 0$ to $x = x$ we obtain $P_A^{(x)}$ in terms of $P_A^{(o)}$

$$P_A^{(x)} = \left[P_A^{(o)} - P_T\right] \exp\left\{\frac{JRTx}{DP_T} + P_T\right\} \tag{3.11}$$

The partial pressure profiles are shown in Figure 3.3.

From the above analysis it can be seen that if the partial pressures at the two ends of the system are known, then the transport rate, J_A, the Stefan velocity, u, and the partial pressures along x can be calculated.

In the above discussion it has been assumed that there are no kinetic barriers to growth at the growth interface. It is possible to calculate the surface barrier if the transport rate is known along with the partial pressures at any two points in the system.

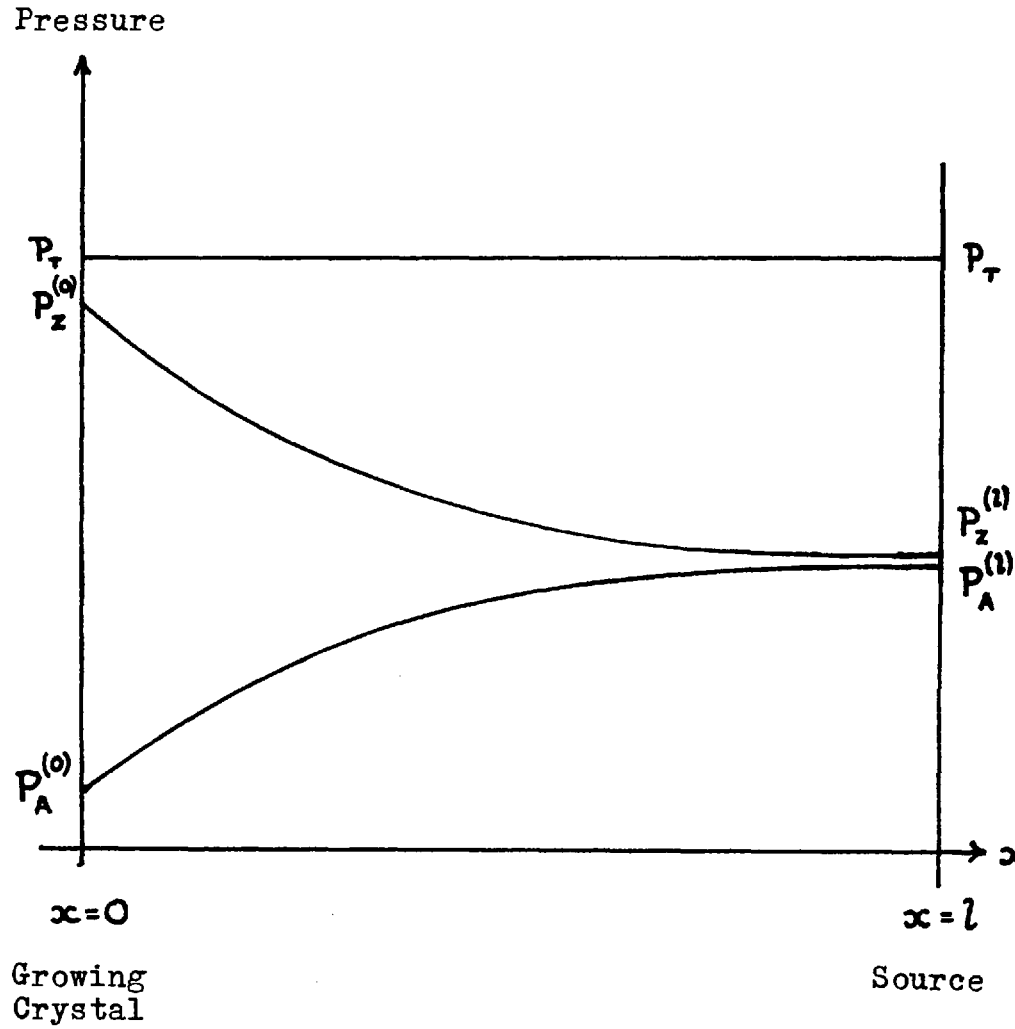

FIG.3.3. PARTIAL PRESSURE PROFILES FOR A SINGLE COMPONENT (A) IN THE PRESENCE OF AN INERT GAS (Z).

3.3 Dissociative Sublimation

The treatment given above for the sublimation of a single component material has been extended to dissociative sublimation[28,31]. The full algebraic treatment is lengthy and therefore only the main features will be summarised here. A theoretical analysis of dissociative sublimation has been reported by White et al[160], following their investigations of the growth of II-VI compounds and their treatment and conclusions are similar to those presented here.

Two new concepts must be introduced when considering dissociative sublimation. The first is that the composition and total pressure of the vapour are not uniquely determined by temperature. In the case of cadmium sulphide where dissociation occurs according to the equation

$$CdS_{(s)} \rightarrow Cd_{(g)} + \frac{1}{2}S_{2(g)} \tag{3.12}$$

The equilibrium constant (K) is given by

$$K = P_{Cd}\, P_{S_2}^{\frac{1}{2}} \tag{3.13}$$

In order to fix both the total pressure and the pressures of cadmium and sulphur, we must define a further parameter (α) which is the ratio of the partial pressures of the components

$$\alpha = \frac{P_{Cd}}{P_{S_2}} \tag{3.14}$$

Since the total pressure P_T is simply $p_{S_2} + p_{Cd}$, using (3.13) and (3.14) we obtain

$$K = \alpha \left(\frac{P_T}{1 + \alpha} \right)^{\frac{3}{2}} \tag{3.15}$$

This equation has been solved for three values of the total pressure P_T for cadmium sulphide and the result is shown in figure 3.4. It is clear that for a given total pressure, the equilibrium temperature may vary considerably, providing that α changes. It is possible therefore to maintain equilibrium over both source and growing crystal, having the same total pressure, but different values of α and T.

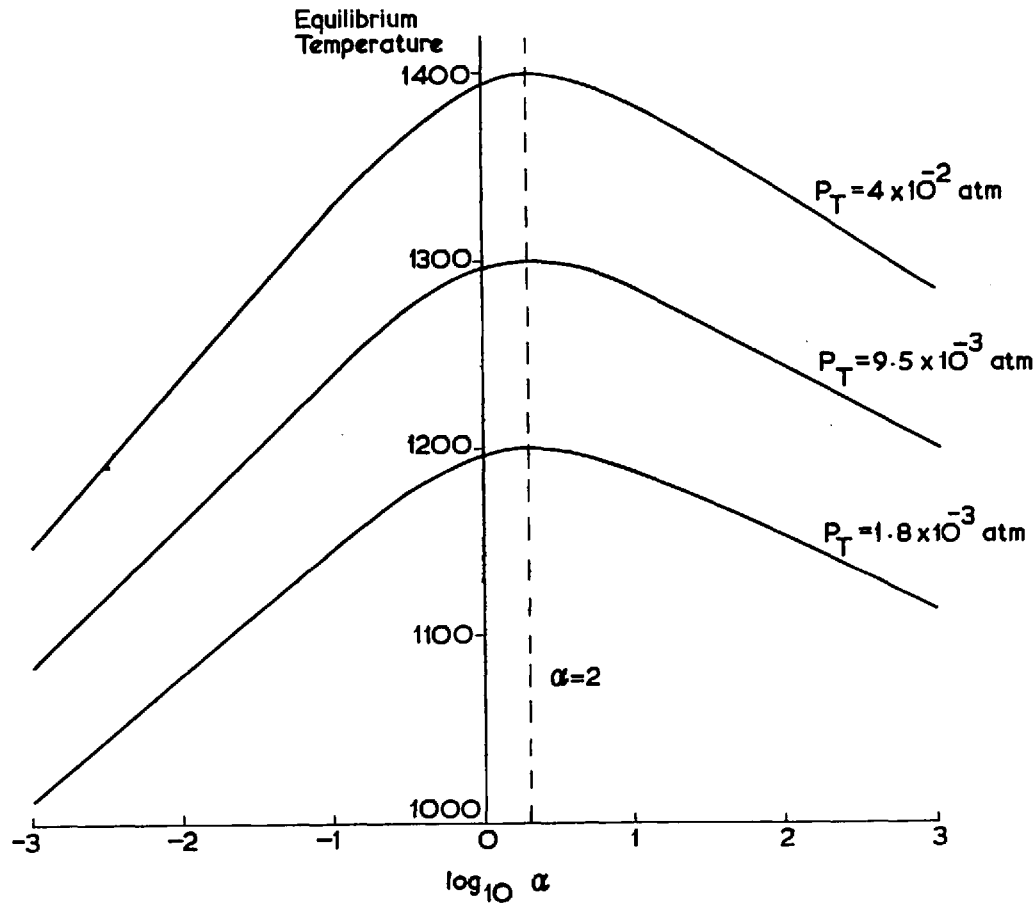

FIG.3.4. VARIATION OF α WITH TEMPERATURE AT CONSTANT TOTAL PRESSURE.

Equation (3.15) is a cubic equation in α and has two positive roots and a physically meaningless, negative one. The two positive solutions refer, one to a system where cadmium is in excess and one where sulphur is in excess. The asymmetry of the plot in figure 3.4 is due to sulphur existing mainly as a dimer in the gas phase.

The second concept is the stoichiometric relationship between the fluxes of the components of the solid in the vapour. In the case of cadmium sulphide where the sulphur is largely diatomic at normal crystal growth temperatures, the flux of cadmium must be twice that of the sulphur.

Following a similar procedure as before, for a compound AB dissociating

$$AB_{n(s)} \rightarrow A_{(g)} + \frac{n}{m} B_{m(g)} \tag{3.16}$$

we now have two fluxes to consider

$$J_A = \frac{uP_A}{RT} - \frac{D}{RT}\frac{dP_A}{dx} \tag{3.17a}$$

and

$$J_B = \frac{muP_B}{RT} - \frac{mD}{RT}\frac{dP_{B_m}}{dx} \tag{3.17b}$$

Integration, followed by substitution for u gives[31]

$$P_A^{(x)} = \left[P_A^{(l)} - \frac{P_T}{s}\right] \exp\left\{(x - l)\frac{JRTs}{P_T D}\right\} + \frac{P_T}{s} \tag{3.18a}$$

$$P_{B_m}^{(x)} = \left[P_{B_m}^{(l)} - \frac{nP_T}{ms}\right] \exp\left\{(x - l)\frac{JRTs}{P_T D}\right\} + \frac{nP_T}{ms} \tag{3.18b}$$

where $s = 1 + \frac{n}{m}$, the relationship between the stoichiometry of the solid and the molecularity of the gaseous components; and $J = J_A = J_{B_n} = \frac{1}{n} J_B$ as fixed by the stoichiometry of the solid.

Equations (3.18a) and (3.18b) have been solved for cadmium sulphide for various values of α and the results are plotted in figure 3.5. Also shown in figure 3.5 is a line marked J_{crit}; this is the critical growth rate for surface stability. The

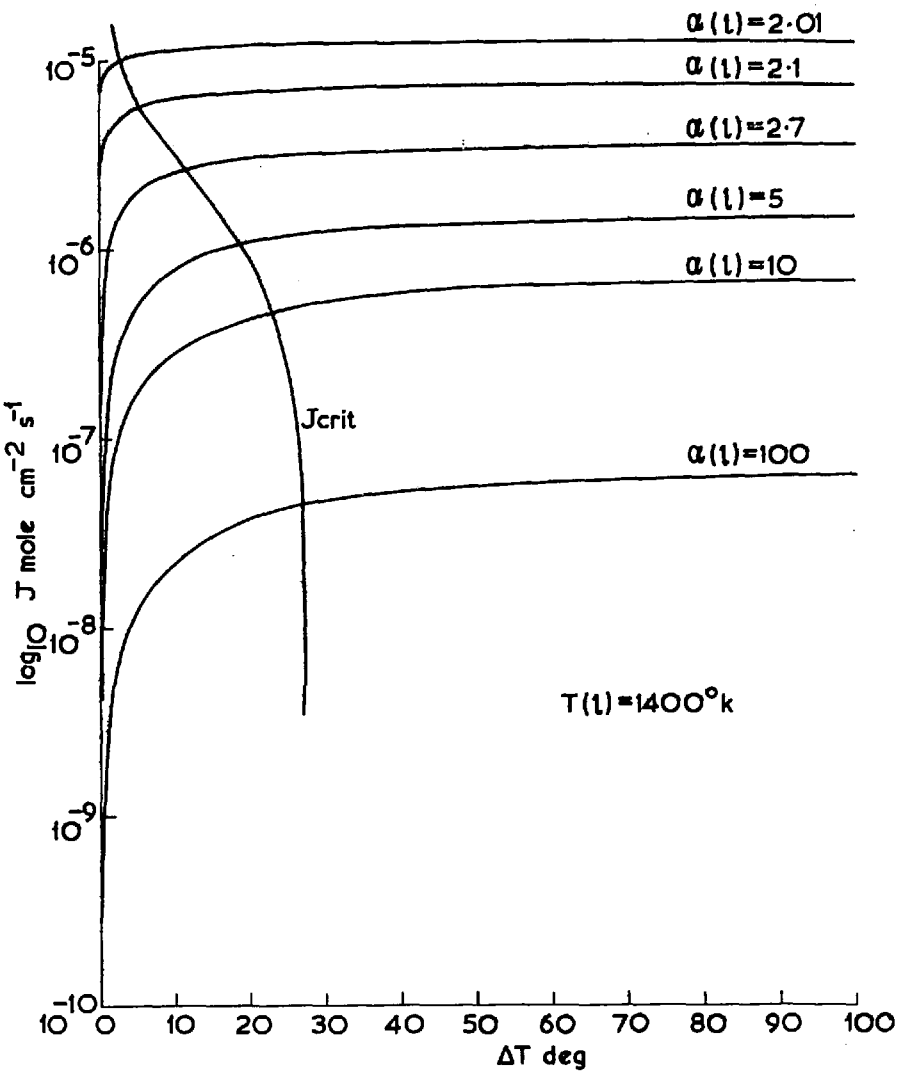

FIG.3.5 GROWTH RATE VERSUS ΔT FOR CADMIUM SULPHIDE.

concept of surface stability and J_{crit} will be discussed at the end of this section on dissociative sublimation. If there is a resistance to growth at the surface, then this resistance may be a function of a at the surface. If $a^{(o)}$ is fixed or prevented from varying to any great extent then the surface resistance will similarly be fixed. This can be done by introducing large amounts of inert gas into the system (see below).

As a approaches 2 in cadmium sulphide transport, the situation becomes comparable with ordinary sublimation of a single component without any inert gas present.

In figure 3.6 the partial pressure profiles of cadmium and sulphur are plotted for a capsule 10 cm long and for three different values of ΔT. The change of $a_{x=0}$ with ΔT is shown more clearly in figure 3.7 where $a_{x=l}$ has been fixed at 2.7. When $\Delta T = 0.1°$, $a_{x=0} \simeq 2.7$ but when $\Delta T = 40°$, $a_{x=0} = 32$. The implications of this variation in composition is that the composition of the solid can be varied within the stoichiometry range by suitable adjustment of growth rate and of a at the source.

If an inert gas in introduced, then there are three main effects on the system:

(a) The variation in composition of the vapour becomes less extreme for a given temperature difference (figure 3.8) e.g. when $\Delta T = 60°$ $a_{x=0} = 13$.

(b) The growth rate is reduced; this effect is most noticeable where the vapour is nearly stoichiometric (figure 3.9).

(c) The critical temperature difference is larger; again the effect is most noticeable if the vapour is nearly stoichiometric.

Figure 3.10 shows the partial pressure profiles for cadmium sulphide in the presence of an inert gas, e.g. argon. In the presence of argon the cadmium partial pressure decreases towards the growing interface.

3.4 Surface Stability and Critical Growth Rates

In the course of the treatment of dissociative sublimation, mention was made of surface stability and a value J_{crit}, the maximum permitted growth rate for surface stability. In this section these concepts will be discussed firstly with reference to a single component sublimation and then to dissociative sublimation.

Reed, La Fleur and Strauss[103, 104] suggested the possibility of constitutional supercooling occurring in vapour phase crystal growth, in an analogous way to that observed

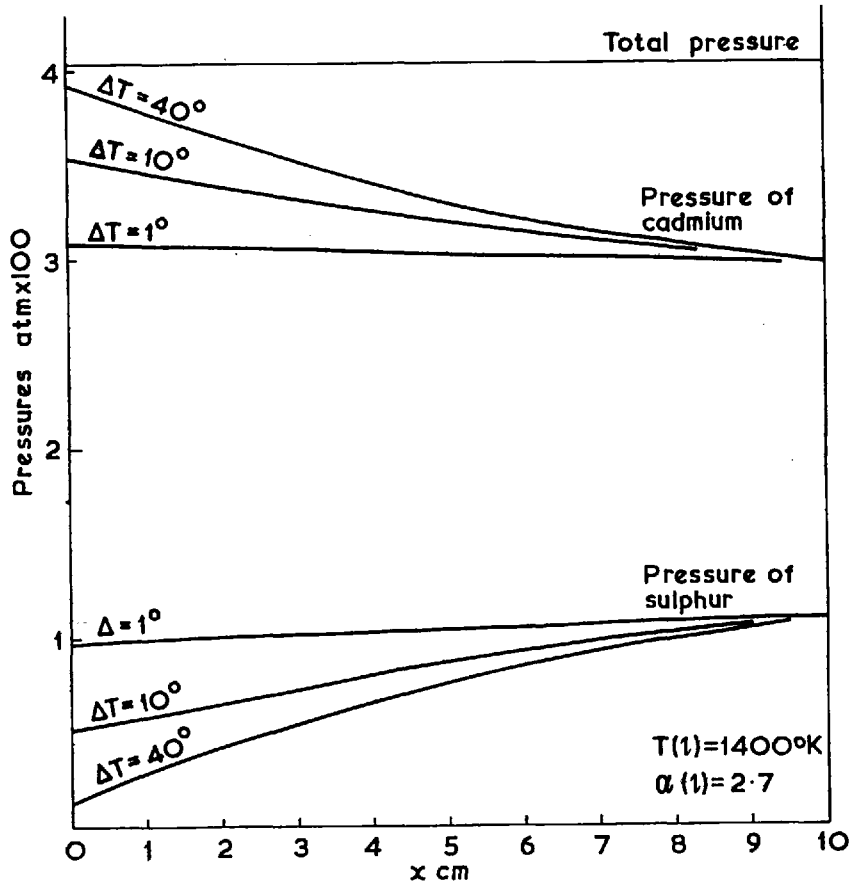

FIG.3.6 PARTIAL PRESSURES OF COMPONENTS AS FUNCTIONS OF x.

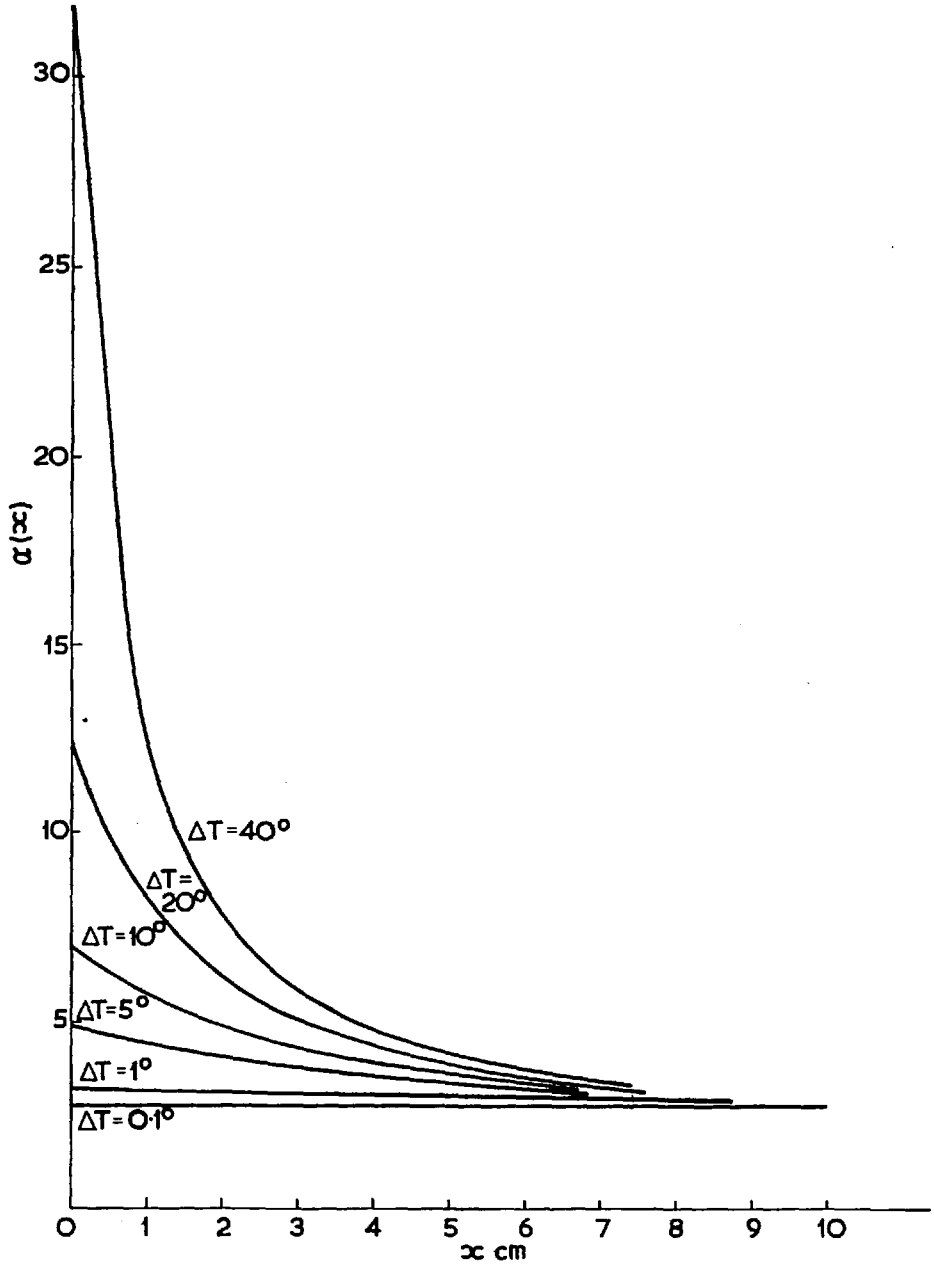

FIG.3.7. PARTIAL PRESSURE RATIO $\alpha(x)$ VERSUS x FOR CADMIUM SULPHIDE.
$T(\ell) = 1400^{\circ}K$; $\alpha(\ell) = 2.7$; $(dT/dx)_{x=0} = 10$ DEG.cm^{-1}

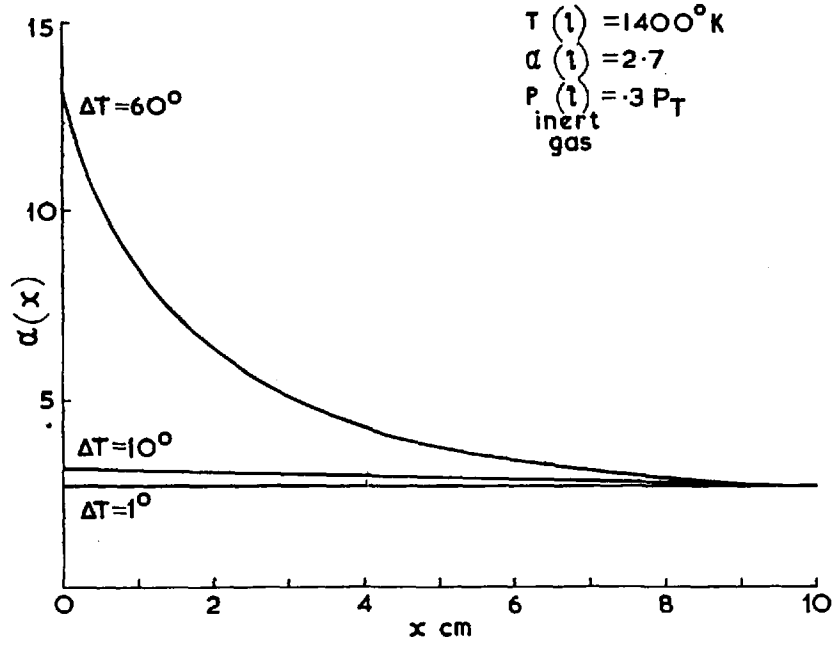

FIG.3.8. PARTIAL PRESSURE RATIO $\alpha(x)$ VERSUS x FOR CADMIUM SULPHIDE WITH AN INERT GAS. $(dT/dx)_{x=0} = 10$ DEG.cm^{-1}

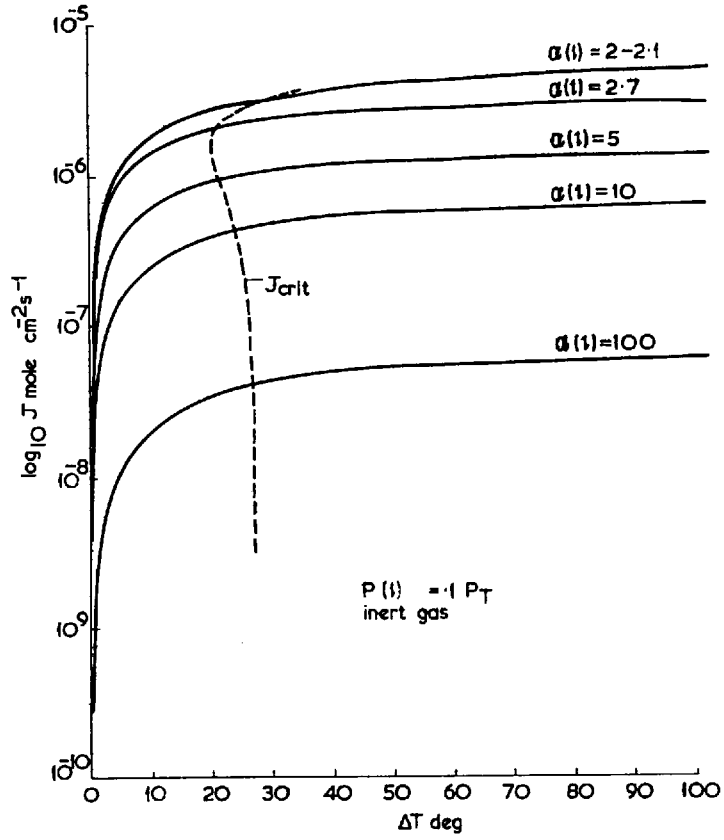

(a)

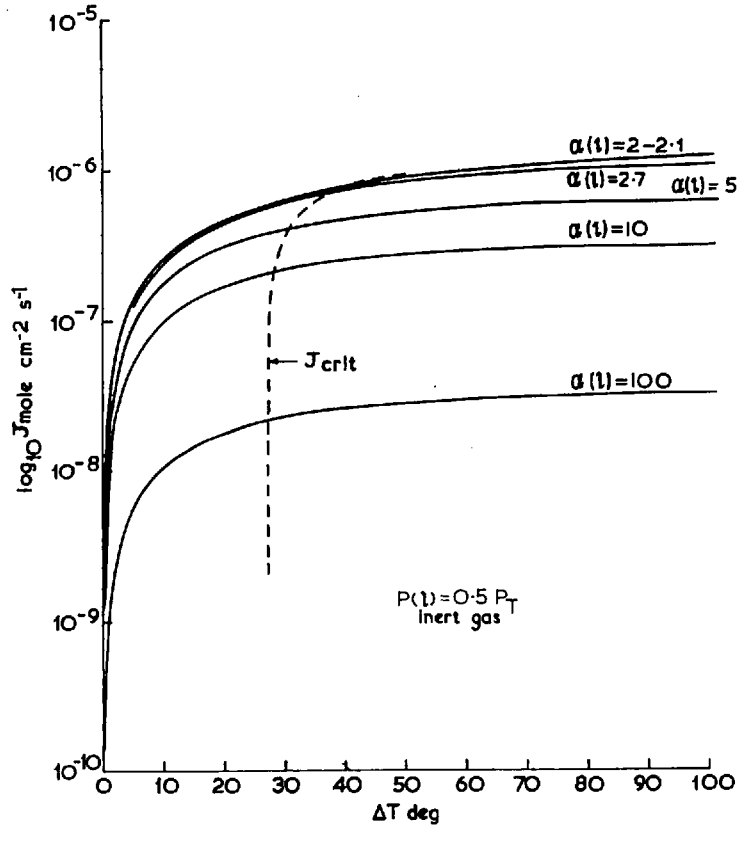

(b)

FIG.3.9. GROWTH RATE AS A FUNCTION OF ΔT FOR CADMIUM SULPHIDE WITH AN INERT GAS. T (ℓ) = 1400°K; ℓ = 10cm; $(dT/dx)_{x=0}$ = 10 DEG.cm^{-1}

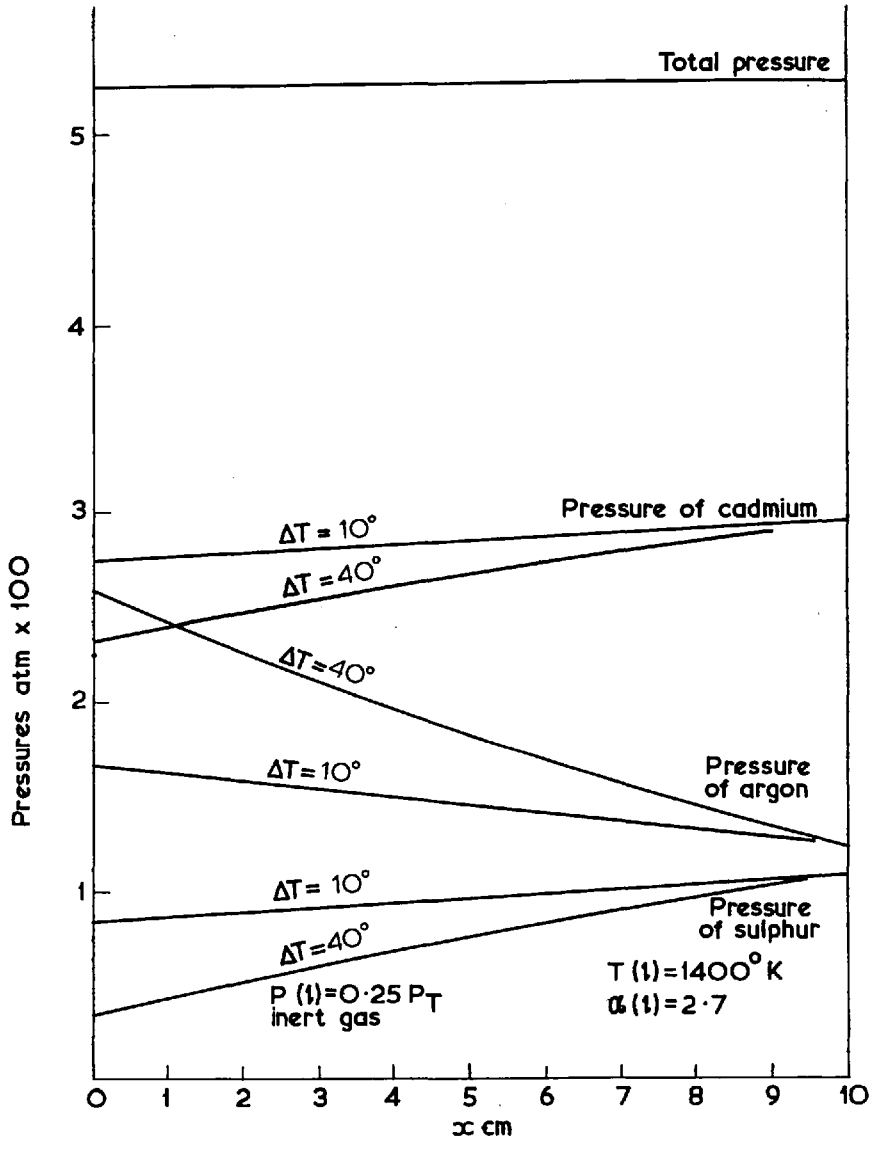

FIG.3.10. VARIATION OF PARTIAL PRESSURES WITH x FOR CADMIUM SULPHIDE WITH AN INERT GAS. $(dT/dx)_{x=0}$ = 10 DEG, cm^{-1}

in liquid phase growth[105]. The actual partial pressure of the active species in the vapour phase is determined by transport processes but the saturated vapour pressure is determined solely by the local temperature. This is illustrated in figure 3.11a assuming a linear temperature gradient between $x = 0$ and $x = l$. The curvature of the saturated vapour pressure line depends upon the enthalpy change of evaporation of substance A (plotted in broken line). The actual partial pressure (plotted with a continuous line) exceeds the saturated vapour pressure everywhere except at $x = 0$ and $x = l$ where we have assumed equilibrium between the solid and vapour. The ratio $P_A/P_{A(sat)}$ is termed the supersaturation and the maximum supersaturation occurs towards the middle of the plot. If this supersaturation is large enough then nucleation could occur on the capsule walls some distance from $x = 0$. It was observed on occasions in experimental systems that nucleation did sometimes occur ahead of the growth interface.

Reed et al.[103,104] suggested that since supersaturation increased going away from the interface into the vapour, then any small protruberances from the surface will grow more rapidly than the rest of the surface. Such a situation they termed constitutional supercooling in the vapour, resulting in a surface which is macroscopically rough. To counteract this they showed that by increasing the temperature gradient near the growth interface the surface becomes more uniform (stable). This can be seen from figure 3.11b, where the dashed line gives the new saturated vapour curve. The vapour is therefore undersaturated going away from the interface into the vapour.

The actual vapour pressure curve is fixed by $P_A^{(o)}$ and $P_A^{(l)}$ and the total pressure P_T. The saturated vapour pressure curve is a function of the temperature profile imposed between $x = 0$ and $x = l$. For surface stability therefore the condition required is that

$$\left[\frac{dP_{A(transport)}}{dx}\right]_{x=0} < \left[\frac{dP_{A(saturation)}}{dx}\right]_{x=0} \qquad (3.19)$$

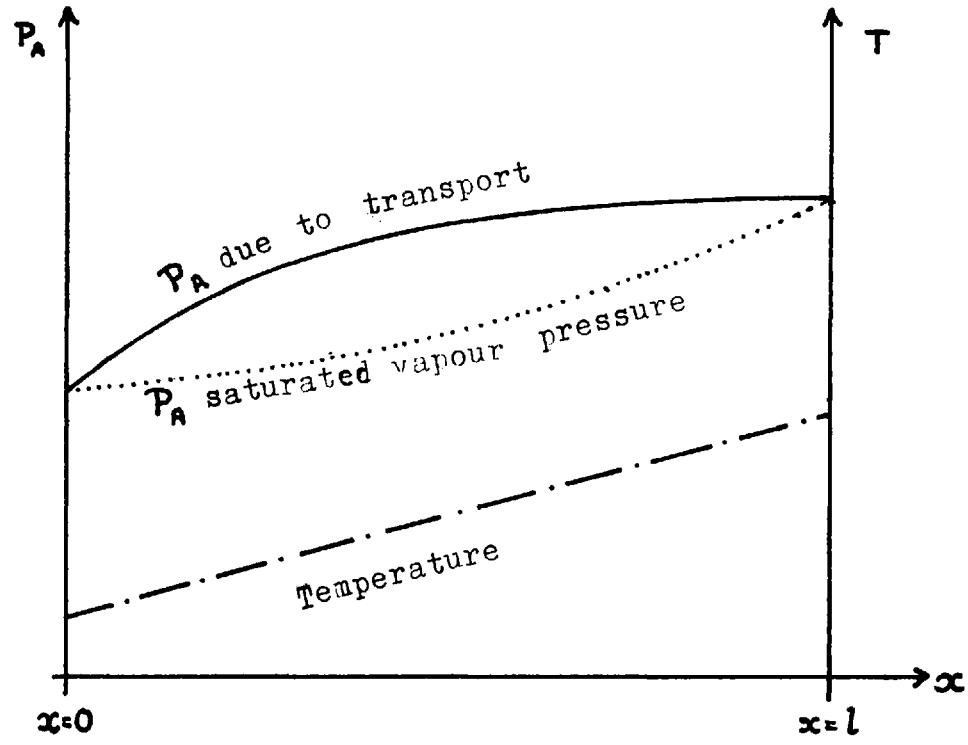

Figure 3.11(a)

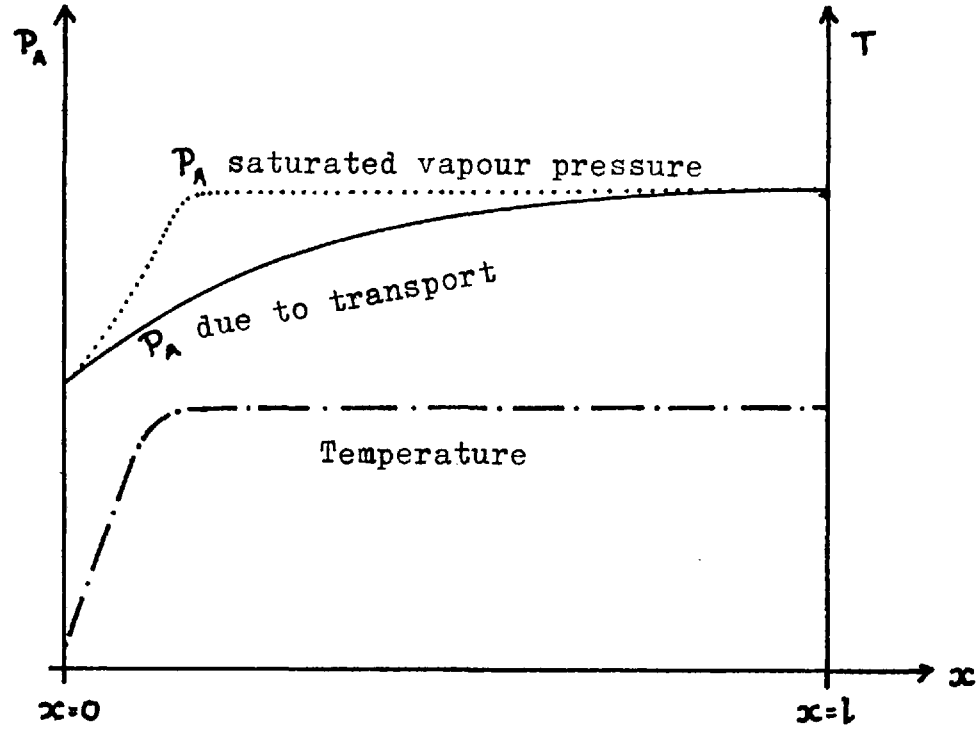

Figure 3.11(b)

FIG.3.11. COMPARISON OF THE PARTIAL PRESSURE PROFILE OF SPECIES 'A' DUE TO TRANSPORT WITH THE SATURATED VAPOUR PRESSURE OF 'A'.

For a given temperature gradient at $x = 0$ there is a critical temperature difference $T^{(l)} - T^{(o)}$ which causes

$$\left[\frac{dP_{A(transport)}}{dx}\right]_{x=0} - \left[\frac{dP_{A(saturation)}}{dx}\right]_{x=0} \tag{3.20}$$

The corresponding growth rate is termed J_{crit}.

When dealing with dissociative sublimation the condition taken for surface stability, is that the activity (a) of a compound AB_n should decrease going away from the growth interface.

i.e. $$\left[\frac{da_{AB_n}}{dx}\right]_{x=0} \leqslant 0 \tag{3.21}$$

The activity of AB_n is given by

$$a_{AB_n} = \frac{P_A (P_{B_m})^{\frac{n}{m}}}{K_T} \tag{3.22}$$

where K_T is the equilibrium constant for reaction (3.16). By substituting the values of $P_A^{(x)}$ and $P_{B_m}^{(x)}$ and K_T for cadmium sulphide in (3.32) it is possible to plot the activity of cadmium sulphide as a function of x. The results obtained are plotted in figure 3.12. Where the activity is greater than 1, solid would form, were it not for nucleation barriers. Where the activity is less than 1, the solid is unstable. It can be seen from figure 3.12, on the basis of the above conditions for a stable interface, that we would expect the growth interface to be smooth for the curves shown when $\Delta T = 1°$ or $10°$ under the conditions specified. [$T^{(l)} = 1400°K$; $\alpha^{(l)} = 2.7$; $(dT/dx)_{x=0} = 10$ deg cm^{-1}] and a rough surface would be expected for the curves where $\Delta T = 20°$ or $40°$.

Although the above considerations of surface stability are helpful for a qualitative understanding of the situation, it would be naive to assume that it is a complete analysis of the problem. In applying the equations and theoretical results to experimental systems there are several factors to be remembered: The model as given is

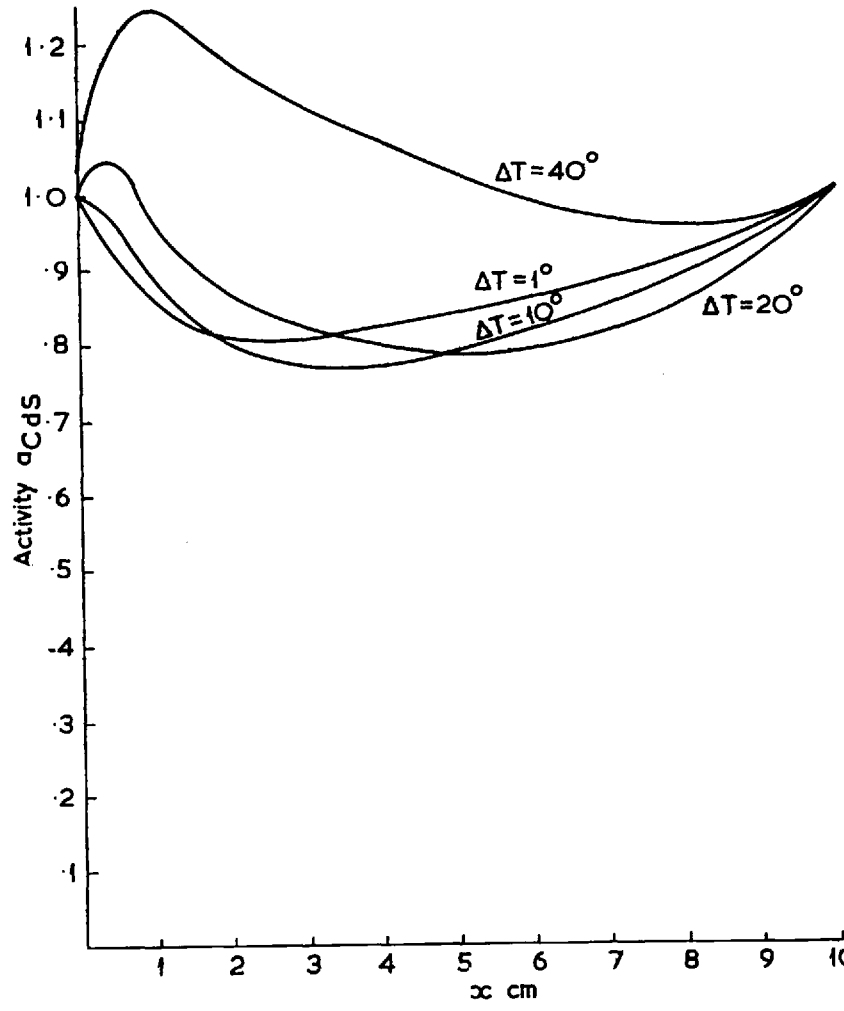

FIG.3.12. VARIATION OF CADMIUM SULPHIDE ACTIVITY WITH x, FOR GROWTH RATES SMALLER AND LARGER THAN THE CRITICAL RATE. $T(\ell) = 1400^{\circ}K$; $\alpha(\ell) = 2.7$; $(dT/dx)_{x=0} = 10$ DEG.cm^{-1}

one-dimensional, any protrusion on the surface of the growing crystal will affect the composition of the gas laterally as well as longitudinally. Gas movement laterally as well as temperature variations across the surface must also be taken into account; convection in the vapour will alter the partial pressure profiles and if the gas composition becomes uniform in the capsule as a result, then it will have the same effect as bringing the source close to the growth interface.

It is possible that requirements of minimum surface free energy may be important, particularly when the crystal is grown under conditions close to equilibrium. A surface may remain flat even if a degree of constitutional supercooling occurs in the vapour or alternatively the surface may become covered in small facets in order to reduce its surface free energy, even if the vapour is undersaturated.

Surface morphology can also be influenced by the presence of impurities in the system[106].

3.5 Chemical Vapour Transport

The treatment given for sublimation and dissociative sublimation has been extended to chemical vapour transport[30,31]. However the increased complexity and variety of possible transporting agents precluded a general treatment, consequently a particular system was used as an example - gallium arsenide/chlorine. The theoretical analysis of that particular system is not described here, since the experimental work carried out for this thesis involved the more commonly used gallium arsenide/arsenic trichloride/hydrogen system. The experimental system used, is described in detail in a later chapter and all that is given here is a brief description of the system. The gallium arsenide source material was contained in a capsule which was sealed except for a small hole. Arsenic trichloride and hydrogen passed into the furnace tube containing the capsule and the hole allowed gases to flow in and out of the capsule, but was sufficiently small for the capsule to be considered as a closed system. A temperature gradient was imposed on the capsule and transport of gallium arsenide occurred to the colder region. A schematic diagram is given in figure 3.13 along with the notation used in the theoretical analysis presented below.

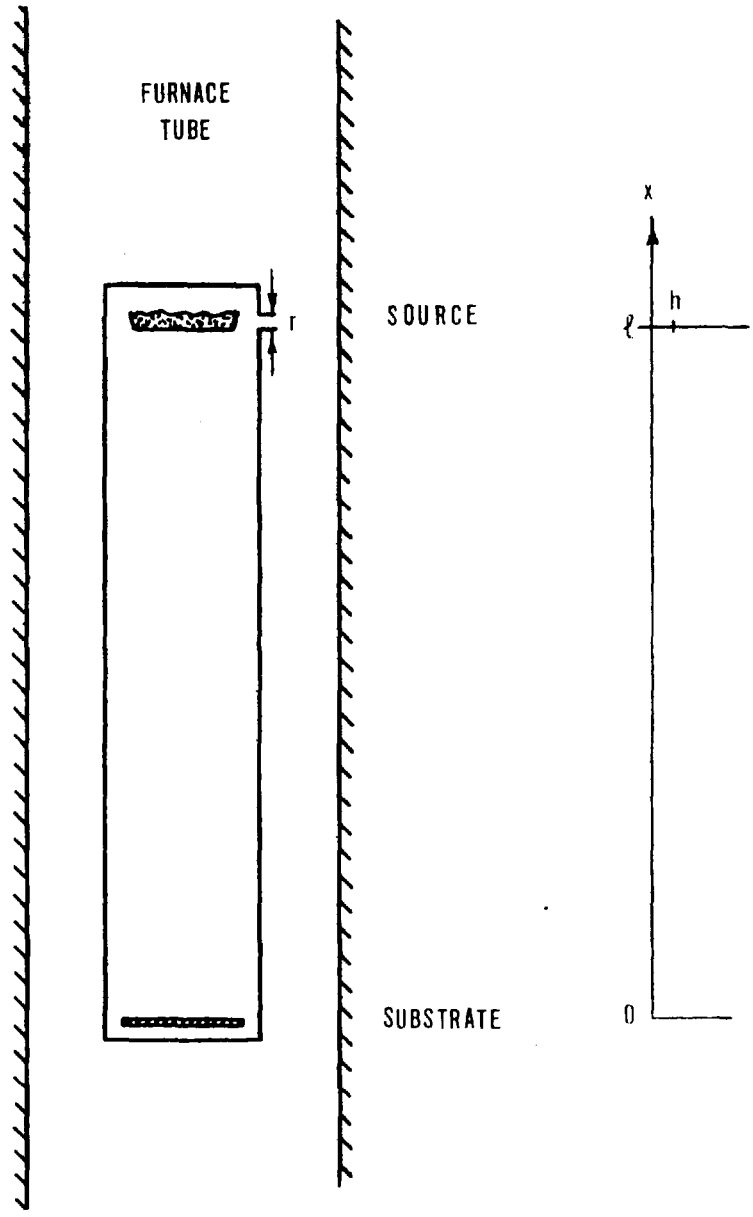

FIG.3.13. SCHEMATIC DIAGRAM OF THE CAPSULE USED IN GaAs – $AsCl_3$ – H_2 SYSTEM WITH THE NOTATION USED IN THE THEORETICAL MODEL.

Equilibria obtaining in the GaAs - $AsCl_3$ - H_2 system

The mixture $AsCl_3/H_2$ was produced experimentally by passing hydrogen through a bubbler containing liquid arsenic trichloride. The partial pressure of arsenic trichloride was varied by altering the bubbler temperature. At room temperature, little reaction occurs between the hydrogen and arsenic trichloride, but on entering the hot furnace, the equilibrium of reaction (3.23) is displaced towards the right-hand side.

$$2\ AsCl_3 + 3\ H_2 \rightarrow \frac{1}{2}As_4 + 6\ HCl \qquad (3.23)$$

At 700-800°C the reaction goes almost to completion.

The gas outside the capsule consists of As_4, HCl and a large excess of H_2.

Inside the capsule there are two possible reactions:

$$GaAs + HCl \rightarrow GaCl + \frac{1}{2}H_2 + \frac{1}{4}As_4 \qquad (3.24)$$

$$GaAs + 3\ HCl \rightarrow GaCl_3 + \frac{3}{2}H_2 + \frac{1}{4}As_4 \qquad (3.25)$$

Other reactions involving species Cl_2, $AsCl_3$ and AsH_3 were ignored since existing thermodynamic data[89,107,108] showed that their equilibrium partial pressures are very small at the normal operating temperatures (700°-800°C). Recently new measurements on arsenic suggest that As_2 is present in significant amounts[109,110] and the modified entrainment method, reported in this thesis, also revealed the presence of $GaCl_2$, however the analysis given here was performed and published[12] before this information was available. The increased accuracy in the growth rate values obtained by including the As_2 and $GaCl_2$ species in the theoretical analysis, would not add significantly to the discussion of the experimental results, since the latter are subject to some uncertainty. It was considered therefore, that the long and tedious computation required was not justified in the case of this crystal growth system. Discussion of the presence of As_2 and $GaCl_2$ is included in the modified entrainment method.

In the system considered, existing thermodynamic data show that the partial pressure of $GaCl_3$ is negligible[107,108]; this was later supported by the modified entrainment, where no evidence for its presence in significant amounts was found. Consequently in the succeeding analysis, reaction (3.24) is the only one considered, and by adopting this

approach the analysis is greatly simplified. The possibility of GaAs molecules or clusters participating significantly in the transport is not considered since no experimental evidence exists other than some mass spectroscopic evidence for GaAs molecules in the vapour over solid GaAs[111]. Such mechanisms have been postulated in other systems[112,113]. If gallium arsenide molecules are present in the gas phase then the number is very small and may be safely ignored.

As in dissociative sublimation it is assumed that equilibrium between GaAs solid and the vapour adjacent to it occurs at both the source and the substrate. Obviously if transport is occurring between the source and the substrate then some departure from equilibrium is inevitable. For rates which are not too large we may write[114,115]

$$J_c = LA \tag{3.26}$$

where

$$A = -\Sigma \nu_i \mu_i \tag{3.27}$$

J_c is the chemical reaction rate and A is the affinity of the reaction, ν_i and μ_i are respectively the stoichiometric coefficient and chemical potential of species i and L is a proportionality constant (phenomenological coefficient). L is frequently a strong function of temperature but at normal growth temperatures we can assume that it is numerically large and A consequently is very small. At equilibrium A = 0.

Determination of the Degrees of Freedom in the system

The phase rule relates the degrees of freedom of system (F) to the number of phases present (P) and the number of components (C) by the equation

$$F = C - P + 2 \tag{3.28}$$

The system described in this section has two phases: solid and gas and four components. Consequently, there are four thermodynamic degrees of freedom. If we choose temperature (T) and total pressure (P_T) along with the partial pressures of two components e.g. p_{H_2} and p_{As_4} then the partial pressures of the other vapour components can be determined from the equilibrium equation

$$K_2 = \frac{p_{GaCl} \; (p_{H_2})^{\frac{1}{2}} \; (p_{As_4})^{\frac{1}{4}}}{p_{HCl}} \tag{3.29}$$

where K_2 is the equilibrium constant for reaction (3.24) and the additional condition:

$$P_T = p_{GaCl} + p_{As_4} + p_{H_2} + p_{HCl} \qquad (3.30)$$

Experimentally it is possible to vary the temperature over a wide range and it is convenient to work at 1 atmosphere total pressure. The level of chlorine species present is fixed by the vapour pressure of arsenic trichloride introduced into the furnace i.e. the equilibrium vapour pressure of the arsenic trichloride as fixed by the temperature of the bubbler (T_b). Use of arsenic trichloride as a source of chlorine imposes a further restriction relating the partial pressures of the arsenic and chlorine. The four degrees of freedom are thus specified and the partial pressures of all species may be calculated - we assume equilibrium at three places:

(a) Between the liquid arsenic trichloride and the vapour over it.

(b) In the gas phase near the capsule.

(c) Between the solid gallium arsenide source material and the vapour above it.

The calculation of these partial pressures is given in Appendix 2.

From equation (3.24) it can be seen that there is a volume change on formation of gallium monochloride. As with sublimation and dissociative sublimation, when a temperature gradient is imposed on the capsule such that the gallium arsenide source is at temperature $T^{(l)}$ and the gallium arsenide substrate at temperature $T^{(o)}(T^{(l)} > T^{(o)})$, there is a nett flow of gas from the source to the substrate.

It is interesting to consider the degrees of freedom at the substrate; as at the source there are four degrees of freedom, the temperature, $T^{(o)}$, is under experimental control and the total pressure is very nearly the same as at the source. The two remaining degrees of freedom are fixed by the fact that there is no nett flow of hydrogen or chlorine in the capsule. It is to be noted that no degree of freedom is necessary for the condition that the gallium and arsenic must be in equal proportions. This is a condition imposed by the stoichiometry of the chemical reaction and is an intrinsic part of the mechanism of approach to equilibrium.

The flow equations for the system

As before, the flux of each species can be expressed as the sum of two components: the diffusive component

$$J_{i\ diff} = \frac{-D}{RT}\frac{dp_i}{dx} \tag{3.31}$$

and a viscous flow component due to the movement of the gas as a whole at velocity U

$$J_{i\ visc} = \frac{Up_i}{RT} \tag{3.32}$$

The flow equations are therefore:

$$J_{Ga} = \frac{Up_{GaCl}}{RT} - \frac{D}{RT}\frac{dp_{GaCl}}{dx} = J \tag{3.33}$$

$$J_{As} = \frac{4\ Up_{As_4}}{RT} - \frac{4\ D}{RT}\frac{dp_{As_4}}{dx} = J \tag{3.34}$$

$$J_H = \frac{U}{RT}(2\ p_{H_2} + p_{HCl}) - \frac{D}{RT}\frac{d}{dx}(2\ p_{H_2} + p_{HCl}) = 0 \tag{3.35}$$

$$J_{Cl} = \frac{U}{RT}(p_{GaCl} + p_{HCl}) - \frac{D}{RT}\frac{d}{dx}(p_{GaCl} + p_{HCl}) = 0 \tag{3.36}$$

J is the growth rate of gallium arsenide in moles/unit area/unit time. It has been assumed that the diffusion coefficients are the same for all species. This is a reasonable assumption where one species (hydrogen) is in large excess and the other species do not have extreme molecular weights[29,30].

From equations (3.33) and (3.36) it can be seen that the flux of HCl is - J. This follows from the fact that the chlorine is transported to the substrate as GaCl and back to the source as HCl so there is no nett flux of chlorine. Similarly there is no nett flux for the hydrogenic species.

By taking a suitable linear combination of the flow equations $\left[(3.33) + \frac{1}{2} \times (3.34) + (3.35) + (3.36)\right]$ and by using equation (3.30), the diffusion terms reduce to zero since P_T is almost constant along the capsule $\left(\text{i.e. } \frac{dP_T}{dx} = 0\right)$. The resulting equation is therefore

$$3\ JRT = 4\ UP_T \tag{3.37}$$

$$\left(\text{c.f. dissociative sublimation } JRT\left(1 + \frac{n}{m}\right) = UP_T;\quad AB_n \rightarrow A + \frac{n}{m}B_m\right)$$

Ignoring the variation of T with x, integration of equations (3.33) - (3.36) using the boundary condition at $x = l$, $p_i = p_i^{(l)}$ gives the partial pressures of the four species as a function of x.

$$p_{GaCl}^{(x)} = \left[p_{GaCl}^{(l)} - \frac{4\,P_T}{3}\right] \exp\left\{\frac{3\,JRT}{4\,DP_T}(x - l)\right\} + \frac{4\,P}{3} \tag{3.38}$$

$$p_{As_4}^{(x)} = \left[p_{As_4}^{(l)} - \frac{P_T}{3}\right] \exp\left\{\frac{3\,JRT}{4\,DP_T}(x - l)\right\} + \frac{P}{3} \tag{3.39}$$

$$p_{HCl}^{(x)} = \left[p_{HCl}^{(l)} + \frac{4\,P_T}{3}\right] \exp\left\{\frac{3\,JRT}{4\,DP_T}(x - l)\right\} - \frac{4\,P}{3} \tag{3.40}$$

$$p_{H_2}^{(x)} = \left[p_{H_2}^{(l)} - \frac{2\,P_T}{3}\right] \exp\left\{\frac{3\,JRT}{4\,DP_T}(x - l)\right\} + \frac{2\,P}{3} \tag{3.41}$$

The growth rate of gallium arsenide (J) is negative as defined since the source is at $x = l$ and substrate at $x = 0$. The value of J may be calculated if the partial pressure of any species at $x = 0$ is known (or at any point between $x = 0$ and $x = l$).

Partial pressures at the substrate

We have already noted that there are four degrees of freedom at the substrate; the easiest to control experimentally is the temperature $T^{(o)}$. The equation corresponding to this degree of freedom may be taken as the equilibrium equation:

$$K_2^{(o)} = \frac{p_{GaCl}^{(o)}\left[p_{H_2}^{(o)}\right]^{\frac{1}{2}}\left[p_{As_4}^{(o)}\right]^{\frac{1}{4}}}{p_{HCl}^{(o)}} \tag{3.42}$$

Since the total pressure is virtually constant along the capsule, then:

$$P_T = p_{GaCl}^{(o)} + p_{As_4}^{(o)} + p_{HCl}^{(o)} + p_{H_2}^{(o)} \tag{3.43}$$

Two further equations are required and these come from the fact that there is zero nett flux of chlorine and hydrogen. These conditions may be expressed as given in equations (3.44) and (3.45) which have been derived from equations (3.38) - (3.41)

$$\frac{p_{HCl}^{(o)} + 2\,p_{H_2}^{(o)}}{p_{HCl}^{(l)} + 2\,p_{H_2}^{(l)}} = \frac{p_{GaCl}^{(o)} - 4\,p_{As_4}^{(o)}}{p_{GaCl}^{(l)} - 4\,p_{As_4}^{(l)}} \qquad (3.44)$$

$$\frac{p_{GaCl}^{(o)} + p_{HCl}^{(o)}}{p_{GaCl}^{(l)} + p_{HCl}^{(l)}} = \frac{p_{GaCl}^{(o)} - 4\,p_{As_4}^{(o)}}{p_{GaCl}^{(l)} - 4\,p_{As_4}^{(l)}} \qquad (3.45)$$

Equations (3.42) to (3.45) can be solved using standard iterative procedures[116] for the partial pressures at the substrate and the transport rate J for gallium arsenide can then be calculated. The results of such a calculation are given for two different temperatures in figures 3.14 and 3.15. The figures by the solid lines are the arsenic trichloride bubbler temperatures in degrees centigrade. The broken lines show J_{crit} and ΔT_{crit} for the temperature gradients indicated, the gradients being given in degrees per centimetre. The derivation of J_{crit} and ΔT_{crit} is given below.

Surface stability in the GaAs - $AsCl_3$ - H_2 chemical vapour transport system

The condition given for surface stability in dissociative sublimation was (Equation 3.21):

$$\left(\frac{da}{dx}\right)_{x=0} < 0$$

The same condition can be used in chemical vapour transport. In the system under discussion the activity of gallium arsenide is given by

$$a_{GaAs} = \frac{p_{GaCl}(p_{H_2})^{\frac{1}{2}}\,(p_{As_4})^{\frac{1}{4}}}{p_{HCl}\,K_2} \qquad (3.46)$$

Differentiating with respect to x we obtain

$$\left(\frac{da}{dx}\right)_{x=0} = a^{(o)}\left[\frac{1}{p_{GaCl}}\cdot\frac{dp_{GaCl}}{dx} + \frac{1}{2\,p_{H_2}}\cdot\frac{dp_{H_2}}{dx} + \frac{1}{4\,p_{As_4}}\frac{dp_{As_4}}{dx} - \frac{1}{p_{HCl}}\frac{dp_{HCl}}{dx} - \frac{1}{K_2}\frac{dK_2}{dx}\right] \qquad (3.47)$$

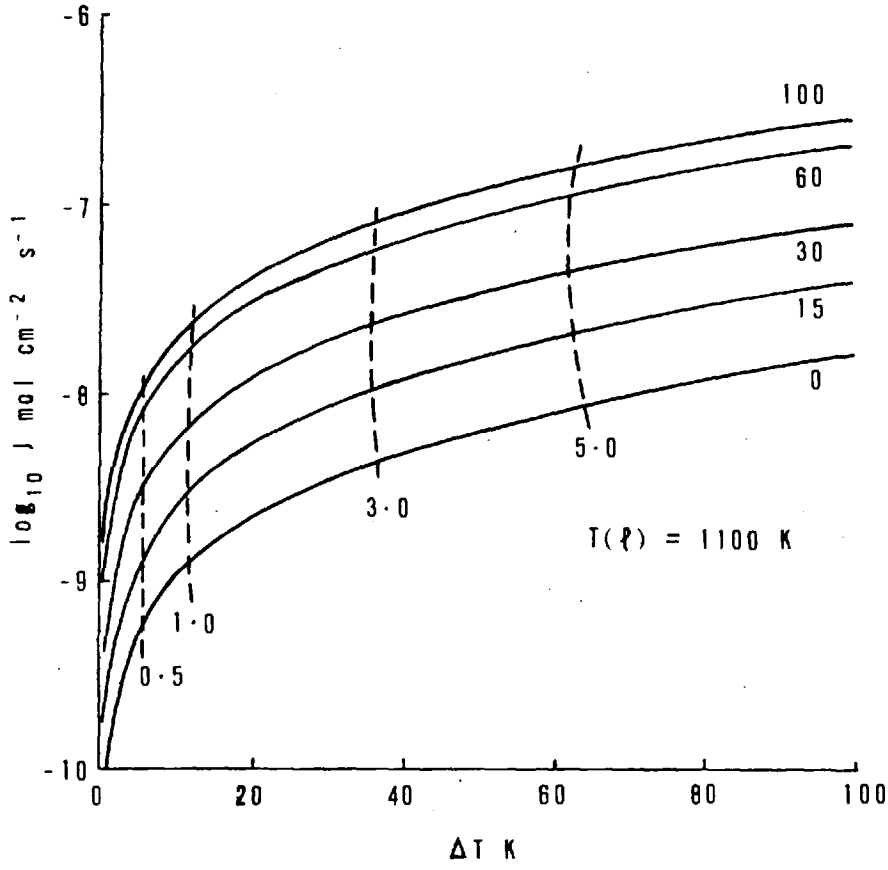

FIG 3 14.THEORETICAL GROWTH RATES vs ΔT

THE NUMBERS BY THE CONTINUDUS LINES INDICATE THE TEMPERATURE (^{o}C) OF THE $AsCl_3$ BUBBLER. THE BROKEN LINES SHOW J_{crit} AND ΔT_{crit} FOR THE TEMPERATURE GRADIENTS INDICATED ($^{o}Kcm^{-1}$)

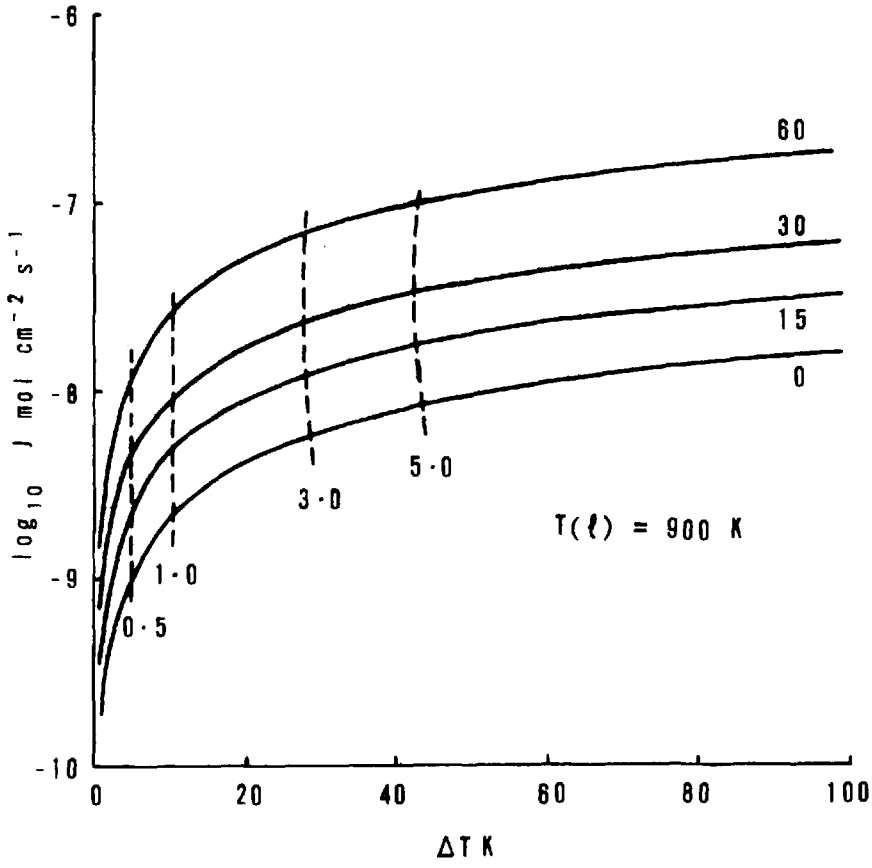

FIG.3.15 THEORETICAL GROWTH RATES vs ΔT

THE NUMBERS BY THE CONTINUOUS LINES INDICATE THE TEMPERATURE (^{0}C) OF THE $AsCl_3$ BUBBLER. THE BROKEN LINES SHOW J_{crit} AND ΔT_{crit} FOR THE TEMPERATURE GRADIENTS INDICATED (^{0}K cm^{-1})

The last term of equation (3.47) is proportional to the temperature gradient at the surface, whereas the other terms are largely unaffected by the temperature profile along the capsule[29].

$$\frac{1}{K_2}\left(\frac{dK_2}{dx}\right)_{x=0} = \left(\frac{d\ (lnK_2)}{dx}\right)_{x=0}$$

$$= \left(\frac{d\ lnK_2}{dT}\right)\left(\frac{dT}{dx}\right)_{x=0} \qquad (3.48)$$

Now van't Hoff's equation states[117] that

$$\frac{d\ lnK_2}{dT} = \frac{\Delta H}{RT^2} \qquad (3.49)$$

where ΔH is the enthalpy of reaction, hence

$$\frac{1}{K_2}\left(\frac{dK_2}{dx}\right)_{x=0} = \frac{\Delta H}{RT^2}\left(\frac{dT}{dx}\right)_{x=0} \qquad (3.50)$$

The first four terms of equation (3.47) have an algebraic total which is positive; the last term is negative since ΔH for reaction (3.24) is positive. The stability of the interface is determined by which of the terms is greater in magnitude. For a given ΔT and conditions at the source, there is a value of $\left(\frac{dT}{dx}\right)_{x=0}$ for which $\left(\frac{da}{dx}\right)_{x=0}$ is zero or conversely for a given $\left(\frac{dT}{dx}\right)_{x=0}$ and conditions at the source, there is a value of ΔT for which $\left(\frac{da}{dx}\right)_{x=0}$ is zero. This value of ΔT is designated ΔT_{crit} and the corresponding growth rate, J_{crit}. Both ΔT_{crit} and J_{crit} are functions of $\left(\frac{dT}{dx}\right)_{x=0}$ and are shown in figures 3.14 and 3.15 for different values of the temperature gradient.

In this chapter a theoretical model[28-33] for transport in the vapour phase has been presented. The theory has been applied to three types of system in order of

increasing complexity:

(a) Sublimation of a single component in the presence of an inert gas.

(b) Dissociative sublimation in the absence and presence of an inert gas.

(c) Chemical vapour transport of gallium arsenide in the GaAs - $AsCl_3$ - H_2 system.

It has been shown that the partial pressure profiles of the species present can be determined at all points along the growth capsule and theoretical growth rates have been obtained for systems close to those in experimental use. The concept of surface stability has been introduced and critical values for growth rates and temperature differences obtained. In chapter 6 the theoretical results are compared with values obtained from experiments in the chemical vapour transport of gallium arsenide.

CHAPTER 4

A MODIFIED ENTRAINMENT METHOD FOR MEASURING VAPOUR PRESSURES AND HETEROGENEOUS EQUILIBRIA INVOLVING REACTIVE GASES

CHAPTER 4

A MODIFIED ENTRAINMENT METHOD FOR MEASURING VAPOUR PRESSURES AND HETEROGENEOUS EQUILIBRIA INVOLVING REACTIVE GASES

4.1 Introduction

The limitations of conventional entrainment methods have been discussed earlier and the Knudsen effusion method, though well proven for vapour pressure measurement, cannot be used for studying equilibria at pressures where the mean free path of the gas molecules is not large compared with the orifice diameter. In the method described here the limitations of the entrainment method have been overcome; it can be used to study equilibria at pressures up to one atmosphere and its versatility has been demonstrated by application to several systems. Initially the method was validated by choosing two materials for vapour pressure measurement operating over different temperature ranges: water at around room temperature and lead at 900°-1050°C. The results obtained are compared with previously reported data. The first reaction equilibrium investigated was that between gallium and water at temperatures above 950°C, and it was chosen for several reasons. Under suitable conditions of temperature and water/hydrogen ratio, volatile gallium compounds are present at significant partial pressures[75,83]. The system is therefore of potential interest in the chemical vapour transport of gallium compounds, e.g. gallium arsenide and some investigations have already been made[76-78]. It also seemed that the gallium-water system was well characterised[75,83] and would be suitable for testing the modified entrainment method in studying reaction equilibria. Finally the method was applied to the systems: gallium-hydrogen chloride and gallium arsenide-hydrogen chloride at temperatures above 500°C. These equilibria form the basis of many chemical vapour transport systems used for the epitaxial growth of gallium arsenide at the present time. Although some thermodynamic data were available[76,107,108,118] the enthalpy of formation of gallium monochloride was not known accurately and also recent measurements of the dissociation of tetrameric arsenic indicated that dimeric arsenic should be included in any analysis of the GaAs/HCl system[109,110].

In the subsequent sections of this chapter, a description of the experimental system and the method of operation are given, followed by a brief account of the theory, in which

reference is made to the four papers appended to this thesis. Finally the results obtained are presented and discussed. For the sake of convenience, the papers attached at the end,will be referred to as Papers I, II, III and IV; paper I being 'Theory and validation of the method using water and lead', Paper II, 'Equilibria in the water-gallium system', Paper III, 'Diffusivity of hydrogen chloride in hydrogen and extension to multicomponent diffusion at 700-1300K' and Paper IV, 'The gallium arsenide - hydrogen chloride system'.

4.2 Experimental System

4.2.1 General Description

The solid or liquid sample to be studied was placed in a small silica bottle which was fitted with a size B5 ground socket joint (figure 4.1). The dimensions of the silica stopper were precisely known: length (usually 20 mm) and internal bore (1 or 2 mm). The bottle was thus fitted with a long narrow channel of known dimensions, variation of these dimensions was achieved by exchanging the stopper. The bottle was suspended from a Cahn RH Electrobalance using the loop on the bottle and a long silica suspension fibre (figure 4.2). The weight of the bottle was monitored continuously and the weight change was plotted out on a chart recorder. The balance, suspension fibre and sample bottle were enclosed in a glass system and the sample was heated by a furnace for temperatures above 300°C and by a controlled temperature water jacket in the range 0-55°C. Two gas inlets were situated at the top of the apparatus, the upper one, directly entering the balance chamber, served to keep the balance in an inert atmosphere, while the lower one was used for introducing reactive gases. Temperatures were measured using platinum/platinum - 13% rhodium thermocouples for the high temperature range and an alcohol-in-glass thermometer positioned immediately below the bottle for the low temperature range. In early experiments the thermocouple was situated outside the furnace tube adjacent to the bottle, but in later experiments the thermocouple was sheathed in thin walled silica and placed inside the furnace tube with the thermocouple bead positioned a few millimetres below the sample bottle. Gas flow rates were measured using Meterate flow meters.

There are certain features in the design of the apparatus which should be stressed. Firstly, the constriction immediately below the balance chamber was included to reduce back diffusion of reactive gases into the chamber thus protecting the balance mechanism.

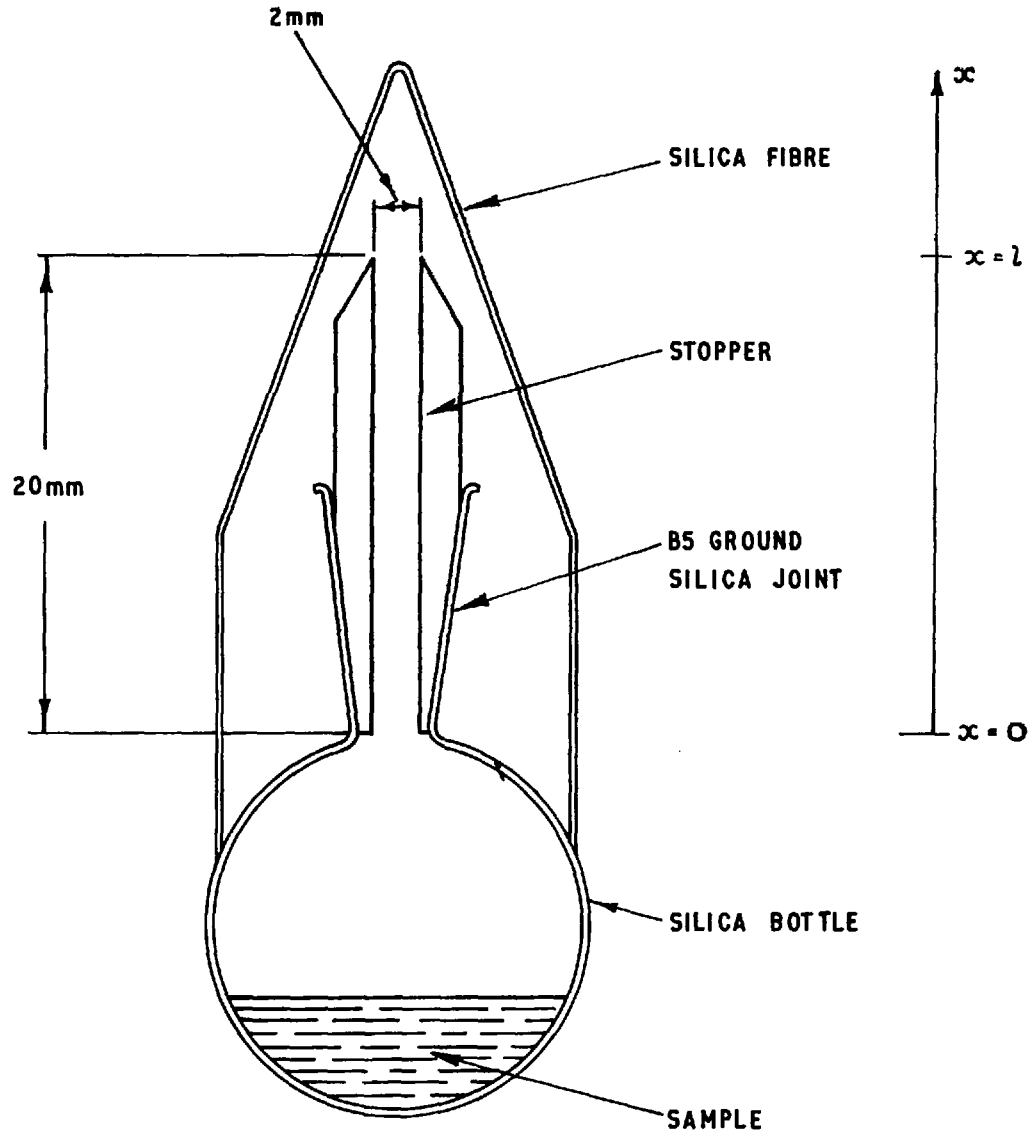

FIG. 4.1. REACTION BOTTLE AND ONE – DIMENSIONAL MODEL FOR GAS TRANSPORT.

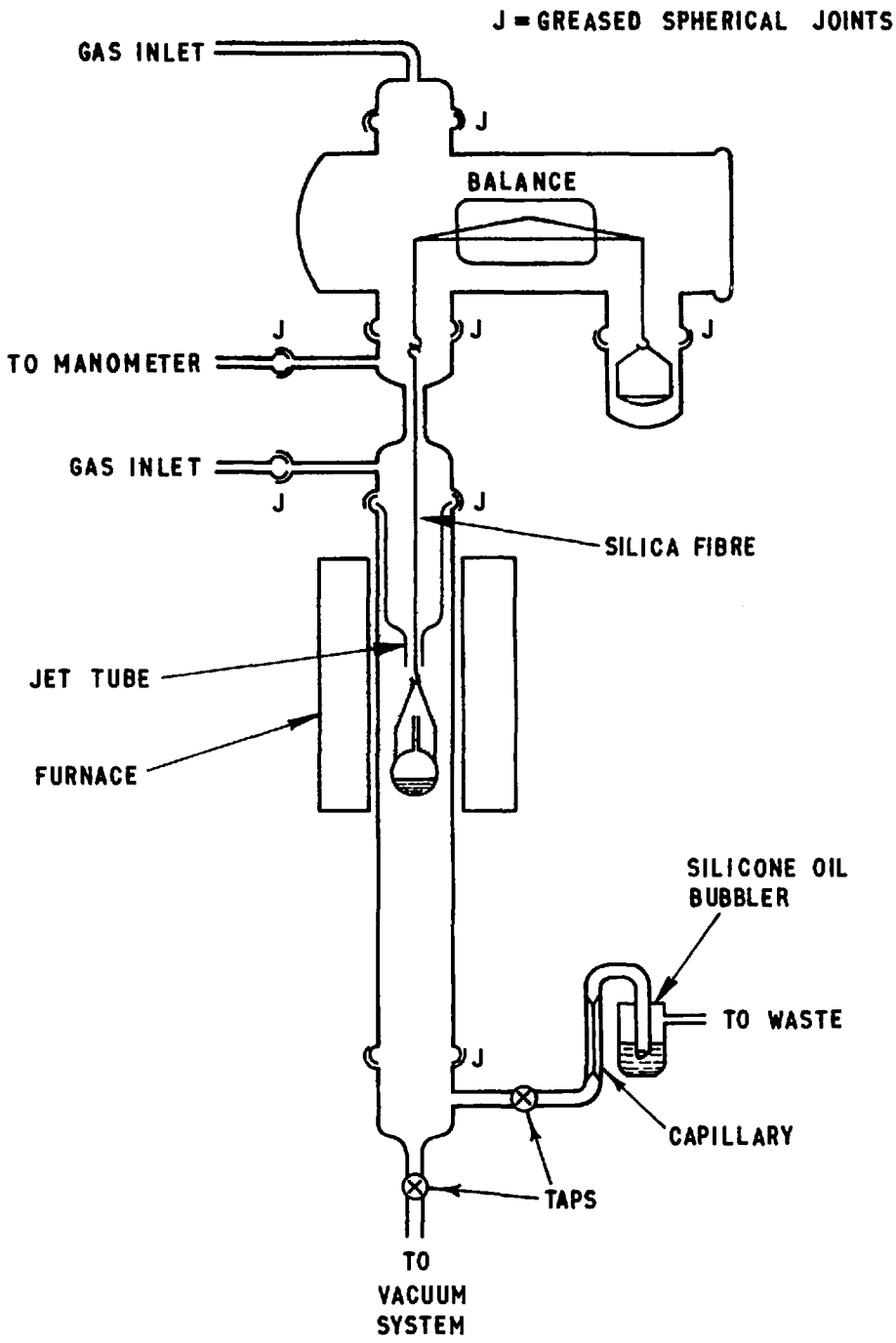

FIG. 4.2. EXPERIMENTAL SYSTEM FOR THE MODIFIED ENTRAINMENT METHOD.

Secondly, preliminary experiments to determine the flow pattern in the furnace tube, using the reaction between ammonia and hydrogen chloride at the top of the tube to form a smoke, indicated that the flow pattern near the exit of the bottle was variable. A jet tube was introduced to direct the flow and increase the linear velocity of the gas and produce a steady flow round the sample bottle. Finally, at the exit of the furnace tube a small capillary was situated, this served two purposes: one was to smooth out pressure fluctuations caused by the oil bubbler and the second was to raise the gas pressure in the system to approximately 20 mm of mercury above atmospheric pressure, this was to prevent any ingress of gas e.g. oxygen from the atmosphere into the system[119].

In operating the system, the apparatus was always evacuated and filled with gas at least three times to ensure that no air was left in the apparatus (particularly important when hydrogen was being used). Also it was confirmed that the rate of weight loss from the bottle was independent of the gas flowrate (see Paper I). For each system studied, the rate of weight loss was studied as a function of temperature.

4.2.2 Water and Lead Vaporisation

For the water evaporation experiment dry nitrogen was used for the inert gas flow and the sample used was double quartz distilled water. The weight loss rate was studied in the temperature range 9°-50°C.

In the case of lead, the carrier gas used was hydrogen (purified using a palladium-alloy diffuser) and the sample was introduced into the bottle as granules (Analar grade; Hopkin & Williams Ltd), the temperature range studied being 890°-1030°C.

4.2.3 Gallium-water system

In the gallium water system, the water content of the gas stream was fixed by passing hydrogen through a bubbler containing water at a controlled temperature. Two experiments were performed, one with hydrogen entering the balance chamber and diluting the reactive gas stream and the other with nitrogen diluting the gas. The gas flows were smoothed out using stagnation chambers and capillaries (See figure 4.3). The gallium was introduced into the bottle as a liquid and was supplied by Mining & Chemical Products Ltd (99.9999% Purity). The temperature range of operation was limited at the upper end by the furnace heating elements and the softening temperature of silica. At a given temperature

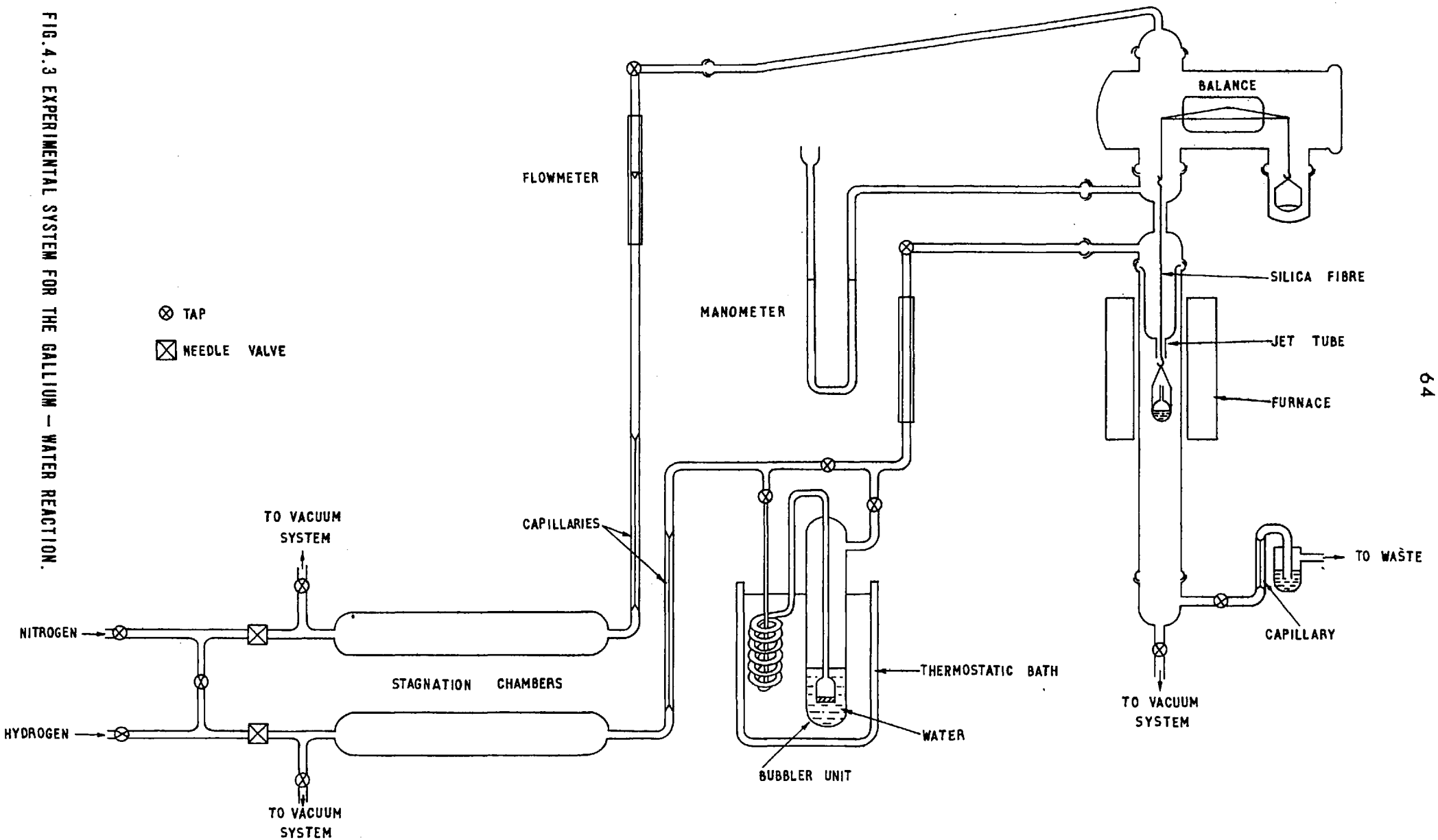

FIG. 4.3 EXPERIMENTAL SYSTEM FOR THE GALLIUM – WATER REACTION.

there is a water vapour/hydrogen ratio at which gallium sesquioxide becomes stable; to prevent the formation of the sesquioxide the water content must be kept as low as possible, this in turn reduces the rate of weight loss and therefore a lower limit is set by the sensitivity of the balance. There is therefore a "window" of operation, the limits of which are given in Paper II. Because of the ease of formation of the sesquioxide on the gallium surface, the sample was always heated to 1030°C first, where the oxide was removed by reduction with gallium.

4.2.4 Gallium-hydrogen chloride and gallium arsenide-hydrogen chloride systems

The experimental gas inlet system used for both of these reactions was very similar to that used for the gallium-water reaction, the only difference being that the bubbler was isolated from the system and an additional gas flow line used to introduce hydrogen chloride into the reactive gas stream. The hydrogen chloride (Electronic grade, 99.99%, Air Products) flow was controlled using two stainless steel needle valves in series for the gallium arsenide experiments and with an automatic flow controller (Drovewood Ltd) for the gallium experiments. The flow rate of hydrogen chloride was measured with a Meterate flowmeter which had been calibrated by determining the HCl content of the HCl/H_2 gas mixture by titration with sodium hydroxide. The gallium arsenide was nominally undoped material supplied by Mining and Chemical Products Ltd and it was introduced into the sample bottle as small chips. The temperature range studied in both systems was 450°-1050°C.

4.3 Theory of Weight Loss

The rate at which material was removed from the sample bottle was dependant upon several factors: the partial pressures of the gaseous species at both ends of the channel and the flow resistance of that channel. It was assumed that the vapour in the bottle was of uniform composition, i.e. all partial pressure variations were confined to the channel. This assumption is reasonable if the diameter of the bulb is large compared with the diameter of the channel (between 50:1 and 100:1 in the system used). It was also assumed that the vapour in the bottle is in equilibrium with the condensed phase; this could be checked by altering the size of channel to see whether the difference in rate of weight loss was consistent with the change in flow resistance of the channel. If the resistance

of the channel was progressively decreased then reaction at the sample/gas interface could ultimately be made to limit the rate of weight loss. This situation is somewhat similar to the Knudsen effusion experiment performed with progressively larger orifices until Langmuir conditions are approached[88]. The final assumption was, that at the exit of the channel, the gas composition was the same as the external gas stream, the vapour from the bottle being rapidly diluted and swept away, i.e. at zero partial pressure at the exit. This assumption was considered in detail (Paper I) and found to be reasonable under the conditions used.

The gas flow in the channel of the sample bottle can be described using the transport equations given in chapter 3. The one-dimensional model was applied as shown in figure 4.1. It can be shown (Paper I) that for the evaporation of a single species (A) in an inert gas, that

$$P_A^{\,o} = P_T[1 - \exp(-\xi)] \tag{4.1}$$

Where ξ is the 'transport function' and is defined as

$$\xi = \frac{J_A RTl}{DP_T} = \frac{\dot{W}RTl}{DP_T M_A C} \tag{4.2}$$

where $\dot{W}$ is the measured weight loss rate from the bottle, M_A is the molecular weight of species A and C is the cross-sectional area of the channel. Since experiments are usually carried out over a wide range of temperature, it is necessary to include the temperature dependance of the diffusion coefficient (D)

$$D = \frac{D_o}{P_T}\left(\frac{T}{T_o}\right)^{1+s} \tag{4.3}$$

where D_o is the value of D at a temperature D_o and 1 atm. pressure and s is a numerical coefficient, the value of which is discussed in Paper I. For small values of $\dot{W}$, equation (4.1) may be approximated to

$$P_A^{\,o} \simeq \frac{\dot{W}RP_T l T_o^{\,1+s}}{D_o T^s M_A C} \tag{4.4}$$

The partial pressure of A can be expressed in terms of the enthalpy and entropy changes on evaporation:

$$l n P_A^{o} = -\frac{\Delta H_v}{RT} + \frac{\Delta S_v}{R} \tag{4.5}$$

Thus from equations (4.4) and (4.5) a plot of $Rln\left(\frac{\dot{W}}{T^s}\right)$ versus $\frac{1}{T}$ has a slope of $-\Delta H_v$ and an intercept of $\Delta S_v - Rln\left(\frac{l R P_T T_o}{D_o M_A C}^{1+s}\right)$

Extension of the theory to heterogeneous reactions is dealt with in detail in Paper I. For a reaction of the type

$$M_{(s)} + HX_{(g)} \rightarrow MX_{(g)} + \frac{1}{2} H_2 \tag{4.6}$$

one obtains

$$P_{MX}^{(o)} = 2 P_T[1 - \exp(-\xi)] \tag{4.7}$$

$$P_{HX}^{(o)} = (P_{HX}^{(l)} + 2 P_T) \exp(-\xi) - 2 P_T \tag{4.8}$$

$$P_{H_2}^{o} = (P_{H_2}^{(l)} - P_T) \exp(-\xi) + P \tag{4.9}$$

where ξ in this case $= \frac{J_M RTl}{2 DP_T} = \frac{\dot{W} RTl}{2 DP_T M_M C}$ (4.10)

The equilibrium constant (K_p) for reaction (4.6) is given by

$$K_p = \frac{P_{MX}^{(o)} \left(P_{H_2}^{(o)}\right)^{\frac{1}{2}}}{P_{HX}^{(o)}} = \exp\left[-\frac{\Delta H_r}{RT} + \frac{\Delta S_r}{R}\right] \tag{4.11}$$

The equilibrium constant can be determined either by calculation of the individual partial pressures $P_{HX}^{(o)}$ etc. from equations (4.7)-(4.9) followed by substitution in equation (4.11) or alternatively by substituting equations (4.7-4.9) into (4.11) and deriving a relationship between K_p and $\dot{W}$. To do this a new term (ϵ) has to be defined where

$$\epsilon = \frac{P_{HX}^{(l)}}{P_T} \tag{4.12}$$

The following results obtain (full derivations in Paper I)

Case (1) $\xi \ll 1$; $\epsilon \sim 1$

$$K_p \simeq \frac{2 P_T \xi \left(P_{H_2}^{(l)} \right)^{\frac{1}{2}}}{P_{HX}^{(l)}} \tag{4.13}$$

Case (2) $\epsilon \ll 1$; $\xi \simeq \epsilon$

$$K_p \simeq \frac{2 \xi P_T^{\frac{1}{2}}}{\epsilon - 2\xi} \tag{4.14}$$

Case (3) $\xi \ll \epsilon \ll 1$

$$K_p \simeq \frac{2 \xi P^{\frac{1}{2}}}{\epsilon} \tag{4.15}$$

In all the preceding theory, an average diffusion coefficient was assumed. The question of multicomponent diffusion is considered in Papers I and III and is not considered here. The theoretical basis of the modified entrainment method as presented was applied to several experimental systems and the results are given in the subsequent sections.

4.4 Results and Discussion

Discussion of the experimental results obtained is brief in this section, since full discussion is given in the appended Papers I-IV.

4.4.1 Water and Lead

The measured weight loss rates for water and lead are given in Tables 4.1 and 4.2 while figures 4.4 and 4.5 show plots of the experimental values obtained for $R\ell nP$ versus $\frac{1}{T}$. The excellent agreement with literature values is shown in Table 4.3 and it confirms the modified entrainment method as being suitable for determining vapour pressures.

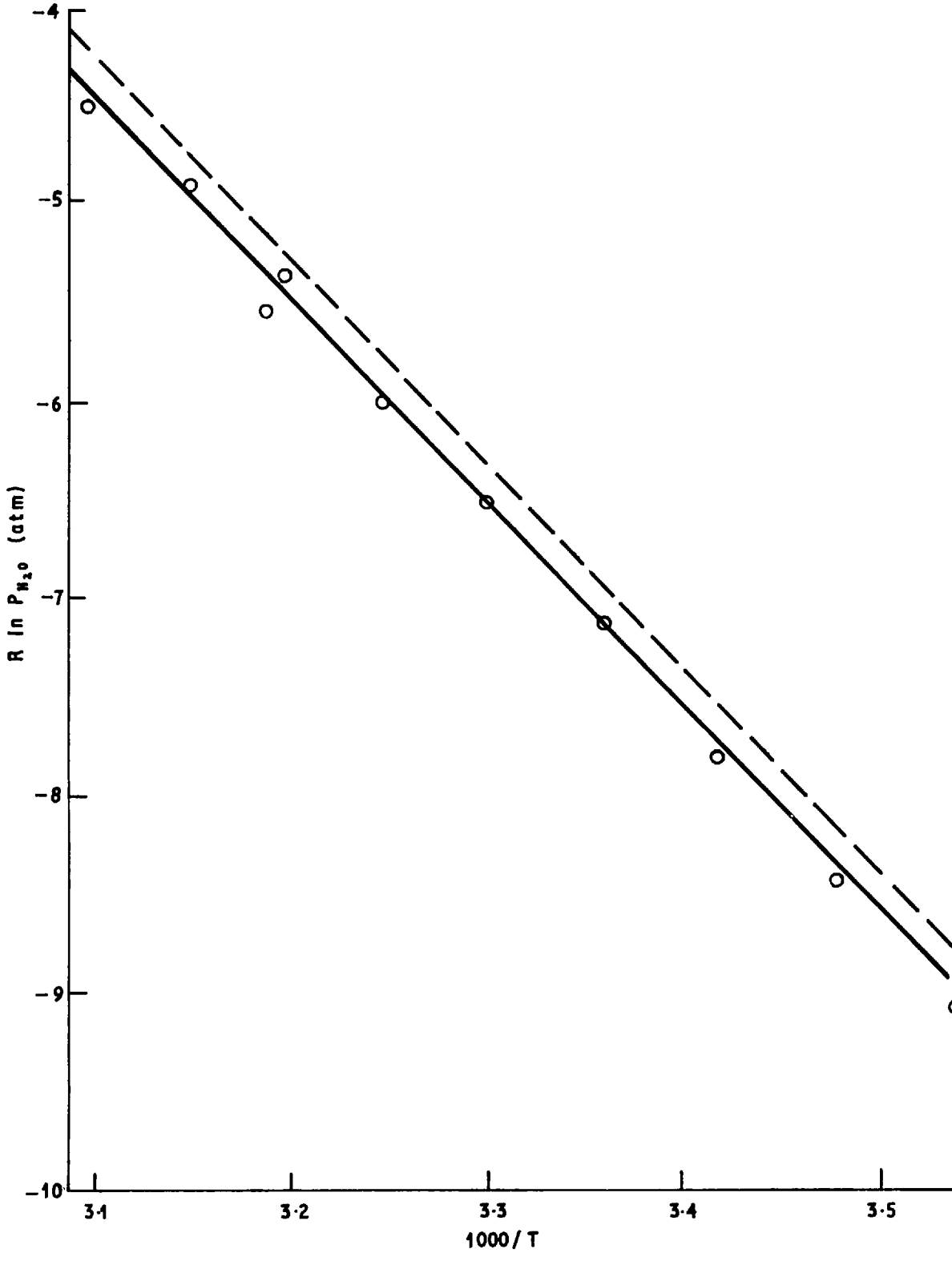

FIG. 4.4. EVAPORATION OF WATER IN NITROGEN.

— — — — — REF.120

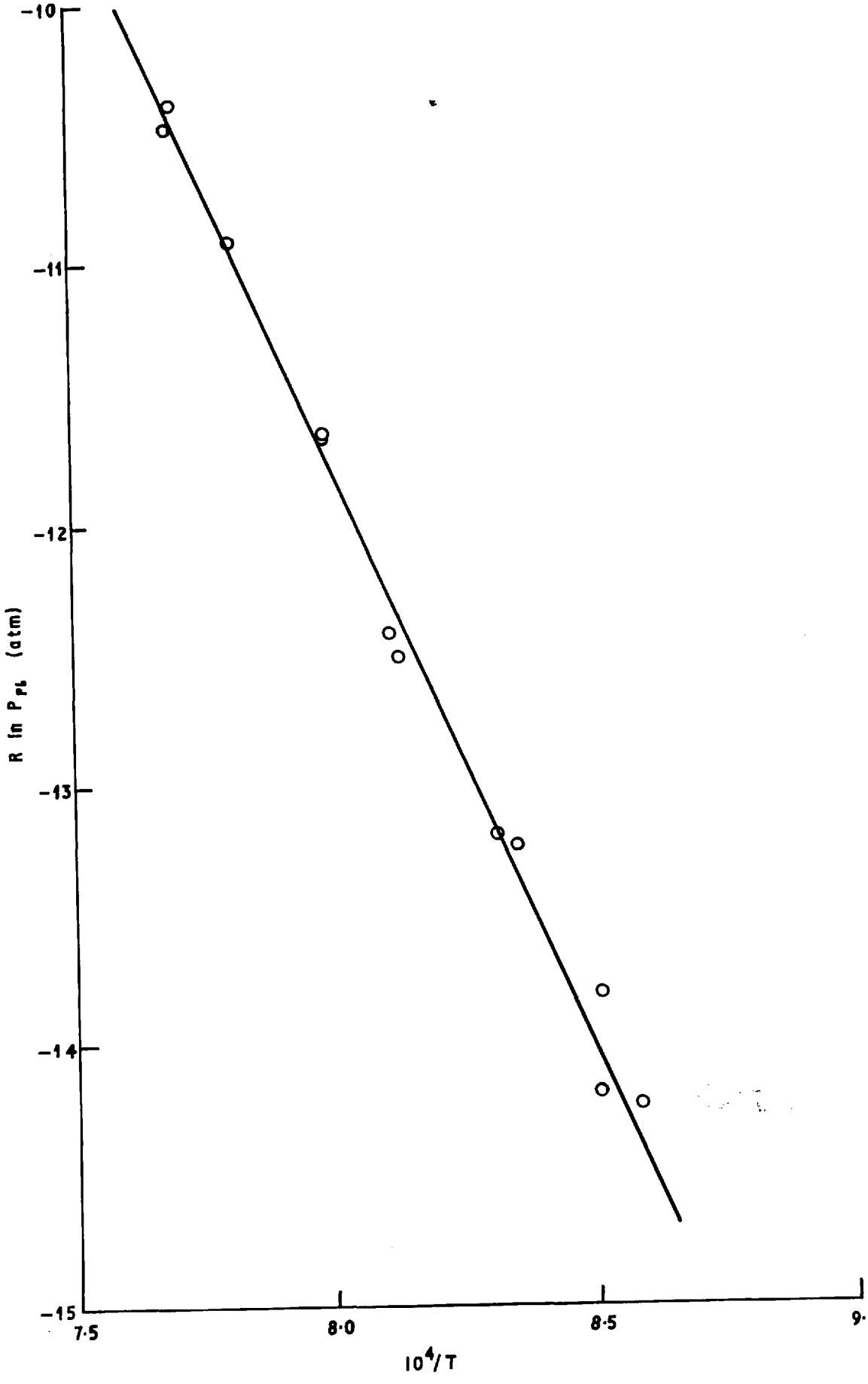

FIG. 4.5 EVAPORATION OF LEAD IN HYDROGEN

Table 4.1

Calibration Experiment:	Water evaporation in nitrogen:
T (° C)	$\dot{W}$ (mg hr^{-1})
9.5	0.0936
14.55	0.135
19.5	0.19
19.5	0.2092
24.6	0.2747
29.9	0.39
34.75	0.5175
39.7	0.74
40.5	0.675
44.5	0.9555
49.7	1.219

Table 4.2

Calibration Experiment:	Lead in hydrogen:
T (° C)	$\dot{W}$ (mg hr^{-1})
892	0.208
902	0.259
902	0.217
925	0.354
930	0.358
958	0.526
961	0.548
979	0.794
979	0.804
1009	1.201
1028	1.510
1028	1.582

Table 4.3

	ΔH°_{298} (kJ mol^{-1})		ΔS°_{298} (J mol^{-1} K^{-1})		
	Present Work	Literature	Present Work	Literature	Ref.
Water	43.6	44.10	116.7	118.70	120
Lead	46.0	46.8	114.0	110.4	121
		45.8			122

Furthermore the results give good support for the theoretical model used for transport in the gas phase.

4.4.2 Gallium-water system

The rates of loss of weight for the two experiments performed are given in table 4.4 along with the water concentrations used in each. Full discussion of the results is found in Paper II.

Table 4.4

Experiment (a) $\frac{P_{H_2O}}{P_{H_2}} = 0.00325$		Experiment (b) $\frac{P_{H_2O}}{P_{H_2}+P_{N_2}} = 0.00163$		$\frac{P_{H_2}}{P_{H_2O}+P_{H_2}+P_{N_2}} = 0.223$
T (° K)	$\dot{W}$ (mg hr^{-1})	T (° K)	$\dot{W}$ (mg hr^{-1})	
1186	0.299	1217	0.157	
1215	0.400	1262	0.181	
1243	0.464	1292	0.220	
1268	0.532	1324	0.281	
1291	0.584			
1291	0.636			
1303	0.646			

It was found that the results could be fitted to straight lines by the linear least squares method to giving the equations

$$ln\dot{W}_a = -\frac{9793.7}{T} + 7.094 \qquad (4.16)$$

(Index of determination -0.991)

and

$$ln\dot{W}_b = -\frac{8680.7}{T} + 5.236 \qquad (4.17)$$

(Index of determination -0.970)

Previous workers[76-78] have assumed that the volatile gallium species in the system is the sub-oxide:

$$2\ Ga_{(l)} + H_2O_{(g)} \rightarrow Ga_2O_{(g)} + H_{2(g)} \qquad (4.18)$$

However the results calculated from the present experimental data assuming this reaction, were at variance with the literature values[75,123]. A second reaction was found to be involved in the system:

$$Ga_{(l)} + H_2O_{(g)} \rightarrow GaOH_{(g)} + \frac{1}{2} H_{2(g)} \qquad (4.19)$$

Evidence for this was found in a variation of the values of the equilibrium constants calculated from the two experiments also the variation was found to depend on temperature (See Table III in Paper II). The composition of the vapour in a capsule containing gallium and wet hydrogen at 1000°C was investigated using a mass spectrometer (VG Micromass 12). Peaks were observed at mass numbers 154, 156, 158 (corresponding to $^{69}Ga_2{}^{16}O$, $^{69}Ga^{71}Ga^{16}O$, $^{71}Ga_2{}^{16}O$) and 86 and 88 (corresponding to $^{69}Ga^{16}O^{1}H$ and $^{71}Ga^{16}O^{1}H$). Unambiguous identification of the peaks was not possible, since the peak heights were only a few times the background height, but the results support the suggestion that reactions (4.19) occurs. Finally estimated entropy and enthalpy changes for the reaction (4.19) indicated that the partial pressures of GaOH and Ga_2O were comparable in the temperature range investigated.

The experimental results were treated first assuming that either reaction dominated, then considering two simultaneous reactions and finally a third law calculation of the results was made. The results are given in Table 4.5 full details being in Paper II.

Table 4.5

Method	Reaction (4.18)		Reaction (4.19)		Ga_2O		GaOH	
	ΔH°_{298}	ΔS°_{298}	ΔH°_{298}	ΔS°_{298}	$\Delta H^\circ_{f\,298}$	S°_{298}	$\Delta H^\circ_{f\,298}$	S°_{298}
Dominant Reaction 2nd Law	120	126	117	109	-121	266	-125	273
Simultaneous Reactions	161 ↓	160 ↓	59 ↓	56 ↓	-80 ↓	300 ↓	-183 ↓	221 ↓
2nd Law	172	165	79	74	-70	305	-163	239
Third Law	151	147	94	84	-90.8 ±8	287 ±6	-148 ±17	248 ±12
Estimated			117 ±20				-125 ±20	
Literature	159				-84			

The range of values for the 2nd law calculations involving simultaneous reactions arise from considerations of the simultaneous linearity of ℓnK versus $\frac{1}{T}$ for each reaction. The equilibrium constants are sensitive to experimental errors and the scatter in results in experiment (b) [See equation (4.17)] is particularly important. However ℓnK must be linear in $\frac{1}{T}$ for both reactions and this imposes a range of uncertainties in the experimental data, e.g. an uncertainty in the slope of $\dot{W}_a(T)$ and $\dot{W}_b(T)$ greater than 10% would lead to a non linear dependence of one equilibrium constant with temperature. The results obtained directly from the experimental data are shown in figure 4.6 and the ranges of results in Table 4.5.

It is clear from the results obtained for the gallium-water system, that great care must be exercised in interpreting measured weight loss rates which appear to give a straight line plot in the temperature range measured. If it had been possible to have taken measurements over a much larger temperature range, then at lower temperatures reaction (4.19) would have dominated and at higher temperatures reaction (4.18) would have dominated and a change of slope might have been perceptible in a plot of $R\ell n\dot{W}$ versus $\frac{1}{T}$. (See results for gallium arsenide - hydrogen chloride system).

4.4.3 Gallium-hydrogen chloride system

Existing data[107, 108, 124, 125] for the reaction of gallium with hydrogen chloride to form gallium monochloride:

$$Ga_{(l)} + HCl_{(g)} \rightarrow GaCl_{(g)} + \frac{1}{2} H_{2(g)} \qquad (4.20)$$

indicate that in the temperature range 700-1300°K the enthalpy ($\Delta H°$) and entropy ($\Delta S°$) changes are +12 (±8) kJ and +65.6 (±4) $J\,K^{-1}$ respectively, thus the equilibrium constant is large and the partial pressure of hydrogen chloride over gallium is almost zero. The possibility of other chlorides of gallium being present in significant amounts has been considered, but under the experimental conditions pertaining in the system, their partial pressures are negligibly small[89] (See also Paper IV). Reaction (4.20) is therefore suitable for studying gaseous interdiffusion since the reaction acts as a sink for the reactant.

The weight loss rates for different concentrations (ϵ) of hydrogen chloride in hydrogen are given in Table 4.6.

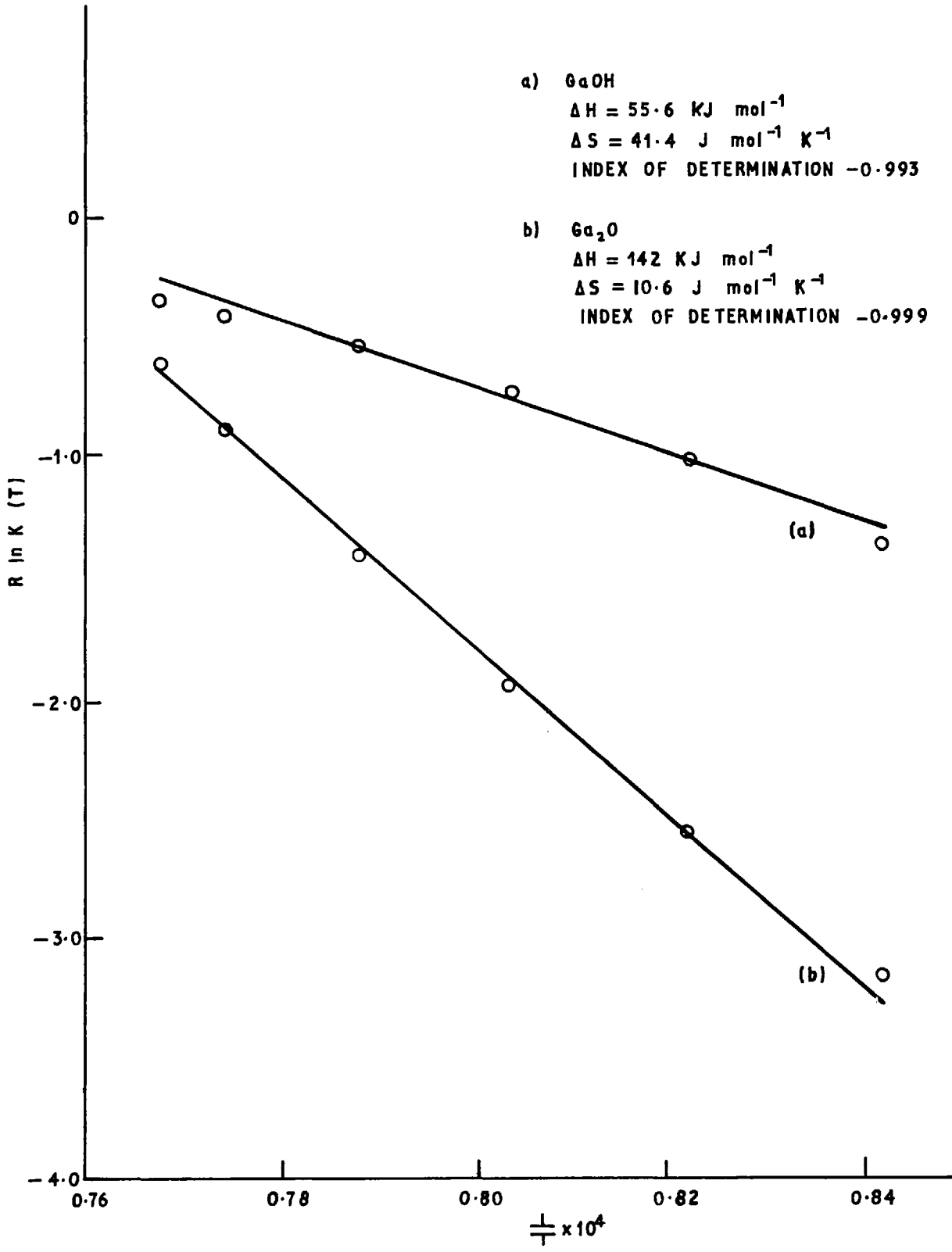

FIG. 4.6 VARIATION OF EQUILIBRIUM CONSTANT WITH TEMPERATURE FOR THE GALLIUM – WATER SYSTEM.

Table 4.6

ϵ = 0.018		ϵ = 0.060		ϵ = 0.100	
T (°K)	$\dot{W}$ (mg hr^{-1})	T (°K)	$\dot{W}$ (mg hr^{-1})	T (°K)	$\dot{W}$ (mg hr^{-1})
1290	1.638	1271	3.570	1248	4.976
1290	1.542	1271	3.449	1248	4.997
1290	1.542	1271	3.592	1019	4.450
1239	1.357	1225	3.271	1019	4.406
1239	1.287	1225	3.438	832	3.644
1239	1.386	1225	3.367	832	3.676
1184	1.350	1183	3.445	832	3.704
1184	1.269	1183	3.281	779	3.463
1184	1.255	1183	3.319	779	3.526
1136	1.366	1129	3.206	779	3.512
1135	1.341	1129	3.151	786	3.512
1135	1.233	1129	3.104	1274	5.268
1082	1.170			1274	5.250
1082	1.136			891	3.836
1082	1.140			891	3.814
1036	1.061			891	3.884
1036	1.031				
1035	1.184				
1035	1.241				
1035	1.151				
984	1.100				
984	1.072				
984	1.084				
935	1.008				
935	0.989				
888	0.937				
888	0.936				

From equation (7), Paper III,

$$\epsilon = 2\,\xi_{HCl}\left(1 + \frac{D_{HCl,m}}{D_{GaCl,m}} \cdot \frac{1}{K_p}\right) \tag{4.21}$$

where

$$\xi_{HCl} = \frac{\dot{W}RTl}{2\,D_{HCl,m}PMA} \tag{4.22}$$

$D_{i,m}$ is the diffusion coefficient of species i in the multicomponent gas mixture and K_p is the equilibrium constant for reaction (4.20). Other symbols are as used in section 4.3.

If K_p is large, $\frac{D_{HCl,m}}{D_{GaCl,m}} \cdot \frac{1}{K_p}$ may be neglected in comparison with unity and thus the diffusion constant for HCl in the gas mixture is given by

$$D_{HCl,m} = \frac{\dot{W}RTl}{PM\epsilon A} \tag{4.23}$$

Using equation (4.23) the diffusion coefficient was calculated for each experimental point. The results, plotted in figure (4.7), show a temperature dependence as expected from equation (4.3) and although s is the same for each value of ϵ, the value of D° increases as ϵ decreases. In Paper III it is shown that the difference in D° arises from the assumption that the minority components, GaCl and HCl can be treated as two independent binary systems (GaCl in H_2 and HCl in H_2). By applying a second-order approximation to multicomponent diffusion the value of D°_{HCl,H_2} was found to be 0.54 ± 0.07 $cm^2\ s^{-1}$ and s = 0.853 ± 0.022. (Figure 4.8).

4.4.4 Gallium arsenide - hydrogen chloride system

The results of two experiments having different values of ϵ are plotted in figure (4.9) and listed in Table 4.7. Each curve may be divided into three regions: two straight sections of different slopes, I and II and a curved region at high temperatures (III). Region III arises from K_p for the dominant reaction, becoming large at high temperature, as K_p becomes large $\dot{W}$ varies less rapidly with temperature:-

$$\dot{W} = \frac{MPAD}{RTl}\left(\frac{K_p\epsilon}{1 + K_p}\right) \tag{4.24}$$

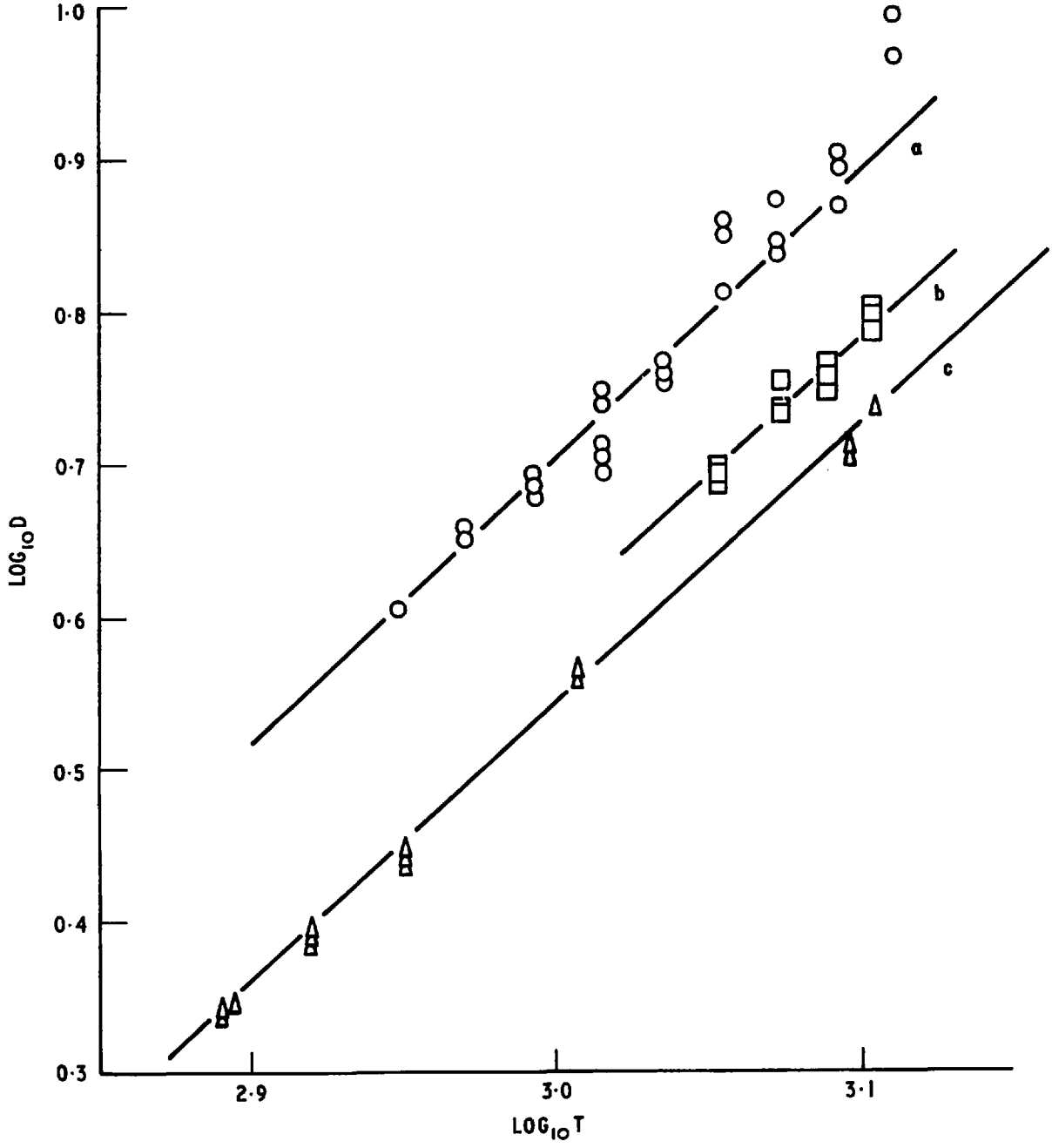

FIG. 4.7. VARIATION OF $D_{HC\ell,H_2}$ WITH TEMPERATURE

a, ϵ = 0.018
b, ϵ = 0.06
c, ϵ = 0.10

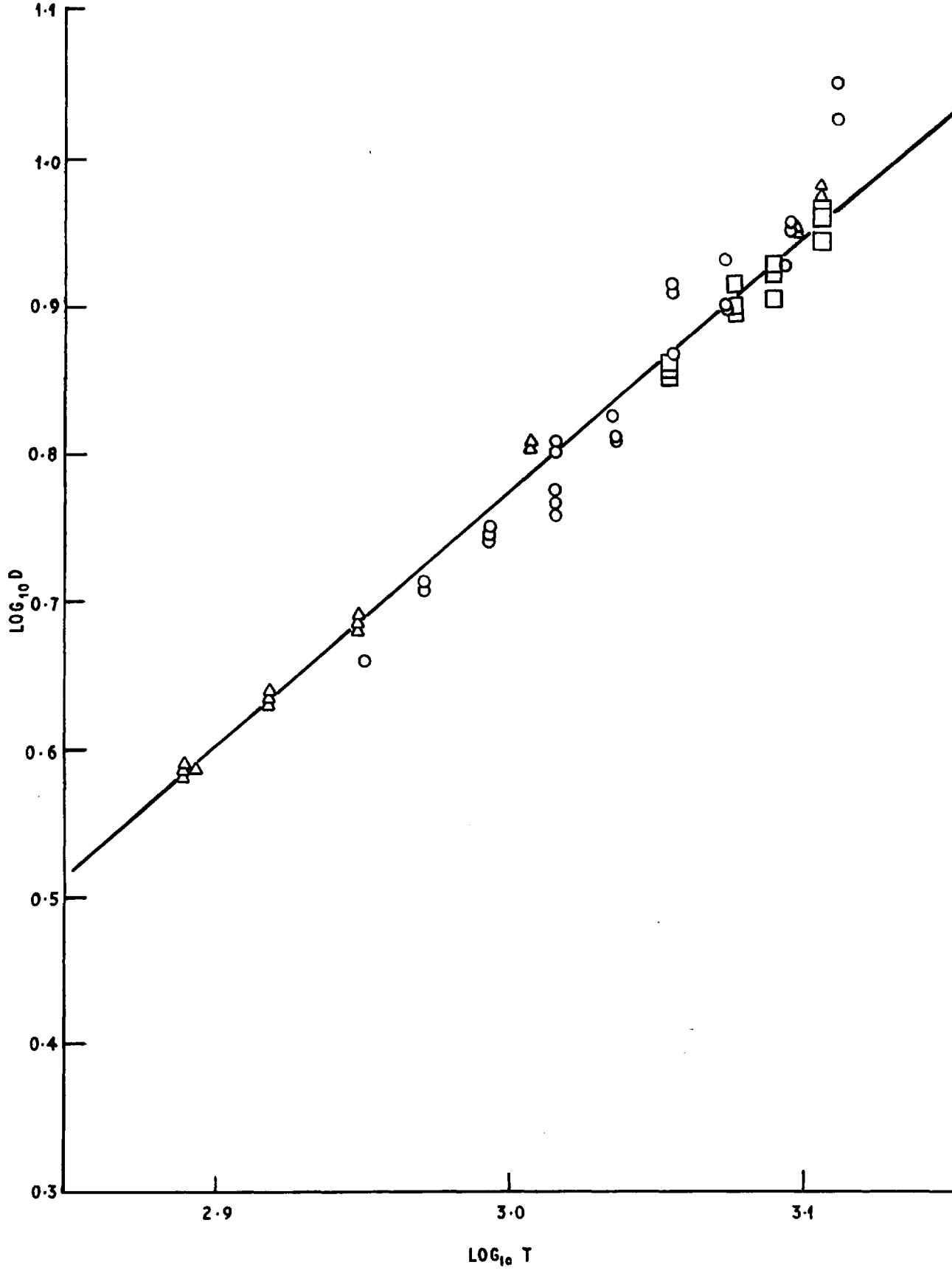

FIG. 4.8. VARIATION OF $D_{HC\ell, H_2}$ WITH TEMPERATURE (SECOND ORDER APPROXIMATION)

○, ϵ = 0.018 □ , ϵ = 0.06 Δ , ϵ = 0.10

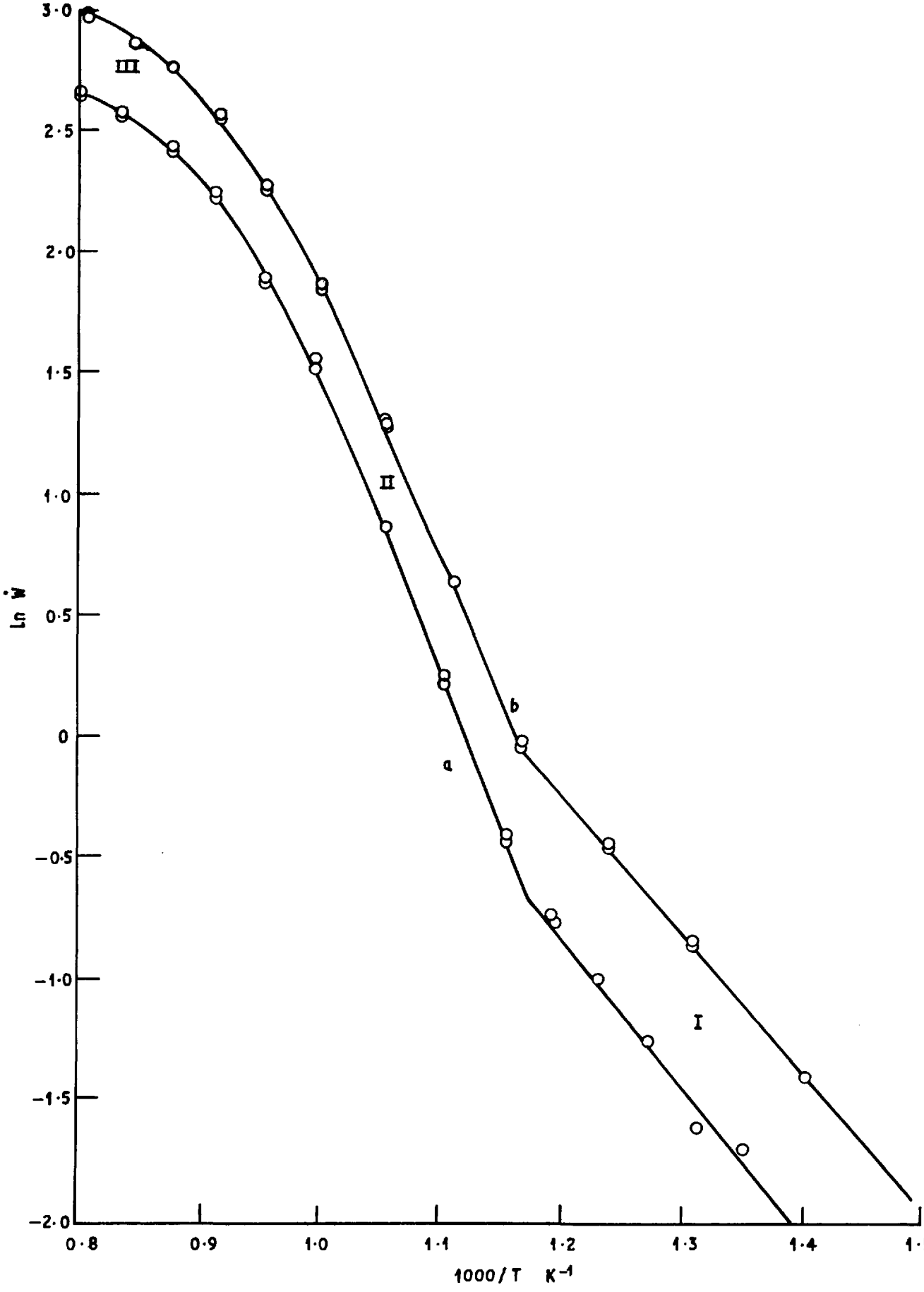

FIG. 4.9. EXPERIMENTAL RESULTS FOR GaAs – HCℓ SYSTEM

a, $\epsilon = 0.051$ b, $\epsilon = 0.083$

Table 4.7

ϵ = 0.083				ϵ = 0.051			
T K	$\dot{W}$ mg h^{-1}	T K	$\dot{W}$ mg h^{-1}	T K	$\dot{W}$ mg h^{-1}	T K	$\dot{W}$ mg h^{-1}
713	0.248	1003	6.295	742	0.183	1200	13.125
763	0.419	1003	6.343	764	0.246	1200	13.170
763	0.430	1003	6.312	788	0.288	1249	14.205
808	0.628	1048	9.696	813	0.369	1249	13.935
808	0.646	1048	9.552	836	0.471	1151	11.244
859	1.049	1048	9.492	840	0.477	1151	11.364
859	0.992	1096	13.080	908	1.220	865	0.651
904	1.916	1096	12.915	908	1.299	865	0.663
904	1.922	1147	15.76	1008	4.507	1054	6.480
904	1.916	1147	15.72	1008	4.555	1054	6.544
950	3.588	1193	18.07	1103	9.180	952	2.408
950	3.708	1193	18.07	1103	9.430	952	2.400
		1244	19.78				
950	3.633	1244	19.46	1200	13.065		

It is generally agreed that the dominant reaction in chemical vapour transport systems, using hydrogen chloride to transport gallium arsenide, is

$$GaAs_{(s)} + HCl_{(g)} \rightarrow GaCl_{(g)} + \frac{1}{4} As_{4(g)} + \frac{1}{2} H_{2(g)} \qquad (4.25)$$

However recent investigations[109,110] of the dissociation of tetrameric arsenic:

$$As_{4(g)} \rightarrow 2\ As_{2(g)} \qquad (4.26)$$

indicate that significant amounts of As_2 are present in such CVT systems at 1000°K. It is shown in Paper IV that region I and II involve different gallium chloride species and $GaCl_2$[126,127] or $Ga(GaCl_4)$[128,129] were considered the most likely for region (I).

$$GaAs_{(s)} + 2\ HCl_{(g)} \rightarrow GaCl_{2(g)} + \frac{1}{4} As_{4(g)} + H_{2(g)} \qquad (4.27)$$

$$GaAs_{(s)} + 2\ HCl_{(g)} \rightarrow \frac{1}{2} Ga(GaCl_4)_{(g)} + \frac{1}{4} As_{4(g)} + H_{2(g)} \qquad (4.28)$$

In solving the equations for three simultaneous reactions scheme 1:- (4.25), (4.26) and (4.27) or scheme 2:- (4.25), (4.26) and (4.28), one arrives at an equation involving four unknowns: the enthalpy and entropy changes for reactions (4.25) and (4.27) or (4.25) and (4.28). Values were then determined which gave the best fit to the experimental data.

The results obtained are shown in figures 4.10 and 4.11. The values used for ΔH and ΔS in each case are given in Table 4.8.

Table 4.8

Scheme 1		Scheme 2	
$\Delta H_{(4.25)}$	157 ± 3 kJ	$\Delta H_{(4.25)}$	159 ± 5 kJ
$\Delta S_{(4.25)}$	134.5 ± 1.5 J K^{-1}	$\Delta S_{(4.25)}$	141 ± 4 J K^{-1}
$\Delta H_{(4.27)}$	44 ± 3 kJ	$\Delta H_{(4.28)}$	67 ± 5 kJ
$\Delta S_{(4.27)}$	35.3 ± 1.5 J K^{-1}	$\Delta H_{(4.28)}$	91 ± 4 J K^{-1}

Clearly the results give a better fit for reaction (4.27) involving the dichloride and it seems likely therefore that reaction (4.27) is the reaction which occurs at low temperature. Full discussion is given in Paper IV. Heats of formation and entropies for GaCl, $GaCl_2$ and $Ga(GaCl_4)$ calculated from the results obtained here are given in Table 4.9 with literature values for comparison.

Table 4.9

Enthalpies of Formation and Entropies of Gallium Chlorides

SCHEME 1

GaCl		$GaCl_2$		References
ΔHf°_{298} kJ mol^{-1}	S°_{298} J mol^{-1} K^{-1}	ΔHf°_{298} kJ mol^{-1}	S°_{298} J mol^{-1} K^{-1}	
-63.2 ± 3	247 ± 2	-267 ± 3	265 ± 2	This work, 2nd law
-67.6	236			Fergusson and Gabor[130]
-84 ± 20	240	-260 ± 25	302	Shaulov and Mosin[126]
-80	240			Hurle and Mullin[25,131]
		-270 ± 10		Combination of (127) and (129)
			279,290 ± 10	Estimates (see Paper IV)

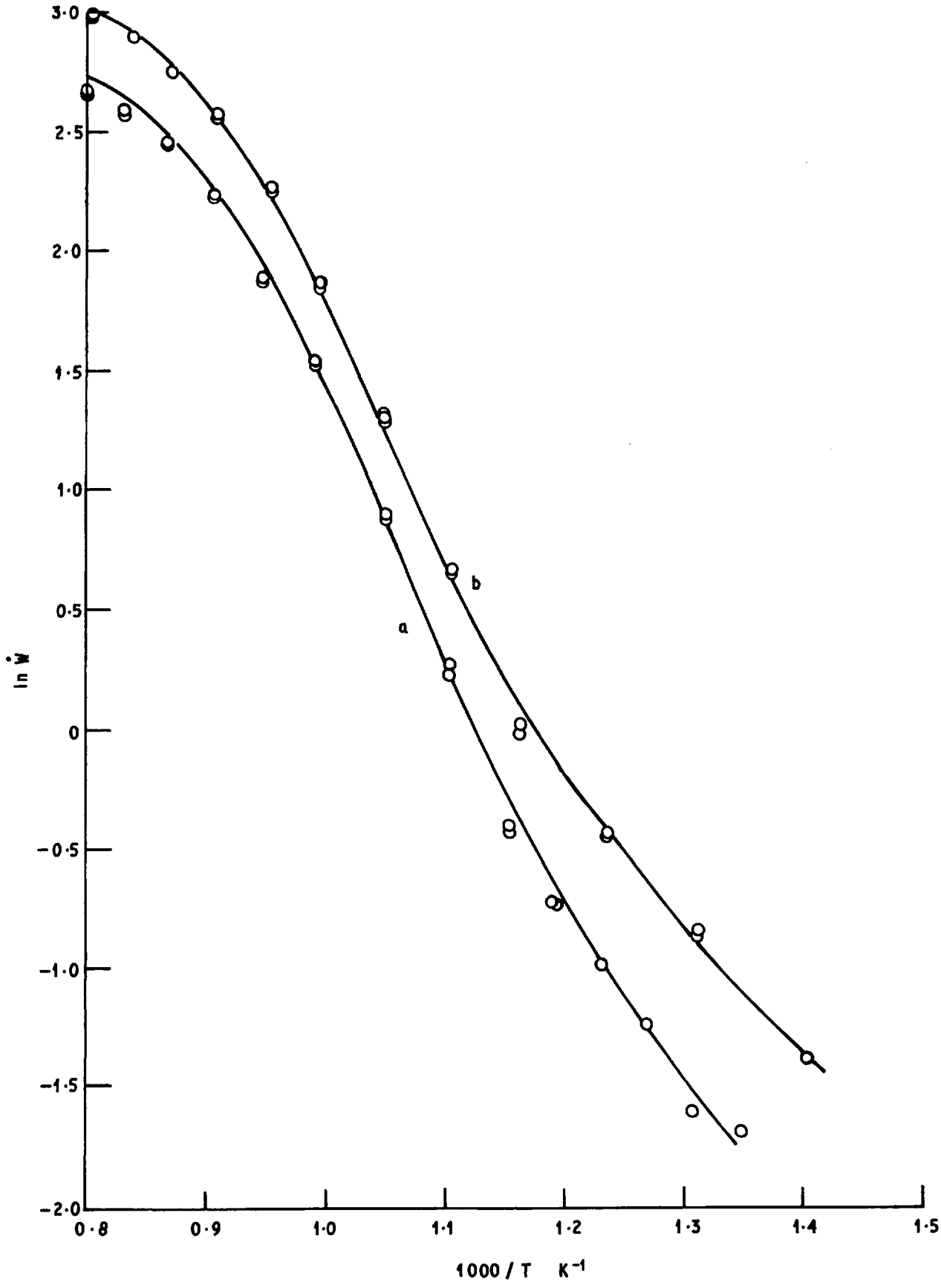

FIG. 4.10. THEORETICAL CURVE FOR GaAs – HCℓ SYSTEM. SCHEME I

a, $\epsilon = 0.051$ b, $\epsilon = 0.083$

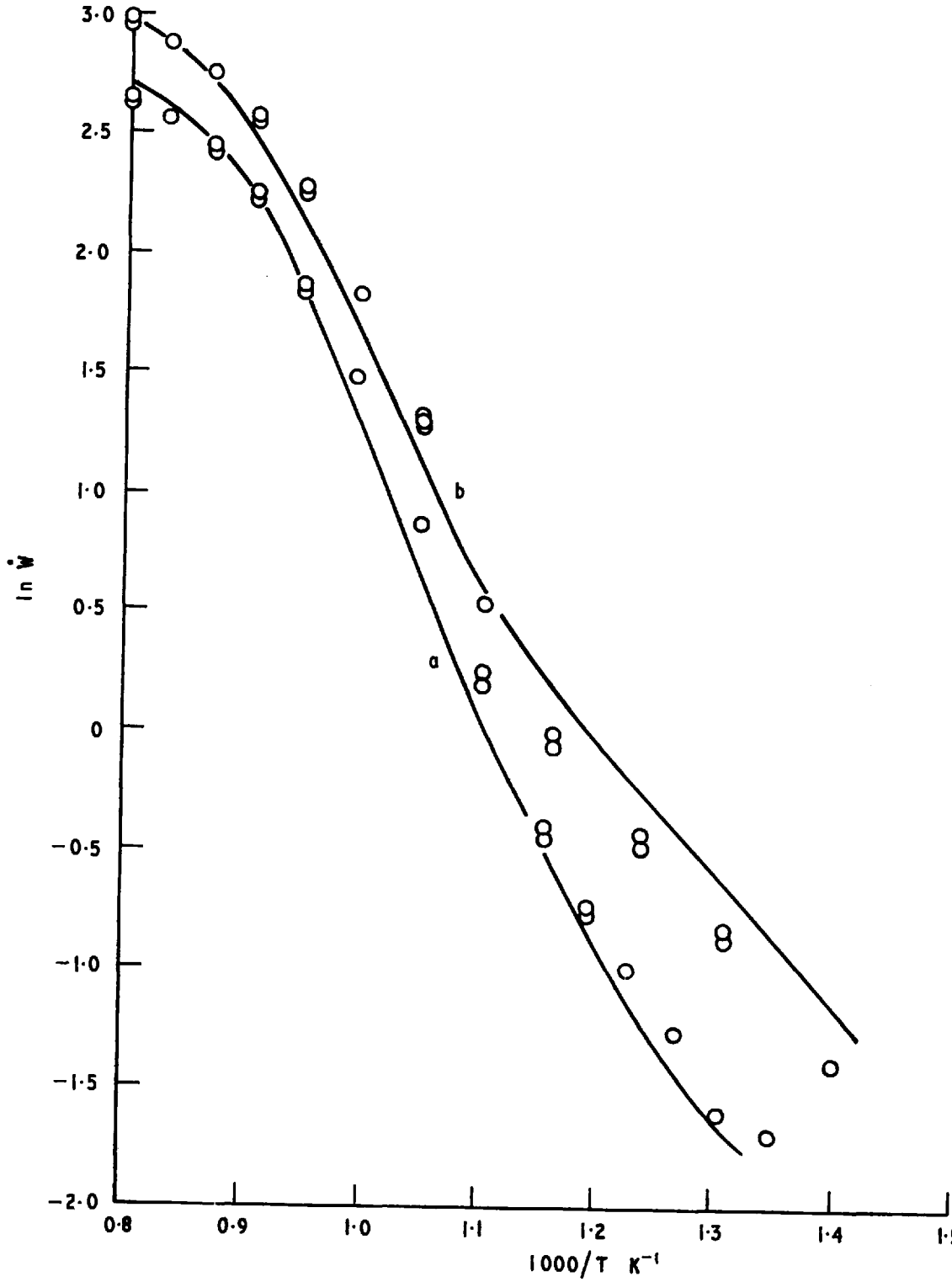

FIG. 4.11. THEORETICAL CURVE FOR GaAs – HCℓ SYSTEM SCHEME 2

a, $\epsilon = 0.051$ b, $\epsilon = 0.083$

Table 4.9 (cont'd)

SCHEME 2

GaCl		$Ga(GaCl_4)$	
ΔHf°_{298}	S°_{298}	ΔHf°_{950}	S°_{950}
kJ mol^{-1}	J mol^{-1} K^{-1}	kJ mol^{-1}	J mol^{-1} K^{-1}
-60 ± 5	250 ± 4	-117 ± 5	161 ± 4

The gallium arsenide - hydrogen chloride system highlights certain dangers in determining thermodynamic data. The two straight-line sections I and II in the experimental data cannot be used directly to calculate enthalpies from the slopes, since the slope is perturbed by another reaction. By using a limited temperature range for measurement the presence of reactions other than (4.25) would not have been revealed thus giving rise to incorrect thermodynamic values for the system, which are similar to the accepted literature ones.

One further point can be seen from this system: even without determining the thermodynamic parameters and undertaking a full analysis of the system, the experimental weight loss rates as plotted in figure 4.9, show immediately the region over which CVT using a temperature gradient can be performed. The optimum region being in section II where there is a significant change of weight loss rate with temperature.

4.5 Conclusion

The modified entrainment method described here has been successfully used to determine vapour pressures and to study reaction equilibria. The results have shown that the use of a narrow channel to confine diffusion effects such that their magnitude may be determined, eliminates many of the problems of the conventional entrainment methods. It has been possible to analyse two systems used for CVT of gallium arsenide (GaAs - H_2O and GaAs - HCl) and provide reliable thermodynamic data. The importance of such data in crystal growth has already been stressed. Finally it has been shown that the modified entrainment method is a tool which can be used to ascertain quickly and accurately the feasibility of different reactions for transporting material by CVT and the temperature range in which to operate, since the sample bottle is effectively half of a growth capsule - the seed being at T = 0°K. The possibility of studying reaction kinetics has already been mentioned.

CHAPTER 5

GALLIUM ARSENIDE VAPOUR PHASE CRYSTAL GROWTH - EXPERIMENTAL

CHAPTER 5

GALLIUM ARSENIDE VAPOUR PHASE CRYSTAL GROWTH - EXPERIMENTAL

5.1 Introduction

Two types of vapour phase crystal growth systems have been used in the Post Office Research Department for growing gallium arsenide: the conventional 'open-flow' method[60] and a new approach using a capsule with an effusion hole, which has been used for producing thin epitaxial layers and for transporting bulk quantities of gallium arsenide. The second method is the main subject of this chapter, although a brief description of the 'open flow' method used, is included for comparison.

There were several reasons for trying a new approach: firstly the immediate requirement was to produce uniform flat layers $\sim 1\mu$ thick with an abrupt change of doping level at the interface between the layer and the substrate. In the 'open flow' system growth rates were 15-60 $\mu\ hr^{-1}$, hence only a few minutes of growth was required for 1μ thickness and it was not easy to define the starting time for growth since initial transients occurred while steady state conditions between the source material and the gas stream and the substrate and the gas stream were set up. Furthermore when two layers of different doping level were required, the time taken to sweep out the gas at the initial dopant concentration was a significant fraction of the total growth time. The effect was that a gradual change in doping level occurred instead of an abrupt change at the interface. Although it was possible to try and arrange for the gas stream to be diverted from the substrate while the new conditions were set up, it seemed desirable to grow at a slower rate. In the capsule system growth rates down to $1\mu\ hr^{-1}$ were achieved and it is possible that this could be reduced further.

Secondly, a method of purifying bulk quantities of gallium arsenide was required and it will be shown that considerable purification was achieved by the capsule method.

Thirdly, the theoretical model for vapour transport presented in chapter 3 was developed before experimental work on gallium arsenide had commenced (at the P.O. Research Dept) and at the time, the theory could not be readily applied to the 'open flow' system. However, the capsule method was suitable for obtaining experimental support for the theory. More recently the theory of transport has been extended and applied to the open flow system by my colleagues at the P.O. Research Department[132].

Finally it was anticipated that the capsule method might be suitable for the growth of large single crystals at modest temperatures (600-850°C).

In the subsequent part of this chapter the experimental equipment is described and the operating procedures for the capsule system are given in detail. Since the capsule system was used for the growth of thin epitaxial layers and also for bulk crystal growth these two applications of the system are described separately for convenience, although the principles of the method are the same in each case.

5.2 Experimental Systems

5.2.1 General

In preparing single crystal epitaxial layers of gallium arsenide, one of the main considerations was the purity of the material and therefore the equipment was designed to keep contamination to a minimum. Impurities in the layers come from three sources:- the reagent materials used (gallium arsenide, gases etc.), the apparatus itself (gas inlet tubes, furnace tube, sample holder etc.) and from small leaks in the system, allowing air or other contaminants to enter. The treatment and handling of the materials used is discussed in section 5.3.4 but the other two sources are considered here.

The apparatus was made as far as possible from glass, the heated parts of the systems being manufactured from high purity silica and the remaining parts (the gas inlet and waste lines) from borosilicate glass. The high purity hydrogen inlet lines were made from stainless steel and the total gas flows were controlled by stainless steel needle valves, which were joined to the glassware using compression couplings with PTFE ferrules. Two types of valve were used in the glassware:- taps (marked T in the diagrams) were manufactured from borosilicate glass. They had two seals; the first, was made to atmosphere using a Teflon O-ring backed by a Viton O-ring, the second, which formed the shut-off in the line, was made by a single Teflon O-ring. These taps were used only where it was essential for a complete seal to be made when the tap was closed. The taps on the bubbler also provided access for filling with arsenic trichloride.

- magnetically operated valves of the type shown in figure 5.1 (marked MV on diagrams) were used wherever possible. The main feature of them was that there was no O-ring or greased seal to the atmosphere, the body of the valve being made entirely from borosilicate glass. The seal in the valve was made by a ground spherical ball joint seating in a

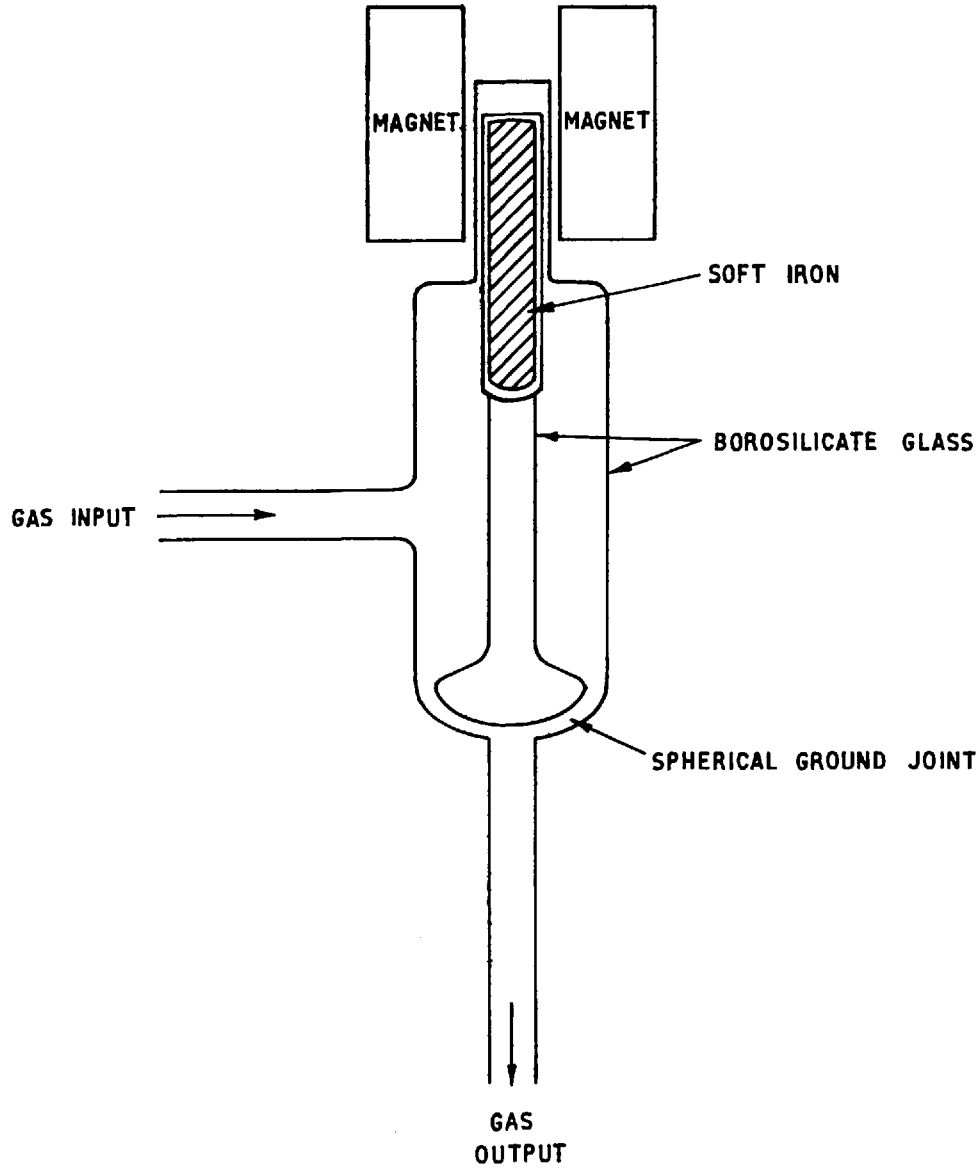

FIG. 5.1. MAGNETICALLY OPERATED GLASS VALVE.

matching socket and the plunger was raised and lowered by the magnet. These valves did not provide a complete seal when closed; there was a small leakage through the ground joint when a large pressure difference was imposed across it, however they provided a good barrier to diffusion.

The end of the furnace tube, used for loading the apparatus, was removable, the seals to atmosphere were made using Viton O-rings or PTFE gaskets. Greased joints were avoided, however it was necessary to use some grease on the rotating seal of the capsule system to ensure smooth operation and a good seal to atmosphere.

All the glassware was degreased using an aqueous solution of nitric acid, hydrofluoric acid and liquid detergent, rinsed thoroughly in water and then soaked in aqua regia for several hours. This was followed by several rinsings in distilled water and finally with double quartz distilled water and high purity isopropanol. On some occasions the glassware was washed with a solution of potassium cyanide to remove traces of heavy metals e.g. copper, iron etc. After cleaning, the whole apparatus was assembled (empty) and heated in hydrogen to $\sim 100^{\circ}$ above the proposed operating temperature, to dry the silica glassware.

Reducing contamination from oxygen or other impurities from the atmosphere was achieved in two ways: firstly joints and taps were kept to a minimum. Every joint or seal was considered a potential source of leaks and in the first systems made, which had many joints, this was found to be true and the quality of the epitaxial layers was poor. Graded glass seals were used to join the silica furnace tubes to the borosilicate glass and flowmeters which could be glass-blown into the apparatus were used in preference to those requiring a mechanical coupling. Furthermore, sealed, magnetically operated glass valves of the type described previously were used in preference to valves having an O-ring seal to atmosphere; only when it was essential to provide a complete shut-off in the gas line were the latter type used.

In addition to the above precautions the second and more significant method of reducing contamination from the atmosphere was to operate the system under positive pressure. A fine capillary tube on the outlet of the system was used to raise the pressure to 10-20 mm of mercury above atmospheric pressure. This was sufficient to keep contamination to less than 1 ppm of air[119]. This pressurisation of the system inevitably means that there is a risk of toxic gases escaping into the atmosphere, therefore the apparatus were kept in a ventilated cabinet, toxic fumes being ducted away.

5.2.2 Crystal Growth Furnaces

Preliminary investigations into the crystal growth of II-VI and III-V compounds by vapour phase techniques showed the need for specialised equipment which would enable one to control the processes occurring. The furnace equipment needed to be versatile to accommodate different systems for growth e.g. growth in vacuo, growth under inert gas at various pressures, facilities for rotation and pulling of the charge. In addition, accurate temperature control over a wide range of temperatures and the ability to produce specific thermal profiles, suited to the individual system, were necessary. Having designed and operated a furnace to satisfy the above requirements the desirability of direct and continuous observation of the charge became apparent, therefore a furnace with direct viewing facilities was produced[133]. Details and principles of the furnace are given in the paper[133] which is attached to this thesis. For the crystal growth of gallium arsenide, new furnaces were made and some details of design were altered but the basic design was the same. The main difference was the replacement of the complex heating element shown in figure 5.2 by two hemicylindrical elements supported in metal brackets so as to leave a viewing slit down one side (figure 5.3). The seal for allowing rotation and pulling of the capsule was also changed to avoid any contact between the metal of the furnace and the gases inside the silica furnace tube. The capsule was suspended from a silica rod for the bulk crystal growth experiments and a seal of the type shown in figure 5.4 was used. In the thin epitaxial layer growth experiments, the capsule was supported from the bottom of the furnace tube on a precision silica tube. Two different seals were used as shown in figures 5.5(a) and (b), the second type (b) being used in later experiments to reduce the surface area of PTFE exposed to the gas stream.

5.2.3 Open Flow System

A diagram of the open flow system used is shown in figure 5.6. Hydrogen entered the system through the stainless steel needle valve, after which the flow was divided into two, one going to the arsenic trichloride bubbler and the other to the dopant source, the relative flows through each being determined by the capillary tubes A and B. The arsenic trichloride bubbler had a sintered glass diaphragm to ensure intimate contact of the hydrogen with the liquid, therefore the hydrogen became saturated with arsenic trichloride at the bubbler temperature and passed into the end of the furnace tube where hydrogen chloride was formed (equation 5.1).

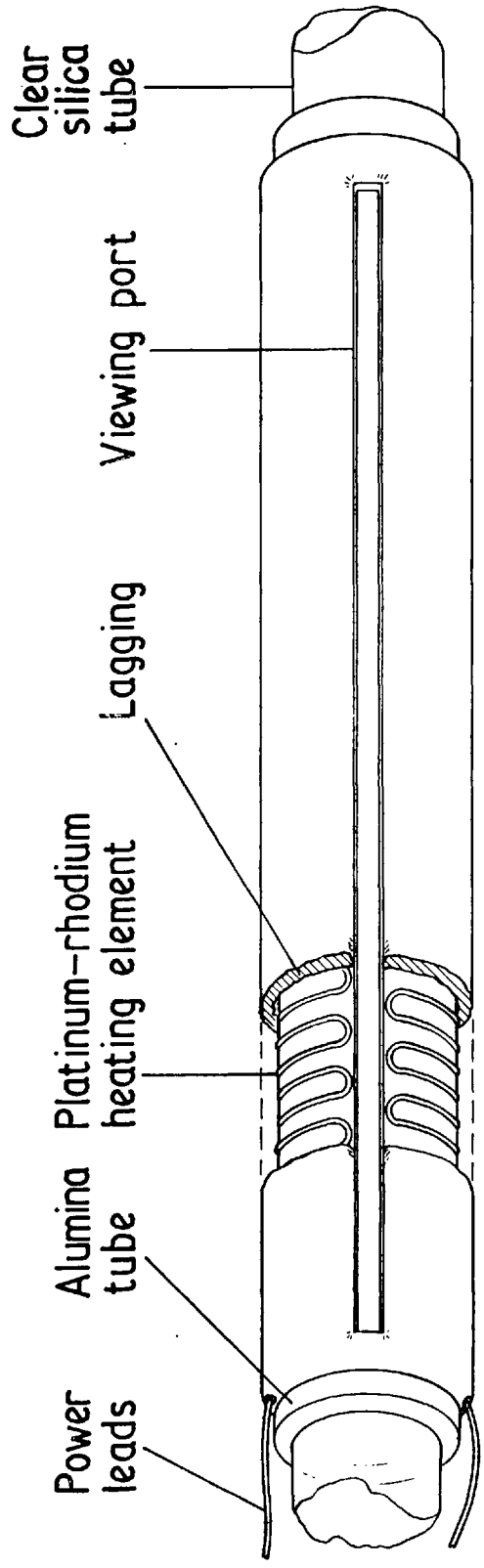

FIG. 5.2. FURNACE HEATING ELEMENT WITH VIEWING SLIT.

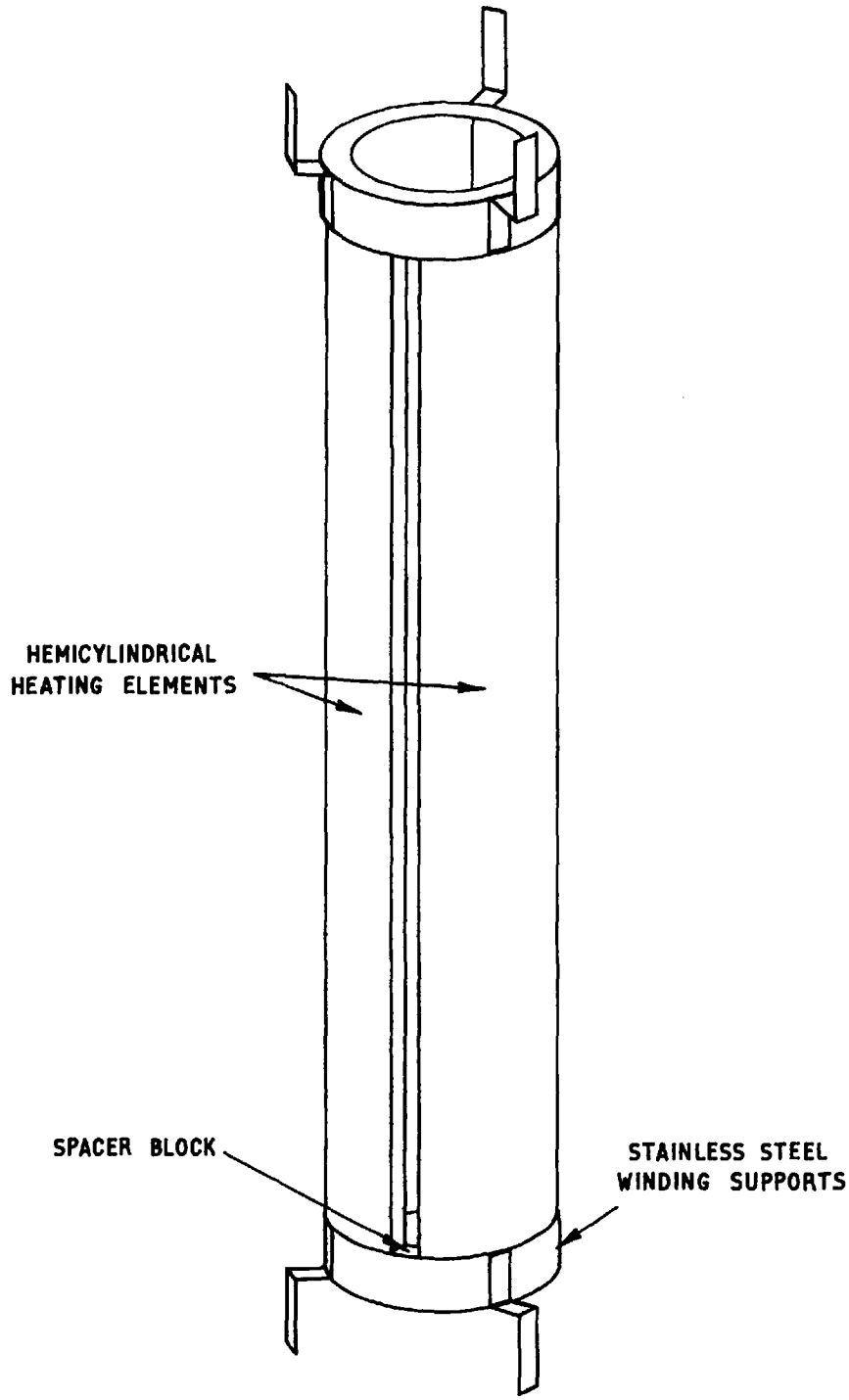

FIG. 5.3. FURNACE HEATING ELEMENTS AND SUPPORT (MODIFIED TYPE)

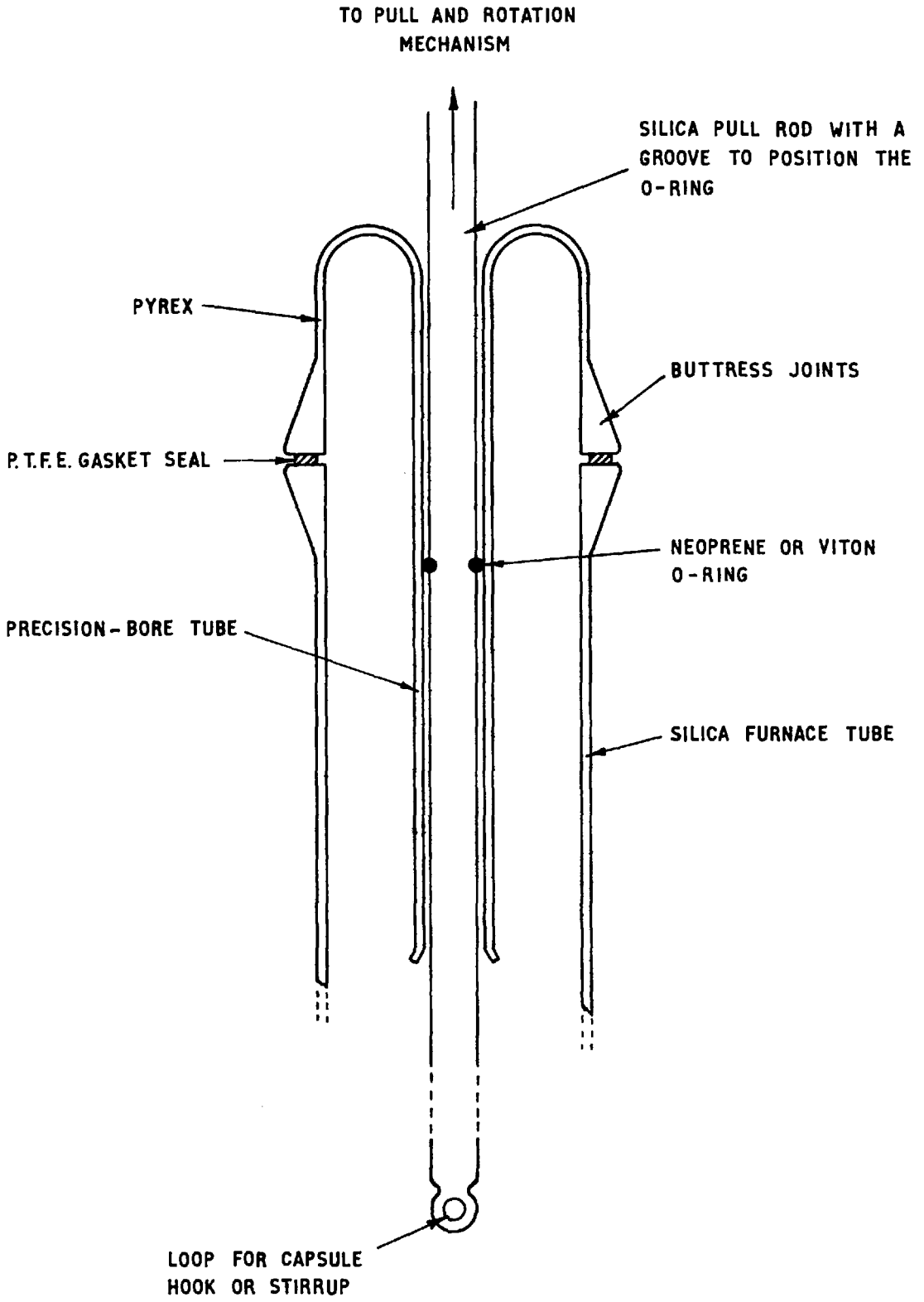

FIG. 5.4. ROTATION SEAL FOR USE WITH CORROSIVE GASES.

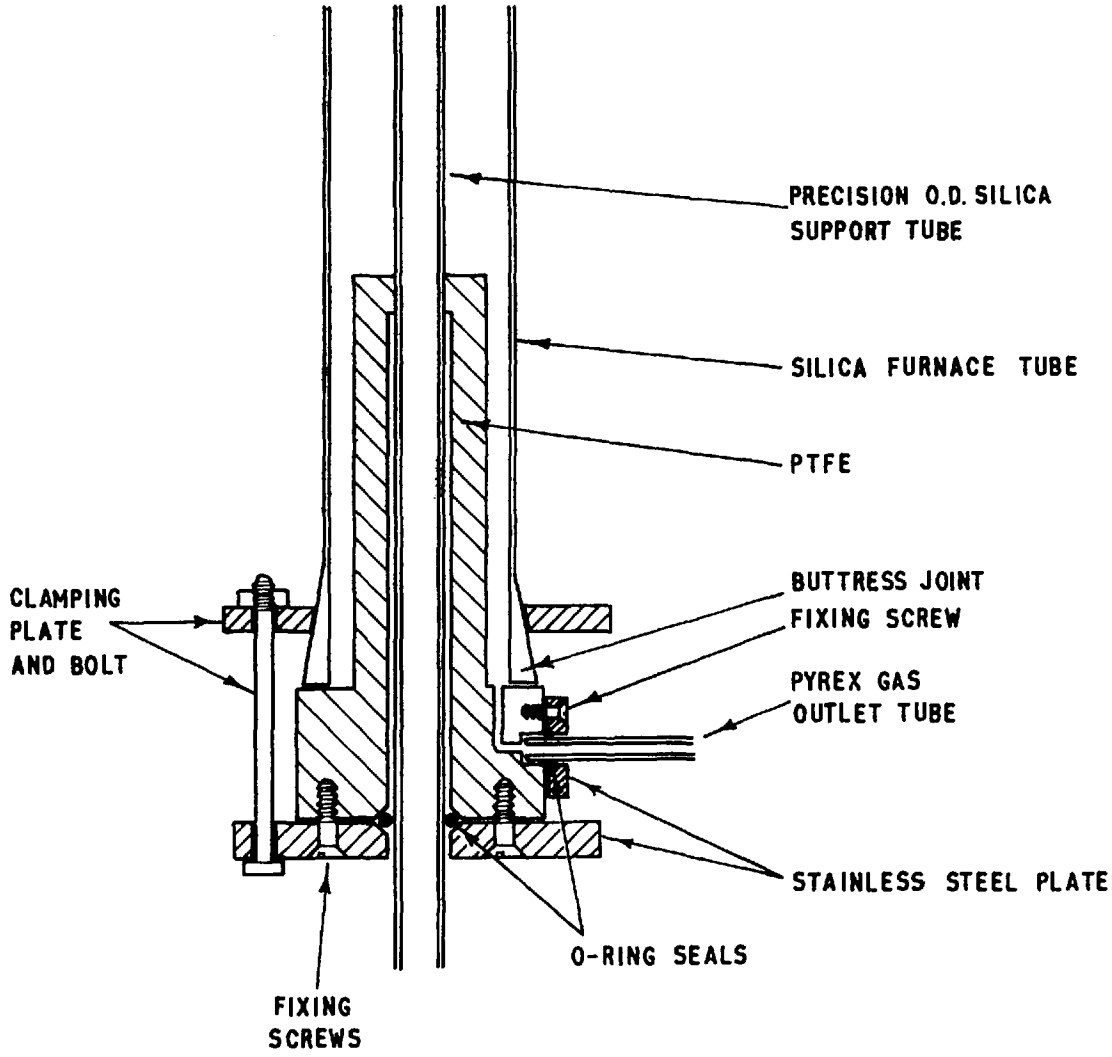

TYPE A

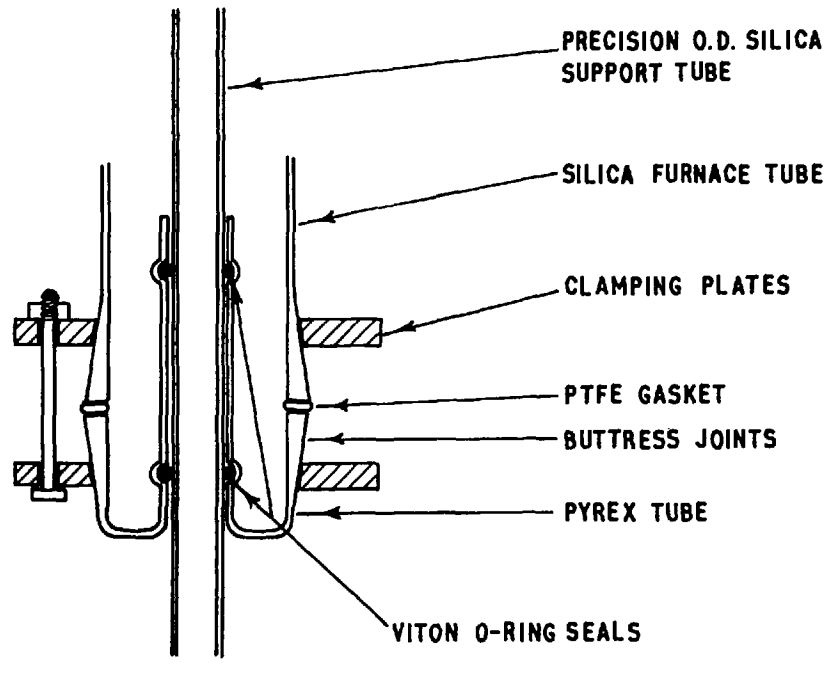

TYPE B

FIG. 5.5. ROTATION SEALS USED IN THIN EPITAXIAL LAYER GROWTH EXPERIMENTS.

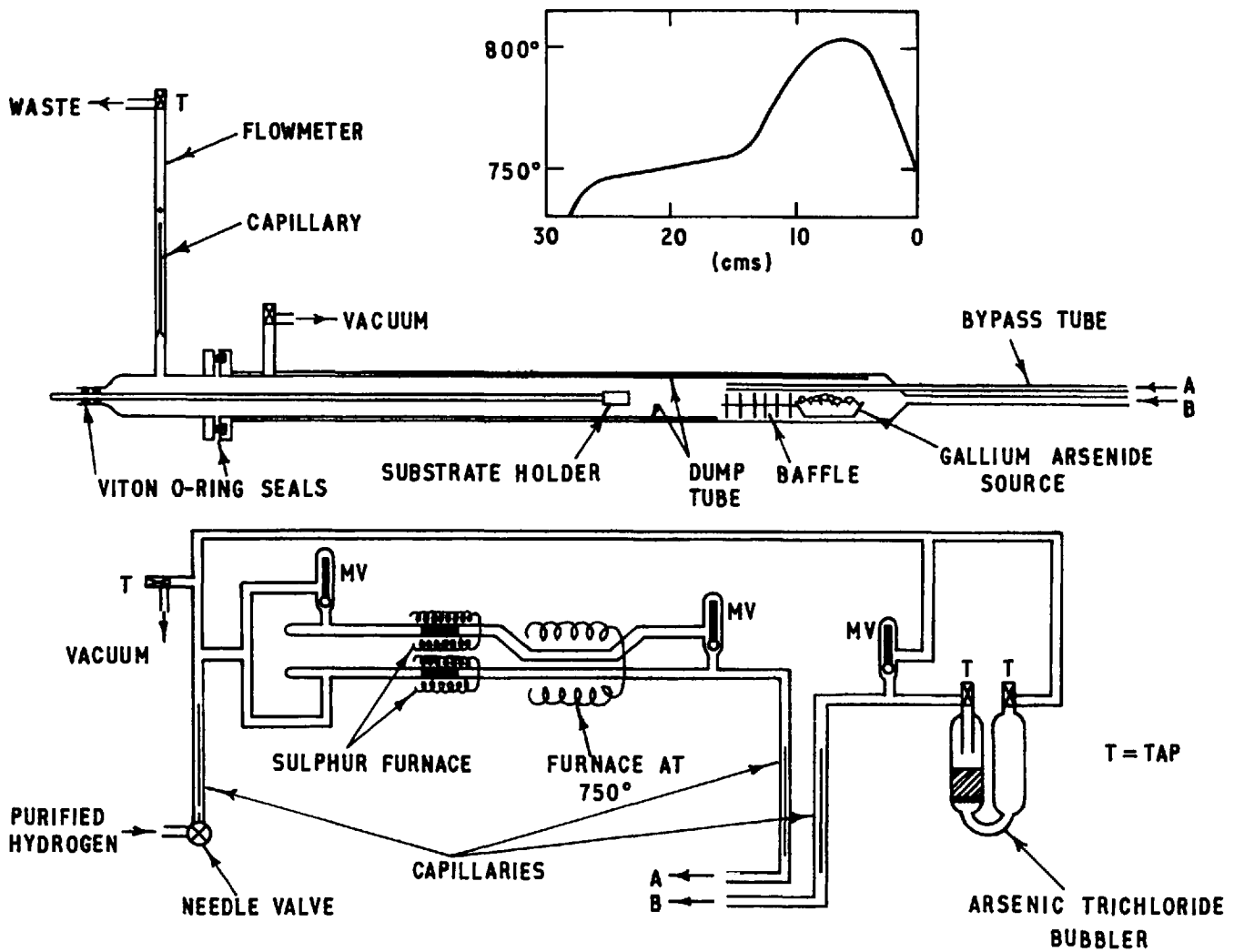

FIG. 5.6. DIAGRAM OF THE OPEN – FLOW SYSTEM

$$2\ AsCl_3 + 3\ H_2 \rightarrow \frac{1}{2}\ As_4 + 6\ HCl \qquad (5.1)$$

The arsenic, hydrogen chloride and hydrogen passed over a silica boat containing gallium arsenide chips at about 800°C, where the hydrogen chloride reacted to form gallium monochloride (equation 5.2).

$$GaAs + HCl_{(g)} \rightarrow GaCl_{(g)} + \frac{1}{4}\ As_{4\,(g)} + \frac{1}{2}\ H_{2\,(g)} \qquad (5.2)$$

When the gas stream reached the substrate at a lower temperature (about 750°C), the equilibrium of reaction (5.2) was moved to the left and gallium arsenide deposited on the substrate, which was supported on a flat silica plate. Some of the vapours condensed onto the 'dump-tube', a close fitting silica tube, lining the furnace tube at the cooler end of the furnace. The dump tube was removed after each experiment and cleaned, thus making it unnecessary to remove the furnace tube so frequently for cleaning, since very little deposit collected on it. The remaining gases passed first through a capillary C, then through a flowmeter which measured the total amount of gas passing through the system and finally into a trap containing soda-lime to remove any poisonous gases remaining. The purpose of capillary C was to raise the total pressure in the system for the reasons stated earlier.

Sulphur was used as a dopant, being contained in a bottle having a capillary outlet and maintained at an elevated temperature e.g. 70°C to give a carrier concentration of $\sim 10^{17}$ cm^{-3} (capillary diameter 0.04 cm and length 1 cm). Sulphur was therefore leaked at a controlled rate into the hydrogen gas stream and heated to 750°C to convert it to hydrogen sulphide. This method was preferred to an open boat of sulphur at room temperature since evaporation rates at lower temperatures are not sufficiently reproducible due to surface contamination[88]. For convenience in changing dopant concentrations abruptly, two boats controlled at different temperatures were used in parallel in the gas stream, one being isolated from the system, when not required, using the magnetic valves at either end of the heated zone.

5.2.4 Capsule System

A diagram of the capsule system used for the growth of thin epitaxial layers is shown in figure 5.7. The gas feed lines were similar to those used in the open flow system, there being a source of arsenic trichloride and a dopant line for introducing controlled amounts of hydrogen sulphide into the gas stream. The gas entered the furnace

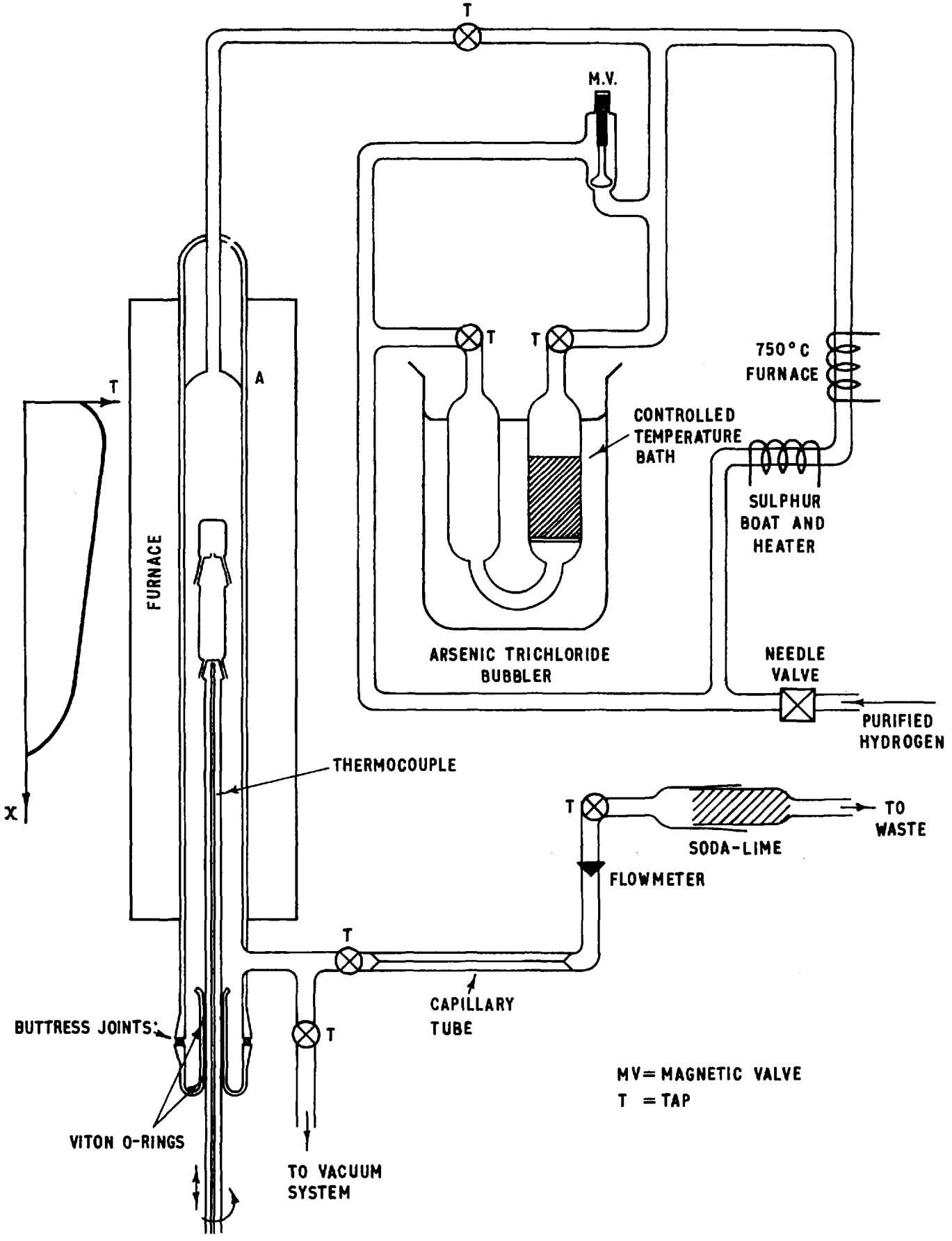

FIG. 5.7. DIAGRAM OF THE CAPSULE SYSTEM

tube at A which is in the hot zone of the furnace, the section of furnace tube above A being present only to facilitate fixing the silica tube into the furnace. The bottom of the furnace had a rotary gas-tight seal to the atmosphere. The support tube for the capsule passed through this seal and had a sealed ground silica joint at the top of it to act as a mounting for the capsule and to support the substrate. This is shown in more detail in figure 5.8. The capsule was formed from three sections, the top of the support tube, a central section with a 'through-cone' at the top of it and an upper section consisting of a domed cap having a small hole in the side 0.007"-0.012" diameter. This hole connected gases inside the capsule with the gases passing outside down the furnace tube. The source material, small chips of gallium arsenide, rested in the annular space formed by the 'through-cone' and the domed cap and the substrate was supported on the flat, polished silica surface of the sealed cone joint. At the lower end of the furnace tube the effluent gases pass through a capillary tube, a flowmeter and finally through a sodalime trap for removing acidic and toxic gases.

The principles of the system used for bulk crystal growth experiments were no different to that used for thin layer growth however there were differences in system design. The main difference was that the capsule was suspended in a stirrup from the top of the furnace as shown in figure 5.9. The gas inlet and waste lines were the same as for thin layer growth except that no provision was made for introducing a dopant. Also the capsule was designed to contain more source material and to ensure that the growing crystal was not adjacent to a ground joint. In the capsule shown in figure 5.8, a large amount of growth would cause the ground joint to be fouled with gallium arsenide and thus make capsule demounting difficult.

Two basic types of capsule were used and they are shown in figure 5.10; (a) was used when gallium arsenide was being purified for use as source material and type (b), was used when a 'seed' plate was introduced for single crystal growth. In type (b), a seed plate of undoped gallium arsenide was cut and polished so as to fit closely into the top of the capsule; it was held in position by an open-ended silica tube which was a close fit inside the top part of the capsule. This liner tube was cut and ground to an exact length, such that, when the capsule was assembled, it rested on the top of the cone joint of the lower part of the capsule and just supported the seed plate against the top of the capsule. It was possible by this method to keep any gap between the seed plate and the capsule to <1mm.

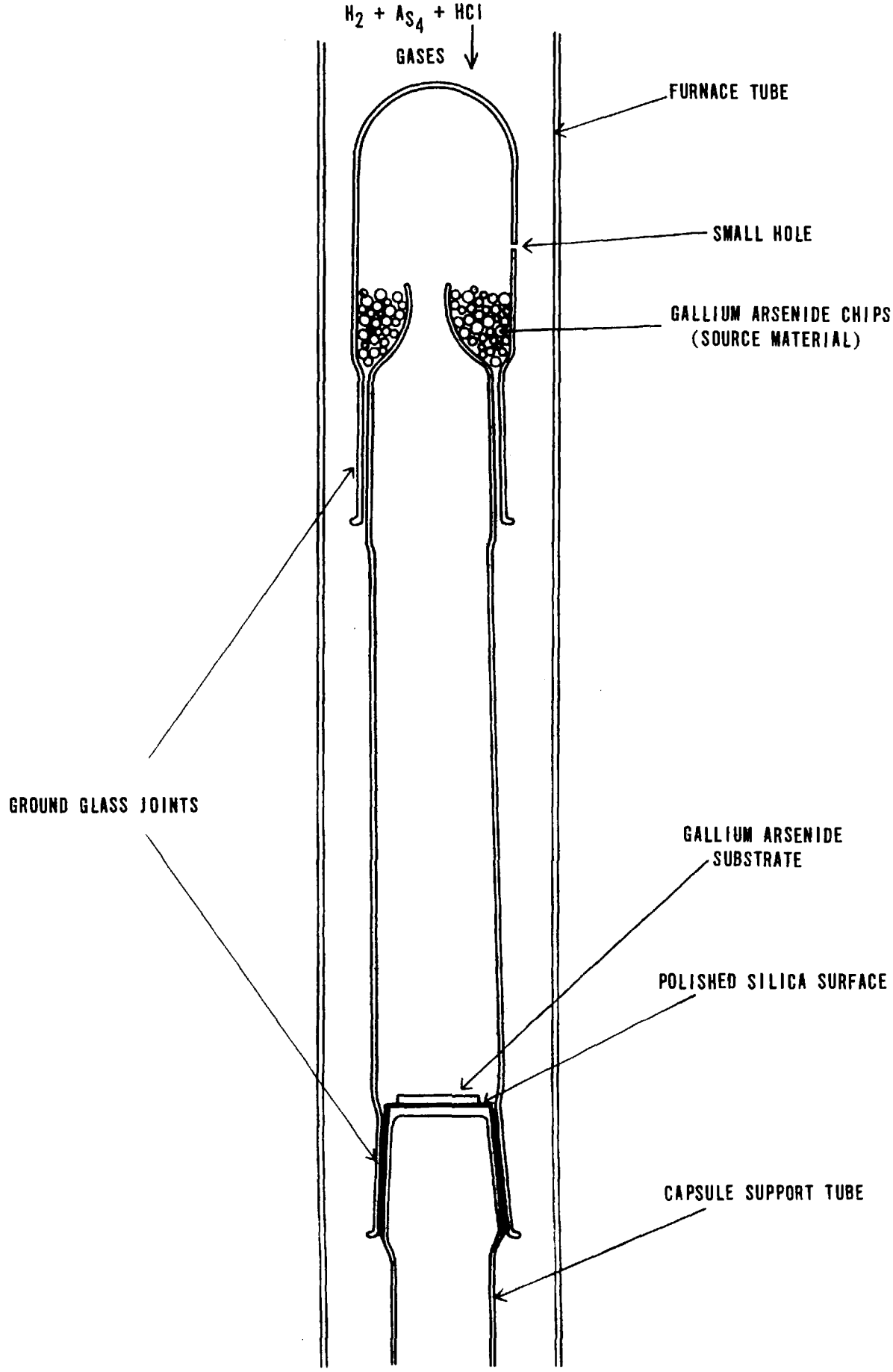

FIG.5.8. SCHEMATIC DIAGRAM OF CAPSULE.

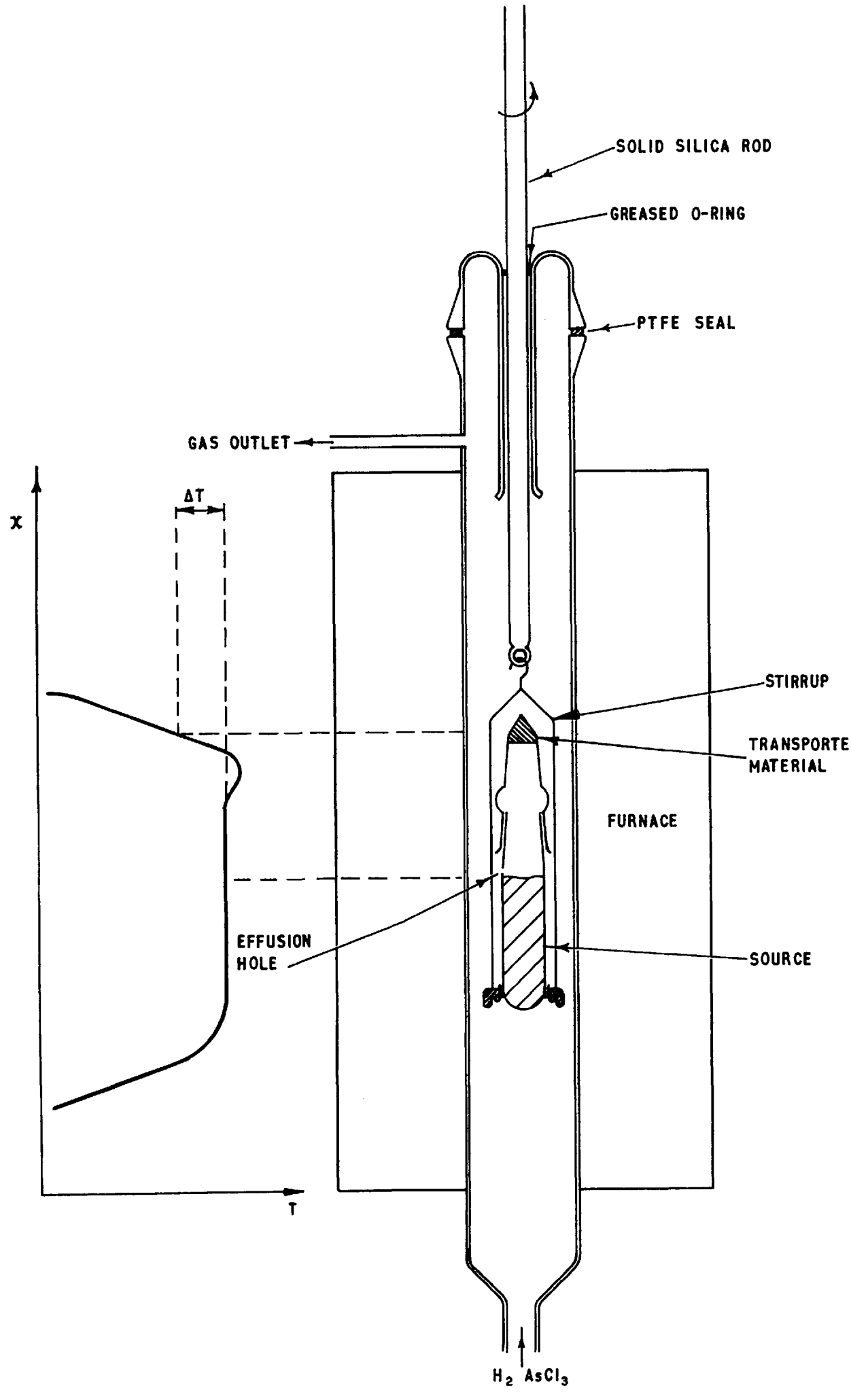
SOLID SILICA ROD
GREASED O-RING
PTFE SEAL
GAS OUTLET
ΔT
X
T
STIRRUP
TRANSPORTED MATERIAL
FURNACE
EFFUSION HOLE
SOURCE
H_2 $AsCl_3$

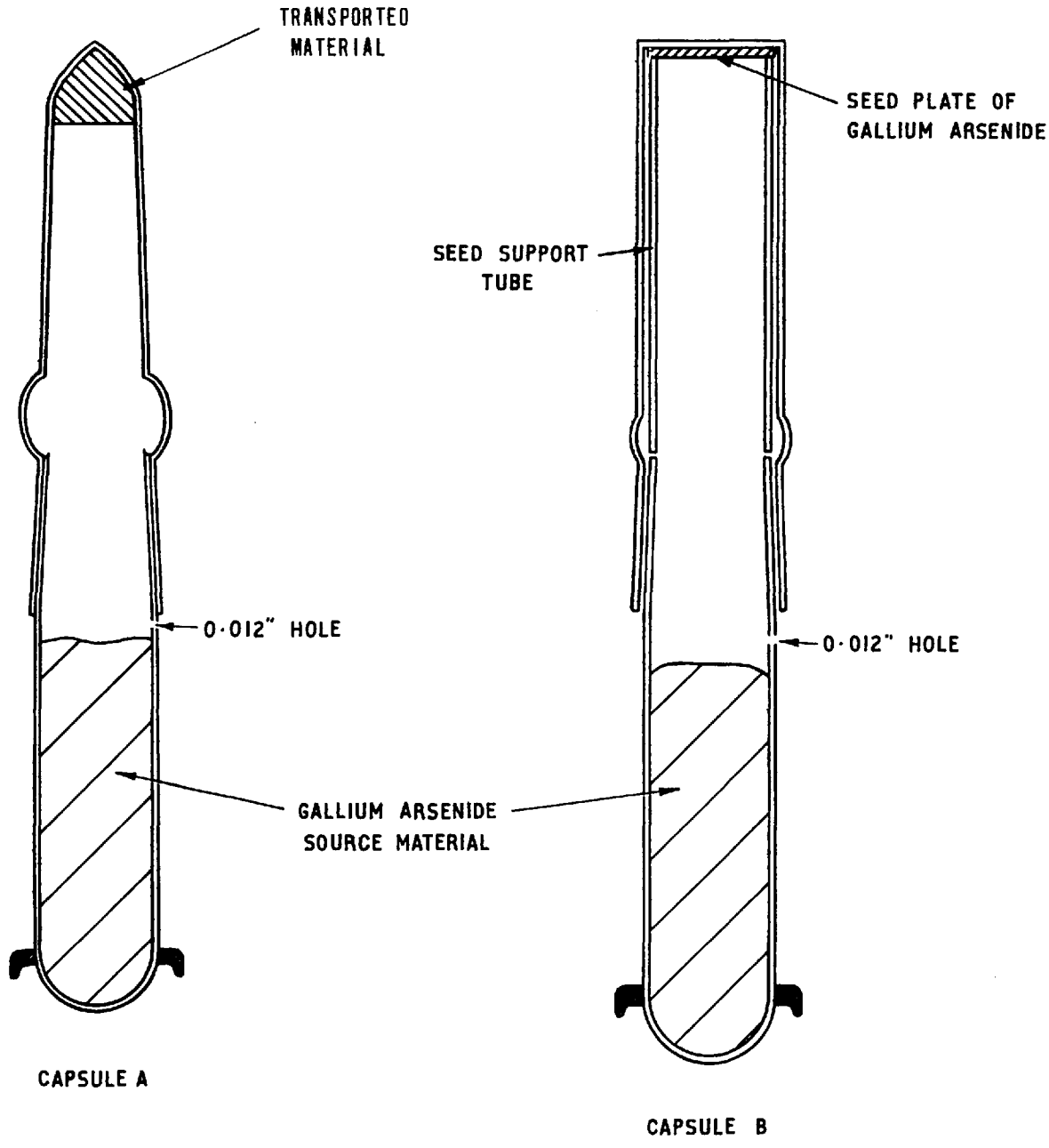

FIG. 5.10. CAPSULES FOR BULK CRYSTAL GROWTH OF GALLIUM ARSENIDE.

5.3 Experimental Procedures and Materials

5.3.1 Operating Procedure for the capsule system

The small size of the hole used in the capsule system meant that the time taken for the gas composition within the capsule to approach a steady state with respect to the gas outside would have been unacceptably long. A procedure for reducing this time was devised and is described below.

The capsule, having been loaded with substrate and source material, was positioned in the furnace and the system was evacuated and filled with arsenic trichloride and hydrogen and this procedure was repeated several times to ensure removal of any air from the capsule. The rate of evacuation of the capsule through the small hole was slow, therefore to gain a measure of the time involved, a capsule was simulated outside the furnace and a pressure gauge used to measure the rate of pressure drop. The system used is shown in figure 5.11. It consisted of a 'through-cone' with a small hole positioned as shown and a glass fitting which had a capsule dial gauge for measuring the pressure above 1 torr and a thermocouple pressure gauge for measuring pressures below 1 torr. Two experiments were carried out, one where the capsule dial gauge had a pressure range of 0–760 torr and one with the range 0–20 torr. The pressure in the capsule was measured as a function of time and the results are plotted in figures 5.12 and 5.13.

The reason for the discrepancy in the time taken to reach 16.5 torr (the starting point for the low pressure readings, figure 5.13) was probably due to the fact that the internal volume of the two dial gauges used were not the same. Furthermore the accuracy of the dial gauges at the low pressure end of their ranges was poor and some 'sticking' of the needle was observed. However the results show clearly that it took $\sim$ 10 minutes to reach 4 torr and thereafter the rate of pressure drop was very slow. In the light of the results thus obtained, the following procedure for pumping the capsule system was adopted. Where a small hole was used in the capsule ($\sim$ 0.007" diameter), the system was pumped for 10 minutes before filling with gas. Most experiments were carried out with a larger hole (0.012" diameter) and here the time for pumping was reduced to 5 minutes. This pumping and filling procedure was repeated 6 times while the system was cold and a further 4 times during heating and when the furnace was at temperature. If the pressure in the capsule

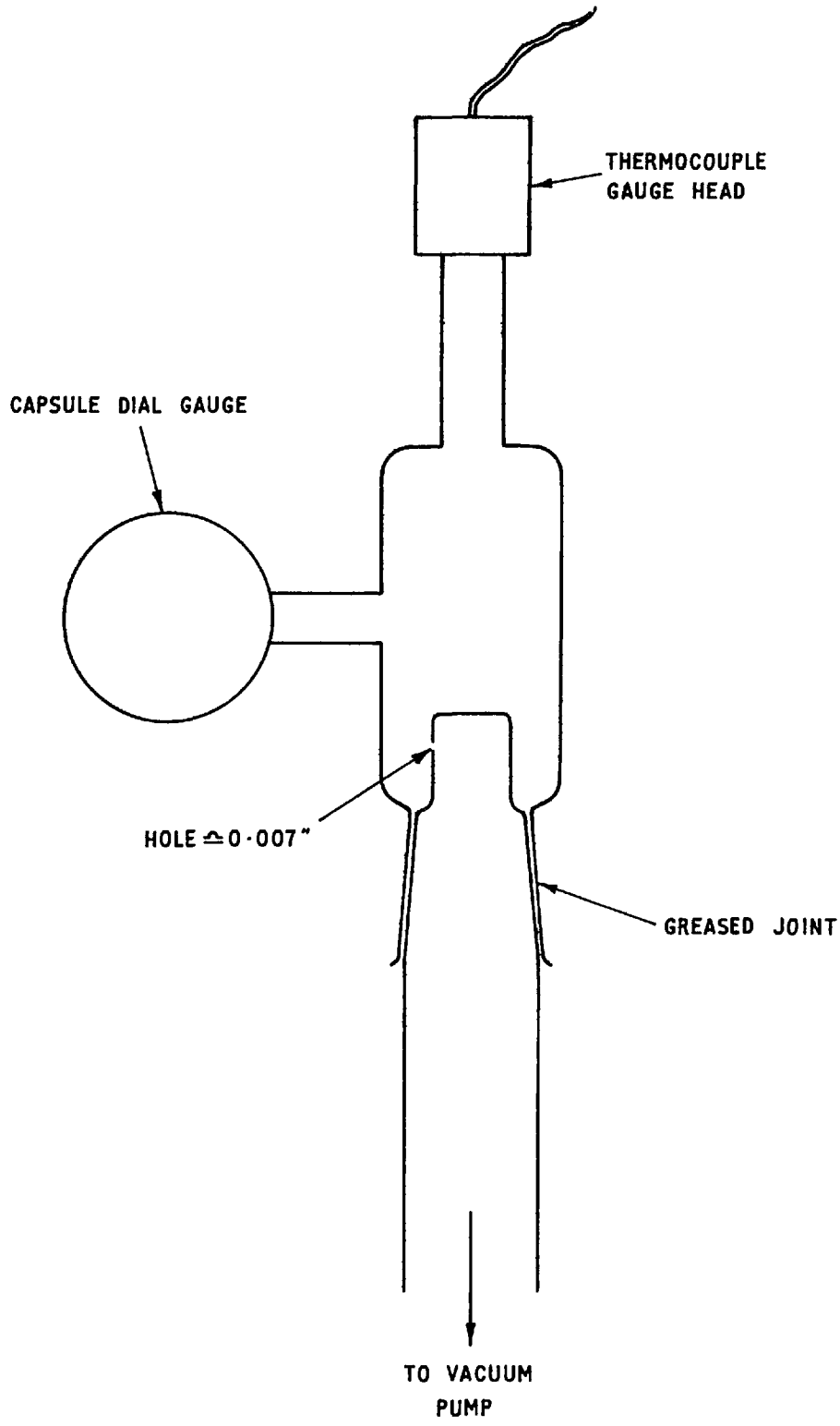

FIG. 5.11 SYSTEM USED TO MEASURE THE RATE OF PRESSURE DROP IN A CAPSULE WHEN PUMPING THROUGH A SMALL HOLE.

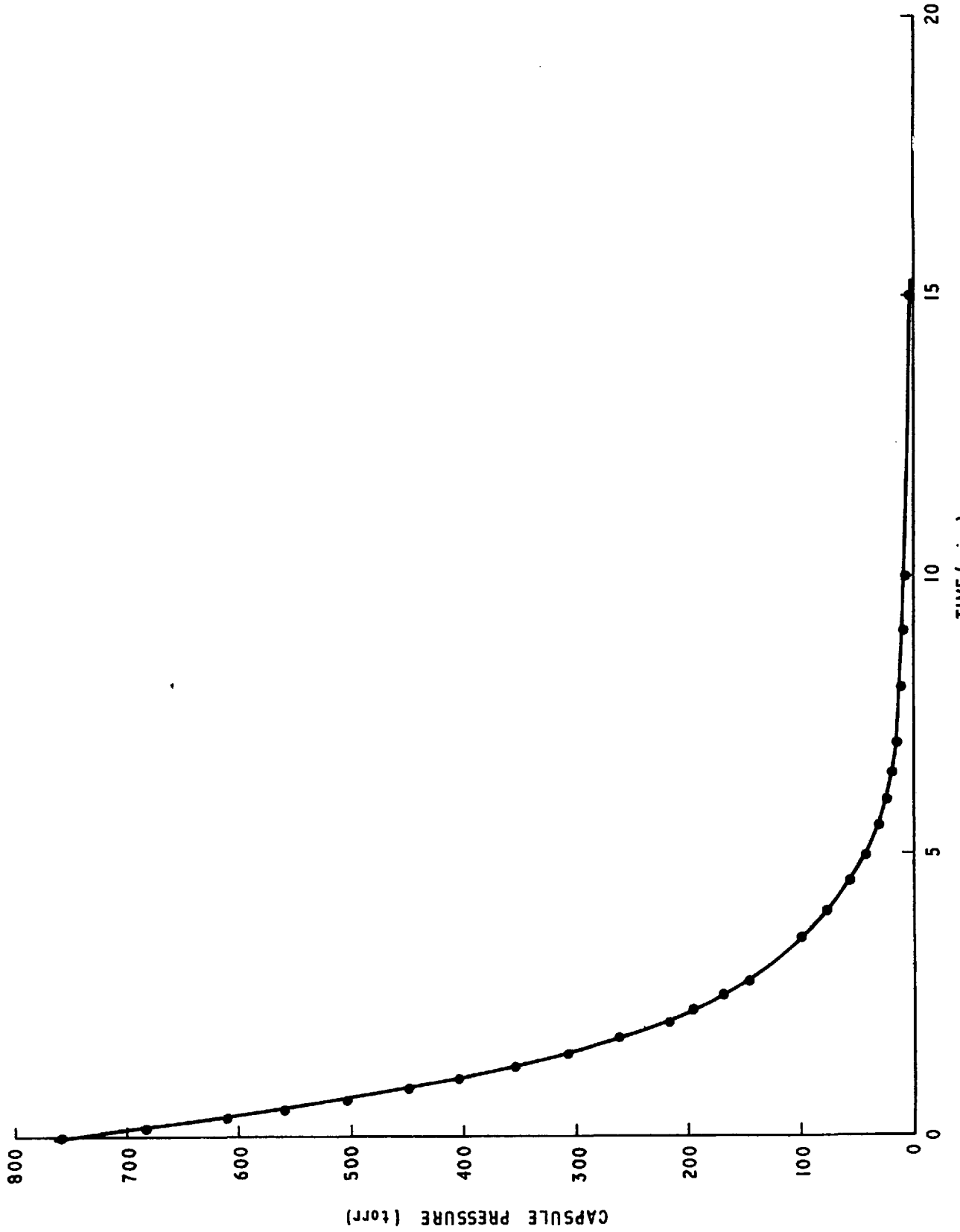

FIG. 5.12. CAPSULE PRESSURE AS A FUNCTION OF TIME.

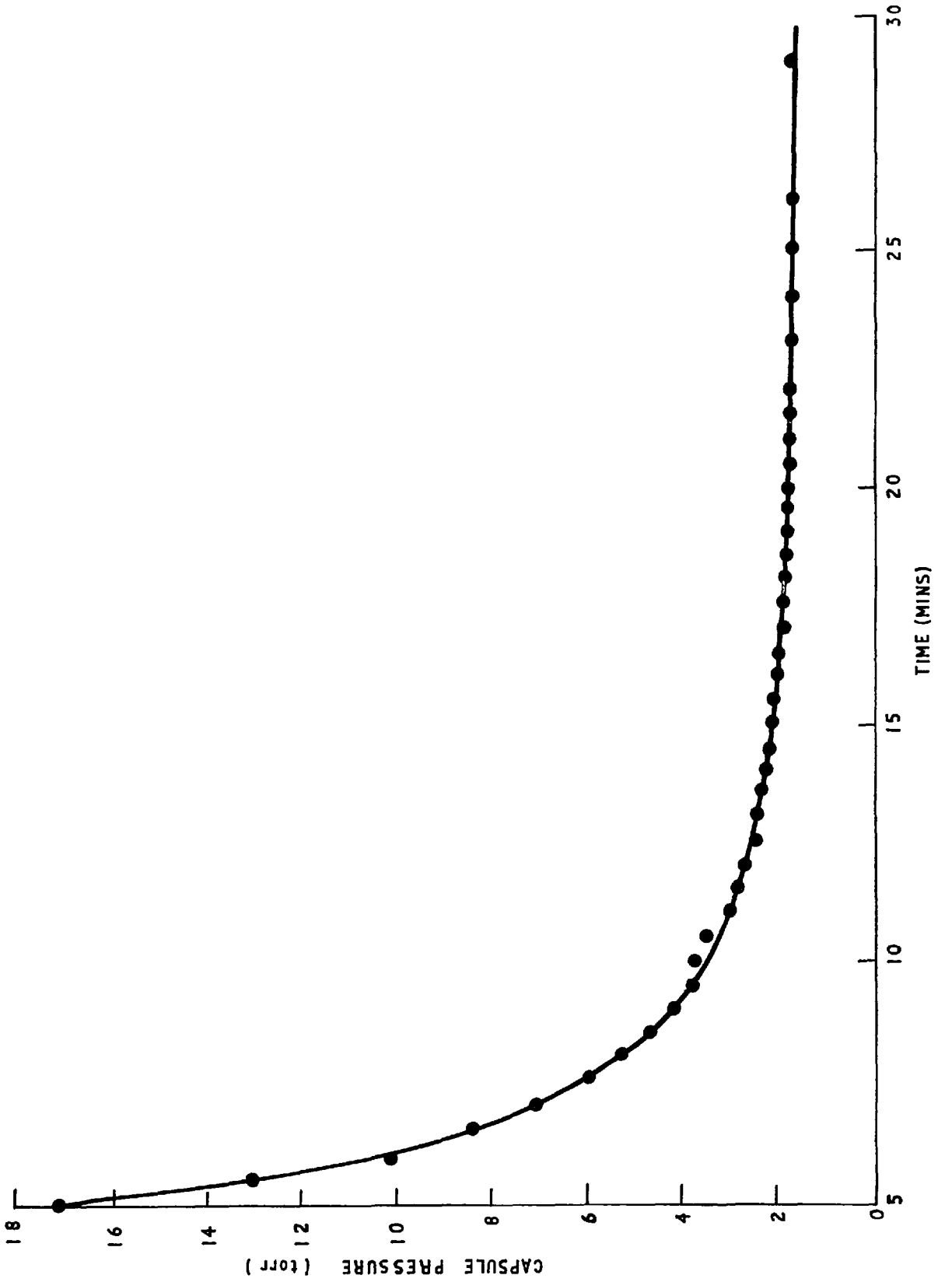

FIG. 5.13. CAPSULE PRESSURE AS A FUNCTION OF TIME (LOW PRESSURE)

reached ~ 4 torr on each pumping cycle then the residual gases in the capsule were reduced to ~ $\frac{1}{200}$ of their pressure each time. After a total of 10 pumpings and fillings the pressure of e.g. oxygen in the capsule would be reduced theoretically to ~ 10^{-23} atmosphere although not all of the gases adsorbed on the walls would be removed by this procedure. Furthermore, silica is known to have a high water content[134, 135] and water would diffuse slowly through the silica to be released into the capsule. It is reasonable to assume however, that the pressure of such species as oxygen and carbon dioxide were reduced to a negligible level. After this procedure was completed the arsenic trichloride, hydrogen and hydrogen sulphide were allowed to flow through the system.

In thin epitaxial layer growth experiments, during the heating of the furnace, the capsule was always positioned so that the substrate was hotter than the source; this was to prevent sudden nucleation on the surface of the substrate during the filling operation. The dopant was allowed into the system only during the final filling of the capsule. Growth was started by lowering the capsule in the furnace until the required temperature difference between the source material and substrate was obtained.

In the bulk growth system the same pumping and filling procedure was used as for thin layer growth. The capsule was initially positioned so that the top of the capsule was hotter than the source material, then when the arsenic trichloride was flowing through the system, the capsule was raised to reverse the temperature gradient. When no seed plate of gallium arsenide was used, the capsule was pulled through the furnace tube at a steady rate until nucleation occurred in the tip of the capsule. At the first visible signs of crystallites, the pulling was stopped to allow the supersaturation to be reduced, the capsule being kept in this position overnight, before pulling was recommenced at a slow rate (up to 1 mm hr^{-1}). When a seed plate was used the capsule was raised until the temperature difference between the source and the seed was ~ 30–40°C then the slow pulling was commenced. Typical growth temperatures used were 700°–800°C.

In both types of capsule system, the growth was terminated by pumping out and filling the system with hydrogen three times, thus preventing further growth and deposition of condensible vapours during the cooling of the furnace.

5.3.2 Temperature Measurement in the capsule systems

The measurement of temperature of the source and substrate was made in various ways. The longitudinal thermal profile of the furnaces was measured at the operating temperatures by a thermocouple inside a silica sheath situated within the furnace tube in the absence of the capsule. The presence of the silica sheath would have had a different effect on the thermal profile from the capsule, therefore temperatures inferred from measurements obtained in this way must be used with caution. However some rough estimate of the temperature differences between the source and the growing crystal were obtained from a knowledge of the thermal profile and the position of the capsule.

At temperatures above 1000°K an optical pyrometer could be used, but here again there are large uncertainties in the results. The emissivity of gallium arsenide is not known with any certainty although when measuring temperature differences this was not required. The greatest source of error in this method arose from the fact that the gallium arsenide has a highly reflecting surface not unlike a polished metal, consequently when using the optical pyrometer, one observed not only the emitted radiation from the gallium arsenide but also the reflected radiation from the furnace walls, which were considerably hotter than the gallium arsenide.

In the thin layer growth a measurement of substrate temperature was obtained by positioning a thermocouple inside the hollow support tube so that the thermocouple bead was touching the underside of the silica plate on which the substrate rested.

Even this was subject to some error since gallium arsenide is fairly transparent to infra-red radiation[136] and consequently the substrate could be very close to some hot object without being at the same temperature as the object.

In view of the uncertainties, it is estimated that measurements of temperature differences were subject to errors of ±5 °K in the thin layer growth with substrate temperatures ±2°K. In the bulk growth experiments the corresponding errors were ± 10°K (for temperature differences) and ±5°K (for the growing crystal).

5.3.3 Measurement of growth rates

Growth rates were determined by weighing the substrates before and after the experiments (in the case of bulk crystal growth by weighing the amount of gallium arsenide transported into the upper part of the capsule). There were two main sources of error in the mean growth rates thus determined. The first arose from the procedure of heating the

capsule initially in a position where the source was cooler than the substrate. In this position, etching of the substrate occurred and the resultant weight loss could not be determined by the method described. The amount of weight loss was dependent not only on the length of time that this position of the capsule was maintained but also on the pumping out and filling of the capsule while at high temperature. The second source of error arose from the fact that growth occurred not only on the top surface of the substrate but also on the sides and back, the amount deposited in these other regions was found to be as much as 25% of the total deposit.

It was not possible to relate growth rates from bulk crystal growth experiments with temperature differences since the growth conditions were not constant throughout the experiment since adjustments to the capsule position were made. In the light of the above sources of error it is estimated that growth rates could be in error by as much as 25-30%.

5.3.4 Materials

Gallium arsenide substrates were obtained mainly from Mining and Chemical Products Ltd (MCP). They were cut from boat-grown ingots using either an annular saw or a Norton saw followed by mechanical lapping to remove the heavily damaged surface. Various types of substrate were used:

(i) Undoped, n-type with a carrier concentration of about 10^{16} cm^{-3} and a room temperature mobility of 4500 cm^2 V^{-1} sec^{-1}.

(ii) Silicon doped n-type ($\sim 10^{18}$ carriers cm^{-3}).

(iii) Tellurium doped n-type ($\sim 10^{18}$ carriers cm^{-3}).

The substrates used were of the (100) orientation although a few (111) oriented slice were used for comparison. A few slices of gallium arsenide grown by the Czochralski method were obtained from the Royal Radar Establishment.

Gallium arsenide source material was obtained as a polycrystalline ingot from MCP which was cleaved into small chips using a tungsten carbide edged knife. The chips were etched in 1 : 1 nitric : hydrochloric acid for 5-10 minutes, washed with double quartz distilled water and dried.

Arsenic trichloride was obtained from two sources:- MCP (99.999% pure) and Johnson Matthey Chemicals (Grade A1). The arsenic trichloride was transferred from the ampoules into the equipment by pouring through a funnel situated in the neck of one of the taps on the bubbler (See e.g. figure 5.7).

The sulphur which was used as an n-type dopant was supplied by Koch-Light (99.9999%) in the form of small crystals.

The hydrogen, supplied by British Oxygen Co. was purified by passing it through a palladium alloy diffuser after which it was transferred in stainless steel pipe to the apparatus.

Chemical reagents used for cleaning glassware etc. were usually analytical grade materials, although cleaning of gallium arsenide by etching was performed using higher purity 'Aristar' grade chemicals supplied by B.D.H. Ltd.

5.3.5 Substrate Preparation

The surfaces of semiconductor slices become damaged when subjected to mechanical treatments, e.g. cutting and polishing. The depth of the damage depends on the process but has been investigated for various semiconductors[137,138]. For epitaxial growth, damage-free surfaces on which to deposit the material were required, therefore the surfaces of the gallium arsenide slices as received were removed by etching. A chemical mechanical polishing process, similar in principle to that described by Sullivan and Kolb[139], was used to obtain flat surfaces as well as to remove the damaged material. A description of the procedure is given below.

(a) The slices, as received, were etched for 5 minutes in a 5% solution of bromine in methanol to remove most of the damaged surface and any particles left by the cutting procedure. When required, small slices were cleaved using a diamond tipped scriber prior to etching.

(b) The slices were mounted onto a PTFE block using a low melting-temperature dental wax, which in turn was attached to the arm of a rotary polishing machine. This machine had a Hyprocel Pellon pad (Type PAN-W) fixed to a flat polythene revolving tray. The pad was rotated at 60 rpm while bromine in methanol was dripped on it slowly and the slice on the PTFE block was traversed to and fro across it. In later experiments it was found that the surface finish of the slice was improved by simultaneously rotating the slice on the PTFE block at 30 rpm. Recently Ridout has reported similar improvements by rotating the slice when using sodium hypochlorite as the etchant[140].

The concentrations of the bromine-methanol solutions used were 5% bromine in methanol for 5 minutes followed by 1% bromine in methanol for 15 minutes. On occasions where the surface finish did not appear good when viewed under a low power microscope a further

5 minutes with 0.5% bromine in methanol was used. During the whole polishing procedure the slice was not allowed to dry off but was kept wet with methanol. Failure to do this meant that when polishing was continued there was an initial deterioration in the surface finish which required extensive polishing to remove it.

(c) The slices were removed from the PTFE block by suspending the block in a silica flask and allowing trichloroethylene vapour to condense on it and dissolve away the wax. When free from the block the slice was transferred to a recycling silica soxhlet containing trichloroethylene and washed for at least 30 minutes to remove the wax. In early experiments the slice was then transferred to a soxhlet containing isopropanol and washed for a further 30 minutes. However the slices appeared to be covered with a non-uniform surface film which caused resistance to epitaxial growth (and chemical vapour etching). Preliminary investigations using Auger spectroscopy indicated that carbon was present on the surface after polishing[141]; this will be discussed in detail later. It is sufficient to point out here that the surface was improved by etching for 5 minutes in 3 : 1 : 1 sulphuric acid: hydrogen peroxide : water, then washing with double quartz distilled water and with isopropanol. A final wash was made in a soxhlet containing 1, 1, 2-trichlorotrifluoroethane for 30 minutes.

The presence of a surface film on gallium arsenide and the variation of film thickness has recently been reported by Adams and Pruniaux[142]. Using ellipsometry they studied the thickness of the surface film as a function of polishing technique and solvents used for washing. Their results indicate that the procedure that has been adopted here should keep the surface film thickness low.

During the whole polishing operation 50-100 μ of gallium arsenide was removed from the substrate leaving a mirror-like surface, although the edges were slightly bevelled, particularly in the case of small slices. An investigation using Lang topography[143] has shown that the polishing process was sufficient to remove the surface damage introduced when the slice was cut from the gallium arsenide ingot.

Substrates prepared in the above way were removed from the soxhlet immediately prior to use, the hot solvent being run off the substrate, then allowing it to dry. The substrate was then placed in the crystal growth apparatus keeping its exposure to air to a minimum, thus limiting the formation of a surface film[142].

CHAPTER 6

RESULTS AND DISCUSSION OF

GALLIUM ARSENIDE CRYSTAL GROWTH

CHAPTER 6

RESULTS AND DISCUSSION OF GALLIUM ARSENIDE CRYSTAL GROWTH

In this chapter the experimental results of vapour phase transport of gallium arsenide are presented and discussed. As indicated earlier, the majority of the crystal growth performed, was carried out in the 'capsule' system; therefore the results given here refer mainly to this method. For convenience of discussion this chapter is divided into three sections:

- studies of the morphology of epitaxial layers,
- experimental growth rates and discussion in the light of the theory given in chapter 3,
- bulk crystal growth experiments.

6.1 Morphology of Gallium Arsenide Epitaxial Layers

6.1.1 General

The aim in growing epitaxial layers of gallium arsenide was to produce flat, uniform layers $\sim 1\ \mu m$ thick. However, initial experiments with the capsule method produced layers which were covered with various morphological features: pyramids, hillocks, pits etc; these were studied therefore in an attempt to understand the causes of them and subsequently to eliminate them. The layers were studied using both optical microscopy and scanning electron microscopy (SEM). The crystalline quality of layers was assessed using Lang and diffractometer techniques. The orientation of facets was determined by measuring the angle of tilt between faces using the standard specimen stage of the SEM instrument (a Cambridge Stereoscan).

The large number of specimens obtained from 'capsule' growth experiments precluded a detailed examination of each one in the time available. All slices were examined by optical microscopy and selected slices were examined using SEM and/or Lang and diffractometer X-ray techniques. The results presented below are taken from a few specimens but may be considered typical of many others that were investigated in less detail.

The gallium arsenide slices were observed throughout the growth process, an external lamp directed towards them giving adequate illumination to observe the condition of the surface by eye. During the initial pumping and filling procedures changes in the surface

appearance (initially smooth and polished) were observed at temperatures in excess of ~ 800°C. On occasions small leaks in the system allowed air to enter on pumping which, when the system was refilled produced a whitening of the slice surface (in cases of very small leaks a slight 'bloom'). Changes in appearance due to air leaks were uniform over the whole slice.

A second type of change in the surface appearance was noted arising from the capsule being positioned so that the slice was initially at a higher temperature than the source material; when gas was admitted into the system, some etching of the slice occurred and the smooth surface acquired a fine matt appearance such that light from the external lamp was back scattered by the surface, at specific positions of the capsule when rotating. The matt surface was probably caused by small facets on the surface of the slice which were formed by etching. Since the slices were of the (100) orientation the facets were probably (111) faces, further evidence for this assignment is given later. Once the capsule was lowered into a position where growth occurred, the matt surface reverted to a smooth one, usually starting at the centre and spreading towards the edges. The surface reacquired its smooth finish within 10 minutes of growth ($\frac{1}{2}$-1μm thickness of deposit). This behaviour, although observed on many specimens, did not always occur, indicating that the slice surfaces were not always in the same condition from one experiment to another. Evidence is presented later that indicates the slice can be covered with an impurity layer which inhibits both etching and growth.

All the observations mentioned above were made during the experiments. Below the results of a more detailed examination of specimens after removal from the growth apparatus are presented.

6.1.2 Etched Specimens

The etching process was kept to a minimum in later experiments, however some etching (up to 1μm deep) always occurred during the initial pumping and filling procedure. Some experiments were terminated after the etching stage of the experiment and before any growth was allowed to occur and it was found that the etched specimens did not all exhibit the same morphology. The results presented below concern mainly one specimen, although the morphology of other specimens will also be discussed.

A silicon doped ($\sim 10^{18}$ carriers cm^{-3}) substrate of nominal (100) orientation was etched by chemical vapour transport (CVT) at $\sim 685°C$ for 100 minutes, the temperature difference being $\sim 20°C$. The specimen had a large number of etch pits in the surface, these are shown in figure 6.1. Some regions were grossly etched and it appeared that the pits had merged into one another; such regions are visible at the top left and top right of the picture. It is also noted that most of the pits are rectangular and are oriented with the longer sides of the pits parallel to one another although a few exceptions were found where the longer side was at right angles to the rest. Closer examination of the pits (figure 6.2) and measurement of the angles between the exposed faces and the top surface showed that the larger faces were (111) type and the smaller rectangular ones were (110) type. The rectangular shape of the pits indicates that the longer sides were the slower etching faces. The (111)A surface of gallium arsenide has gallium atoms exposed, the (111)B has arsenic atoms exposed and Shaw[144, 145] investigating the growth rates of the A and B faces in an open flow system (using a gallium source with arsenic trichloride and hydrogen) found the ratio of growth rates (A to B) to be 40 : 1. This suggests that the slowest etching faces were (111)B type, the length to width ratio of the pits giving the ratio of etch rates of (111)A to (111)B faces. A statistical examination of the etch pits gave a length to width ratio of 1.6 : 1 with a standard deviation of ~ 0.3.

The discrepancy between the values of the ratio obtained by Shaw and that obtained here is very large. Different experimental conditions such as temperature and gas composition could account for some of the discrepancy but it is unlikely to be a factor of 25. Impurities on a crystal can alter the etch rate (or growth rate) of a particular surface[106]. Such an effect could explain the differences of result.

Rectangular pits were also found on the underside of the slice, even though it was resting on a flat silica plate and the longer sides of these pits were at 90° to those on the top surface. The (111)A and (111)B surfaces would also be rotated through 90°, which confirms the assignment of the faces given in figure (6.2).

Figure (6.3) shows a general view of the surface; the rectangular etch pits were found to be scattered over the surface between grossly etched regions (which appear as light coloured patches in the photograph). These grossly etched regions were all of a similar depth into the material ($\sim 10\ \mu m$ deep). There were some line features on the

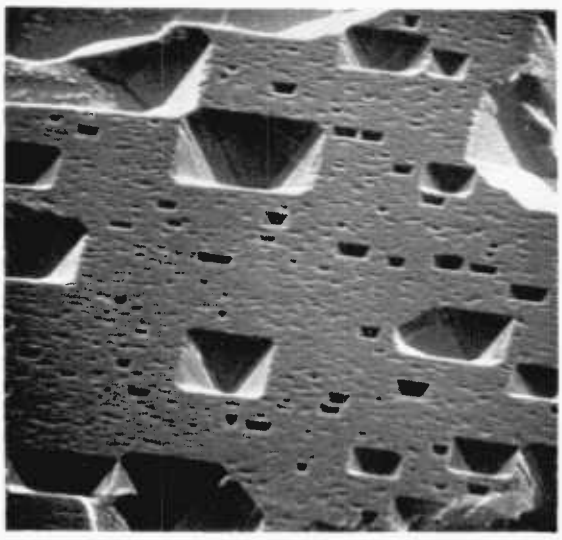

Figure 6.1

Scanning electron micrograph of etched specimen

Angle of tilt: 30°
Magnification: x1400

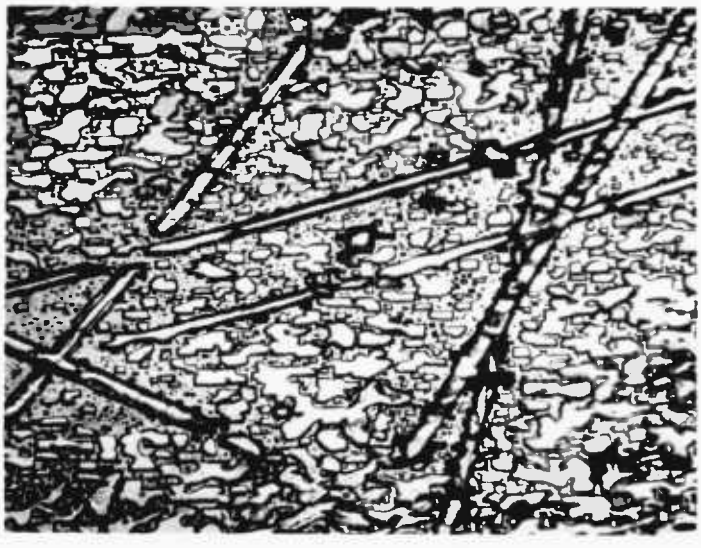

Figure 6.3

Optical micrograph showing a general view of the etched surface

Magnification: x70

Figure 6.4

Optical micrograph of a deep etching effect on a specimen, the other half of which was coated with a 150 Å thick carbon film

Magnification: x575
Etching temperature: 690° C
$AsCl_3$ temperature: 0° C

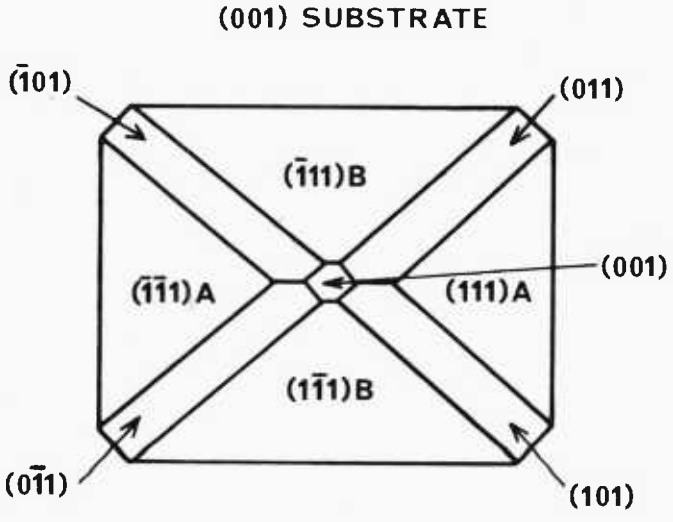

Figure 6.2

Scanning electron micrograph of a typical etch pit, with faces indexed

Angle of tilt: 0°
Magnification: x1400

surface, which were also deeply etched into the slice and it is most probable that the causes of these features were scratches on the surface of the slice formed either during the polishing procedure or as a result of the subsequent handling of the slice. Silicon doped slices were particularly susceptible to being scratched during mechanico-chemical polishing. It is possible that any inert granular impurities in the gallium arsenide, released as the surface was removed, became embedded in the polishing pad and caused the scratching. The rectangular pits varied in length from 1 to ~ 15 μm, and the etch pit density on the high regions was ~ 2×10^6 cm^{-2} (counting pits of 1 μm length or greater). It can be seen in figure (6.1), that between the pits there were a large number of shallow hollows, which could have been incipient pits generated by the CVT etching.

The morphology described above was observed on several other specimens etched in the manner described, but when etching was allowed to occur to a greater extent, the morphology was more irregular (figure 6.4). The morphology shown in figures (6.1)-(6.3) appeared to be an intermediate stage before the grosser features of figure (6.4) were formed. If the surface of the slice was covered with a layer of impurity (as discussed later) then it is probable that the initial etching behaviour was different from subsequent etching when the top surface had been removed.

6.1.3 Grown Specimens

In order to observe the early stages of growth of an epitaxial layer, growth on substrates etched as described above, was terminated before a complete epitaxial layer was formed and the resulting morphology studied. Growth had occurred on definite centres on the substrate surface in the form of regular almost isometric pyramids (figure 6.5). Such pyramids were observed only on incomplete epitaxial layers never where the initial substrate surface had been completely covered by growth. The pyramids were aligned along the (110) directions (figures 6.6 and 6.7), the longer edges of the rectangular pyramids being parallel to each other (occasional exceptions were found). Measurement of the angles between the pyramid faces showed that the large side faces were (111) type, with very narrow (110) faces at the edges (figure 6.8) and the top surface was a (100) face, although not all pyramids exhibited it (figure 6.9). Using the same arguments as for etch pits, the smaller side faces are (111)A (faster growing) and the larger faces are (111)B, the ratio of the two giving a measure of the relative growth rates of the faces. A statistical

Figure 6.5

Scanning electron micrograph of some regular pyramids

Angle of tilt: 45°
Magnification: x840
Growth temperature: 740° C
Temperature difference between source & substrate: 10° C
$AsCl_3$ temperature: 20° C

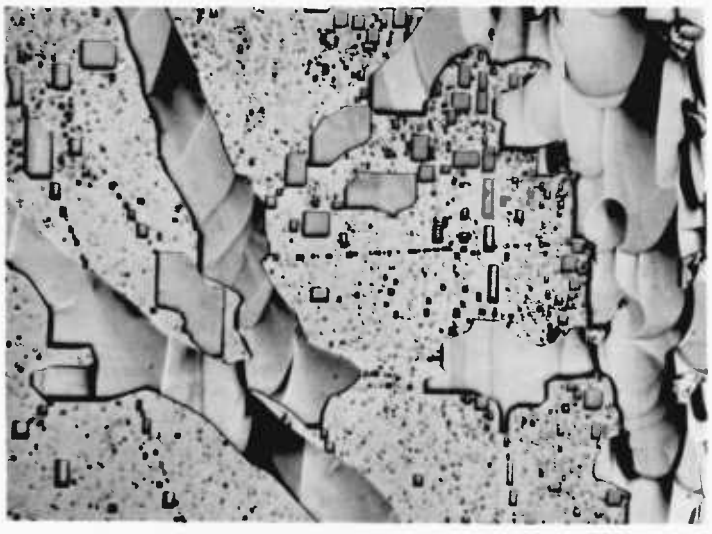

Figure 6.6

Optical micrograph of another specimen with epitaxial regular pyramids

Magnification: x100
Growth temperature: 625° C
Temperature difference between source & substrate: 30° C
$AsCl_3$ temperature 0° C

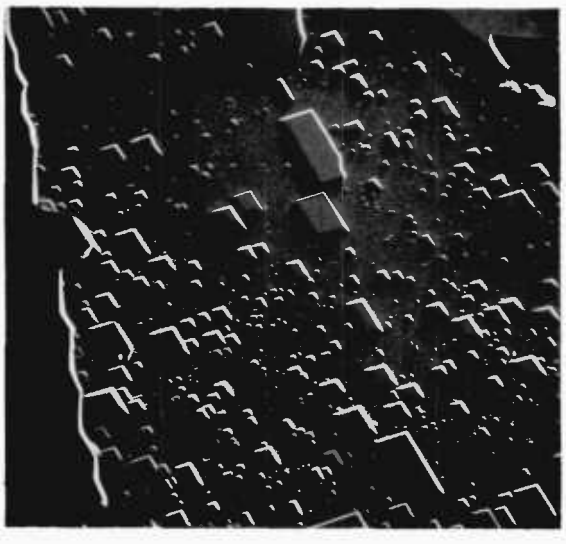

Figure 6.7

Scanning electron micrograph of same specimen as Figure 6.6

Angle of tilt: 30°
Magnification: x150

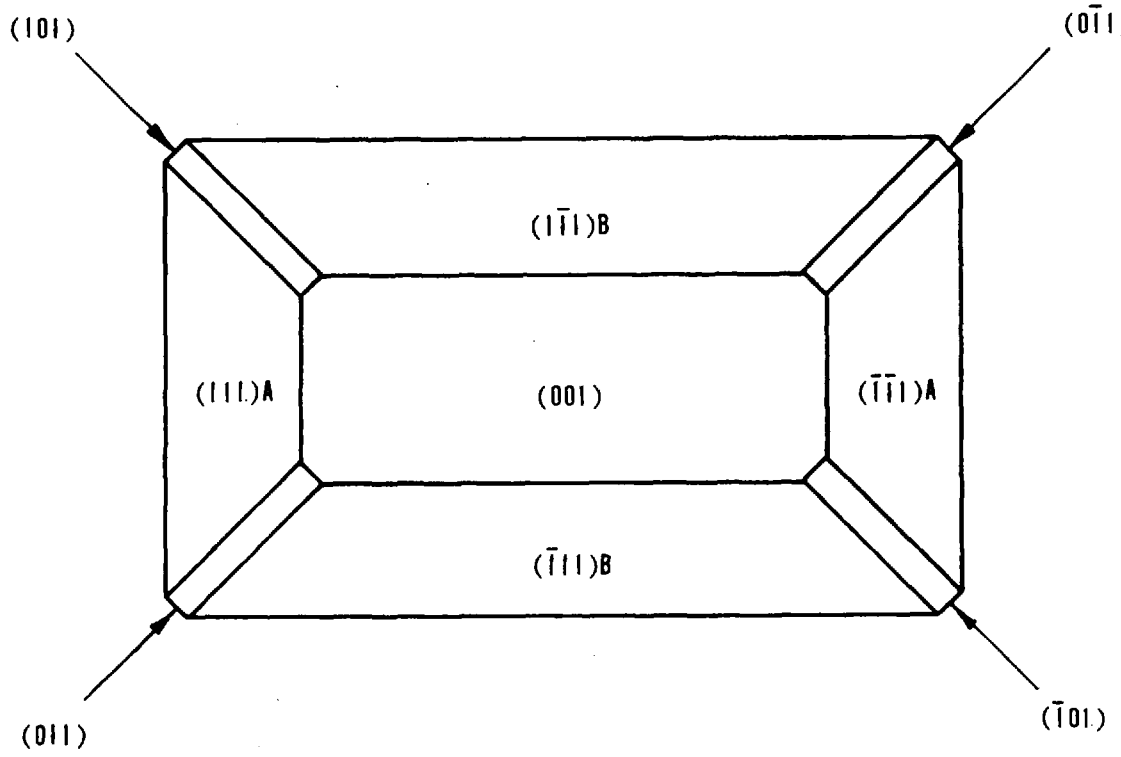

FIG.6.8. SCHEMATIC DIAGRAM OF A REGULAR PYRAMID IDENTIFYING THE EXPOSED FACES.

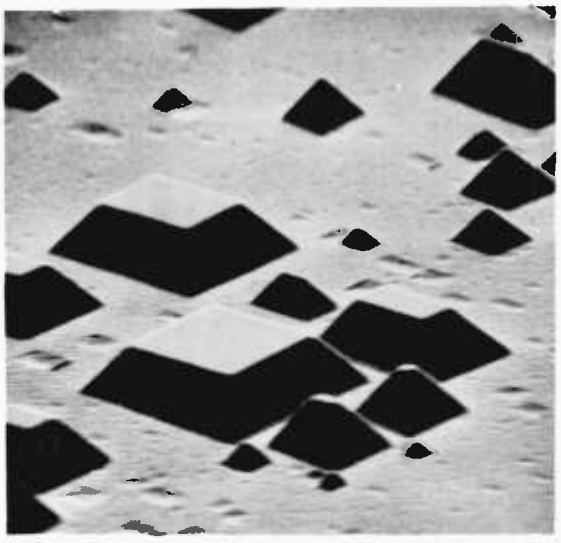

Figure 6.9

General view of regular pyramids and etch pits. Same specimen as inFigure 6.6 Scanning electron Micrograph

Angle of tilt: 60°
Magnification: x 1500

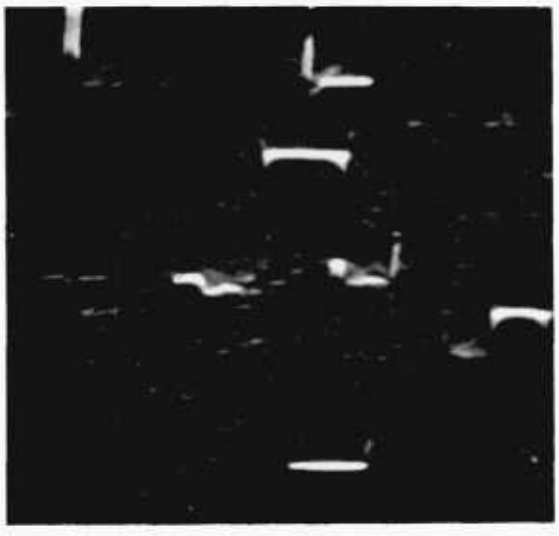

Figure 6.10

Scanning electron micrograph of same specimen as Figure 6.6 showing pyramids growing at the edges of etch pits

Angle of tilt: 30°
Magnification: x 3850

Figure 6.11

Optical micrograph of an epitaxial layer showing step structure on growth hill

Magnification: x100
Growth temperature: 720° C
Temperature difference between source & substrate: 30° C
$AsCl_3$ temperature: 21° C
Layer thickness: ~400μm

examination of the dimensions of the growth pyramids was performed on two different specimens. The ratio of length to width was found to be 1.2 : 1 with a standard deviation of 0.4 on the specimen shown in figures 6.6, 6.7, 6.9, 6.11 and 2.1 : 1 (standard deviation 0.5) for the specimen shown in figure 6.5. It was mentioned earlier that Shaw[144,145] found a ratio of 40 : 1 and reasons for the discrepancy between the results were suggested. The difference between the two specimens quoted here could be due to differences in the gas composition and temperature, although impurities may also have taken some part in determining the precise ratio. A few small pyramids were observed on the underside of the substrate, the side which had been resting on the silica plate. The direction of the longer edges of the pyramids was at right angles to those on the top surface, supporting the conclusion that the side faces of the pyramids were (111)A and (111)B.

Figure (6.6) shows that the distribution of pyramids was not entirely random over the slice. As mentioned earlier in the case of etched specimens, light scratches were present on the surface of some substrates before the growth experiments were performed. There appears to have been preferential growth along these scratch marks and in some cases the growth was continuous and not in the form of isolated pyramids. The remaining pyramids had a fairly random distribution over the surface and a distribution density of $\sim 2 \times 10^6$ cm^{-2}, very similar in fact to the etch pit density mentioned previously. The size of the pyramids varied, with lengths from 1 μm – 25 μm, but the maximum height achieved (with few exceptions) was $\sim$ 10 μm.

Some small pyramids were observed to be growing on the sides of etch pits (figures 6.9 and 6.10). The growth on such sites is unlikely to have been due to dislocations since they would be expected to be situated in the centre of the etch pit. From figure 6.10 it is clear that growth has occurred at the edges of the pits and not on any particular side, but in a variety of positions around the edge. The presence of an inert impurity film could have been responsible for this behaviour: if evaporation occurred at some weak point in a surface film of impurity, then as evaporation proceeded, the impurity film could have collapsed into the etch pit. It is conceivable that in such a situation, the edges of the etch pit would have least impurity allowing nucleation to occur preferentially at the edges of the pits when growth was started. This explanation it must be emphasised is purely

speculation and there is no evidence to substantiate it other than the growth morphology that has been described.

Features of the type described above were observed on approximately 20 specimens and therefore certain general comments summarizing the type of growth observed can be made. Pyramids did not occur on surfaces where a complete epitaxial layer had been formed during growth, only on regions of the original substrate surface. Even on specimens where most of the initial substrate surface was covered, pyramids were observed in the remaining regions. There is evidence that the initial layer on the substrate is formed by coalesence of pyramids and this is supported by the fact that in figure 6.7 it can be seen that the complete epitaxial layer is bounded by (111) faces. These faces would be expected if the layer was formed by coalesence of pyramids. Growth of "ribbon" layers resulted from preferential nucleation along line features, possibly scratches on the surface, followed by coalesence. Figure 6.6 shows some line features where the ribbon layer is not completed. Figure 6.6 also shows rounded growth hillocks on the ribbon layer, which were similar to those found on complete epitaxial layers and such hillocks always had defects visible at their peaks (figure 6.11). The defect shown in figure 6.11 had a spiral step structure radiating from it. Short line defects are visible and these have been ascribed to stacking faults by other workers[146].

Growth hillocks or pyramids on gallium arsenide have been previously reported[71,106,146-148] and their formation has been attributed to particles of impurity[106], surface contamination of unknown origin[71,146] and gallium droplets on the surface of the substrate[147,148] or gallium inclusions[148] acting by vapour-liquid-solid growth to form hillocks. However the hillocks described were not isometric, but were usually rounded and more irregular in shape. Such pyramids were observed on heavily tellurium doped substrates ($\sim 2 \times 10^{18}$ carriers cm^{-3}) during the present work and these are shown in figure 6.12. It is possible that non-uniformity in the substrate material was responsible e.g. segregation of tellurium, since the distribution of hillocks was not random over the slice.

The isometric pyramids referred to in this thesis were only observed on the original substrate surface and not on an epitaxial layer, indicating that the initial epitaxial layer growth was different from the subsequent growth. The possibility of lattice defects being the cause of pyramid growth has been discussed and it was noted that pyramids often

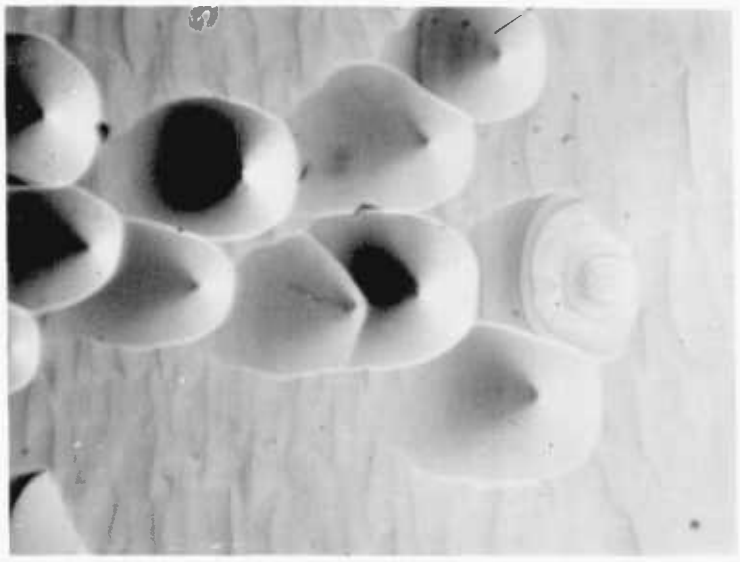

Figure 6.12

Growth hillocks on a tellurium doped gallium arsenide substrate.
Magnification: X40

formed on the edges of etch pits and never in the centre. If this is typical of all pyramid formation then it is unlikely that lattice defects are the cause since any defect would be expected at the centre of the etch pit. If pyramid formation was due to inclusions or segregation then a variation in pyramid distribution over the slice would be expected; however this was not observed.

6.1.4 Growth on specimens coated with a layer of carbon

Contamination is well known to affect crystal growth and morphology, e.g. Booker and Joyce[149] studying the epitaxial growth of silicon by silane molecular beam found that the presence of hydrocarbon vapours in the equipment affected the substrate surface and subsequent growth. Gallium arsenide has been shown to possess a film of impurity after polishing[142] (see also earlier section on slice preparation) and Auger spectroscopy studies[141] showed that the substrates used in this work had carbon on the surface at least 20 Å thick. Since such a film is highly likely to affect epitaxial growth, a few experiments were performed using substrates which had been deliberately coated with carbon. A slice prepared in the usual manner was placed in a vacuum chamber and half of the surface was covered with a carbon film by evaporation; the other half of the slice being shielded from the evaporated carbon beam and used as a control sample.

Considering first chemical vapour etching, a slice with a 150 Å carbon film was etched for several hours and a dramatic alteration in the etching rate was observed: the carbon coated side etched at a much slower rate than the control side. Figure 6.4 shows the control side which was grossly etched and figure 6.13 shows the carbon coated side which had a much shallower etch structure with a few regions of more gross etching. Some regions of the carbon coated side were high compared with the surrounding surface and appeared to have had only a small amount of material removed.

The effect of a carbon film on growth was equally dramatic, very little growth occurring on a slice having ~ 100 Å of carbon on the surface, while the control side had grown significantly (figure 6.14). The ratio of the amount grown on the coated side to that of the control side was approximately 1 : 15. Small, fairly regular pyramids were found on the coated side of the slice, although the facets on the pyramids were less well defined than those discussed earlier (figure 6.15). Similar results were obtained with a 15 Å thick film. One notable feature of the pyramids was that they were epitaxially related

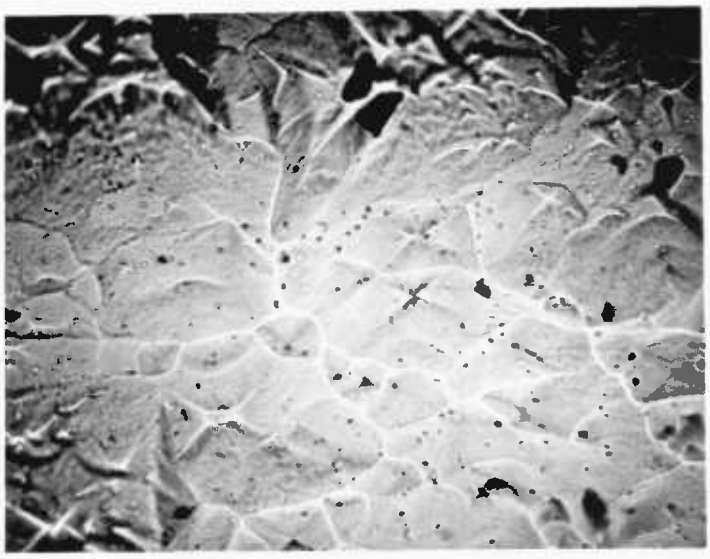

Figure 6.13

Optical micrograph of etched surface on the carbon coated side (150 Å) of the same specimen as in Figure 6.4

Magnification: x575

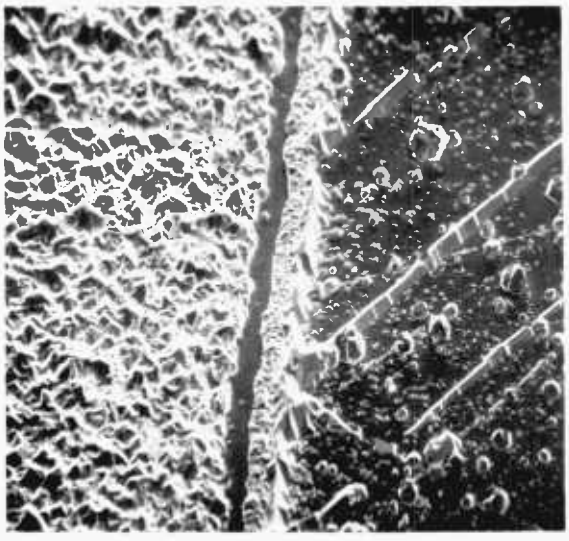

Figure 6.14

Scanning electron micrograph showing growth on a specimen half covered with a 100 Å thick carbon film. The carbon coated side is on the right

Angle of tilt: 45°
Magnification: x85

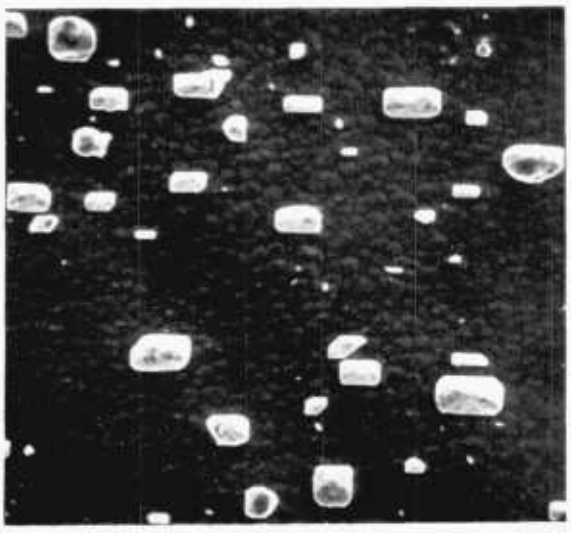

Figure 6.15

Scanning electron micrograph showing details of growth on a specimen coated with a 100 Å thick carbon film

Angle of tilt: 0°
Magnification: x1050
Growth temperature: 815° C
Temperature difference between source & seed: 53° C
$AsCl_3$ temperature: 0° C

to the substrate despite the thick carbon film. Similar phenomenon of orientation through a thick amorphous carbon layer have been reported by Distler et al[150,151], who suggested that the presence of long-range active centres was responsible for the epitaxial relationship. This conclusion was questioned by Chopra[152,153] after unsuccessful attempts to reproduce Distler's results. Ackermann et al[154] subsequently showed that long-range centres can be due to direct contact through faults in the amorphous film. It is therefore possible that the carbon film deposited in the present work could have been discontinuous in places thus allowing some epitaxial relationship between the pyramids and the substrate to be established. This conclusion is supported by the fact that growth on carbon coated slices was found to take place preferentially at certain places, giving rise to lines of growth (figure 6.14). Such line features could well have been formed along cracks in the carbon film; they were shown by Lang topographical X-ray techniques to be extensively twinned with respect to the substrate as were some of the larger irregular island features visible in figure 6.14.

6.1.5 General discussion of growth morphology

The results obtained on carbon coated slices showed a marked similarity to those described earlier on uncoated slices. It is likely therefore that isolated growth (instead of uniform growth) on substrates prepared by the polishing method described earlier, was due to the presence of an impurity film on the surface of the slice. Since the pyramid features were often 10 μm high, they were unacceptable where layers of 1 μm thickness are required. In order to achieve less contaminated surfaces, the cleaning procedures used in slice preparation were made more rigorous, e.g. solvents were changed more frequently, slices were cleaned in the soxhlets for longer periods of time and, in later experiments, by etching with 3 : 1 : 1 sulphuric acid : hydrogen peroxide : water (as described in the section on slice preparation). Following this careful attention to the cleanliness of substrate surfaces, uniform, thin layers were obtained. Figure 6.16 shows an interference micrograph of a layer 2 μm thick, the parallel lines indicating the planarity of the epitaxial layer.

Summarising then, the type of growth was dependent on the initial surface of the substrate: if a film of impurity was present then pyramids and uneven growth occurred, if the film was absent or very thin, then a thin uniform growth occurred.

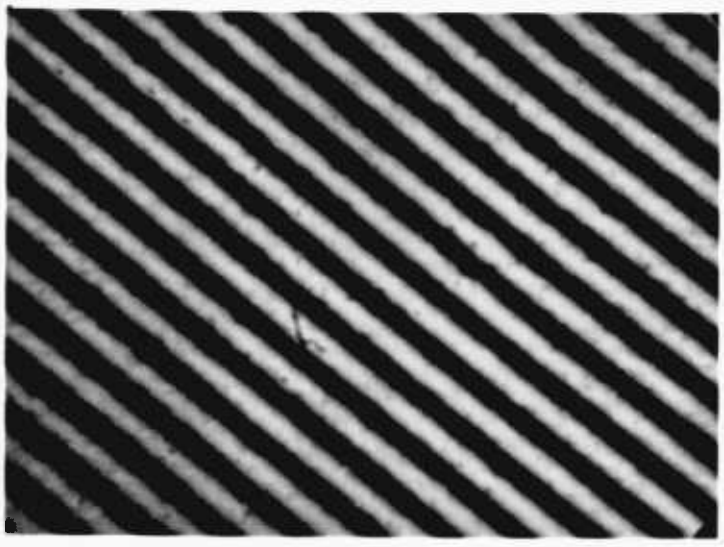

Figure 6.16

FIG 16 An interference micrograph (using sodium light) of a flat epitaxial layer

Magnification: x300
Growth temperature: 745° C
Temperature difference between source & substrate: 35° C
$AsCl_3$ temperature: 0° C
Layer thickness: ~2μm

Two other factors affected the morphology of the layers and will be mentioned briefly. Firstly, leaks in the system, the effects of which have already been described. By operating the system under a small positive pressure above atmospheric pressure (20–30 torr), the ingress of oxygen during growth was prevented[119]. This increase in pressure was produced by a fine capillary at the outlet of the furnace (see figure 5.7). However, during the pumping procedures at the beginning and end of an experiment it was still possible for oxygen to enter the system if leaks were present. Secondly, small marks visible on the substrate surface prior to loading into the system usually gave rise to growth hills or regions of zero growth. These marks were either due to non-uniformity in the substrate or drying marks left by the solvents on evaporation after the cleaning procedure.

6.1.6 Ring Structures

In all the previous discussion, only the morphology determined by the substrate was considered and no account was taken of the effects of the vapour composition above the substrate. In the subsequent section morphology which appeared to be related to the gas composition and flows within the capsule is discussed.

It was noted earlier that the surface of the substrate had a slightly matt appearance after the initial etching. As growth proceeded the centre region of the slice became smooth and polished, the smooth surface then spread outwards covering most of the slice. Frequently this resulted in a 'ring' structure being formed on the surface which was usually smooth in the centre, surrounded by rings of varying degrees of surface roughness. Parts of such ring structures are shown in figures 6.17 and 6.18. (The sample in figure 6.18 was cracked and this is responsible for the dark line across it.) On some occasions the centre region subsequently became rough (figure 6.19) and this rough region was surrounded in turn by a smooth ring and a further rough region. Ring structures were always concentric with the capsule and slices displaced to one side of the capsule exhibited partial ring structures (figure 6.18), while small slices positioned in the centre of the capsule did not show ring structures at all. The shape of the substrate seemed to affect the shape of the ring (figure 6.20), but the effect was only small. The ring structure shown in figure 6.20 is complex, one side of the slice had a facet as indicated by the small ring, also there seemed to be a ring which did not exactly coincide

Figure 6.17

Part of a ring structure with a smooth centre region.
Magnification: approx. X12

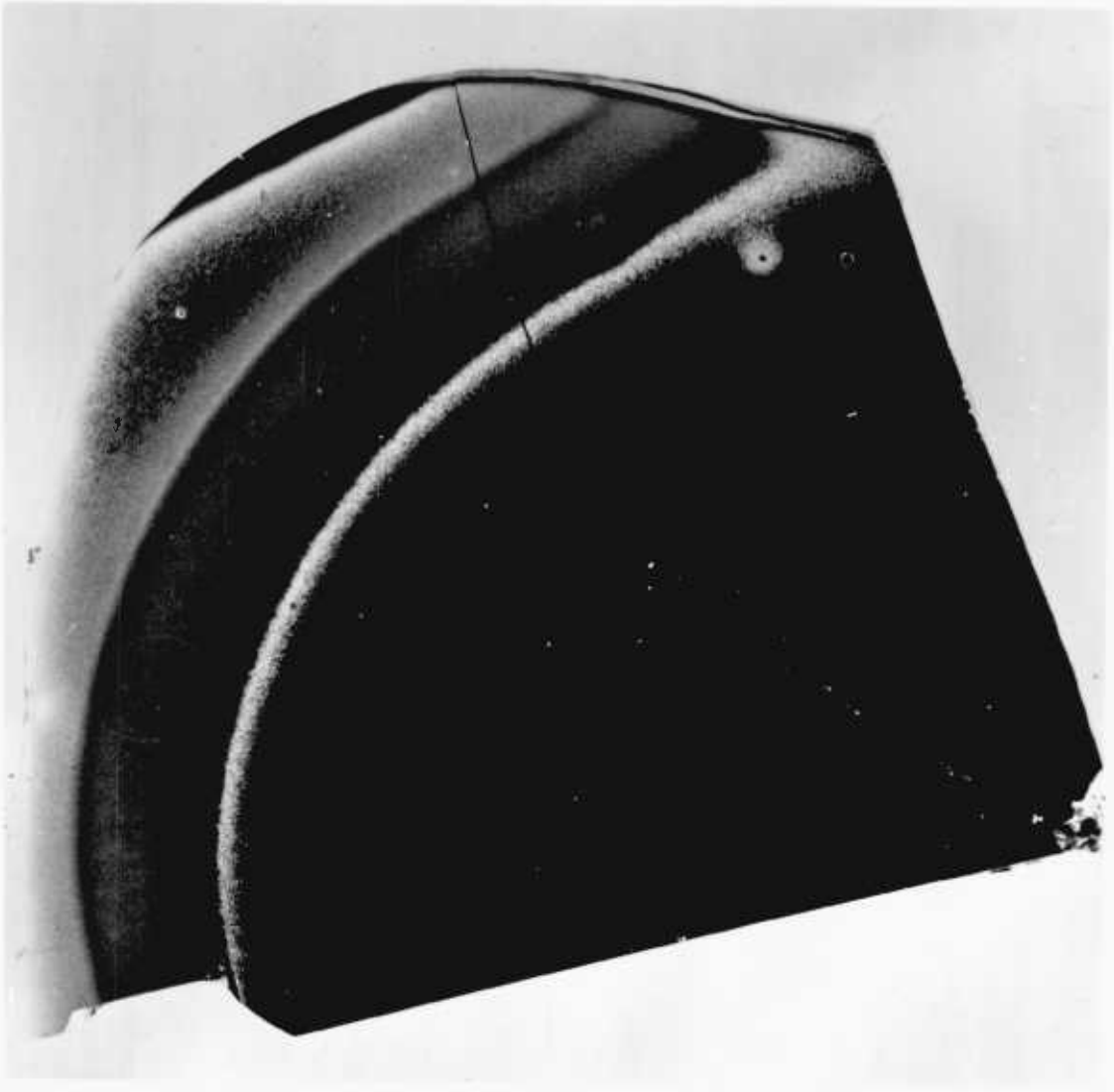

Figure 6.18

Part of a ring structure with a smooth centre.
Magnification: approx. X12

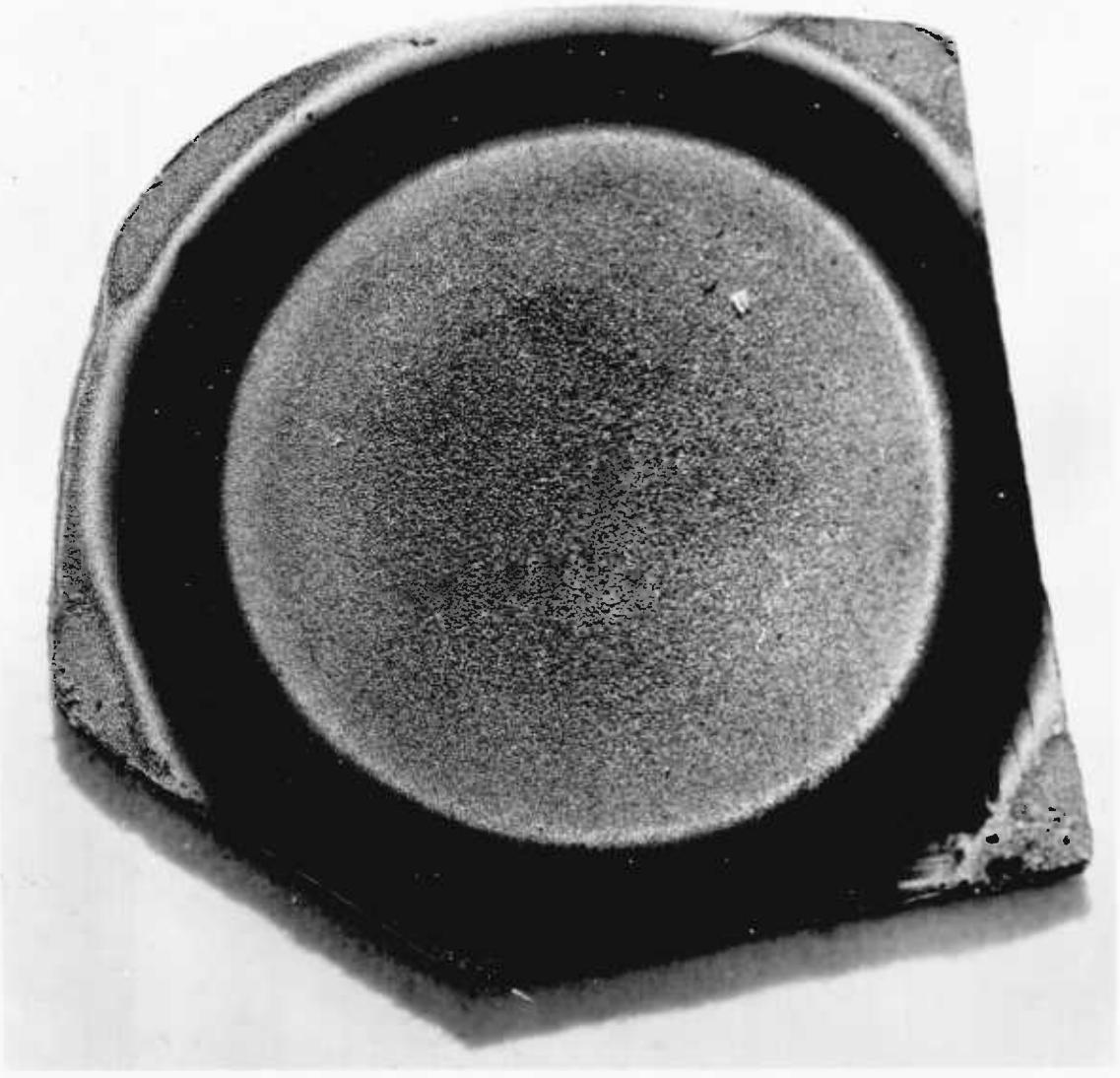

Figure 6.19

Ring structure with a rough centre.
Magnification: approx. X9.5

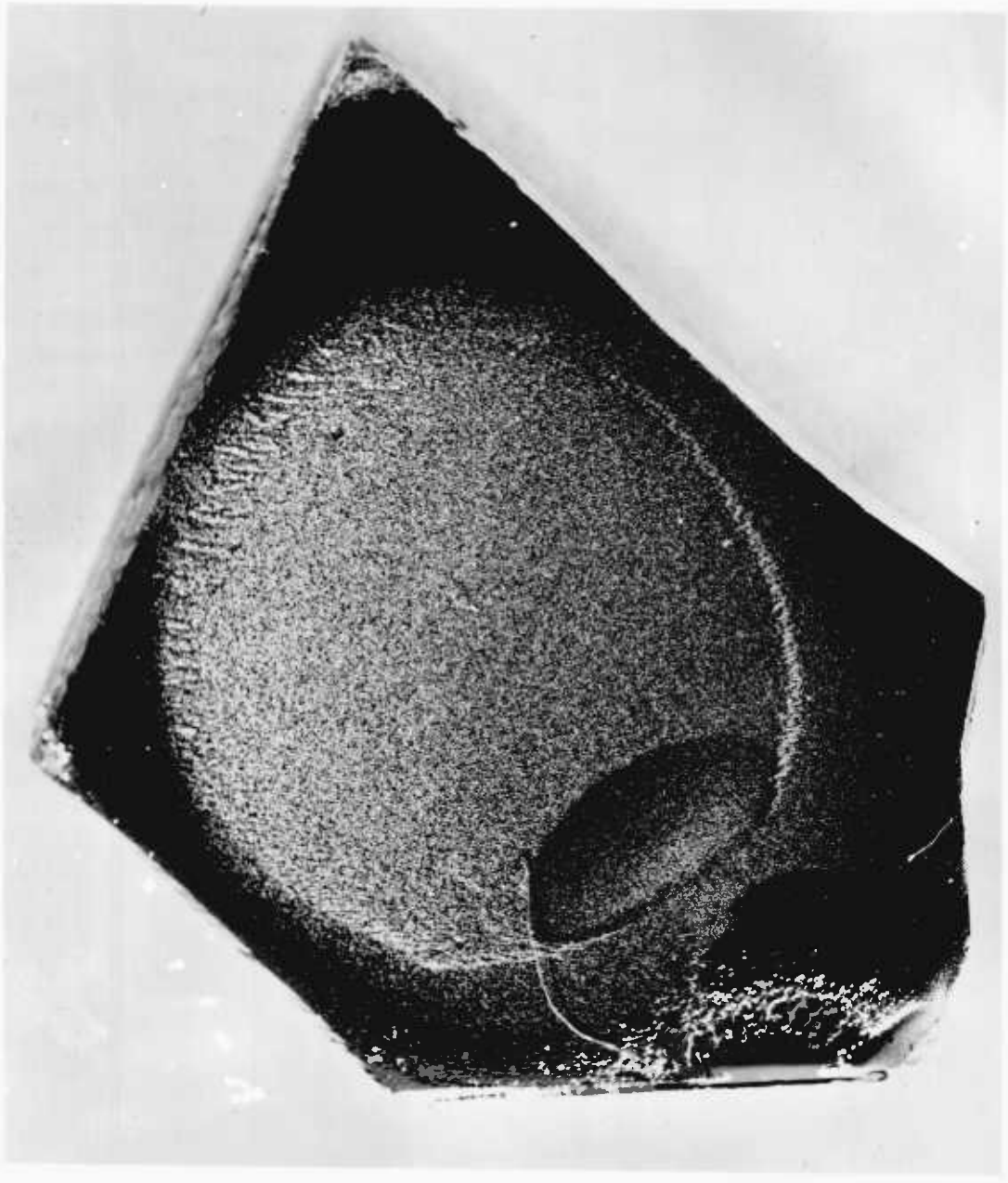

Figure 6.20

An asymmetric ring structure.
Magnification: approx. X9

with the smooth-rough boundary. The centre regions of the ring structures was found to have more material deposited on it than at the edges, which is consistent with the observation that the rings developed from the centre and grew out towards the edges.

The formation of 'ring' structures cannot be explained in terms of the one-dimensional theoretical model presented earlier in the thesis. However it is possible to consider the subject qualitatively in the light of that model. Application and discussion of the theoretical model to the capsule system will be given later in this chapter, for the moment discussion will be confined to finding an explanation for ring structures.

There are two possible factors which could be involved in ring formation: temperature variations across the slice and convection in the capsule. In addition there will inevitably be some interplay between these affecting the growth rate and any impurities on the surface of the substrate. Impurity effects alone are unlikely to have caused ring structures so clearly defined and so reproducibly. Temperature variations across the slice could be present, since the lateral temperature gradients across a tube furnace are such that the centre is always cooler than the walls of the tube, due to radiative heat losses from the ends of the furnace tube. Attempts were made to even out any temperature gradients across the slice by resting the slice on a single crystal alumina plate. It was expected that the alumina, being a better thermal conductor than silica, would smooth out any temperature variations but no difference was observed in the results obtained. It was not possible to detect any temperature differences across the slice using an optical pyrometer (resolution $\sim 2^{\circ}K$). It would appear therefore that temperature variations across the slice were small and therefore unlikely to play a major part in ring formation.

Viscous forces in the gas phase give rise to lateral variations in the flow velocity in the capsule: at the walls of the capsule the gas velocity will be zero and at the centre it will be a maximum. A parabolic variation in flow velocity with the radial co-ordinate was anticipated as predicted by Poiseuille's analysis. This variation meant that the nett flux of material down the capsule was a maximum in the centre of the capsule. The precise way that the flux varies across the capsule is not known since radial partial pressure gradients will be formed as a result of the variation in flow velocity. The above analysis is consistent with the centre region of the slices usually having a thicker deposit than the edges.

Convection in the gas phase arises from variations in density gradient which can be caused by temperature gradients, this is referred to as thermal convection. Changes in gas composition along a capsule can also cause density variations which result in compositional convection. In chapter 3 it has been shown how the gas composition within a crystal growth capsule may be determined and in the table below the results are given for a hypothetical experiment with no convection (T = 1000°K; temperature difference, 50°K; and arsenic trichloride bubbler temperature, 0°C).

Species	Molecular Weight	Pressure at source (atm)	Pressure at substrate (atm)
GaCl	105.5	0.01132	0.006482
As_4	300	0.005146	0.003946
H_2	2	0.9671	0.9681
HCl	36.5	0.01649	0.02143

The density difference due to composition change is 15% greater at the source than at the substrate and the density difference due to temperature is ~ 5%. In the experimental system under discussion growth was from the top to the bottom of the vertical capsule, thus thermal and compositional convection were opposed, leaving a 10% density change which could have given rise to convection. In a system where the source is at the bottom and the substrate is at the top, convection is not possible since the denser gas is at the bottom. The convective flow pattern in the present system was dependent upon the capsule shape and temperature field within the capsule, thus if the walls of the capsule were hotter than the centre then a circulatory motion of the gas would occur with the gas at the walls rising and that at the centre falling. The transverse gas velocity variation is depicted in figure 6.21(a) and by superimposing the Stefan velocity as shown in figures 6.21(b) and 6.21(c) we arrive at two different flow velocities depending on the direction of the Stefan flow (assuming also that the magnitudes of the contributing velocity distributions are similar). Such a resultant velocity distribution could give rise to ring growth since changes in the surface morphology could arise if the critical growth flux J_{crit} is exceeded locally across the slice. To check the above explanation, a full two-dimensional analysis of the system, including convection would be required; such an analysis is not available and the task to produce one is formidable.

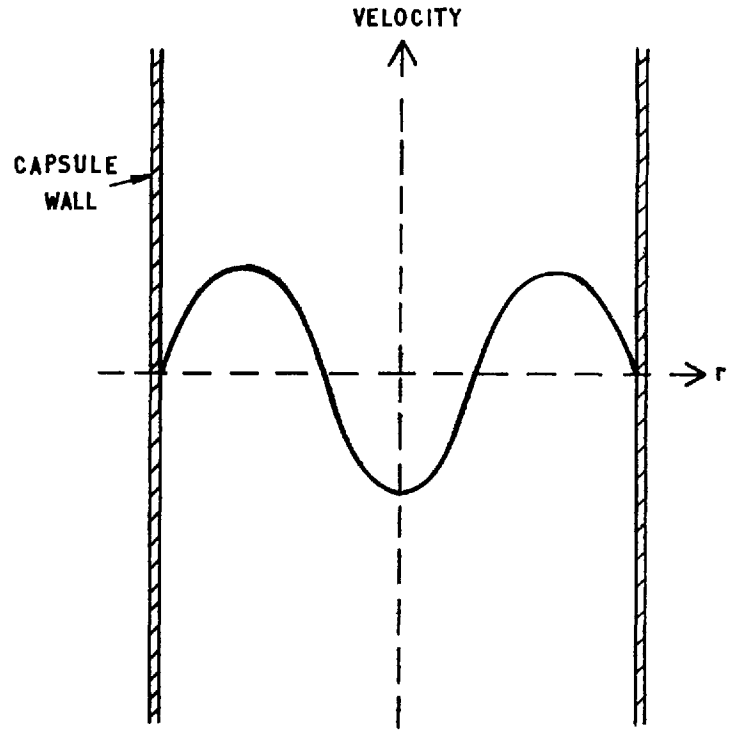

(a)

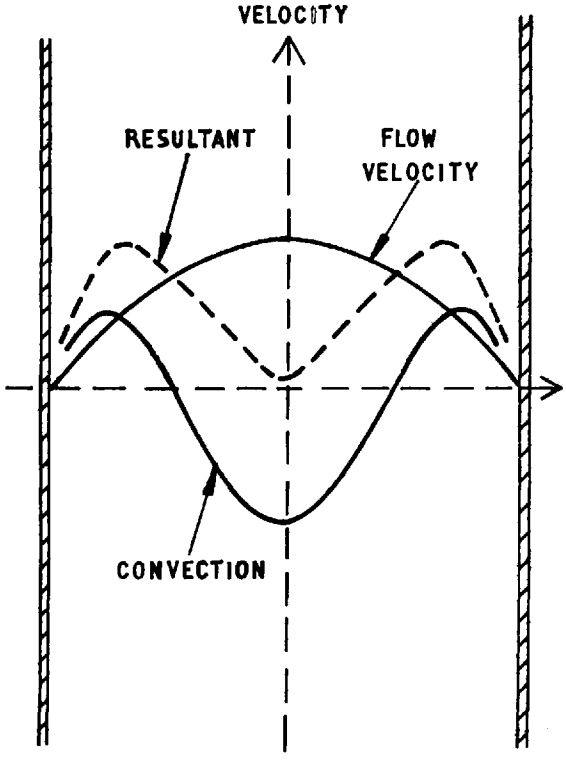

(b) UPWARDS

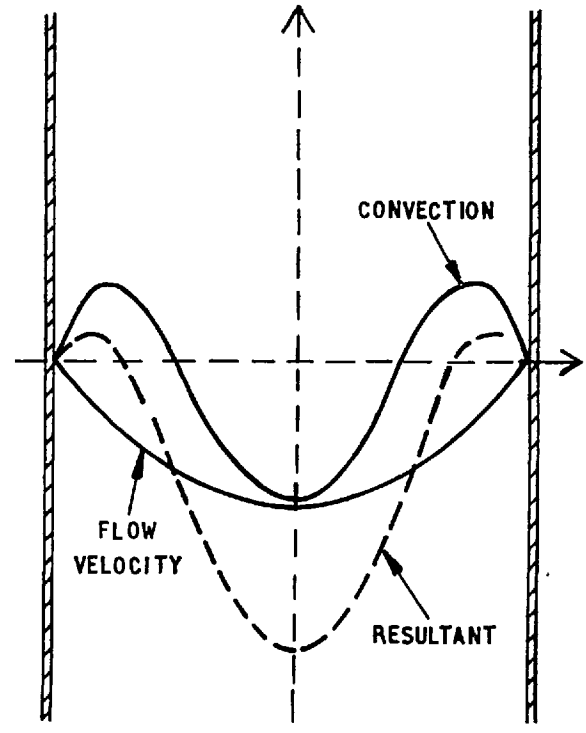

(c) DOWNWARDS

FIG. 6.21. CONVECTION AND FLOW VELOCITIES IN A CAPSULE.

One further possible explanation could account for the ring structure formation. The examples shown in figures 6.17 and 6.18 had smooth centre regions which were observed to be formed from the centre and spread outwards. Maximum growth occurred at the centre of the ring, the rough edge regions were usually pitted and might be regions where only the initial etching had occurred and subsequent growth had been absent or only very slight. In cases where the centre region was rough, as in figure 6.19, if a thin impurity film had built up on the smooth surface, then subsequent nucleation may have caused the rough finish in the centre of the slice. The remains of the smooth region can be seen as a ring round the central rough area.

In conclusion, the formation of 'ring' structures was due to a variety of factors or a combination of them but a complete explanation is not possible with the present one dimensional model and much more experimentation would be required even if a suitable model became available. Convection is undesirable if smooth uniform epitaxial layers are to be produced by the capsule method and therefore the best approach is to eliminate or at least minimise convection. A system of baffles or a method of stirring the vapour in the capsule could help and growing from the bottom to the top of the capsule would keep the more dense gas at the bottom. In connection with this last point it is worth noting that in bulk crystal growth experiments where a seed plate was used at the top of a capsule, no ring structures were observed, however, further work would be required to ascertain whether this inversion was the reason for their absence.

6.2 Comparison of Experimental and Theoretical Growth Rates

In chapter 3 a one-dimensional model of chemical vapour transport in the gallium arsenide-arsenic trichloride-hydrogen system was derived. In this section some quantitative comparison of experimental and theoretical results is made. The experimental measurement of growth rates and temperatures was presented in the preceding chapter and the uncertainties of the measurements were discussed.

Epitaxial layers of gallium arsenide on gallium arsenide substrates were deposited at temperatures in the range 950°-1100°K. The experimental values of growth rate at two temperatures 970°K and 1020°K are plotted in figure 6.22 along with the theoretical lines. The results are scattered but generally fall on or below the theoretical lines, but the errors of measurement are not sufficient to give an entirely satisfactory explanation of

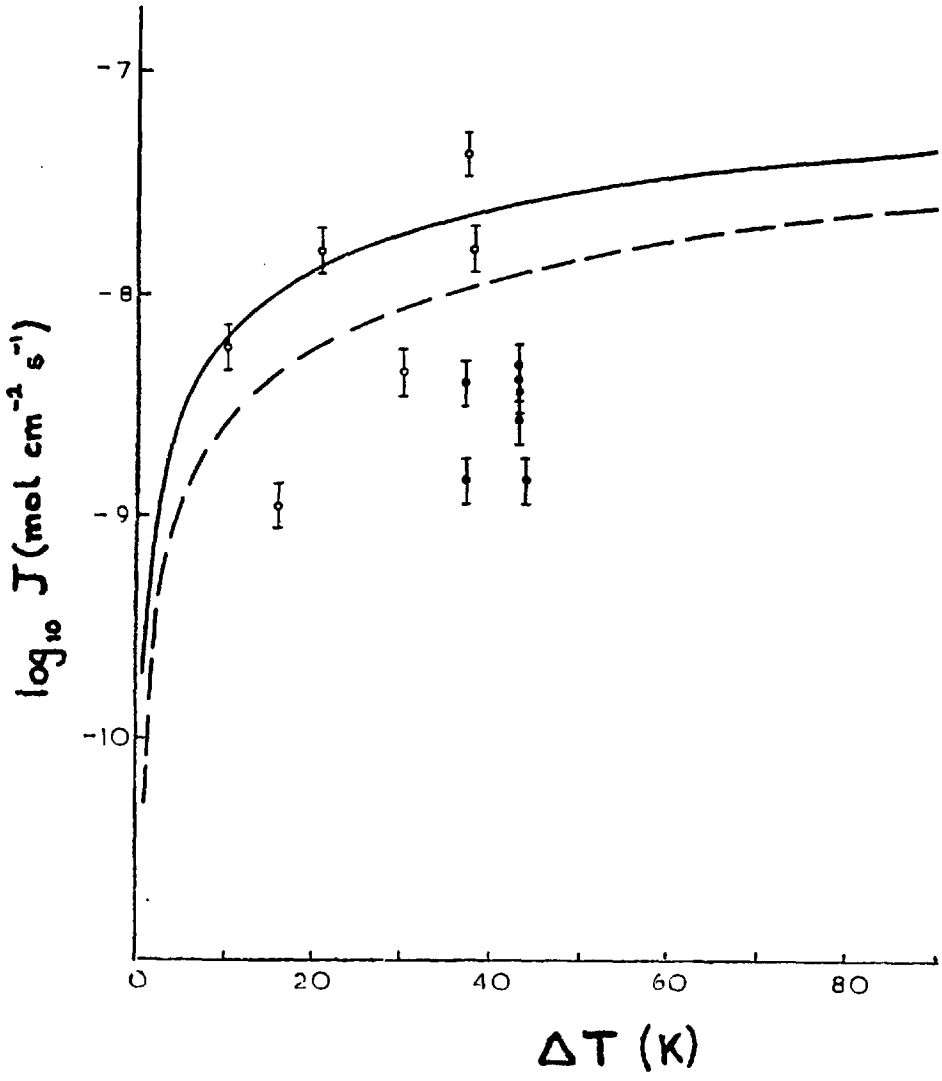

FIG. 6.22 COMPARISON OF EXPERIMENTAL AND THEORETICAL GROWTH RATES.

Solid line, $T(1)=970K$, $T_b=20C$, ○ experimental points.
Broken line, $T(1)=1020K$, $T_b=0C$, ● experimental points.

the scatter. It is possible that there is an activational barrier to the surface reaction and this barrier varies from one slice to another, this is supported by the fact that the results fall below the theoretical lines. Variations in the activational barrier could arise from an impurity layer which alters in thickness from one slice to another, e.g. the presence of a carbonaceous impurity layer of the type already discussed. A further possibility is a small variation in crystallographic orientation from one substrate to another. The theoretical growth rates appear to be in reasonable agreement with the maximum rates measured, these values probably occurred when the activational barrier was low.

There are two main limitations of the theory which are apparent in the light of the experimental evidence:- (1) the need for the theory to be extended from a one-dimensional model to a three-dimensional model and (2) the need to assume equilibrium at the source and the seed to obtain the boundary conditions to solve the flow equations. The theory has been extended to take the latter into account in the case of a simpler system[32] and work is also in progress on extending the theory to open flow gallium arsenide deposition systems and to include the possibility of non-equilibrium conditions between solid and vapour[132].

6.3 Bulk Crystal Growth Experiments

Bulk quantities (20g) of gallium arsenide were purified to provide source material for thin film epitaxy experiments by the chemical vapour transport method described in the previous chapter. In addition, a few experiments were made to assess the method as a means of growing large single crystals.

In experiments where no seed plate was used, many crystallites ($\sim$ 100) were formed in the tip of the capsule. As these crystallites grew, some would dominate and develop until there were approximately a dozen crystals growing. Further nucleation occurred during growth forming more crystals and the final boule was composed of small crystals up to 150 mm^3 in size (figures 6.23 and 6.24). Some of the small crystals exhibited large facets at the growth interface, which were probably slow growing faces of the crystals. The reasons for nucleation of further crystals on these faces will be discussed when considering the growth of large single crystals.

Figure 6.23

Gallium arsenide crystal boule (side view).
Magnification: approx. X9

Figure 6.24

Gallium arsenide crystal boule (plan view).
Magnification: approx. X9

Some regrowth of the source material occurred during the experiment (figure 6.25) since it was in a part of the furnace where the temperature gradient made the bottom of the source material cooler than the top and therefore growth towards the bottom of the capsule occurred. There is also clearly visible a black fibrous material on the surface of the source material and on the walls of the capsule where the gallium arsenide had been during the early stages of the experiment. This fibrous residue, though often observed was not always present in such large amounts and it remained when the gallium arsenide was removed by chemical vapour transport.

The residue appeared to be some impurity present in the original boat grown material and was found to be fairly inert to the common inorganic acids. A sample was sent for analysis to AERE, Harwell. The small quantities available precluded complete analysis, but a spark source mass spectrograph showed silicon to be the main constituent with gallium and arsenic as minor species. The analysis did not include tests for carbon, nitrogen, oxygen and tantalum but all other elements between boron and uranium were looked for and trace amounts of the following elements were found: sodium, potassium, chromium, aluminium, nickel and cobalt.

The above evidence indicated that some purification was occurring in the capsule system and that further investigation of the purity of the material was desirable. Samples of the gallium arsenide were therefore investigated by cathodoluminescence, where a high energy electron beam was directed at a sample of gallium arsenide and the intensity of the luminescence was measured. Five different bands were observed[155,156]:-

(i) at 1.5eV which corresponds to transitions between shallow donor levels to the valence band

(ii) at 1.46eV which corresponds to transitions between shallow donor levels to shallow acceptor levels

(iii) at 1.36eV corresponding to arsenic vacancies

(iv) at 1.25eV corresponding to gallium vacancies associated with acceptors

(v) at 1.0eV the origin of which is not known.

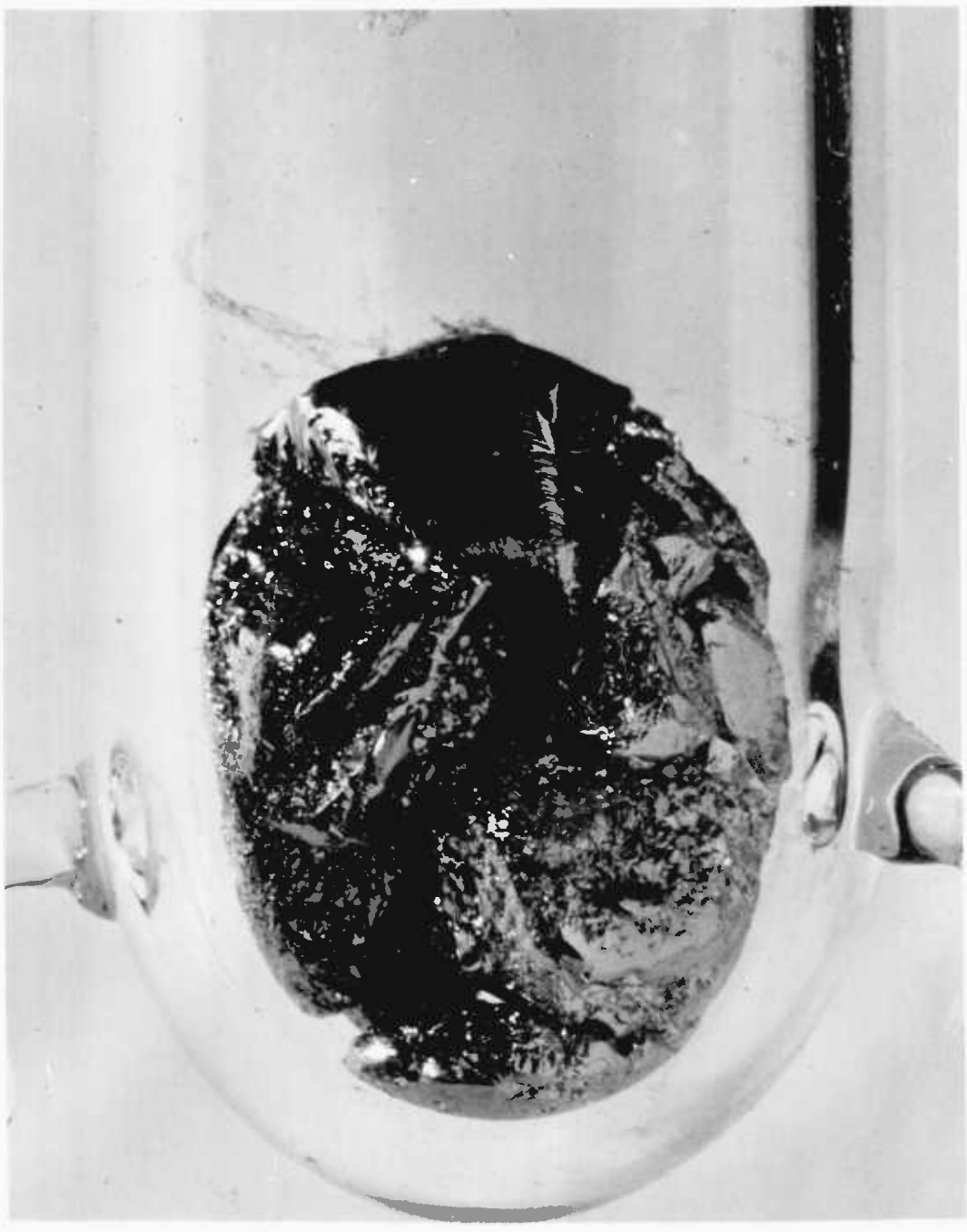

Figure 6.25

Gallium arsenide source material.
Magnification: approx. X5

In the table below the figures are in arbitrary units, all measurements being made under identical conditions, the figures taken being the peak maxima. The following samples taken from one experiment were studied:

(a) the original starting material as received from the suppliers

(b) the residue left at the source end of the capsule after the experiment

(c) the translocated material, a sample of the gallium arsenide deposited in the early stages of the experiment

(d) the translocated material, a sample of the gallium arsenide deposited in the later stages of the experiment.

Band	Sample			
	(a)	(b)	(c)	(d)
(i)	85	15	15	5
(ii)	2	15	n.d.	n.d.
(iii)	90	700	60	60
(iv)	n.d.	100	n.d.	n.d.
(v)	n.d.	300	n.d.	n.d.

n.d. - not detected

The results given in the table confirm that considerable purification occurred in translocating the material. The decrease in the 1.5eV band indicates a decrease in the number of shallow donors present. There also seems to have been some further improvement in the purity of the transported material as the growth proceeded (as far as shallow donors are concerned). The decrease in the 1.46eV band indicates a decrease in the number of acceptors. An improvement is also observed in the decrease of arsenic vacancies. It should be mentioned that copper would also give rise to a band at 1.36eV but attributing this peak to copper was not favoured[157]. One feature of the results is a little difficult to understand and that is the high intensity of the 1.36, 1.25 and 1.0eV bands in the residue, all of which are considerably greater than in the original starting material. The increase is larger than can reasonably be explained by the impurities removed from the translocated material being concentrated in the residue since approximately only one half of the material placed in the capsule was transported. It is possible that the impurities remaining in the source material could have been concentrated at the surface of the gallium arsenide and thus give a reading which was not typical of all the material. The

results of the cathodoluminescence studies confirm that the translocation of gallium arsenide by the capsule method purifies the material considerably.

Having presented the experimental evidence for the purification method, brief consideration will now be given to the principles behind it. For convenience of discussion, impurities may be divided into two types: those which readily form volatile species and those which do not. The less volatile impurities have small partial pressures and hence their rate of transport to the seed is small. Inert and involatile impurities remain on the surface of the source as they become uncovered during the experiment. The degree of purification obtained is high in the case of the less volatile impurities.

Volatile impurities enter the vapour as they diffuse out or are uncovered by transport of the gallium arsenide. The Stefan flow sweeps the impurities towards the growing crystal where they accumulate. Some of the impurity is lost through the effusion hole, so the concentration of impurity above the surface of the growing crystal will reach a steady state value, determined by the rate at which it enters the gas phase at the source, the rate of incorporation into the growing crystal and the rate of removal through the hole. If the impurity enters the gas phase by reaction with hydrogen chloride and if the reaction is exothermic, then the impurity in the gas phase will transport from the cold seed to the hot source and purification will be better than if the reaction is endothermic. Any initial enrichment of impurity in the gas phase will leak out through the hole. If an impurity is present in large amounts throughout the source material and it is transported slower than the gallium arsenide then the activity of the impurity at the source will reach unity; a second condensed phase will be formed on the surface of the source and thus the activity of the gallium arsenide at the source will be decreased.

In some cases the transport of impurity can be depressed relative to the transport of gallium arsenide by adjusting the ratio of hydrogen chloride to hydrogen e.g. an impurity M forming a trihalide

$$M + 3\,HCl \rightarrow MCl_3 + \frac{3}{2} H_2 \qquad (6.1)$$

The equilibrium constant for this reaction K_M is given by

$$K_M = \frac{P_{MCl_3} \cdot P_{H_2}^{\frac{3}{2}}}{a_M \cdot P_{HCl}^3} \qquad (6.2)$$

K_M is a function of $\left(\frac{P_{H_2}^{\frac{1}{2}}}{P_{HCl}}\right)^3$ whereas with gallium arsenide:

$$GaAs + HCl \rightarrow GaCl + \frac{1}{4}As_4 + \frac{1}{2}H_2 \qquad (6.3)$$

K is a function of $\left(\frac{P_{H_2}^{\frac{1}{2}}}{P_{HCl}}\right)$ since

$$K = \frac{P_{GaCl} \cdot P_{H_2}^{\frac{1}{2}} \cdot P_{As_4}^{\frac{1}{4}}}{a_{GaAs} \cdot P_{HCl}} \qquad (6.4)$$

where a_M and a_{GaAs} in the above equations are the activities of impurity M and gallium arsenide respectively.

The value of K_M for a given temperature and total pressure is clearly more sensitive to the ratio of hydrogen to hydrogen chloride than K and could be made small relative to K, increasing the degree of purification.

It has already been mentioned that preliminary investigations were made into the possibility of growing large single crystals by the capsule method. To do this a seed plate of nominally undoped gallium arsenide, (100) orientation, was used and the experiment performed as described in chapter 5. Initially the slice grew uniformly maintaining a flat and polished interface, but as growth continued, facets developed at the edges: four facets inclined to the (100) surface one on each of the four sides of a square. When 2-3 mm of growth had occurred on the original slice, small crystals were formed on two opposite facets. Owing to a power failure, the experiment was terminated earlier than intended and the resulting material is shown in figures 6.26, 6.27 and 6.28. The centre region of the material appeared to be single crystal, probably having the same orientation as the original substrate. The two facets not having additional crystal outcrops on them showed a form of patterning consisting of variations in surface roughness. The centre region of the pattern on the facet visible in figure 6.26 is shown in more detail in figures 6.29 and 6.30, figure 6.29 being an optical micrograph under normal reflected light, and figure 6.30, the same region using interference contrast. Despite the poor surfaces of these two facets it was possible to make some measurements using a goniometer and they were identified as being (111) faces assuming the large central flat region is (100). The threefold symmetry

Figure 6.26

Gallium arsenide crystal.
Magnification: approx. X9

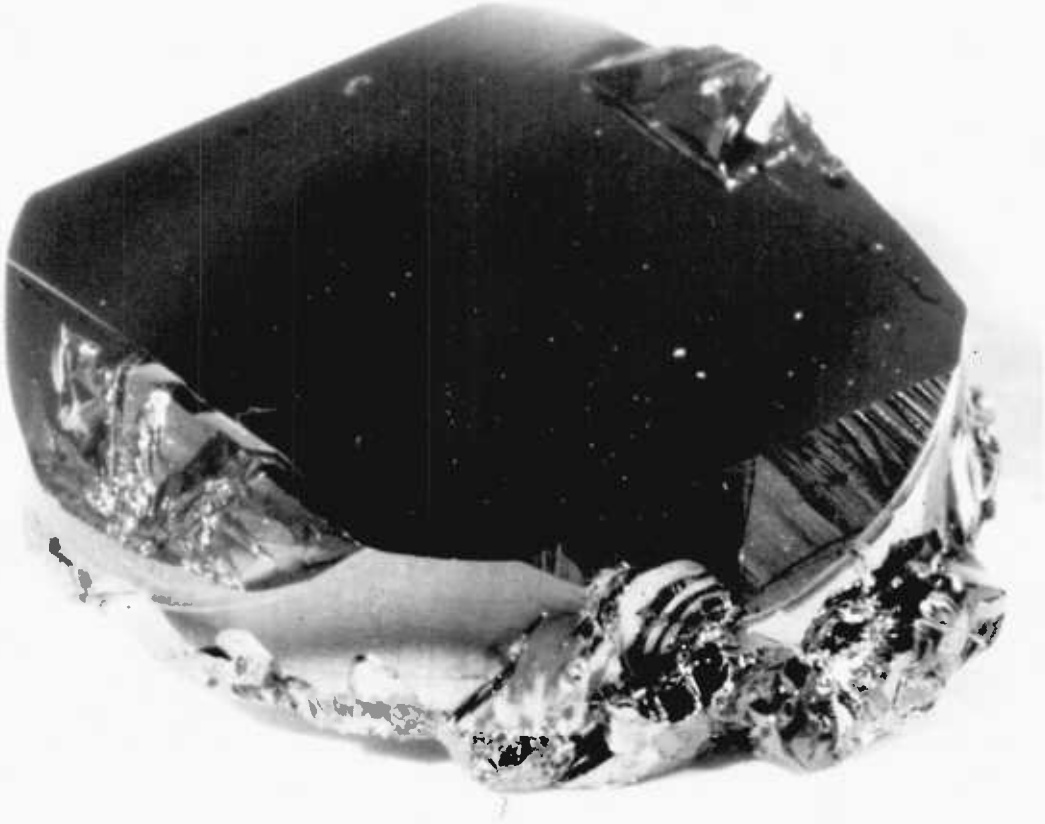

Figure 6.27

Gallium arsenide crystal.
Magnification: approx. X9

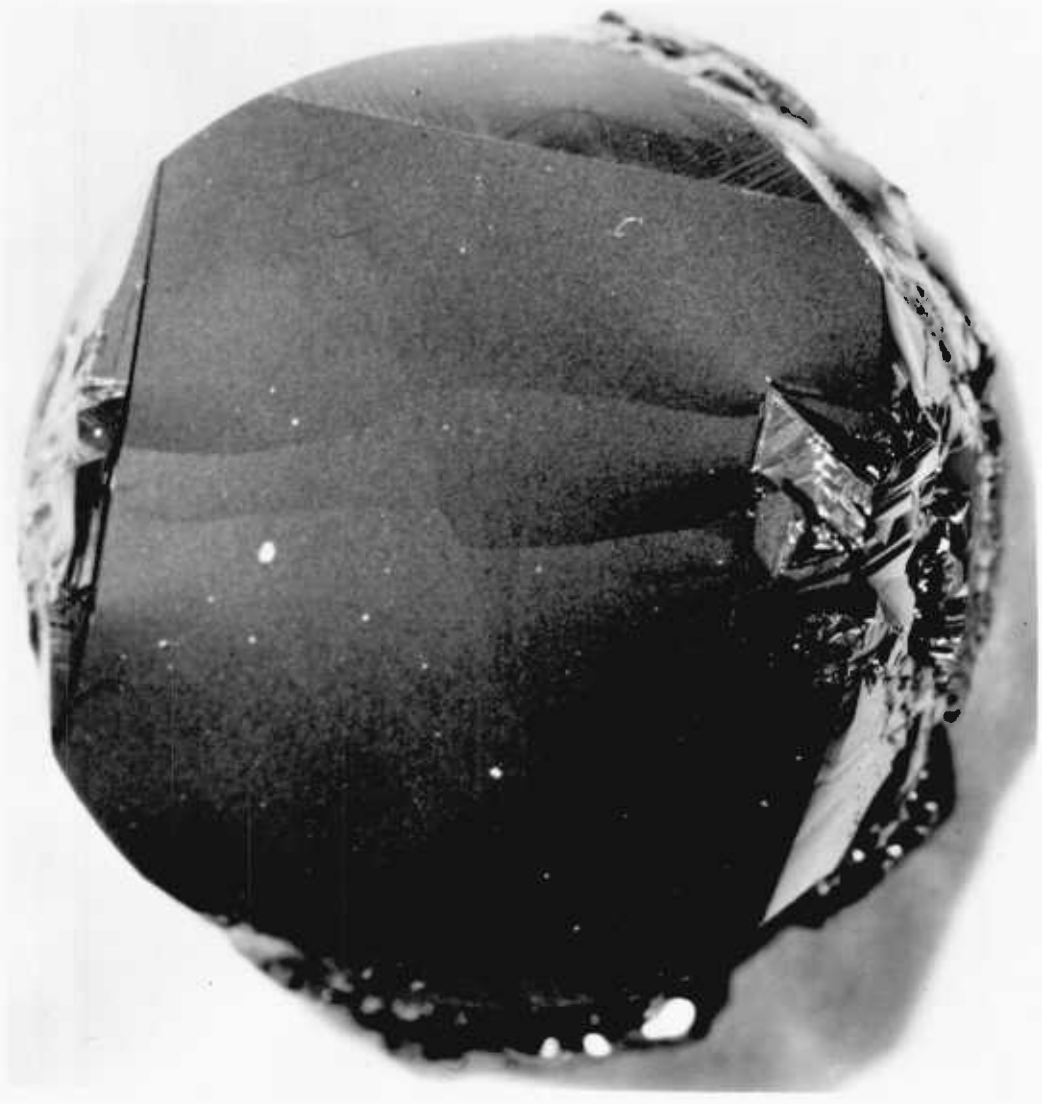

Figure 6.28

Gallium arsenide crystal.
Magnification: approx. X9

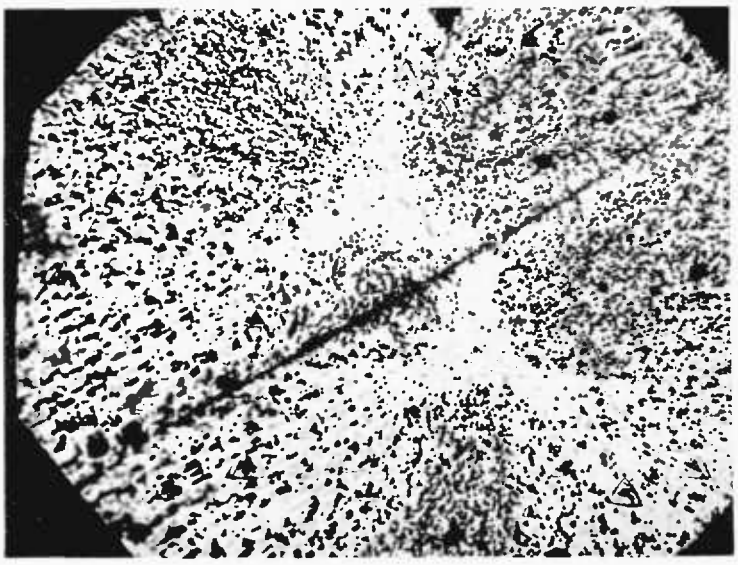

Figure 6.29

Part of a facet on the gallium arsenide crystal shown in Figure 6.26.
Magnification: approx. X100

Figure 6.30

As figure 6.29 but using interference contrast

of some of the features on the facet (figure 6.30) supports the above assignment[148].

Figure 6.28 shows a diagonal line across the central region with further lines radiating from the small crystal outcrops on the edges. Using interference contrast on the microscope it was found that steps spreading out from these crystals covered much of the slice (figure 6.31). The crystals at the edge seemed to be of a different orientation from the original substrate. To confirm this and to check on the crystal quality, reflection Lang X-ray topographs were taken and figure 6.32 shows a topograph of a $6\bar{2}0$ reflection using copper Kα radiation. The topograph shows that the centre region of the slice was single crystal although there were fairly high dislocation densities in places (indicated by the light coloured patches). The extra crystals at the edges were not of the same orientation as the rest of the crystal and they were subsequently identified as twinned regions by selecting a 440 reflection which reflects only twinned regions.

Summarising the results obtained, it has been shown that the material obtained was single crystal over most of the slice having (111) facets forming at the edges of the (100) surface. Two of the opposite (111) facets had twinned regions of the crystal growing on them, and these were beginning to affect the growth on the 100 face by acting as centres of growth, layers spreading out from them across the surfaces.

Although only preliminary experiments were carried out on single crystal growth the results obtained were encouraging, indicating that the capsule method could be used for this purpose. The method has been shown to purify the normal boat-grown material, therefore high purity single crystals could well be obtained by this method. Typical growth rates for bulk transport experiments were up to 0.06 g hr^{-1} at approximately 750°C depending upon the arsenic trichloride concentration in the gas stream. The rate of loss of material from the capsule (averaged over the experiment) was equivalent to $\sim$ 10% of the growth rate in a capsule with two holes each 0.012" diameter.

Figure 6.31

Growth steps on (100) surface of the gallium arsenide crystal shown in Figure 6.28.
Magnification: X50

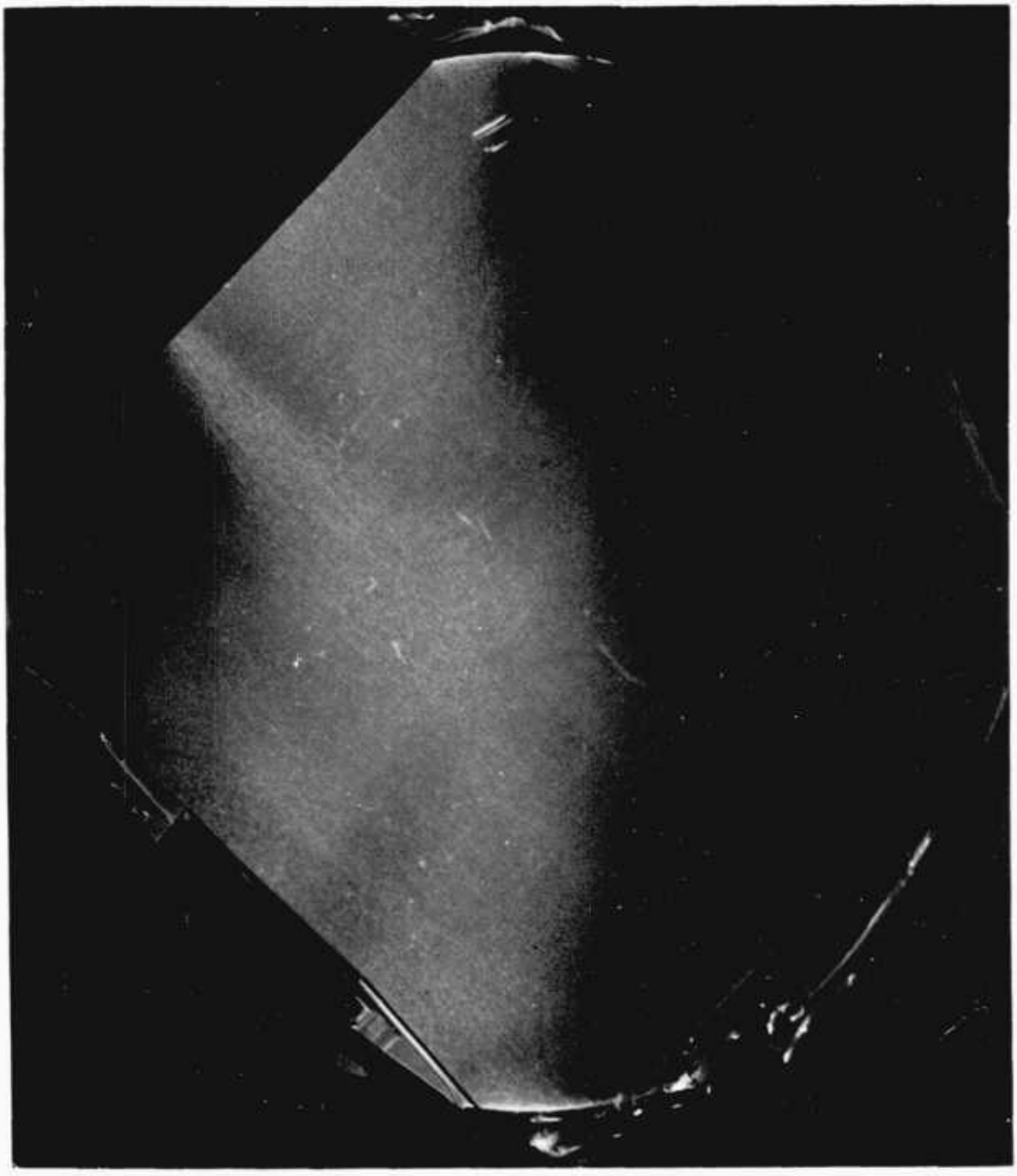

Figure 6.32

Reflection Lang X-ray topograph of the crystal shown in Figure 6.28
$6\bar{2}0$ reflection. CuKα radiation. Magnification: X12

CHAPTER 7

CONCLUSIONS

CHAPTER 7

CONCLUSIONS

In an interdisciplinary subject such as crystal growth, the possible lines of research are numerous and it is always easier to decide which subjects should have been investigated, and in which order, having completed a research programme, than it is to make those decisions at the beginning. In consequence, the order in which the research, presented in this thesis, was carried out, was not the logical one that has been used in reporting the results and observations. On entering the crystal growth field, or a new branch of it, due to an initial lack of bearing and insight, large amounts of information, covering a range of topics too large to cover adequately, were collected. It was soon clear that one's effort had to be confined to one or two aspects if any significant understanding of the subject was to be achieved.

It was obvious that different laws governed the sequential processes involved in crystal growth; for a simple system this would involve gas transport and surface kinetics, but as systems become more complex, parallel processes also occur. Much of the research performed in crystal growth has been based on a purely empirical approach: control as many variables as possible, alter them a little at a time until adequate results are achieved. Understanding of the processes involved was frequently poor, with vague, qualitative statements about surface or diffusion controlled growth. It was considered important therefore, to try and provide a more concise formalism and the theoretical model presented in chapter 3 is the result of many years of discussion (and argument) amongst my colleagues and myself at the Post Office Research Department.

Figure 7.1 is a picture which is helpful in understanding the processes involved in crystal growth, it is a plot of free energy versus distance in the growth system. The right hand part of the picture shows the variation in $RT\ell nK^*$ resulting from transport considerations: the potential difference between the source at $x = l$ and the crystal surface at $x = 0$, is the free energy required to drive the transport. The potential difference $RT\ell n\left(\frac{K^{*(o)}}{K^{(o)}}\right)$ is the free energy required to drive the surface processes. The broken line marked $RT\ell nK^{(x)}$ is not a function of any transport consideration, but is solely dependent upon the local temperature, $T^{(x)}$, and the vertical distance between this line and

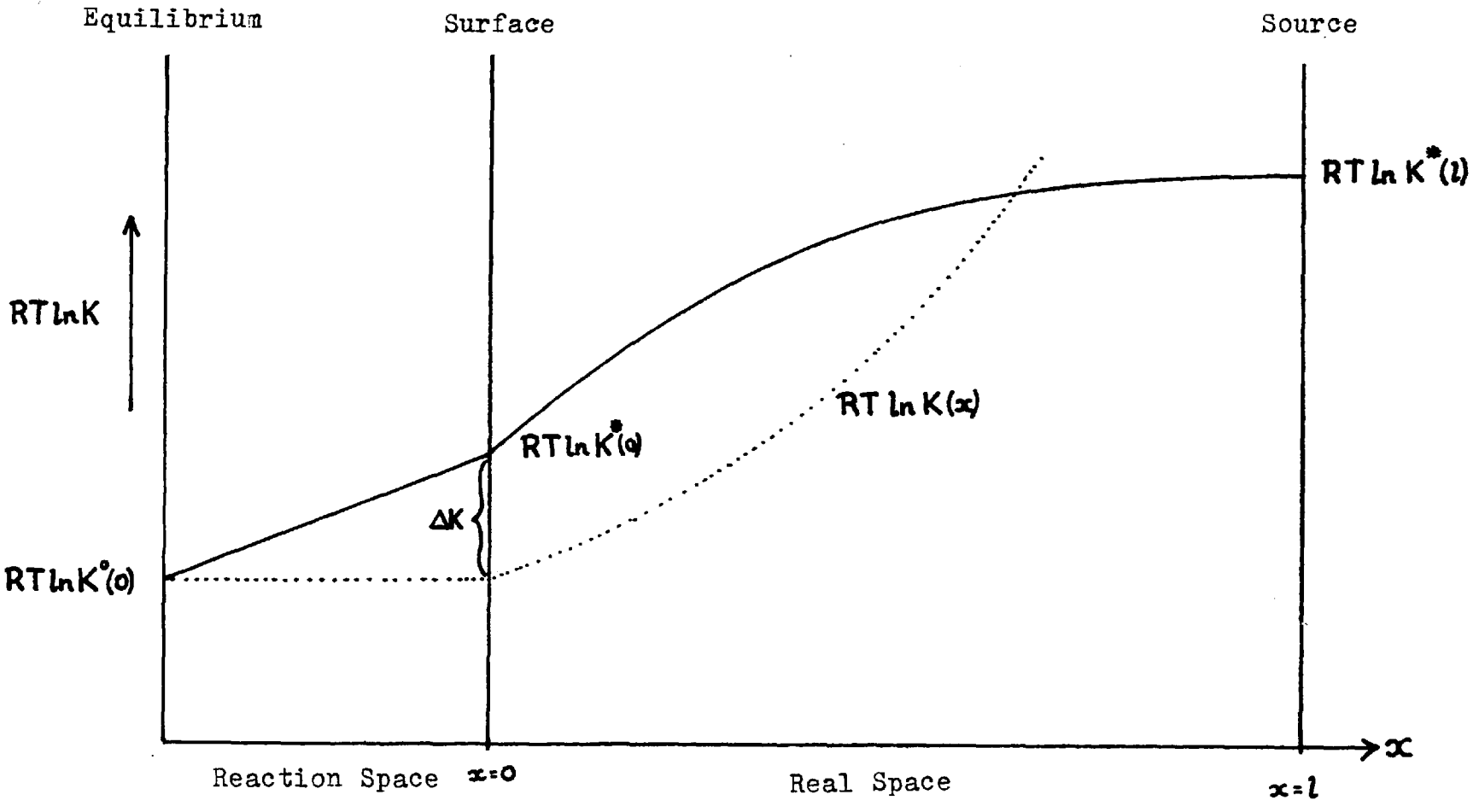

FIG. 7.1. SCHEMATIC VARIATION OF FREE ENERGY IN REAL AND REACTION SPACE.

the continuous line $RT\ln K^*$ represents the overpotential or supersaturation in the vapour (ΔK at $x = 0$). Now the equilibrium value $K^{o(o)}$ is obtained from thermodynamic data, K^* can be determined, using the theory given in chapter 3, from a knowledge of either $K^{*(l)}$ and the growth rate or from two values of $K^{*(x)}$, hence the true overpotential ΔK can be obtained.

The need for accurate thermodynamic data was apparent and a technique for obtaining them which was facile, accurate and versatile was needed. The modified entrainment method was therefore devised and it confirmed the validity of the theoretical model of transport using materials with accurately known thermodynamic parameters and provided reliable data for chemical vapour transport reactions, used in growing gallium arsenide. In addition, the method demonstrated, by working over an extended temperature range, that linear behaviour by $\ln\dot{W}$ versus $\frac{1}{T}$ must be interpreted with caution since two reactions occurring simultaneously can give an approximately straight line over several hundred degrees. Entropies deduced for compounds must be checked with third law calculations. Inconsistencies suggest the presence of additional species to those being considered. In this way GaOH and $GaCl_2$, previously unsuspected, were shown to be present in significant amounts in the systems investigated.

Experimental values of diffusion coefficients of reactive gases at high temperature were obtained using a second-order approximation to multicomponent diffusion. Results for $D^{\circ}_{HCl\ :\ H_2}$ were obtained and it has been shown how values for $D^{\circ}_{GaCl\ :\ H_2}$ and $D^{\circ}_{HCl\ :\ GaCl}$ can be obtained empirically.

The modified entrainment method also provides a quick and easy way of checking the usefulness of a particular system as a transport process and to indicate the optimum temperature range of operation. Finally the method has potentialities for studying surface kinetics: if the resistance of the channel of the sample bottle is steadily decreased, then the increase in $\dot{W}$ due to that decrease will become less than expected when surface kinetics become significant in comparison to the gas phase resistance in the channel.

For the future, armed with the modified entrainment method and the theoretical model of gas transport, there is good reason to believe that the many years of empirical research that have been expended on each new growth system, can be significantly reduced.

Furthermore, having a basic understanding of the processes occurring in the gas phase, the way is open to study the processes occurring at the surface.

The 'nearly closed' capsule method for purification and single crystal growth has considerable possibilities; it is versatile and further research into this technique could well prove fruitful. The present investigation into the growth of epitaxial layers by this method also revealed the importance of substrate preparation and further work is required in this area. In the capsule growth experiments, the ability to observe the capsule throughout an experiment proved invaluable, both in preventing long abortive experiments and in allowing the various growth stages to be noted. The furnace described in this thesis, has thus played a significant part in arriving at our present state of understanding of vapour phase crystal growth.

It is the belief of the author that the understanding of crystal growth has been increased as a result of the work reported in this thesis and that it opens up many promising lines of future research.

REFERENCES

REFERENCES

1. The Holy Bible, Job ch. 28 verses 12-19
2. A. van Hook, "Crystallisation, Theory and Practice", Reinhold Publ. Corp. (1961)
3. J. J. Gilman, "The Art and Science of Growing Crystals", J. Wiley & Sons Inc. (1963)
4. J. R. Arthur & J. J. LePore, J. Vacuum Sci. & Tech., 6, 545 (1969)
5. W. G. Burgers in "The Art and Science of Growing Crystals" (ed. J. J. Gilman) J. Wiley & Sons Inc., (1963), p. 416
6. P. Hartman, ed., "Crystal Growth: an Introduction", North-Holland Pulb. Co. Amsterdam & London (1973)
7. R. A. Laudise, "The Growth of Single Crystals", Prentice-Hall, New Jersey (1970)
8. I. Tarjan & M. Matrai, eds, "Laboratory Manual on Crystal Growth", Akademai Kiado, Budapest (1972)
9. H. Schafer, "Chemical Transport Reactions", Academic Press, New York & London (1964)
10. W. W. Piper & S. J. Polich, J. Appl. Phys., 32, 1278 (1961)
11. S. D. Sharma & L. K. Malhotra, J. Cryst. Growth, 10, 199 (1971)
12. M. M. Faktor, I. Garrett & R. H. Moss, J. Chem. Soc., Faraday Trans. I, 69, 1915 (1973)
13. C. Hilsum in "Progress in Semiconductors", eds A. F. Gibson & R. E. Burgess, Vol. 9, Heywood (1965), p. 137
14. S. M. Ku, J. Electrochem. Soc., 110, 991 (1963)
15. B. I. Miller, E. Pinkas, I. Hayashi & R. J. Capik, J. Appl. Phys., 43, 2817 (1972)
16. D. de Nobel & M.T. Vlaardingerbroek, Philips Tech. Rev. 32, 328 (1971)
17. G. A. Acket, R. Tijburg & P. J. de Waard, Philips Tech. Rev. 32, 370 (1971)
18. H. T. Minden, Solid State Tech., 31 (January 1973)
19. H. Kressel & H. Nelson, RCA Rev., 106 (March 1969)
20. J. C. Bass, Electronic Engineering, 61 (November 1970)
21. F. A. Kroger, "The Chemistry of Imperfect Crystals", 2nd revised ed., North-Holland Publ. Co. (1973)
22. R. L. Parker, in Solid State Physics, Vol. 25 (1970) eds. H. Ehrenreich, F. Seitz & D. Turnbull, Academic Press, New York & London p. 151

23. N. N. Greenwood, "Ionic Crystals, Lattice Defects and Non-stoichiometry", Butterworths, (1968)

24. R. A. Swalin. "Thermodynamics of Solids", John Wiley & Sons, (1962)

25. J. S. Anderson, Proc. Roy. Soc., A185, (1946), 69

26. D. R. Frankl & J. A. Venables, Advances in Physics, 19 (1970) 409

27. A. van Hook, "Crystallization, Theory & Practice", Reinhold Publ. Co (1961)

28. M. M. Faktor, R. Heckingbottom & I. Garrett, J. Chem. Soc. (A), 2657 (1970)

29. M. M. Faktor, R. Heckingbottom & I. Garrett, J. Chem. Soc. (A), 1 (1971)

30. M. M. Faktor & I Garrett, J. Chem. Soc. (A), 934 (1971)

31. M. M. Faktor, I. Garrett & R. Heckingbottom, J. Cryst. Growth, 9, 3 (1971)

32. M. M. Faktor & I. Garrett, J. Cryst. Growth, 9, 12 (1971)

33. M. M. Faktor & I. Garrett, Lecture given at a Summer School on Vapour Transport at Imperial College of Science & Technology, London University (1972)

34. D. Effer, J. Electrochem. Soc., 112, 1020 (1965)

35. R. L. Newman & N. Goldsmith, J. Electrochem. Soc., 108, 1127 (1961)

36. H. Welker, Z. Naturforsch., 7a, 744 (1952)

37. J. M. Whelan, in "Semiconductors", ed. N. B. Hannay, Reinhold Publ. Corp. New York (1959)

38. J. H. Westbrook, ed., "Intermetallic Compounds", John Wiley & Sons London (1967) p. 521

39. O. G. Folberth in "Compound Semiconductors", Vol. 1., Preparation of III-V Compounds, Ed. R. K. Willardson & H. L. Goering, Reinhold Publ. Corp. New York (1962) p. 21.

40. N. A. Goryunova, "The Chemistry of Diamond-like Semiconductors", ed. J. C. Anderson, trans. by Scripta Technica Inc., Chapman & Hall, London (1965)

41. J. van dem Boomgaard & K. Schol, Philips Research Repts., 12, 127 (1957)

42. R. K. Willardson & H. L. Goering, eds., "Compound Semiconductors", Vol. 1., Preparation of III-V Compounds, Reinhold Publ. Corp., New York (1962)

43. J. Frey, "Gallium Arsenide, a Review", UKAEA Research Group, Harwell, Report No. AERE - R5757 (March 1968)

44. J. W. Harrison, Solid State Technol., 48 (January 1973)

45. F. A. Cunnell in "Compound Semiconductors", Vol. 1. Preparation of III- V Compounds Ed. R. K. Willardson & H. L. Goering, Reinhold 1962, p. 207

46. R. Gremmelmaier, Z. Naturforsch, 11A, 511 (1956)

47. H. Nelson, RCA Rev., 24, 603 (1963)

48. M. B. Panish, S. Sumski & J. Hayashi, Metallurgical Trans., 2, 795 (1971)

49. J. M. Woodall & R. M. Potomski, J. Electrochem, Soc., 119, 277 (1972)

50. G. H. B. Thompson & P. A. Kirkby, Electronics Letters, 9, 295 (1973)

51. S. Knight, L. R. Dawson, J. V. DiLorenzo & W. A. Johnson, Proc. 3rd Int. Symp. on Gallium Arsenide: Inst. Phys. Phys. Soc. Conf. Ser. No. 9, 108 (1971)

52. E. A. Giess, J. P. Kuptsis & E. A. D. White, J. Cryst. Growth, 16, 36 (1972)

53. R. H. Deitch, J. Cryst. Growth, 7, 69 (1970)

54. J. A. Donahue & H. T. Minden, J. Cryst. Growth, 7, (1970) 221

55. H. P. Kleinknecht & A. H. Oberholzer, U.S. Patent, 3,755,011 (1973)

56. G. R. Antell & D. Effer, J Electrochem, Soc. 106, 509 (1959)

57. A. Hagenlocher, J. Electrochem Soc., 108, 213C (1961)

58. F. A. Pizzarello, J. Electrochem. Soc., 110, 1059, (1963)

59. R. R. Moest & B. R. Shupp, J. Electrochem., Soc. 109, 1061 (1962)

60. D. Effer & G. R. Antell, J. Electrochem Soc., 107, 252 (1960)

61. R. R. Moest, J. Electrochem. Soc., 113, 141 (1966)

62. D. Effer, J. Electrochem Soc., 112, 1020 (1965)

63. R. L. Newman & N. Goldsmith, J. Electrochem Soc., 108, 1127 (1961)

64. S. W. Ing & H. T. Minden, J. Electrochem. Soc., 109, 995 (1962)

65. G. R. Cronin, R. W. Conrad & S. Borrello, J. Electrochem. Soc., 113, 1336 (1966)

66. R. W. Conrad, R. A. Reynolds & M. W. Jeffcoat, Solid State Electronics, 10, 507 (1967)

67. J. R. Knight, D. Effer & P. R. Evans, Solid State Electronics, 8, 178 (1965)

68. J. Whitaker & D. E. Bolger, Solid-State Commun., 4, 181 (1966)

69. D. V. Eddols, Phys. Status Solidi, 17, 67 (1966)

70. L. C. Bobb, H. Holloway, K. H. Maxwell & E. Zimmerman, J. Phys. Chem Solids, 27, 1679 (1966)

71. H. Holloway & L. C. Bobb, J. Appl. Phys., 38, 2893 (1967)

72. A. Bradshaw & J. E. Knappett, Solid State Technol., 45, (October 1970)

73. J. J. Tietjen & J. A. Amick, J. Electrochem. Soc., 113, 724 (1966)

74. J. J. Tietjen, V. S. Ban, R. E. Enstrom & D. Richman, J. Vacuum Sci. & Tech., 8, S5 (1971)

75. C. J. Frosch & C. D. Thurmond, J. Phys. Chem., 66, 877 (1962)

76. M. Michelitsch, W. Kappallo & G. Hellbardt, J. Electrochem. Soc., 111, 1248 (1964)

77. K. L. Lawley, J. Electrochem. Soc., 113, 240 (1966)

78. C. Lin, L. Chow & J. J. Miller, J. Electrochem. Soc., 117, 407 (1970)

79. H. M. Manasevit, Appl. Phys. Letters, 12, 156 (1968)

80. H. M. Manasevit, & W. I. Simpson, J. Electrochem. Soc., 116, 1725 (1969)

81. S. Ito, T. Shinohara & Y. Seki, J. Electrochem. Soc., 120, 1419 (1973)

82. R. R. Moest & D. T. Lassota, J. Electrochem. Soc., 114, 110 (1967)

83 C. N. Cochran & L. M. Foster, J. Electrochem. Soc., 109, 149 (1962)

84. M. E. Weiner, J. Electrochem. Soc., 119, 496 (1972)

85. H. Miki, M. Ito & T. Oda, Japan. J. Appl. Phys., 11, 623 (1972)

86. H. T. Minden, J. Cryst. Growth, 8, 37 (1971)

87. V. K. Jain & S. K. Sharma, Solid-State Electronics, 13, 1145 (1970)

88. An. N. Nesmeyanov, "Vapour Pressure of the Elements", Infosearch (1963)

89. O. Kubaschewski, E. L. Evans & C. B. Alcock, "Metallurgical Thermochemistry", Pergamon Press (1967)

90. M. Knudsen, Ann. Physik, 28, 75 (1909)

91. M. Knudsen, Ann. Physik, 28, 999 (1909)

92. P. Clausing, Ann. Physik, 12, 961 (1932)

93. L. Brewer & J. S. Kane, J. Phys. Chem. 59, 105 (1955)

94. P. Goldfinger & M. Jeunehomme, Trans. Far. Soc. 59, 2851 (1963)

95. M. Volmer, Z. Physik Chem, Bodenstein Festband, 863 (1931)

96. J. L. Margrave, J. Chem. Phys. 27, 1412 (1957)

97. R. D. Freeman, Technical Documentary Report No. ASD TDR 63-754, Part II Air Force Materials Laboratory, Wright-Patterson Base, Ohio (1965)

98. K. D. Carlson in "The Characterization of High Temperature Vapours", J. L. Margrave (ed), J. Wiley & Sons, Inc. (1967) p.115

99. R. C. Paule & J. L. Margrave in "The Characterization of High Temperature Vapours", J. L. Margrave (ed), J. Wiley & Sons, Inc. (1967) p.130

100. U. Merton & W. E. Bell in "The Characterization of High Temperature Vapours" J. L. Margrave (ed), J. Wiley & Sons. Inc. (1967) p.91

101. M. M. Faktor & J. I. Carasso, J. Electrochem. Soc., 112, 817 (1965)

102. J. Stefan, Ann. Phys. Chem. 17, 550 (1882)

103. T. B. Reed & W. J. La Fleur, Appl. Phys. Letters 5 (1964), 191

104. T. B. Reed, W. J. La Fleur & A. J. Strauss, J. Crystal Growth 3, 4 (1968), 115

105. W. A. Tiller, K. A. Jackson, J. W. Rutter & B. Chalmers, Acta Metallurgica, 1, 428 (1953)

106. D. W. Shaw, J. Crystal Growth, 12, 249 (1972)

107. D. J. Kirwan, J. Electrochem. Soc., 117, 1572 (1970)

108. G. F. Day, Varian Report No. 324-6Q, Air-Force Contract No. AF33 (615) - 1988 Project No. 4460, Task No. 446006 'Heterojunction Device Concepts'.

109. J. J. Murray, C. Pupp & R. F. Pottie, J. Chem. Phys., 58, 2569 (1973)

110. C. Pupp, J. J. Murray & R. F. Pottie, J. Chem. Thermodynamics, 6, 123 (1974)

111. G. de Maria, L. Malaspina, V. Piacente, J. Chem. Phys., 52, 1019 (1970)

112. B. M. Bulakh, J. Crystal Growth, 5, 243 (1969)

113. R. J. Caveney, J. Crystal Growth, 7, 102 (1970)

114. S. R. de Groot, "Thermodynamics of Irreversible Processes", North-Holland Publishing Co. Amsterdam (1952)

115. I. Prigogine, "Introduction to Thermodynamics of Irreversible Processes" Charles C. Thomas, Illinois (1955)

116. J. Hawgood, "Numerical methods in Algol", McGraw-Hill Publishing Co. Ltd, London (1965)

117. K. Denbigh. "The Principles of Chemical Equilibrium", Cambridge University Press, (1961)

118. A. Boucher & L. Hollan, J. Electrochem. Soc., 117, 932 (1970)

119. D. Battat, M. M. Faktor & M. A. Savva, Chem. & Ind., 263 (March 1974)

120. D. Ambrose & I. J. Lawrenson, J. Chem. Thermodynamics, 4, 755 (1972)

121. A. C. Egerton, Proc. Roy. Soc. (A), 103, 469 (1923)

122. P. Gross, C. S. Campbell, P. J. C. Kent & D. L. Levi, Disc. Faraday Soc., 4, 206 (1948)

123. C. N. Cochran & L. M. Foster, J. Electrochem. Soc., 109, 144 (1962)

124. R. Hultgren, R. L. Orr, K. K. Kelley, "Supplements to Selected Values of Thermodynamic Properties of Metals and Alloys", University of California (up to 1972)

125. J. B. Mullin, D. T. J. Hurle, J. Luminescence, 7, 176 (1973)

126. Yu. Kh. Shaulov & A. M. Mosin, Zh. Fiz. Khim., 47, 1131 (1973)

127. A. W. Laubengayer & F. B. Schirmer, J. Amer. Chem. Soc., 62, 1578 (1940)

128. J. D. Beck, R. H. Wood & N. N. Greenwood, Inorg. Chem., 9, 86 (1970)

129. P. I. Fedorov & G. A. Lovetskaya, Zh. Neorg. Khim., 13, 3357 (1968)

130. R. R. Fergusson & T. Gabor, J. Electrochem. Soc., 111, 585 (1964)

131. D. T. J. Hurle & J. B. Mullin, J. Phys, Chem. Solids, Suppl. No. 1, 241 (1967)

132. M. M. Faktor, M. A. Savva & D. Battat, Private Communication.

133. G. W. Lord & R. H. Moss, J. Phys. E, Scientific Instruments, 3, 177 (1970)

134. G. Hetherington & K. H. Jack, Physics & Chemistry of Glasses, 3, 129 (1962)

135. T. P. Browell & G. Hetherington, J. British Soc. Scientific Glassblowers, 3, 1 (1965)

136. W. G. Spitzer & J. M. Whelan, Phys. Rev., 114, 59 (1959)

137. T. M. Buck in "The Surface Chemistry of Metals and Semiconductors" John Wiley & Sons Inc. 107 (1960)

138. R. Stickler & G. R. Booker, Scientific Paper 62-125-546-P3, Westinghouse Research Laboratories, Pittsburgh, Pennsylvania (1962)

139. M. V. Sullivan & G. A. Kolb, J. Electrochem Soc., 110, 585 (1963)

140. V. L. Rideout, J. Electrochem, Soc., 119, 1778 (1972)

141. C. J. Todd, Private Communication

142. A. C. Adams & B. R. Pruniaux, J. Electrochem. Soc., 120, 408 (1973)

143. C. R. Elliott, Private Communication

144. D. W. Shaw, 1968 Symposium on Gallium Arsenide, Institute of Physics and Physical Society, Conference Series No. 7, 50 (1969)

145. D. W. Shaw, J. Electrochem Soc, 115, 777 (1968)

146. M. S. Abrahams & C. J. Buiocchi, J. Phys. Chem. Solids, 28, 927 (1967)

147. B. D. Joyce & J. B. Mullin, 1968 Symposium on Gallium Arsenide, Institute of Physics and Physical Society, Conference Series No. 3

148. B. D. Joyce, Electronic Components, 1389, December 1968

149. G. R. Booker & B. A. Joyce; Phil. Mag. (GB), 14, 301 (1966)

150. G. I. Distler & B. B. Zvagin, Nature, 212, 807 (1966)

151. G. I. Distler, S. A. Kobzareva & Y. M. Gerasimov, J. Crystal Growth, 2, 45 (1968)

152. K. L. Chopra, J. Appl. Phys., 40, 906 (1969)

153. K. L. Chopra, Surface Sci., 20, 201 (1970)

154. M. Ackermann, J. S. Vermaak & H. C. Snyman, Surface Sci., 34, 394 (1973)

155. H. B. Bebb & E. W. Williams in "Semiconductors and Semimetals", Vol. 8, eds. R. K. Willardson & A. C. Beer, Academic (1972) p.321

156. The results of cathodoluminescence studies were obtained and supplied by Dr. D. H. Newman of the Post Office Research Dept.

157. D. H. Newman, Private Communication

158. R. Nitsche in "Metallphysik", ed. O. Madelung, Pergamon Press (1968), p.42

159. D. Battat, M. M. Faktor, I. Garrett & R. H. Moss to be published in J. Chem. Soc., Faraday I, (1974)

160. D. W. G. Ballentyne, S. Wetwatana & E. A. D. White, J. Cryst. Growth, 7, 79 (1970)

APPENDICES

APPENDIX 1

The derivation of equations for linear and saturation regions of equation (3.7) plotted in Figure (3.2).

(a) Linear Region - Equation (3.8)

$$J_A \simeq \left(\frac{DP_T}{R^2\ T^3}\right)\left(\frac{\Delta H}{l}\right)\frac{P_A^{(l)}}{P_g^{(l)}}\ .\ \Delta T \qquad \text{when } \Delta T \text{ is small}$$

The general equation (3.7) is

$$J_A = \left(\frac{DP_T}{RTl}\right) ln\left\{\frac{P_T - \exp\left[\frac{-\Delta H}{RT^{(o)}} + \frac{\Delta S}{R}\right]}{P_T - \exp\left[\frac{-\Delta H}{RT^{(l)}} + \frac{\Delta S}{R}\right]}\right\}$$

$$\exp\left\{J_A \frac{RTl}{DP_T}\right\} = \frac{P_T - \exp\left[\frac{-\Delta H}{RT^{(o)}} + \frac{\Delta S}{R}\right]}{P_T - \exp\left[\frac{-\Delta H}{RT^{(l)}} + \frac{\Delta S}{R}\right]} \qquad (A1)$$

To express R.H.S. in terms of ΔT subtract 1 from either side of equation (A1) and express the R.H.S. over a common denominator.

$$\exp\left\{J_A \frac{RTl}{DP_T}\right\} - 1 = \frac{\left\{P_T - \exp\left[\frac{-\Delta H}{RT^{(o)}} + \frac{\Delta S}{R}\right]\right\} - \left\{P_T - \exp\left[\frac{-\Delta H}{RT^{(l)}} + \frac{\Delta S}{R}\right]\right\}}{P_T - \exp\left[\frac{-\Delta H}{RT^{(l)}} + \frac{\Delta S}{R}\right]} \qquad (A2)$$

Consider R.H.S. only, this reduces to

$$= \frac{\exp\left[\frac{-\Delta H}{RT^{(l)}} + \frac{\Delta S}{R}\right] - \exp\left[\frac{-\Delta H}{RT^{(o)}} + \frac{\Delta S}{R}\right]}{P_T - \exp\left[\frac{-\Delta H}{RT^{(l)}} + \frac{\Delta S}{R}\right]} \qquad (A3)$$

$$= \frac{\exp\left[\frac{-\Delta H}{RT^{(l)}} + \frac{\Delta S}{R}\right]\left\{1 - \frac{\exp\left[\frac{-\Delta H}{RT^{(o)}} + \frac{\Delta S}{R}\right]}{\exp\left[\frac{-\Delta H}{RT^{(l)}} + \frac{\Delta S}{R}\right]}\right\}}{P_T - \exp\left[\frac{-\Delta H}{RT^{(l)}} + \frac{\Delta S}{R}\right]} \qquad (A4)$$

$$= \frac{\exp\left[\frac{-\Delta H}{RT^{(l)}} + \frac{\Delta S}{R}\right]\left\{1 - \exp\left[\frac{-\Delta H}{RT^{(o)}} + \frac{\Delta H}{RT^{(l)}}\right]\right\}}{P_T - \exp\left[\frac{-\Delta H}{RT^{(l)}} + \frac{\Delta S}{R}\right]} \qquad (A5)$$

$T^{(o)}T^{(l)} \simeq T^2$ and $\Delta T = T^{(l)} - T^{(o)}$, therefore

$$\exp\left\{J_A \frac{RTl}{DP_T}\right\} - 1 = \frac{\exp\left[\frac{-\Delta H}{RT^{(l)}} + \frac{\Delta S}{R}\right]\left\{1 - \exp\left[\frac{-\Delta H}{RT^2} \cdot \Delta T\right]\right\}}{P_T - \exp\left[\frac{-\Delta H}{RT^{(l)}} + \frac{\Delta S}{R}\right]} \qquad (A6)$$

Now $P_A^{(l)} = \exp\left[\frac{-\Delta H}{RT^{(l)}} + \frac{\Delta S}{R}\right]$ and $P_T = P_A^{(l)} + P_Z^{(l)}$

$$\therefore \exp\left\{J_A \frac{RTl}{DP_T}\right\} = \frac{P_Z^{(l)} + P_A^{(l)}\left\{1 - \exp\left[\frac{-\Delta H}{RT^2} \cdot \Delta T\right]\right\}}{P_Z^{(l)}} \qquad (A7)$$

$$\text{or } \exp\left\{J_A \frac{RTl}{DP_T}\right\} = \frac{P_T - P_A^{(l)} \exp\left[\frac{-\Delta H}{RT^2} \cdot \Delta T\right]}{P_Z^{(l)}} \qquad (A8)$$

expanding $\exp\left\{\frac{-\Delta H}{RT^2} \cdot \Delta T\right\}$ when ΔT is small gives

$$\exp\left\{J_A \frac{RTl}{DP_T}\right\} \simeq \frac{P_T - P_A^{(l)}\left\{1 - \frac{\Delta H}{RT^2} \cdot \Delta T\right\}}{P_Z^{(l)}} \qquad (A9)$$

Taking logarithms of both sides

$$J_A \simeq \frac{DP_T}{RTl}\left\{ln\left(1 + \frac{P_A^{(l)}}{P_Z^{(l)}} \cdot \frac{\Delta H}{RT^2} \cdot \Delta T\right)\right\} \qquad (A10)$$

Now expanding the logarithm when ΔT is small gives (A11) which is the same as equation (3.8)

$$J_A \simeq \frac{DP_T}{R^2T^3l} \cdot \frac{P_A^{(l)}}{P_Z^{(l)}} \cdot \Delta H \cdot \Delta T \qquad (A11)$$

(b) Saturation Region - Equation (3.9)

$$J_{A_{assymptote}} = \left(\frac{DP_T}{RTl}\right) ln\left\{1 - \frac{P_A^{(l)}}{P_Z^{(l)}}\right\}$$

Equation (A8) is

$$\exp\left\{J_A \frac{RTl}{DP_T}\right\} = \frac{P_T - P_A^{(l)} \exp\left\{\frac{-\Delta H}{RT^2} \cdot \Delta T\right\}}{P_Z^{(l)}} \qquad (A8)$$

As ΔT becomes large $\exp\left\{\frac{-\Delta H}{RT^2} \cdot \Delta T\right\} \rightarrow 0$. The limit of ΔT is $\Delta T \rightarrow T$ when the exponential becomes $\exp\left\{\frac{-\Delta H}{RT}\right\}$ this will be almost zero since ΔH is numerically larger than RT at normal operating temperatures.

Since $P_T = P_Z^{(l)} + P_A^{(l)}$, equation (A8) becomes

$$\exp\left\{J_A \frac{RTl}{DP_T}\right\} = 1 - \frac{P_A^{(l)}}{P_Z^{(l)}} \qquad (A12)$$

which gives

$$J_A = \left(\frac{DP_T}{RTl}\right) ln\left\{1 - \frac{P_A^{(l)}}{P_Z^{(l)}}\right\} \qquad (A13)$$

APPENDIX 2

Calculation of partial pressures of As_4, GaCl, H_2 and HCl inside a capsule for the chemical vapour transport system GaAs - $AsCl_3$ - H_2

Hydrogen passes through a bubbler containing arsenic trichloride as described earlier. It is assumed that the resulting gas mixture is in equilibrium with the liquid $AsCl_3$ at the bubbler temperature T_b, i.e.

$$K_3\ (T_b) = \frac{(p_{As_4})^{\frac{1}{2}}\ (p_{HCl})^6}{(p_{AsCl_3})^2\ (p_{H_2})^3} \qquad (A2.1)$$

where K_3 is the equilibrium constant for the reaction (3.23)

$$2\ AsCl_3 + 3\ H_2 \rightarrow \frac{1}{2}\ As_4 + 6\ HCl \qquad (3.23)$$

The equilibrium vapour pressure (in atm) of arsenic trichloride is given by[108]

$$\log_{10} p_{AsCl_3} = -\frac{2660}{T} - 2.53\ ln\ T + 21.88\ atm \qquad (A2.2)$$

The stoichiometry dictates that

$$p_{HCl} = 12\ p_{As_4} \qquad (A2.3)$$

and the total pressure is

$$P_T = p_{AsCl_3} + p_{H_2} + p_{As_4} + p_{HCl} \qquad (A2.4)$$

The four equations (A2.1) - (A2.4) can be solved for the partial pressures in the gas stream leaving the bubbler. The equilibrium of reaction (3.23) is displaced to the right as the temperature increases on entering the furnace. At the capsule temperature $T^{(l)}$, the component partial pressures can be calculated using equations (A2.1) - with K_3 at temperature T^l on the left hand side, (A2.2), (A2.3) and (A2.5) which states that the hydrogen/chlorine ratio remains constant once the gas stream has left the bubbler:

$$\left(\frac{2\ p_{H_2} + p_{HCl}}{3\ p_{AsCl_3} + p_{HCl}}\right)_{at\ capsule} = \left(\frac{2\ p_{H_2} + p_{HCl}}{3\ p_{AsCl_3} + p_{HCl}}\right)_{at\ bubbler} \qquad (A2.5)$$

Equation (A2.5) holds providing diffusion rates are much smaller than the gas flow rate in the pipe from the bubbler to the furnace.

Consider now the flow of gas through the effusion hole and the partial pressures over the source. The equilibrium equation at the source is

$$K_2^{(l)} = \frac{p_{GaCl}^{(l)} \left[p_{H_2}^{(l)}\right]^{\frac{1}{2}} \left[p_{As_4}^{(l)}\right]^{\frac{1}{4}}}{p_{HCl}^{(l)}} \qquad \text{(A2.6)}$$

The partial pressures of GaCl, H_2, As_4 and HCl are unknown and also the total pressure which may be greater than that outside the capsule if the effusion hole is small.

Poiseuille's equation for viscous flow through the effusion hole is:

$$u' = \frac{1.013 \times 10^6 \ r^2 \ \Delta P}{8 \ \eta h} \qquad \text{(A2.7)}$$

where u' is the flow velocity in mm s^{-1}, r is the hole radius in mm, ΔP the difference in pressure through the hole in atm, η is the viscosity coefficient in poise and h is the length of the hole in mm. Four flow equations, (33) - (36), can be solved for the flow of gases through the hole, it is assumed that the pressure of gallium monochloride is negligible outside the capsule. The resulting equations are:

$$0 = \left[p_{GaCl}^{(l)} - \frac{JRT}{u}\right] f + \frac{JRT}{u} \qquad \text{for gallium} \qquad \text{(A2.8)}$$

$$p_{AsCl_3}^{(h)} + p_{As_4}^{(h)} = \left[4 \ p_{As_4}^{(l)} - \frac{JRT}{u}\right] f + \frac{JRT}{u} \qquad \text{for arsenic} \qquad \text{(A2.9)}$$

$$2 \ p_{H_2}^{(h)} + p_{HCl}^{(h)} = \left[2 \ p_{H_2}^{(l)} + p_{HCl}^{(l)}\right] f \qquad \text{for hydrogen} \qquad \text{(A2.10)}$$

$$3 \ p_{AsCl_3}^{(h)} + p_{HCl}^{(h)} = \left[p_{GaCl}^{(l)} + p_{HCl}^{(l)}\right] f \qquad \text{for chlorine} \qquad \text{(A2.11)}$$

where (h) denotes the partial pressures outside the effusion hole, J is the nett flux of material through the hole and

$$f = \exp\left\{\frac{uh}{D}\right\} = \exp\left\{\frac{1.013 \times 10^6 \ r^2 \ \Delta P}{8 \ \eta D^o \ (T/273)^{1.8}}\right\} \qquad \text{(A2.12)}$$

D^o is the diffusion coefficient at 273°K.

Finally we have the total pressure in the capsule

$$p_{GaCl}^{(l)} + p_{As_4}^{(l)} + p_{H_2}^{(l)} + p_{HCl}^{(l)} = P + \Delta P \qquad \text{(A2.13)}$$

Eliminating J from (A2.8) and (A2.9) gives

$$p_{AsCl_3}^{(h)} + p_{As_4}^{(h)} = [4\, p_{As_4}^{(l)} - p_{GaCl}^{(l)}]\, f \qquad \text{(A2.14)}$$

Using the six equations (A2.6), (A2.10), (A2.11), (A2.12), (A2.13) and (A2.14) the unknown partial pressures can be determined along with the total pressure. The calculation requires a double iterative procedure because equation (A2.6) is of the seventh order and equations (A2.10), (A2.11) and (A2.14) are transcendental. The problem was solved on a Burroughs B5500 computer.

PUBLICATIONS

Journal of Physics E : Scientific Instruments, 1970, Volume 3, pp177–179

A furnace for growing crystals by vapour phase transport in which growth can be continuously observed

G W Lord and R H Moss
Post Office Research Department, Dollis Hill, London NW2

MS *received 10 September 1969, in revised form 18 November 1969*

Abstract A furnace of low inherent thermal stability but which is screened from ambient temperature variations and has its temperature controlled to close limits is described. The capsule in which vapour transport is performed can be rotated and moved axially through the temperature profile in the furnace. Continuous observation of the capsule is possible up to the maximum operating temperature of 1100 °C. Any desired profile over a length of 30 cm can be obtained subject to the limits: ±0·5 degC for a uniform temperature zone over 15 cm and a maximum temperature gradient of 15 degC cm $^{-1}$.

1 Introduction

Research in the field of crystal growth has increased rapidly in recent years and has shown the need for specialized furnaces. Many are now available for growth from flux or melt but not for growth by vapour phase transport.

In the course of investigations into the growth of group II–VI semiconducting compounds by vapour phase transport a furnace has been designed and built having special features to facilitate control over the process. It has a specific thermal profile with flat zones and steep temperature gradients between zones. The temperature is controlled more accurately than has hitherto been usual, and the furnace has facilities for pulling and rotating the capsule *in vacuo*. A later version of this furnace has all these facilities plus that of viewing the contents of the furnace during an experiment. The maximum working temperature is 1100 °C.

The basic idea of winding a heating element for direct viewing was reported by Gibbs *et al.* (1957). More recently Reed (1969) described a furnace in which a thin layer of gold, transparent in the visible region, is deposited on the inside of a Pyrex tube and forms an efficient heat reflector through which a growing crystal can be observed. No attempt however is made to control either the shape of the profile or the environment of the Pyrex tube. The furnace described here, although originally designed for the growth of cadmium sulphide is of general use for the growth of II–VI, III–V and other related compounds that can be grown from the vapour phase.

Some advantages of the furnace include direct observation which eliminates long abortive runs: also optical pyrometry is possible, and direct measurement of growth rates can be made. The vital early stages of oriented seeding experiments can be watched, and continuous observations of the shape of the growing face of the crystal can be made.

2 General description

The furnace body consists of concentric cylindrical components and is shown in section in figure 1. The work tube is made of transparent silica (bore 40 mm, length 98 cm) and the water jacket of Pyrex tubes (bores 100 mm and 150 mm, lengths 76 cm and 60 cm respectively). The platinum-rhodium winding is on an alumina tube having a slit for viewing along almost its entire length, and the wire is wound up to the edge of the slit and held in position by alumina cement (figure 2). The length of the heating element is approximately 40 cm. The required thermal profile is obtained by grading the winding and by applying small amounts of lagging to selected

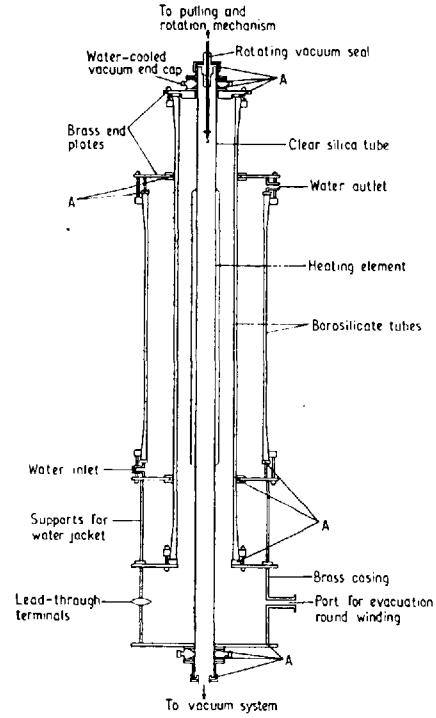

Figure 1 Furnace assembly. A, position of O-ring or gasket

areas of the element. The lagging used is either woven silica fibre or ceramic fibre blanket. The water jacket is formed by two standard borosilicate glass tubes and the space between the inner one and the work tube, which includes the winding, is partially evacuated to reduce heat losses and thermal profile 'smearing' by convection currents. Except for the viewing slit the inner surface of the water jacket is coated with gold leaf to reduce power consumption. The final temperature profile depends on the balance between all these factors.

3 Temperature control

3.1 *Controller*

A three term solid state temperature controller is used. The sensor is a platinum-platinum/13% rhodium thermocouple placed close to the element wire and is terminated on lead-through terminals on the casing. Compensating cable is used between the thermocouple terminals and the controller and

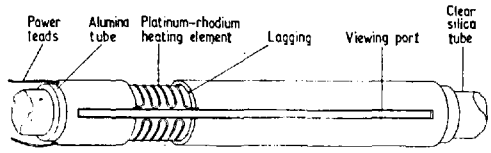

Figure 2 Furnace winding

the connections at each end are lagged to minimize and delay the effects of ambient temperature changes. The pressure in the jacket round the winding is maintained at a value in the range 5 to 10 torr. Lower pressures increase the risk of flash-over and tracking between the power terminals whilst higher pressures increase thermal instability and heat losses by convection.

3.2 *Winding characteristics*

The winding is deliberately made with a minimum of lagging to keep its time constant small and to limit the amount of heat conduction from one zone to another. The furnace is therefore extremely responsive to environmental changes around the winding and to variations in applied power. This is why the water jacket and three term controller with its characteristics carefully tuned to the constants of the furnace are used. It will be apparent that the furnace is capable of very fast heating rates, and in fact the risk of thermal shock to the alumina base of the winding forces the acceptance of a maximum heating rate of 400 degC h^{-1}. The use of porous alumina for winding support would reduce this effect. Thus the furnace is programmed up to temperature, and down again at the end of a run. The gold layer inside the water jacket limits the power consumption to approximately 2 kW at 1100°C.

4 Pulling and rotating mechanisms

A lead screw of 1 mm pitch is suspended through the correspondingly threaded hub of a spur gear supported in its turn by a thrust race. A fifteen-speed gear box couples a clock motor to a worm wheel which meshes with a spur gear. The lead screw is prevented from rotating by means of a rod fixed at right angles to it which runs between a vertical pair of guides. The position of the rod relative to a scale fixed to one of the guides indicates how far pulling has progressed. A cage at the lower end of the lead screw carries another clock motor and in effect its spindle carries and rotates the charge. Rotation speed is altered by changing the motor. The rod carrying the capsule and charge is brought out of the furnace through a rotating vacuum seal consisting of an O-ring (seated in a groove formed by two metal rings fixed to the rod) which is a sliding fit in a long, precision-bore tube at the top of the furnace. Pulling rates can be varied over a range of 120:1 by means of the gear box; changes outside this range are achieved by changing the pulling clock motor.

5 Pumping equipment

The work tube is evacuated by a 2 in air-cooled diffusion pump backed by a single stage rotary pump. A glass liquid nitrogen-cooled vapour trap is placed between the work tube and the diffusion pump. Work tube pressure is 10 μtorr to 0·1 mtorr when the pressure at the top of the pump is 1 μtorr. The partial pressure around the windings is set either by sealing the system at the required pressure with the furnace at working temperature or by continuous pumping against a leak controlled by a needle valve. This valve is placed near the pump to prevent a flow of air over the winding.

6 Performance

6.1 *Thermal profile*

Preplanned thermal profiles have been obtained in which uniform zones of 15 cm at $\pm 0{\cdot}5$ degC are close to regions having gradients of 15 degC cm^{-1}. Well defined peaks of 2 to 100°C have been achieved in an otherwise smooth profile. Profiles can be adjusted by small local additions of lagging to the winding. Some smoothing out of the thermal gradients occurs by axial conduction through the crystal charge. Spare windings of different wire distribution can be held to enable completely different profiles to be provided at short notice.

6.2 *Thermal stability*

For a given winding the thermal profile is basically the same over the temperature range 700 to 1100°C. The shape of one profile which has been used is shown at three different temperatures in figure 3. The diagram shows that as the temperature

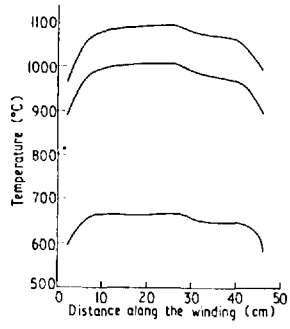

Figure 3 A thermal profile shown at three different temperatures

is increased through this range, the centre of the profile becomes slightly hotter with respect to the ends. It may be necessary therefore to make slight adjustments of the lagging to maintain a uniform zone (within the limits specified in §6.1) over a range of working temperatures. The profile has proved to remain constant for at least 1000 hours of running. As the temperature is controlled at the hottest part of the winding where deterioration is quickest, ageing shows by relative cooling of the rest of the winding rather than by development of a hot spot. Though the viewing slit causes radial distortion of the temperature profile, the effect on the charge appears to be eliminated by rotating it.

O-ring (seated in a groove formed by two metal rings fixed to the rod) which is a sliding fit in a long, precision-bore tube at the top of the furnace. Pulling rates can be varied over a range of 120:1 by means of the gear box; changes outside this range are achieved by changing the pulling clock motor.

5 Pumping equipment

The work tube is evacuated by a 2 in air-cooled diffusion pump backed by a single stage rotary pump. A glass liquid nitrogen-cooled vapour trap is placed between the work tube and the diffusion pump. Work tube pressure is 10 μtorr to 0·1 mtorr when the pressure at the top of the pump is 1 μtorr. The partial pressure around the windings is set either by sealing the system at the required pressure with the furnace at working temperature or by continuous pumping against a leak controlled by a needle valve. This valve is placed near the pump to prevent a flow of air over the winding.

6 Performance

6.1 *Thermal profile*

Preplanned thermal profiles have been obtained in which uniform zones of 15 cm at $\pm 0{\cdot}5$ degC are close to regions having gradients of 15 degC cm^{-1}. Well defined peaks of 2 to 100°C have been achieved in an otherwise smooth profile. Profiles can be adjusted by small local additions of lagging to the winding. Some smoothing out of the thermal gradients occurs by axial conduction through the crystal charge. Spare windings of different wire distribution can be held to enable completely different profiles to be provided at short notice.

6.2 *Thermal stability*

For a given winding the thermal profile is basically the same over the temperature range 700 to 1100°C. The shape of one profile which has been used is shown at three different temperatures in figure 3. The diagram shows that as the temperature

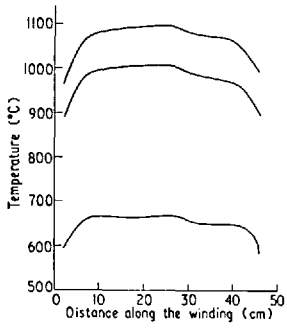

Figure 3 A thermal profile shown at three different temperatures

is increased through this range, the centre of the profile becomes slightly hotter with respect to the ends. It may be necessary therefore to make slight adjustments of the lagging to maintain a uniform zone (within the limits specified in §6.1) over a range of working temperatures. The profile has proved to remain constant for at least 1000 hours of running. As the temperature is controlled at the hottest part of the winding where deterioration is quickest, ageing shows by relative cooling of the rest of the winding rather than by development of a hot spot. Though the viewing slit causes radial distortion of the temperature profile, the effect on the charge appears to be eliminated by rotating it.

It has never been the prime object to measure the temperature of the charge extremely accurately but only the variations with time and position along the work tube. An output from the controller is proportional to the difference between the reference standard and the control thermocouple, the maximum difference has been found to be less than $\pm 0{\cdot}1$ degC during a run lasting for over four weeks. Variations within the work tube have been shown to be less than $\pm 0{\cdot}5$ degC. Thermal stability is limited by the following. (i) The temperature stability of the connexions to the control couple. Insulation of the junctions from draughts of air at different temperatures is vital. (ii) The residual gas around the windings causing temperature variations due to convection. (iii) Room temperature variations alter (a) the loss rate from the fan-cooled ends and (b) the rate at which heat is lost from, and hence the temperature gradient along, the water jacket. (iv) Temperature variations in the supply of cooling water. (v) Stability of the standard reference voltage in the controller.

6.3 *Viewing facility*

At temperatures above 850°C the non-black-body characteristics of the visible radiation from the furnace are sufficient to permit observation of the charge. External illumination enables fine detail to be seen. Crystal growth can be observed during the early stages of experiments, crystallites being re-evaporated if too many are formed. This is done by moving the capsule so as to reverse the temperature gradient. One of the major difficulties of seeded experiments in vapour phase growth is the positioning of a capsule in a furnace so that the seed is neither evaporated nor covered with a layer of polycrystalline material. In this furnace the seed can be observed and the capsule position adjusted to achieve slow growth or evaporation. Algae make cleaning of the water jacket essential at about six monthly intervals, but a recirculating system with inhibitors would prevent this.

7 Conclusions

The furnace described has been shown to operate most reliably; the viewing facility is highly advantageous in crystal growth experiments. Cadmium sulphide has been successfully grown in the furnace using both seeded and self-nucleated experiments. The furnace may also be applied to any other field where high temperature stability, and viewing of the charge are required. Expected element life with insignificant drift will be several thousand hours provided the furnace is not used above 1100°C.

Acknowledgments

The authors wish to acknowledge the advice of Dr M M Faktor during the development of this equipment. The information used in this paper is published by permission of the Senior Director, Development, Post Office Telecommunications Headquarters.

References

Gibbs D F Kay H F Short M A and Wills H H 1957 *J. Sci. Instrum.* **34** 121–2

Reed T B 1969 *MIT Report* No. I 21–3

Offprinted from the *Journal of The Chemical Society, Faraday Transactions I*, 1973, vol. 69

Growth of Crystals from the Gas Phase

Part 4.—Growth of Gallium Arsenide by Chemical Vapour Transport, and the Influence of Compositional Convection

BY M. M. FAKTOR, I. GARRETT AND R. H. MOSS

P.O. Research Dept., Brook Road, Dollis Hill, London NW2 7DT

Received 12*th January*, 1973

An experimental system for crystal growth by chemical vapour transport has been devised, so as to be compatible with the model used in a theoretical treatment described previously. The correlation between the experimental and theoretical growth rates is discussed and the influences of compositional convection and surface barriers to growth are considered.

Gallium arsenide is a commercially important semiconductor. It is produced by chemical vapour transport in either the open flow type of system [1, 2] or in sealed capsules.[3, 4]

The sealed capsule system is the more amenable to theoretical discussion, but we have shown before [5] that it is impossible to control the vapour composition adequately. The total lack of control over the morphology and electronic properties of all the compounds grown by this method supports our contention. The open flow system, on the other hand, while yielding acceptable material, requires a more sophisticated theoretical model than is at our command, at present.

We have therefore designed an "almost closed capsule" system, which may be described with acceptable accuracy by our one-dimensional model,[5] while yielding useful material under well-controlled conditions. The theoretical study reported here, with a modest amount of experimentation, has produced a self-consistent model, with good predictive capabilities.

EXPERIMENTAL AND MODEL SYSTEMS

While the open flow type of system [1, 2] remains the most popular way of depositing thin films of gallium arsenide, the problems of hydrodynamics and chemical engineering involved in a theoretical analysis of that system are intractable.[6] Adjustment of doping level and crystalline perfection rely on trial and error. In an attempt to narrow the gap between theory and practice, we have devised an "almost closed capsule" apparatus, shown in fig. 1. This system may be described usefully by a one-dimensional model, since the region of interest, between the gallium arsenide source material and the substrate, is shielded from the flow of gas through the furnace tube, communicating with it only through a hole about 0.2 mm in diameter.

THEORETICAL TREATMENT

1. EQUILIBRIA IN THE SYSTEM

HCl is produced by the reduction of $AsCl_3$ in hydrogen: eqn (1)

$$2AsCl_3 + 3H_2 \rightarrow \tfrac{1}{2}As_4 + 6HCl. \qquad (1)$$

Purified hydrogen is bubbled through $AsCl_3$ at 0–25°C. When the resulting gas mixture enters the hot part of the furnace, reaction (1) takes place, the equilibrium being far to the right at our operating temperature of 700-800°C. Thus the atmosphere in the furnace tube consists of As_4 and HCl, with a considerable excess of hydrogen.

Inside the capsule, the transport reaction (2) takes place

$$GaAs(s)+HCl(g) \rightarrow GaCl(g)+\tfrac{1}{4}As_4(g)+\tfrac{1}{2}H_2(g). \quad (2)$$

There is much thermodynamic and mass-spectrometric evidence that this reaction is by far the dominant process under the experimental conditions prevailing in gallium arsenide deposition apparata.[7-9]

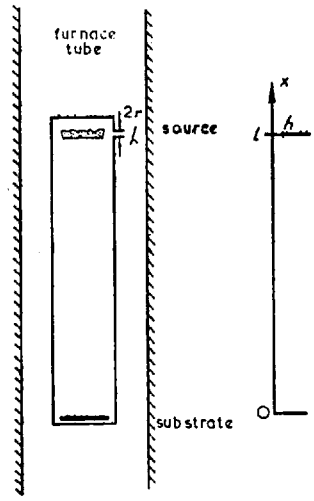

FIG. 1.—Capsule and model systems.

For the purposes of this analysis, we will assume that the solid source and the substrate are in thermodynamic equilibrium with the vapour phase in their immediate vicinities, although the composition of the vapour alters smoothly in the intervening region. This assumption is to be regarded as a reasonable and useful approximation.

2. EQUILIBRIUM AT THE SOURCE

There are four thermodynamic degrees of freedom in this system. We choose to assign arbitrary values to the parameters: source temperature $T(l)$ total pressure P ($\simeq$ 1 atm) and the partial pressures p_{H_2} and p_{As_4} of hydrogen and arsenic. The other partial pressures p_{HCl} and p_{GaCl} may then be calculated from eqn (3) and (4)

$$K_2 = p_{GaCl}(p_{H_2})^{\frac{1}{2}}(p_{As_4})^{\frac{1}{4}}/p_{HCl} \quad (3)$$

$$P = p_{GaCl}+p_{H_2}+p_{As_4}+p_{HCl}. \quad (4)$$

The use of $AsCl_3$ as a source of chlorine imposes a restriction relating the partial pressures of arsenic and chlorine species, as well as determining the total level of chlorine species. Thus the four degrees of freedom are reduced to two once the temperature T_b of the $AsCl_3$ bubbler is fixed, and it is possible to calculate the partial pressures of all species in terms of P, $T(l)$, and T_b. The details of this calculation are given in the Appendix. For the moment we imagine that we have independent control of p_{H_2} and p_{As_4}.

3. EQUILIBRIUM OVER THE SUBSTRATE

The four degrees of freedom are accounted for as follows: we fix the temperature $T(0)$; the total pressure P is taken as being constant all along the capsule since it is about 2 cm in diameter.[5] The remaining two degrees of freedom are removed by the requirements that there must be zero fluxes of hydrogen and of chlorine. No degree of freedom is removed by the requirement that the gallium and arsenic fluxes must be in the correct stoichiometric ratio, as this restriction is imposed by the stoichiometry of the reaction, i.e., by the mechanism of the approach to equilibrium.

4. FLOW EQUATIONS

Each vapour species is transported by diffusion, and also by Stefan flow resulting from the molar volume change accompanying reaction (2).[5, 10-12] The flow equations are therefore:

$$J_{Ga} = \frac{Up_{GaCl}}{RT} - \frac{D}{RT}\frac{dp_{GaCl}}{dx} = J \tag{5}$$

$$_{As} = \frac{4Up_{As_4}}{RT} - \frac{4D}{RT}\frac{dp_{As_4}}{dx} = \tag{6}$$

$$J_H = \frac{U}{RT}[2p_{H_2} + p_{HCl}] - \frac{D}{RT}\frac{d}{dx}[2p_{H_2} + p_{HCl}] = 0 \tag{7}$$

$$J_{Cl} = \frac{U}{RT}[p_{HCl} + p_{GaCl}] - \frac{D}{RT}\frac{d}{dx}[p_{HCl} + p_{GaCl}] = 0 \tag{8}$$

where J is the growth rate of gallium arsenide, U is the mole-average (Stefan) velocity of the gas mixture, and D is the diffusion coefficient, which for formal simplicity we assume is the same for all species. The general treatment of multicomponent diffusion is complicated.[13] We could improve our accuracy by making the very reasonable assumption that the minor species GaCl, As_4, and HCl diffuse independently in the hydrogen, so that we have, in effect, three independent binary diffusion systems. However, the assumption of a single diffusion coefficient is sufficiently accurate here. If we wished to use eqn (10)-(13) below to calculate partial pressures at the substrate in terms of a measured growth rate, the improvement would be necessary. We have taken a value of 0.45 $cm^2\ s^{-1}$ for D_0 (273 K).[14]

From the flow equations (5)-(8) it follows (i) that $J_{HCl} = -J$, i.e., chlorine is transported one way as GaCl and the other way as HCl, (ii) by suitable linear combination of the equations, that:

$$3JRT = 4UP. \tag{9}$$

Thus if T does not vary much along x, U is essentially constant (conservation of matter).

Ignoring the small variation [10] of T with x, we can easily solve the flow equations to obtain the partial pressures as functions of x in terms of the boundary conditions, i.e., the partial pressures over the source:

$$p_{GaCl}(x) = \left[p_{GaCl}(l) - \frac{4P}{3}\right]\exp\left\{\frac{3JRT}{4DP}(x-l)\right\} + \frac{4P}{3} \tag{10}$$

$$p_{As_4}(x) = \left[p_{As_4}(l) - \frac{P}{3}\right]\exp\left\{\frac{3JRT}{4DP}(x-l)\right\} + \frac{P}{3} \tag{11}$$

$$p_{HCl}(x) = \left[p_{HCl}(l)+\frac{4P}{3}\right]\exp\left\{\frac{3JRT}{4DP}(x-l)\right\}-\frac{4P}{3} \tag{12}$$

$$p_{H_2}(x) = \left[p_{H_2}(l)-\frac{2P}{3}\right]\exp\left\{\frac{3JRT}{4DP}(x-l)\right\}+\frac{2P}{3}. \tag{13}$$

Inserting the boundary condition over the substrate, i.e., the equilibrium partial pressures, into any of these equations yields an expression for the nett growth rate J, e.g.,

$$J = \frac{4DP}{3RTl}\ln\left[\frac{p_{GaCl}(l)-4P/3}{p_{GaCl}(0)-4P/3}\right]. \tag{14}$$

From eqn (10)-(13) we can also extract the conditions for zero nett flow of chlorine and hydrogen, which represent two of the degrees of freedom at the substrate (see section 3):

$$\frac{p_{HCl}(0)+2p_{H_2}(0)}{p_{HCl}(l)+2p_{H_2}(l)} = \frac{p_{GaCl}(0)-4p_{As_4}(0)}{p_{GaCl}(l)-4p_{As_4}(l)} \tag{15}$$

$$\frac{p_{GaCl}(0)+p_{HCl}(0)}{p_{GaCl}(l)+p_{HCl}(l)} = \frac{p_{GaCl}(0)-4p_{As_4}(0)}{p_{GaCl}(l)-4p_{As_4}(l)}. \tag{16}$$

Thus we may calculate the theoretical growth rates J for given input conditions ($T(l)$, P, T_b, and $T(0)$) and capsule length l. The results, shown in fig. 2, are discussed in section 6.

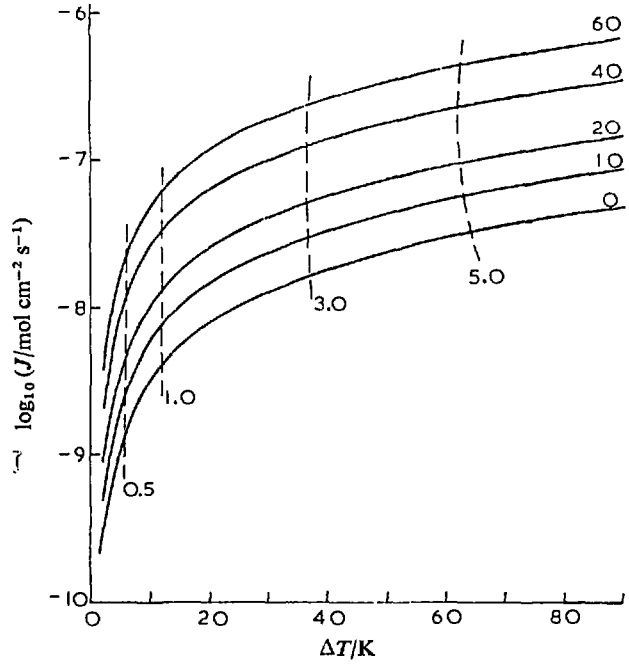

FIG. 2.—Theoretical growth rate (J) as a function of temperature difference (ΔT). $T(l) = 1100$ K. The numbers against the solid lines indicate the temperature of the arsenic trichloride bubbler in °C. The broken lines show $J_{crit.}$ and $\Delta T_{crit.}$ for the temperature gradients indicated (K cm^{-1}).

5. STABILITY OF THE SUBSTRATE SURFACE

For the epitaxial layers of gallium arsenide to be usable for manufacturing devices, they must be smooth single crystal layers a few microns thick. It is essential to prevent pits and hillocks forming as the layers grow, since these blemishes can grow to vertical dimensions exceeding the thickness of the layer. Both pits and hillocks are suppressed if the vapour is undersaturated with respect to gallium arsenide for $x > 0$ and supersaturated for $x < 0$, i.e.,

$$(\partial a/\partial x)_{x=0} \leqslant 0 \tag{17}$$

where a is the activity of solid gallium arsenide, given by:

$$a = \frac{p_{GaCl}(p_{H_2})^{\frac{1}{2}}(p_{As_4})^{\frac{1}{4}}}{p_{HCl}K_2}. \tag{18}$$

We therefore require that:

$$\left(\frac{\partial a}{\partial x}\right)_{x=0} = a(0)\left[\frac{1}{p_{GaCl}}\frac{dp_{GaCl}}{dx}+\frac{1}{2p_{H_2}}\frac{dp_{H_2}}{dx}+\frac{1}{4p_{As_4}}\frac{dp_{As_4}}{dx}-\frac{1}{p_{HCl}}\frac{dp_{HCl}}{dx}-\frac{1}{K_2}\frac{dK_2}{dx}\right] \leqslant 0. \tag{17a}$$

The gradients in partial pressures may be obtained by differentiating eqn (10)-(13) with respect to x.

We have shown previously [10, 11] that the partial pressure gradients depend almost entirely on conditions at the source and the substrate, being very little affected by the temperature profile in between. For given values of $T(l)$, P, T_b, and $T(0)$ (the input conditions), the first four terms on the right of equation (17a) are constant. The last term may be written as:

$$\frac{1}{K_2}\left(\frac{dK_2}{dx}\right)_{x=0} = \frac{\Delta H}{RT(0)^2}\left(\frac{dT}{dx}\right)_{x=0} \tag{19}$$

using van't Hoff's equation, where ΔH is the enthalpy of reaction (2). The first four terms have a positive total, from which the last term, which is also positive since ΔH is positive, is to be subtracted. The stability of the interface thus depends on the magnitude of this last term, i.e., on the temperature gradient over the substrate $(dT/dx)_{x=0}$. For a given temperature gradient, there will be a critical temperature difference $T(l)-T(0) = \Delta T$, for which $(\partial a/\partial x)_{x=0} = 0$, and a corresponding growth rate J_{crit}. Both $\Delta T_{crit.}$ and $J_{crit.}$ are functions of $(dT/dx)_{x=0}$, and are indicated in fig. 2.

6. DISCUSSION OF THEORETICAL RESULTS

The range of ΔT shown in fig. 2 corresponds to that which is easily achieved in practice. Growth rates spanning three orders of magnitude may be achieved, using bubbler temperatures in the range 0-20°C. The fastest rates are suitable for translocating gallium arsenide in bulk to purify it. The slowest rates, corresponding to 0.5 μm/h may be used for fine control over the thickness of epitaxial layers.

The stability of the growth rate to small temperature fluctuations is characterised by the slope of the curves in fig. 2. Acceptable stability is obtained if $\Delta T \geqslant 10$ K, since the furnace is designed to reduce fluctuation of temperature to less than 0.5 K, which would result in a change in growth rate of a few per cent only. Such a fluctuation would, however, alter the composition of the vapour over the growing layer,

resulting in a change in the stoichiometry of the layer and hence in its electronic properties.

The critical conditions for surface stability are approached if the temperature gradient is linear, especially for small gradients. That is, for small ΔT (< 20 K, say) $\Delta T_{\text{crit.}} \simeq l\,(\mathrm{d}T/\mathrm{d}x)_{x=0}$. It is undesirable to operate near the critical conditions, since (i) fluctuations in ΔT may result in a change from sub-critical to super-critical conditions (ii) the radial properties of the problem (i.e., radial temperature gradients, viscosity effects in the vapour) may result in a radial variation in surface stability. Unfortunately, the capsule itself acts as a heat-conduction path and tends to make the temperature profile imposed by the furnace more linear.

The thermochemical data for reaction (2) have been taken from a recent critical appraisal of the literature values :[15]

$$\ln K_2 = (-33\,400/RT + 30.0/R) \tag{20}$$

in the temperature region of interest (700-800°C). The enthalpy of reaction is thus 140 kJ. We have investigated the effect of error in this quantity, in the following way. Clearly, an uncertainty in ΔH for the reaction is equivalent to an uncertainty in the temperature, apart from the relatively small effect of temperature changes on the quantity $4DP/3RT$ which appears in eqn (14) for example. We have therefore calculated the growth rate J as a function of temperature in the range 900-1200 K, for several input conditions, as shown in fig. 3. The calculated growth rate passes through a maximum at about 1050 K. The slope of J against temperature at 1100 K is about 1 % per degree. Hence the error in J arising from an error in ΔH would be about 1 % for an error of 0.13 kJ (8 % per kJ). It is regrettable that the likely error in ΔH is several kJ. The sensitivity of J to ΔH emphasises the need for reliable thermodynamic data for chemical vapour transport systems.

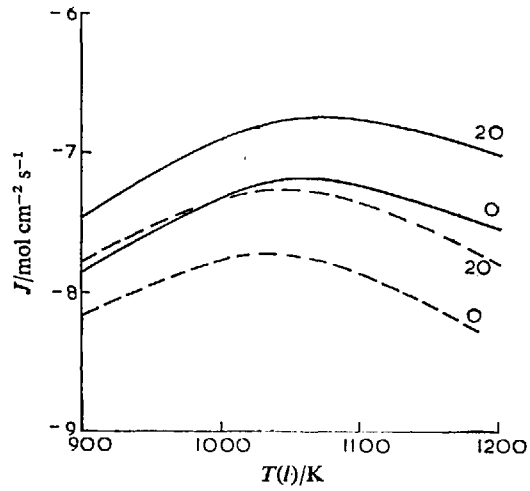

FIG. 3.—Theoretical growth rate (J) as a function of absolute temperature $T(l)$. The numbers against the lines indicate bubbler temperature in °C. Solid line, $\Delta T = 100$ K; broken line, $\Delta T = 30$ K.

The maximum in the growth rate as a function of temperature may be explained as follows: consider the partial pressure of gallium monochloride, p_{GaCl}. The maximum in J represents a compromise between the largest p_{GaCl} over the source, and the largest change in p_{GaCl} between the source and the substrate. When the

temperature is high, p_{GaCl} is large but does not change much for a given ΔT. When the temperature is low, p_{GaCl} is small and cannot change much. The temperature at which J is a maximum increases with increasing temperature of the $AsCl_3$ bubbler.

EXPERIMENTAL BASIS

Layers have been deposited on gallium arsenide substrates using the apparatus shown schematically in fig. 1, at temperatures between 950 and 1100 K. Typical results are shown in fig. 5. We observe that the results are scattered, but generally fall on or below the theoretical lines. There are several sources of experimental error, since the growth rates were determined simply as the difference in weight of the substrate before and after deposition. The main sources of error are (1) we cannot measure the amount of weight lost during the initial vapour etching of the substrate to clean it immediately before growth (2) material deposited on the edges and the back of the substrate contributes to the weight increase. These two effects are in opposition, but the second one is probably larger, and results in the experimental points being too high; (3) the grown layers were frequently far from uniform in thickness.

We consider that the scatter in our experimental points is too great to be explained entirely by the errors mentioned above. The fact that our experimental growth rates fall consistently below our theoretical predictions lends support to the idea that there is an activational barrier to the surface reaction which is significant at our temperature of operation, and which varies from one substrate to another. Such variation might be due to slight variation in crystallographic orientation or to films of contamination such as carbon. It appears, however, that the theoretical rates of growth are in good agreement with the maximum rates achieved experimentally, which probably occur when the surface activational barrier is low.

LIMITATIONS OF THE THEORY

The two most serious short-comings of the theory are (1) that it is one-dimensional, (2) that at present it is necessary to assume equilibrium between solid and vapour in order to obtain numerical boundary conditions for the flow equations. This second short-coming may be overcome with little difficulty, as has been shown formally for a simpler system.[16]

The one-dimensional analysis fails to take into account the viscous interaction of the vapour with the capsule walls, the possibility of a non-uniform distribution of the activational barriers to growth on the substrate surface, and the possibility of convection currents in the capsule. We have nothing to say about the first two effects here, but some useful information about the possibility of convection currents may be obtained from the present model.

Convection currents are driven by a vertical density gradient, which may arise from the temperature difference (thermal convection) or from the change in composition of the gas along the capsule (compositional convection). We avoid the first cause of convection currents by arranging for the bottom of the capsule to be colder than the top. However, in a typical experiment at 1000 K with a temperature difference of 50 K and a bubbler temperature of 0°C, we calculate the compositions of the vapour over the source and over the substrate to be those given in table 1.

The density of the vapour is decreased by 5 % at the top of the capsule by the temperature gradient, but increased by 15 % by the composition change. The nett density difference of 10 % is available to drive convection currents.

TABLE 1

species	mol. wt.	pressure at source/atm	pressure at substrate/atm
GaCl	105.5	0.01132	0.006482
As_4	300	0.005146	0.003946
H_2	2	0.9671	0.9681
HCl	36.5	0.01649	0.02143

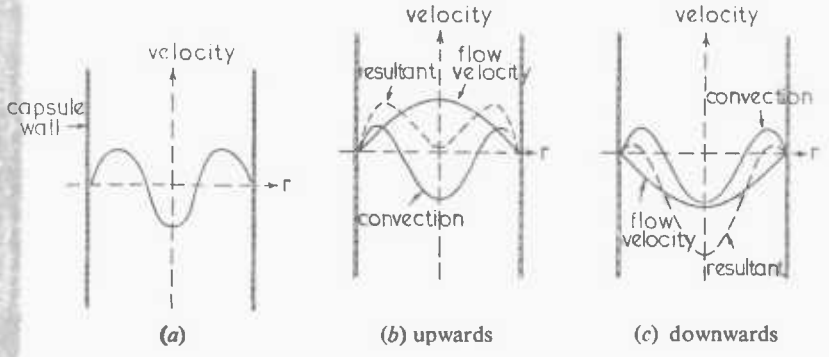

(*a*) (*b*) upwards (*c*) downwards

FIG. 4.—Convection and flow velocities.

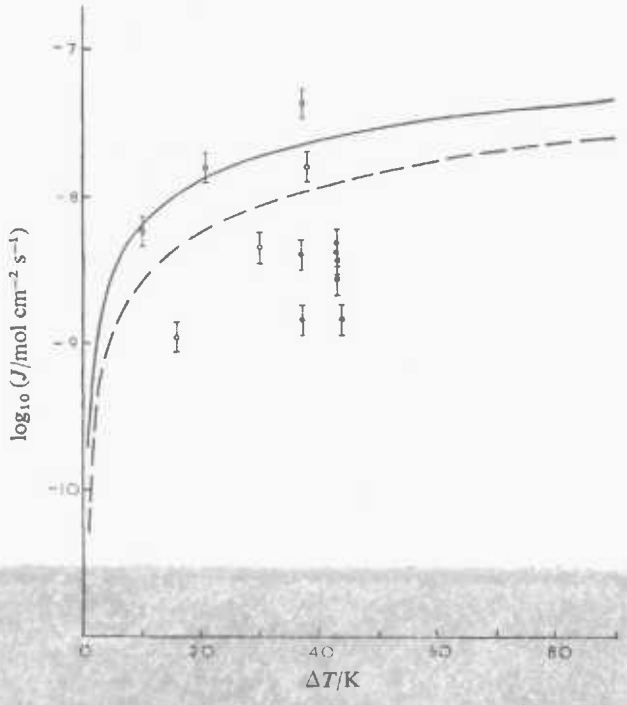

FIG. 5.—Comparison of experimental and theoretical growth rates (l = 20 cm). Solid line, $T(l)$ = 970 K, T_b = 20°C. ○, experimental points. Broken line, $T(l)$ = 1020 K, T_b = 0°C. ●, experimental points.

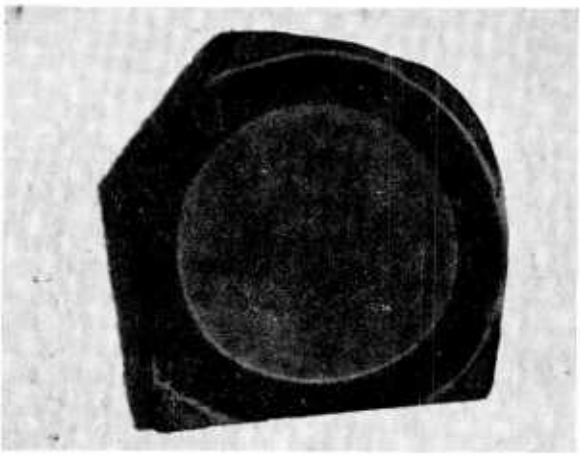

PLATE 1.—Ring pattern deposit on the {100} surface of gallium arsenide.

To face page 1923]

The convective flow pattern of the gas will depend on the geometry of the capsule and on the temperature field. We expect the gas near the capsule walls to be hotter than that at the axis of the capsule, as is inevitable in a tube furnace. We postulate a circulatory motion of the gas, with the gas near the wall rising and that at the centre falling. The transverse velocity variation, in absence of any other motion of the gas, would be as depicted in fig. 4(*a*). On this variation we have to superimpose the Stefan flow velocity, which would have approximately the parabolic variation given by Poiseuille's analysis. If the Stefan velocity is upwards, the situation sketched in fig. 4(*b*) arises when the two velocity contributions are of similar magnitude. Such a resultant velocity could clearly cause a ring of growth on the substrate instead of a uniform layer. The opposite situation, sketched in fig. 4(*c*), results in enhanced growth in the centre. If the growth rate here exceeds $J_{crit.}$ under the existing experimental conditions, a ring structure delineated by changes in surface morphology may result. Such ring structures have been observed by us, e.g., plate 1, and we ascribe them tentatively to this cause.

CONCLUSIONS

Calculated growth rates for the "almost closed capsule" are in reasonable agreement with the maximum growth rates obtained experimentally, which are probably obtained when the surface activational barriers are low. Our model is thus correct in its essential features. The calculated rates are sensitive to errors in the thermodynamic data for the transport reaction, which emphasises the need for more precise data. The experimental conditions are such that the growing surface should be stable, according to our stability criterion $(\partial a/\partial x)_{x=0} \leqslant 0$.

The one-dimensional model can deal qualitatively with the possibility of convection in the capsule. Other three-dimensional phenomena require a more sophisticated model.

APPENDIX

CALCULATION OF PARTIAL PRESSURES INSIDE THE CAPSULE

The purified hydrogen gas is bubbled through arsenic trichloride at room temperature or below. We assume that the resulting gas mixture is in equilibrium with liquid arsenic trichloride at the bubbler temperature T_b, i.e.:

$$\frac{(p_{As_4})^{\frac{1}{4}}(p_{HCl})^6}{(p_{AsCl_3})^2(p_{H_2})^3} = K_1(T_b) \tag{27}$$

where K_1 is the equilibrium constant for the reaction:

$$2AsCl_3 + 3H_2 \rightarrow \tfrac{1}{4}As_4 + 6HCl \tag{28}$$

and also, the partial pressure of arsenic trichloride is the equilibrium vapour pressure, given by:[9]

$$\log_{10}(p_{AsCl_3}/\text{atm}) = -2660\,\text{K}/T - 2.53\ln(T/\text{K}) + 21.88. \tag{29}$$

The stoichiometry of reaction (28) dictates that:

$$p_{HCl} = 12p_{As_4}. \tag{30}$$

The total pressure is given by

$$P = p_{AsCl_3} + p_{H_2} + p_{As_4} + p_{HCl}. \tag{31}$$

The four equations (27), (29), (30), (31) may be solved for the four component partial pressures in the gas stream leaving the bubbler. This gas stream enters the furnace, and as its temperature rises, the equilibrium of reaction (28) moves to the right. At the capsule

temperature $T(l)$ we can calculate the component partial pressures, using eqn (27) with $K_1T(l)$ on the right hand side, eqn (30) and (31), and an equation expressing the fact that the hydrogen/chlorine ratio remains constant once the gas stream has left the bubbler:

$$\left(\frac{2p_{H_2}+p_{HCl}}{3p_{AsCl_3}+p_{HCl}}\right)\text{outside the capsule} = \left(\frac{2p_{H_2}+p_{HCl}}{3p_{AsCl_3}+p_{HCl}}\right)\text{at the bubbler.} \quad (32)$$

Eqn (32) is a good approximation if diffusion fluxes are very much smaller than the gas flow rate in the pipe connecting the bubbler to the furnace. This condition is certainly fulfilled in practice.

We now turn to consider the flow of gas through the effusion hole and the partial pressures over the source.

The equilibrium equation is:

$$K_2(l) = \frac{p_{GaCl}(l)[p_{H_2}(l)]^{\frac{1}{2}}[p_{As_4}(l)]^{\frac{1}{4}}}{p_{HCl}(l)}. \quad (33)$$

The unknowns are: $p_{GaCl}(l), p_{H_2}(l), p_{As_4}(l), p_{HCl}(l)$, and the total pressure inside the capsule, which may exceed the total pressure outside by an appreciable amount if the effusion hole is small. The equations at our disposal are: Poiseuille's equation for viscous flow through the effusion hole:

$$U = 1.013\times10^6 r^2\Delta P/8\eta h \quad (34)$$

where U is the flow velocity in mm/s, r the hole radius in mm, ΔP the difference in total pressure through the hole in atm, η the viscosity coefficient in poise, and h the length of the hole in mm; four flow equations, (10)-(13), which, when solved assuming that the partial pressure of gallium monochloride outside the hole is negligible, give:

$$0 = [p_{GaCl}(l) - JRT/U]f + JRT/U \quad \text{for gallium} \quad (35)$$

$$p_{AsCl_3}(h) + p_{As_4}(h) = [4p_{As_4}(l) - JRT/U]f + JRT/U \quad \text{for arsenic} \quad (36)$$

$$2p_{H_2}(h) + p_{HCl}(h) = [2p_{H_2}(l) + p_{HCl}(l)]f \quad \text{for hydrogen} \quad (37)$$

$$3p_{AsCl_3}(h) + p_{HCl}(h) = [p_{GaCl}(l) + p_{HCl}(l)]f \quad \text{for chlorine} \quad (38)$$

where (h) denotes partial pressures outside the effusion hole, J is the nett flux of material through the hole, and

$$f = \exp\left\{\frac{Uh}{D}\right\} = \exp\left\{\frac{1.013\times10^6 r^2\Delta P}{8\eta D^0(T/273)^{1.8}}\right\}. \quad (39)$$

Finally, we have, for the total pressure:

$$p_{GaCl}(l) + p_{As_4}(l) + p_{H_2}(l) + p_{HCl}(l) = P + \Delta P. \quad (40)$$

We eliminate J between eqn (35) and (36):

$$p_{AsCl_3}(h) + 4p_{As_4}(h) = [4p_{As_4}(l) - p_{GaCl}(l)]f. \quad (41)$$

We now have five equations, viz.: (33), (40), and (37), (38), (41) with (39) substituted for f, which are to be solved for the unknown partial pressures and the total pressure. The calculation requires a double iterative procedure because eqn (33) is of the seventh order and eqn (37), (38) and (41) are transcendental. The problem was solved on a Burroughs B5500 computer.

Acknowledgement is made to the Director of Research of the Post Office for permission to publish this paper.

[1] J. J. Tietjen and J. A. Amick, *J. Electrochem. Soc.*, 1966, **113**, 724.
[2] D. Effer, *J. Electrochem. Soc.*, 1965, **112**, 1020.
[3] R. R Moest and B. R. Shupp, *J. Electrochem. Soc.*, 1962, **109**, 1061.

[4] H. Shafer, *Chemical Transport Reactions* (Academic Press, London, 1964).
[5] M. M. Faktor, R. Heckingbottom and I. Garrett, *J. Chem. Soc. A*, 1970, 2657.
[6] B. G. Secrest, W. W. Boyd and D. W. Shaw, *J. Cryst. Growth*, 1971, **10**, 251.
[7] V. S. Ban, *J. Electrochem. Soc.*, 1971, **118**, 1473.
[8] D. J. Kirwan, *J. Electrochem. Soc.*, 1970, **117**, 1572.
[9] G. F. Day, Varian Report No. 324-6Q, Air Force Contract No. AF33(615)-1988, Project No. 4460, Task No. 446006, *Heterojunction Device Concepts.*
[10] M. M. Faktor and I. Garrett, *J. Chem. Soc. A*, 1971, 934.
[11] M. M. Faktor, R. Heckingbottom and I. Garrett, *J. Chem. Soc. A*, 1971, 1.
[12] J. Stefan, *Ann. Phys. Chem.*, 1882, **17**, 550.
[13] S. Chapman and T. G. Cowling, *The Mathematical Theory of Non-uniform Gases* (Cambridge, 1960).
[14] W. H. Shepherd, *J. Electrochem. Soc.*, 1965, **112**, 988.
[15] D. Battat, M. M. Faktor and M. A. Savva, unpublished work.
[16] M. M. Faktor and I. Garrett, *J. Cryst. Growth*, 1971, **9**, 12.

Journal of The Chemical Society, Faraday Transactions I, 1974 , Volume 70, pp2267–2279

Modified Entrainment Method for Measuring Vapour Pressures and Heterogeneous Equilibrium Constants

Part 1.—Theory, and Validation of the Method using Water and Lead

By David Battat, Marc M. Faktor,* Ian Garrett and Rodney H. Moss

Post Office Research Station, Dollis Hill, London NW2 7DT

Received 27*th March*, 1974

A method of evaluating vapour pressures and equilibrium constants for heterogeneous reactions is proposed. It replaces the usually indeterminate contribution of gaseous transport in the conventional entrainment method by a calculable amount. The method was successfully applied at around room temperature to the evaporation of water, and to the vaporisation of lead in the temperature range 900-1050°C.

1. INTRODUCTION

The thermodynamics of heterogeneous equilibria provides the corner-stone for many branches of physical and chemical science, for example, materials preparation, corrosion and combustion. For reacting systems the enthalpy and entropy changes for the reactions which are involved have in the past been measured by various methods. Vapour pressures and dissociation pressures have been measured by calorimetry, manometry, effusion, torsion-effusion, mass-spectrometry, entrainment, and other methods,[1, 2] and a similar variety of techniques is available for determining the equilibrium constants for chemical reactions. For vapour-solid and vapour-liquid reactions, entrainment has long been a popular method. We present a method which is a modification of the normal entrainment method. Before doing so, we briefly appraise the normal method.

A stream of reactive gas is passed over the solid or liquid maintained at a given temperature and the amount of product formed in a given time is found from the loss of weight of the solid or liquid, or by condensing or dissolving the products out of the gas stream and determining them by standard analytical techniques. While this method is both simple and flexible, it suffers from the disadvantage that the effect of *flowing* the reactants at a finite rate must somehow be accounted for or eliminated. If the gas-flow is very fast, the vapour is not fully equilibrated with the condensed phase, whereas if the flow is very slow, products may travel away from the zone in which equilibrium is being established at a significant rate by diffusion. Furthermore, unmixing of the gas by thermal diffusion becomes a serious source of error, particularly if the gas mixture contains hydrogen.[3] Traditionally, extrapolation to zero flow rate has been used, but this results in error for the reasons given above. By constricting the flow channel either side of the equilibrium zone containing the condensed phase the effect of diffusion at low flow rates can be reduced. If the apparent partial pressure of the product is plotted as a function of flow rate, there may be a range of flow rates in which the apparent partial pressure does not alter greatly, and this " plateau " value is often taken as representing the true partial pressure.[4] In well-designed apparatus this assumption may be justifiable, but because equilibrium is established only at the surface of the condensed phase, there must always be some

diffusion of reactants towards the surface and of products away from the surface. The region in which diffusion operates is usually ill-defined. This diffusion can be made less limiting by causing turbulent mixing of the gas in the reaction zone, or by flowing the gas stream fast to reduce the boundary layer over the solid or liquid. Inevitably there is some composition change in the gas in a direction normal to the surface of the condensed phase, and this is an eventual limitation of the method. When a " plateau " in the plot of apparent partial pressure against flow rate is not found, the true partial pressure is in doubt.

In the new method described in this paper, we have come to terms with the unavoidable diffusion effect by confining its region of action to a long, narrow channel of *known* geometry (typically 2 cm long, 1 mm diameter). One end of the channel is connected to a bulb or reservoir containing the condensed phase under study, and the other end is directed into the stream of reactive gas. The reservoir and channel are suspended from a recording microbalance, so that the loss of weight can be measured continuously. By making the gas flow resistance of the channel high, we can ensure that the rate at which the sample substance loses weight is limited by gas transport kinetics in the channel, the effects of which can be calculated accurately. As a good approximation, we assume that the vapour has a uniform composition in the reservoir above the condensed phase, so that the partial pressure variations are confined to the channel. It would not be difficult to relax this assumption. When the vapour leaves the open end of the channel, it is rapidly diluted and swept away in the fast stream of gas.

This paper presents the simple theory of the method, showing how the enthalpy and entropy changes for the reaction, evaporation, or dissociative sublimation may be found from the rate at which the sample loses weight. We also give the results of calibration and test experiments performed on evaporating water and lead. These results are in excellent agreement with the other values reported in the literature.

By varying the dimensions of the channel so as to decrease its resistance to gas flow, and by decreasing the surface area of the condensed phase, the chemical reaction or evaporation process at the surface can be made to limit the rate at which weight is lost. Here we have an analogy with a Knudsen effusion experiment, performed with larger and larger orifices, until Langmuir evaporation conditions are approached. Our method, then, may be used to study both equilibria and chemical kinetics for heterogeneous reactions.

2. THEORY OF WEIGHT LOSS

2.1 MODEL SYSTEM USED

We describe the channel through which the vapour in the bulb communicates with the stream of reactive gas by a simple one-dimensional model (see fig. 1). At the point $x = 0$, we assume that the vapour composition is the same as that over the surface of the condensed phase, and at $x = l$, we assume that the composition of the vapour in the channel has become identical with that in the external gas stream. The first assumption is reasonable if the bulb diameter is large compared with the channel diameter. The second assumption is investigated in detail in section 2.5, and is a very good approximation under the conditions of flow used.

2.2 SIMPLE THEORETICAL DESCRIPTION

We consider first the evaporation of a single species A in a stream of inert gas Z. Because of the increase in molar volume when species A evaporates, a " wind " or Stefan flow is generated in the channel,[5] which sweeps both species upwards. The

partial pressure gradient of A, and the corresponding gradient of Z, cause diffusion fluxes which must result in zero nett flow of species Z. We can thus write the flow equations in the form [6, 7]:

$$J_A = \frac{Up_A}{RT} - \frac{D}{RT}\frac{dp_A}{dx} = \frac{\dot{W}}{M_A C} \tag{1}$$

$$J_Z = \frac{Up_Z}{RT} - \frac{D}{RT}\frac{dp_Z}{dx} = 0 \tag{2}$$

where D is the binary diffusion coefficient, U is the " wind " or Stefan velocity, $\dot{W}$ is the measured rate of weight loss, M_A is the molecular weight of species A, and C the cross-sectional area of the channel. In writing the diffusion fluxes in terms of dp_A/dx, instead of $d(p_A/P)/dx$, we are assuming that the total pressure is essentially constant all along the channel. Although some pressure gradient is necessary to maintain the Stefan flow, this gradient is negligible unless the channel is very narrow.[6]

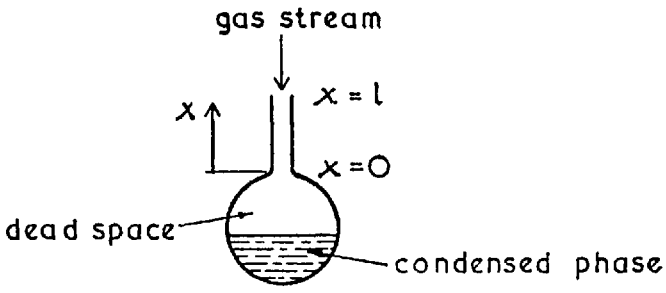

FIG. 1.—Reaction bottle.

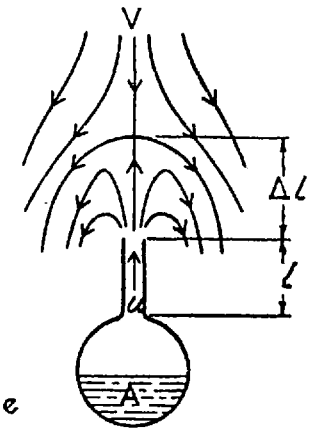

FIG. 2.—Streamline pattern in vicinity of channel exit.

Addition of eqn (1) and (2) causes the diffusion terms to cancel out, and we obtain:

$$J_A = UP/RT \tag{3}$$

where P is the total pressure. We now substitute eqn (3) in eqn (1) to eliminate U, and integrate from $x = 0$ to $x = l$. At $x = l$, p_A is zero (see section 2.5), and at $x = 0$, p_A is the saturated vapour pressure of species A, p_A°. Thus:

$$p_A^\circ = P[1 - e^{-\xi}] \tag{4}$$

where $\xi = J_A RTl/DP = WRTl/DPM_A C$ is the " transport function ".

If the rate of weight loss is not large, we may approximate the exponential in eqn (4) to obtain:

$$p_A^\circ \approx \dot{W}RTl/DM_A C. \tag{5}$$

If measurements of weight loss are carried out over a fairly restricted temperature range, it may be acceptable to assume that T/D is a constant, in which case a plot of

$R \ln \dot{W}$ against $1/T$ has a slope of $-\Delta H_v$ and an intercept at $1/T = 0$ of $\Delta S_v - R \ln(RTl/DM_AC)$, since

$$R \ln p_A^\circ = -\Delta H_v/T + \Delta S_v$$

where ΔH_v and ΔS_v are the enthalpy and entropy changes of evaporation of substance A.

However, it is preferable to carry out measurements of weight loss over as wide a temperature range as possible, for which reason it is necessary to correct for the temperature dependence of the diffusion coefficient. Over a range of temperature, the expression

$$D = \frac{D_0}{P}\left(\frac{T}{T_0}\right)^{1+s} \tag{6}$$

holds,[8] where D_0 is the value of D at a reference temperature T_0 and 1 atm pressure, and s lies usually between 0.5 and 1, frequently near 0.8 (but see section 3 for a case where $s \approx 1.5$ for water in nitrogen). Eqn (5) now becomes (still for small $\dot{W}$):

$$p_A^\circ \approx \dot{W}RPlT_0^{1+s}/D_0T^sM_AC. \tag{7}$$

A plot of $R \ln(\dot{W}/T^s)$ against $1/T$ again has a slope of $-\Delta H_v$, and an intercept at $1/T = 0$ of $\Delta S_v - R \ln(lRPT_0^{1+s}/D_0M_AC)$. We thus have a method for establishing the enthalpy and entropy changes of evaporation or sublimation which gives results that can be made independent of the rate at which the external stream of gas flows. Because of uncertainties about diffusion coefficients and their variation with temperature, ΔH_v and ΔS_v are subject to small errors, which will be discussed in section 2.4. In section 4 we present the results of two calibration experiments, which show the accuracy that can quite easily be achieved.

Next we consider a heterogeneous reaction of a fairly simple but general type:

$$M(s) + HX(g) \rightarrow MX(g) + \tfrac{1}{2}H_2\ (g) \tag{8}$$

where M is the condensed phase, assumed to be a single component, and X could be a halogen or, with the necessary changes in stoichiometric coefficients, oxygen or sulphur, for example. The equilibrium constant for reaction (8) may be expressed as:

$$K_p = \frac{p_{MX}^\circ (p_{H_2}^\circ)^{\frac{1}{2}}}{p_{HX}^\circ} = \exp\left[-\frac{\Delta H_r}{RT} + \frac{\Delta S_r}{R}\right] \tag{9}$$

where p_{MX}°, etc. are the equilibrium vapour pressures which we assume exist at $x = 0$.

Since reaction (8) involves an increase in the number of vapour phase molecules, there will again be a " wind " in the channel. The flow equations are:

$$J_M = \frac{Up_{MX}}{RT} - \frac{D}{RT}\frac{dp_{MX}}{dx} = \frac{\dot{W}}{M_MC} \tag{10}$$

$$J_H = \frac{U}{RT}(p_{HX} + 2p_{H_2}) - \frac{D}{RT}\frac{d}{dx}(p_{HX} + 2p_{H_2}) = 0 \tag{11}$$

$$J_X = \frac{U}{RT}(p_{MX} + p_{HX}) - \frac{D}{RT}\frac{d}{dx}(p_{MX} + p_{HX}) = 0. \tag{12}$$

Here we assume an average value for D. We discuss this point in the next section.

As there are no sources or sinks for hydrogen or X inside the channel or the bulb (neglecting absorption in the condensed phase), the fluxes of these species are zero. Again, addition of the flow equations eliminates the diffusion terms, and yields:

$$J_M = 2UP/RT. \tag{13}$$

We again eliminate U from eqn (10) using eqn (13), and integrate from $x = 0$ to $x = l$. At the exit of the channel, $p_{MX}(l) \sim 0$ (see section 2.5), so that:

$$p^{\circ}_{MX} = 2P(1-e^{-\xi}) \tag{14}$$

where now $\xi = J_M RTl/2DP = \dot{W}RTl/2DPM_M C$.

By similar integration, we also find:

$$p^{\circ}_{HX} = (p^{(l)}_{HX}+2P)e^{-\xi}-2P \tag{15}$$

$$p^{\circ}_{H_2} = (p^{(l)}_{H_2}-P)e^{-\xi}+P. \tag{16}$$

Note that the sum of the partial pressures is constant and equal to the total pressure in the system.

Measurement of the rate of weight loss allows us to calculate the equilibrium partial pressures, p°_{MX} etc., and hence arrive at the equilibrium constant using eqn (9). Alternatively, we may formulate the equilibrium constant from eqn (14)-(16) and hence derive a relation between K_p and $\dot{W}$.

Let us define the fraction of reactive species in the free stream as:

$$p^{(l)}_{HX}/P = \varepsilon. \tag{17}$$

We consider various approximate expressions for the equilibrium constant K_p in terms of the transport function ξ, and reactive species fraction ε, which arise when $\xi \ll 1$, i.e. small rate of weight loss. This situation occurs if either ε is small (there is little reactant in the system) or if the equilibrium of reaction (8) is well to the left ($K_p \ll 1$). We treat each case separately.

CASE (1) $\xi \ll 1$, $\varepsilon \sim 1$.—Eqn (14)-(16) become:

$$p^{\circ}_{MX} = 2P\xi$$

$$p^{\circ}_{HX} = P(\varepsilon-\varepsilon\xi-2\xi)$$

$$p^{\circ}_{H_2} = P(1-\varepsilon+\varepsilon\xi).$$

Thus

$$K_p \approx 2\left(\frac{\xi}{\varepsilon}\right)P^{\frac{1}{2}}(1-\varepsilon)^{\frac{1}{2}} \qquad \text{for } \varepsilon \sim 1,\ \xi \ll 1$$

or

$$K_p \approx 2P\xi(p^{(l)}_{H_2})^{\frac{1}{2}}/p^{(l)}_{HX}. \tag{18}$$

In this case, a plot of $R \ln \dot{W}$ against $1/T$ yields ΔH_r and ΔS_r, directly from the slope and the intercept.

CASE (2) $\varepsilon \ll 1$, $\xi \sim \varepsilon$.—Then

$$p^{\circ}_{MX} \approx 2P\xi$$

$$p^{\circ}_{HX} \approx P(\varepsilon-2\xi)$$

$$p^{\circ}_{H_2} \approx P(1-\varepsilon).$$

(Note that since $p^{\circ}_{HX} > 0$, ξ cannot be greater than $\varepsilon/2$.) For this case we find:

$$K_p \approx \frac{2\xi\sqrt{P}}{\varepsilon-2\xi}. \tag{19}$$

In this case, a plot of $R \ln \dot{W}$ against $1/T$ does not yield ΔH_r and ΔS_r directly. It is necessary to calculate K_p at each temperature from eqn (19). However, if ξ is near $\varepsilon/2$, the reaction has gone essentially to completion, K_p is very large and the experiment will not be revealing.

CASE (3) $\xi \ll \varepsilon \ll 1$.—Eqn (19) reduces to

$$K_p = \frac{2\xi\sqrt{P}}{\varepsilon} \tag{20}$$

and a plot of $R \ln \dot{W}$ against $1/T$ yields ΔH_r and ΔS_r directly, as in case (1).

2.3 MULTICOMPONENT DIFFUSION

The treatment of multicomponent diffusion is lengthy,[8] and we will not apply it to this problem. However, it frequently happens that one species is present in considerable excess. It is then permissible to consider the diffusion of each minority species in the majority species as an independent binary diffusion system. For a ternary system, this approximation can be justified rigorously.[9] We ignore diffusion of one minority species into another, because the collisions which give rise to these diffusion phenomena are rare.

The flow equations can now be re-written in the form :[9]

$$J_{MX} = \frac{U}{RT}p_{MX} - \frac{D_{MX}}{RT}\frac{dp_{MX}}{dx} = J_M \tag{21}$$

$$J_{HX} = \frac{U}{RT}p_{HX} - \frac{D_{HX}}{RT}\frac{dp_{HX}}{dx} = -J_M \tag{22}$$

$$J_{H_2} = \frac{U}{RT}p_{H_2} + \frac{D_{MX}}{RT}\frac{dp_{MX}}{dx} + \frac{D_{HX}}{RT}\frac{dp_{HX}}{dx} = \tfrac{1}{2}J_M \tag{23}$$

where D_{MX} and D_{HX} are the binary diffusion coefficients of MX and HX in hydrogen, and the relations between the J values for each species result from the conditions :

$$J_H = J_{HX} + 2J_{H_2} = 0$$
$$J_X = J_{HX} + J_{MX} = 0$$

as before. By summing eqn (21)-(23), the diffusion fluxes cancel out, and eqn (13) is obtained again. Eliminating U and integrating from $x = 0$ to $x = l$ yields :

$$p^\circ_{MX} = 2P[1 - e^{-\xi_{MX}}] \tag{24}$$

$$p^\circ_{HX} = [p^{(i)}_{HX} + 2P]e^{-\xi_{MX}} - 2P \tag{25}$$

where

$$\xi_{MX} = \frac{J_M RTl}{2D_{MX}P} \quad \text{and} \quad \xi_{HX} = \frac{J_M RTl}{2D_{HX}P}.$$

For hydrogen, we simply subtract the minority partial pressures from the total pressure :

$$p^\circ_{H_2} = P - p^\circ_{MX} - p^\circ_{HX}. \tag{26}$$

Eqn (24)-(26) may be used to calculate the equilibrium partial pressures from the measured rate of weight loss.

Since the flow eqn (21)-(23) hold for a mixture with one majority species only, $p^{(i)}_{HX}$ is a small fraction of the total pressure P ($\varepsilon \ll 1$). Furthermore, the transport functions ξ_{HX} and ξ_{MX} cannot be greater than $\varepsilon/2$ and $(D_{HX}/D_{MX})(\varepsilon/2)$ respectively. Hence we can usefully simplify the expression for the partial pressures and for K_p :

$$p^\circ_{MX} \approx 2P\xi_{MX}$$
$$p^\circ_{HX} \approx p^{(i)}_{HX} - 2P\xi_{HX}$$
$$p^\circ_{H_2} \approx p^{(i)}_{H_2} - P[2\xi_{MX} - 2\xi_{HX}].$$

Hence

$$K_p \approx \frac{2P\xi_{MX}}{p_{HX}^{(I)} - 2P\xi_{HX}} \qquad \text{for } \varepsilon \ll 1. \tag{27}$$

If, in addition, $\xi \ll \varepsilon$, then

$$K_p \approx 2\xi_{MX}/\varepsilon. \tag{28}$$

In practice, we found eqn (28) was applicable to our calibration experiments, described in section 3.

2.4 ERRORS IN ENTHALPY AND ENTROPY CHANGES

We will not consider errors in measurement of temperature and partial pressures in the external stream of gas. Also we assume that the dimensions of the channel and the total pressure are known well. Our concern here is with the effect of errors in the diffusion coefficient D_0 and the index of its temperature variation s on the experimental values of enthalpy and entropy changes.

The parameter D_0 appears only in the expression for the entropy, and then only as a logarithm. An uncertainty of a factor of two in the diffusion coefficient contributes an error of 6 J mol^{-1} K^{-1}. While the value of D_0 may not be known accurately, it may be estimated from critical-point data,[10, 11] by comparison with pairs of similar gases for which D_0 is known,[12, 13] or from empirical curves such as that of Shepherd.[14]

The index s affects both ΔH and ΔS. We can find the error $\delta(\Delta H)$ introduced by an error $\delta(s)$:

$$-\Delta H = \frac{\mathrm{d}}{\mathrm{d}(1/T)}(R \ln \dot{W} - Rs \ln T)$$

$$= \frac{\mathrm{d}}{\mathrm{d}(1/T)}(R \ln \dot{W}) + RsT.$$

Hence

$$\delta(\Delta H) = -RT\,\delta(s).$$

Thus an error of 0.1 in s at 1200 K produces an error of 1 kJ mol^{-1} in ΔH. The index s is, of course, not known for species for which the diffusion coefficient has not been measured as a function of temperature. This includes the products of many high-temperature reactions. For most pairs of gases, s is in the range 0.5-1.[8] However, anomalous values of s for some combinations of gases are known, e.g. ≈ 1.5 for $H_2O + N_2$, as calculated from the experimental data of Schwertz and Brow.[15]

Similarly we find the error $\delta(\Delta S)$ caused by an error $\delta(s)$ in the index s, and one calculates

$$\delta(\Delta S) \approx -R\delta(s)[1 + \ln(T/T_0)].$$

Thus an error of 0.1 in s introduces an error in ΔS of 1 J mol^{-1} K^{-1} at 320 K and 2 J mol^{-1} K^{-1} at 1200 K, if $T_0 = 273$ K.

2.5 HYDRODYNAMICS OF THE FLOW AT THE CHANNEL EXIT

We have assumed so far that at $x = l$, i.e. at the exit of the channel, the gas becomes rapidly diluted and swept away by the external stream. Let us examine the flow pattern near the channel exit. The vapour leaving the channel spills out into a region of length Δl, and on reaching the bounding streamline, its concentration has

been reduced effectively to zero. We take Δl as being the distance from the exit of the tube to the stagnation point (fig. 2).

According to potential flow theory,[16] the flow in the stagnation region may be constructed by superposition of the uniform flow of the external stream at velocity V, and the flow issuing from the channel. The flow from the channel may be approximated by a point source, from which the flow falls off as $1/r^2$ in accordance with the conservation of matter.[16] For this flow, the velocity $u(x)$ a distance x from the source is given by:

$$2\pi x^2 u(x) = UC = \dot{W}RT/PM$$

where U is the Stefan velocity in the channel. At the stagnation point, $x = \Delta l$ and $u(x) = V$, hence

$$\Delta l = (\dot{W}RT/2\pi VPM)^{\frac{1}{2}}. \tag{29}$$

On substituting $(l+\Delta l)$ for l in the expression for ξ (the transport function), we obtain V as a function of $\dot{W}$ from eqn (4):

$$V = \frac{\dot{W}^3 RT/2\pi PM}{\left[\dfrac{CD_0PM}{RT_0}\left(\dfrac{T}{T_0}\right)^s \ln\left\{1-\dfrac{p_A^\circ}{P}\right\}+l\dot{W}\right]^2}. \tag{30}$$

We have investigated the dependence of the rate of weight loss due to simple evaporation, as a function of the velocity V of the external stream and of the length l of the channel. The substance evaporating was water, in a stream of nitrogen (this system has also been investigated experimentally for calibration and testing the method, see section 3). Solutions to this equation are presented in fig. 3. The left-hand limit, for zero V, corresponds to the entire volume of the apparatus reaching the saturated vapour pressure p_A°, where $\dot{W}$ becomes zero. As V increases, Δl decreases and $\dot{W}$ increases, until a limit is approached asymptotically. Having a rough idea of the

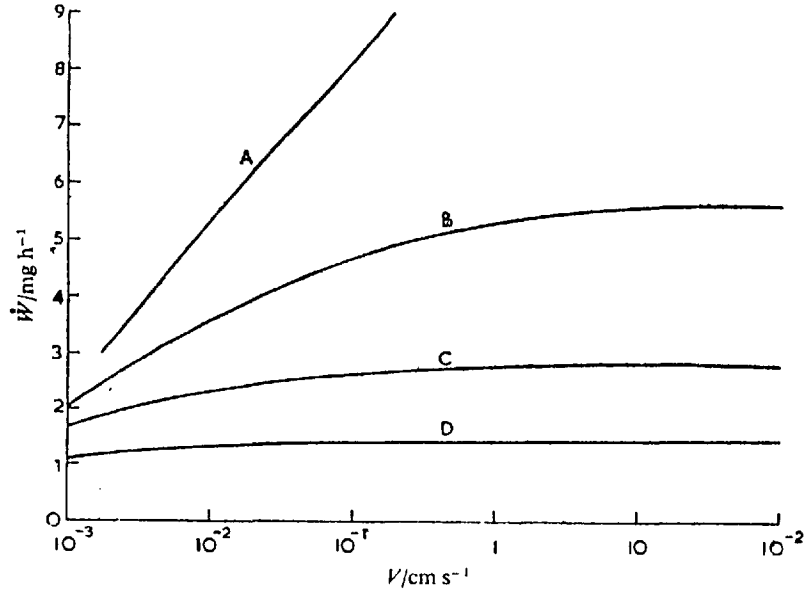

FIG. 3.—Effect of external stream velocity on rate of weight loss. (A) l = 0.1 cm; (B) l = 0.25 cm; (C) l = 0.5 cm; (D) l = 1 cm. T = 40°C, P = 1 atm, channel diam. = 2 mm.

maximum value of $\dot{W}$ to be expected (say within a factor of 10), it is a simple matter to calculate the necessary velocity for the external stream to make $\Delta l \ll l$. For our apparatus, we calculate a maximum value of Δl of around 0.1 mm at the speed $V = 1\ \mathrm{cm\ s^{-1}}$.

3. EXPERIMENTAL

3.1 APPARATUS

The apparatus is illustrated schematically in fig. 4. The reaction bottle, shown in fig. 4.(i), was suspended on a silica fibre from a Cahn RH electrobalance, and hung inside a furnace tube which could be heated with a small furnace to temperatures in the range 300-1100°C, or with a water jacket (condenser) in the range 0-55°C. Two gas inlets are provided

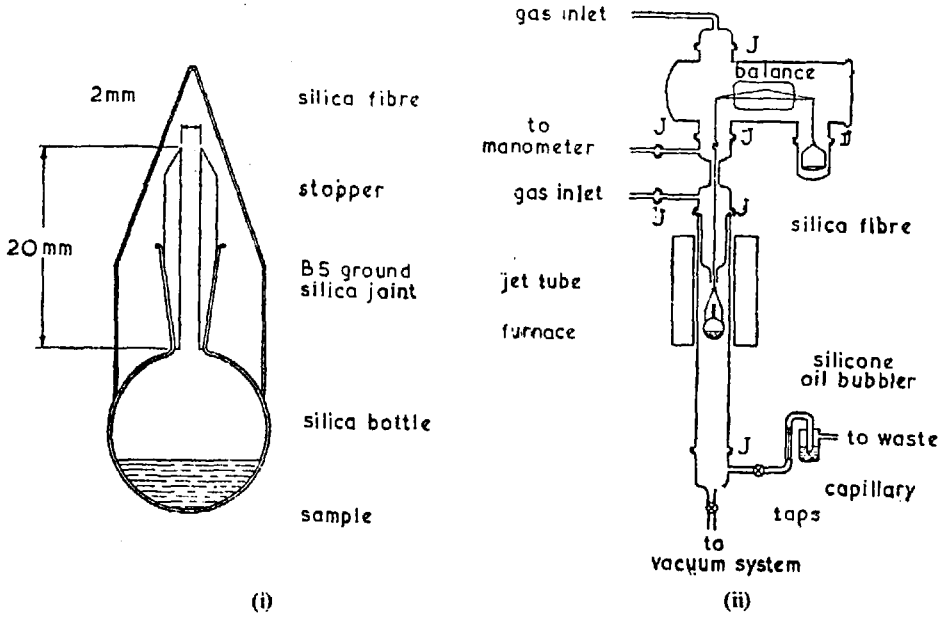

FIG. 4.—(i) Reaction bottle; (ii) experimental system.

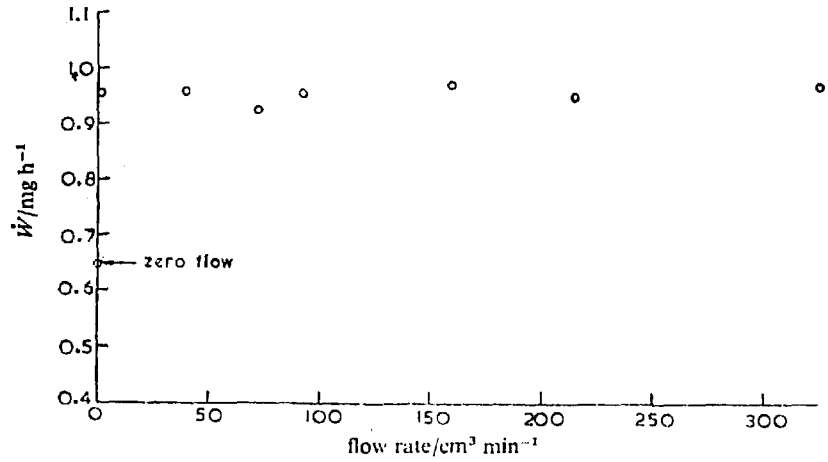

FIG. 5.--Effect of flow rate on rate of evaporation. $T = 44.4$°C, $P = 1$ atm, H_2O/N_2.

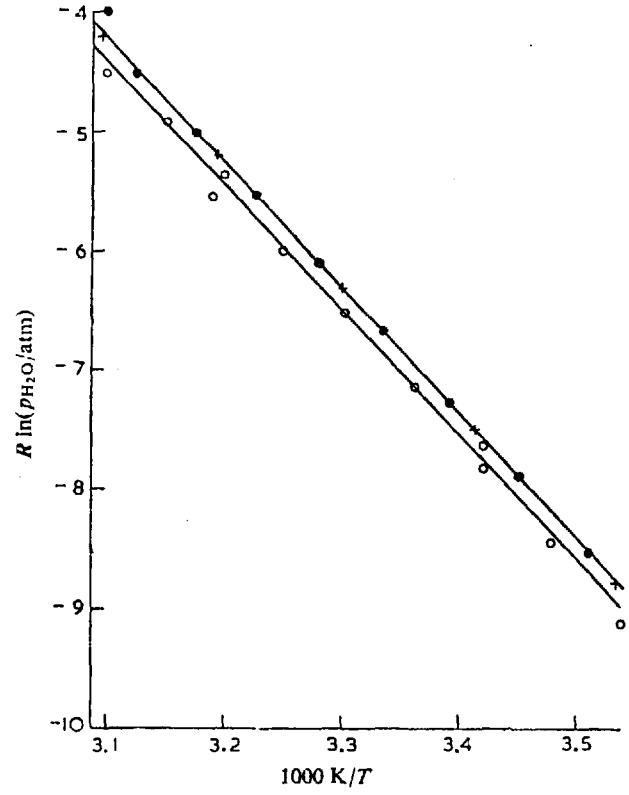

FIG. 6.—Evaporation of water in nitrogen. ●, ref. (17); +, ref. (18); ○, this work.

near the top of the apparatus: the lower one will pass reactive gases into the furnace tube in future experiments, the upper one, directly into the balance chamber, serves to keep the chamber free of reactive gases. The temperature of the gas stream was measured with a Pt/Pt–13 % Rh thermocouple on the outside of the furnace tube for high temperatures, and an alcohol-in-glass thermometer positioned with its bulb immediately below the reaction bottle for the lower temperature work. Gas flow rates were measured using Meterate flow meters.

TABLE 1.—CALIBRATION DATA

(*a*) water in nitrogen		(*b*) lead in hydrogen	
T/°C	$\dot{W}$/mg h^{-1}	T/°C	$\dot{W}$/mg h^{-1}
9.5	0.0936	892	0.208
14.55	0.135	902	0.259
19.5	0.19	902	0.217
19.5	0.2092	925	0.354
24.6	0.2747	930	0.358
29.9	0.39	958	0.526
34.75	0.5175	961	0.548
39.7	0.74	979	0.794
40.5	0.675	979	0.804
44.5	0.955	1009	1.201
49.7	1.219	1028	1.510
		1028	1.582

3.2 FLOW VISUALISATION EXPERIMENTS

Preliminary experiments demonstrated the need for controlling the gas flow near the exit of the neck of the bottle (channel). The flow pattern was made visible by passing ammonia and hydrogen chloride through the furnace tube so that they mixed at the top of the furnace tube and reacted to form a smoke. At the flow rates used (about 100 cm^3 min^{-1}), no steady flow pattern developed in the wide (20 mm) furnace tube. The main flow was down one side of the tube, but this pattern changed erratically with temperature and flow rate. To direct the flow and increase the linear velocity by a factor of 10 a constriction or jet tube was introduced, which resulted in a steady flow around the reaction bottle.

3.3 DEPENDENCE OF WEIGHT LOSS ON FLOW RATE

The theoretical basis for the dependence of the rate of weight loss on the velocity of the external stream of gas was given in section 2.5. We find that, with the jet tube fitted, the rate of weight loss of a reaction bottle containing water is independent of the rate of flow of nitrogen in the furnace tube over the entire range of flows under our control (1-350 cm^3 min^{-1}), corresponding to linear velocities of 0.6 to 200 mm s^{-1}). The results are shown in fig. 5.

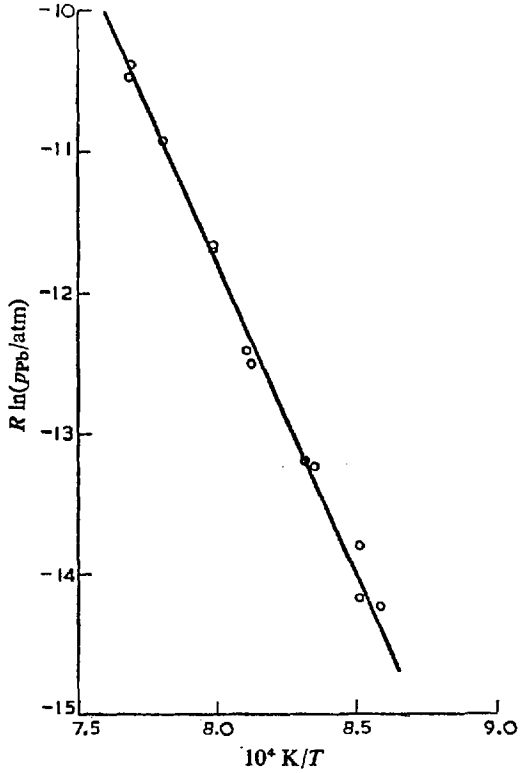

FIG. 7.—Evaporation of lead in hydrogen.

4. RESULTS

4.1 EVAPORATION OF WATER

The sample material was deionized, double quartz-distilled water. The experimental results are given in table 1(*a*) as rate of weight loss at various temperatures. We have converted these weight loss rates to partial pressures of water, using eqn (4), and taking the diffusion coefficient for water in nitrogen from Schwertz and Brow.[15]

Fig. 6 shows a plot of our experimental values for $R \ln(p^{\circ}_{H_2O}/\text{atm})$ against $1/T$, with literature values [17, 18] for comparison. From our plot we calculate the following second-law values for ΔH°_{v} and ΔS°_{v} (at our mean operating temperature of 30°C) as 43.6 kJ mol^{-1} (10.4 kcal mol^{-1}) and 116.7 J mol^{-1} K^{-1} (27.9 e.u.) respectively.

4.2 EVAPORATION OF LEAD

The sample material was lead granules (AnalaR; Hopkins and Williams Ltd.). The experimental rates of weight loss at various temperatures are given in table 1(*b*). These results have been converted to partial pressures using eqn (4). The diffusion coefficient of lead in hydrogen was estimated from Shepherd's curve [14] to be 0.16 cm^2 s^{-1}, and we have taken s to be 0.8 as discussed in section 2.4. Our values for $R \ln(p^{\circ}_{Pb}/\text{atm})$ are plotted against $1/T$ in fig. 7, and from this plot we calculate the second-law values of ΔH°_{v} and ΔS°_{v} (at our mean operating temperature of 960°C) as 180 kJ mol^{-1} (43.0 kcal mol^{-1}) and 94.7 J mol^{-1} K^{-1} (22.6 e.u.) respectively.

5. DISCUSSION

Our value for ΔH°_{v} for water is in excellent agreement with the literature value of 43.6 kJ mol^{-1}, but our value for ΔS°_{v} is too high by 0.8 J mol^{-1} K^{-1} (0.2 e.u.).

For the evaporation of lead, we find the following values for ΔH°_{v} in the literature:

ΔH°_{v}/kcal mol^{-1} 298 K	ΔH°_{v}/kcal mol^{-1} 1235 K	ref.
46.36	43.36 (181.2 kJ mol^{-1})	19
46.615	43.615 (182.3 kJ mol^{-1})	20
46.47	43.47 (181.7 kJ mol^{-1})	21
47.06	44.06 (184.2 kJ mol^{-1})	21
46.80	43.8 (183.1 kJ mol^{-1})	22
45.8±0.7	42.8±0.7 (178.9±3 kJ mol^{-1})	1
	43.0 (180 kJ mol^{-1})	this work

The value of ΔS°_{v} at 1235 K, calculated from the data of Stull and Sinke,[22] is 91.1 J mol^{-1} K^{-1}, in good agreement with the data recommended as reliable by Nesmeyanov, and 3.6 J mol^{-1} K^{-1} below our value.

The effect of errors in the diffusion coefficient and in its temperature dependence have been discussed in section 2.4. Other errors arise in the measurement of $\dot{W}$, T, C and l. The dimensions of the channel, C and l, were measured with a travelling microscope. Small systematic errors originate from the channel being slightly oval in section and the ends not being quite perpendicular to the axis. Measurement of $\dot{W}$ introduces very small systematic errors from inaccuracies of the balance, and larger random errors, which may be as large as 5 %. One serious source of systematic error at the high temperature is in the measurement of temperature. The cold gas entering the furnace is accelerated in the jet tube, so that we would not have been surprised to find indications that our temperature measurements were too high. This would have resulted in a low value for the entropy of evaporation, whereas we find too high a value.

Our analysis in section 2 is based on a one-dimensional model, wherein the flux J is uniform over the entire cross-section C of the channel. Obviously, this is not so, Stefan's velocity U will have a parabolic distribution due to viscosity forces, and the more realistic problem is one of axi-symmetric (diffusion) flow in two dimensions. For small rates of evaporation, the variations of the flow quantities in the channel are small and we would expect the mean flow described by the one-dimensional model to yield a good approximation.

In view of the systematic and random errors which are involved, we consider our results for water to be in excellent agreement with the literature values. For lead, we will discuss the possible errors from two points of view. Looking at our experiment as a calibration of the method, we find that by choosing $D_0 = 0.168$ cm^2 s^{-1}, and $s = 0.64$ for the diffusion of lead in hydrogen, and taking the measured temperatures to be 1 % too low, we bring our results into line with those recommended by Stull and Sinke. Alternatively, looking at the experiment as a measurement of ΔH_v and ΔS_v for lead, and assessing the likely errors to be 10 % in D_0, 25 % in s, and possibly as large as 2 % in T, we calculate uncertainties in our values for ΔH_v and ΔS_v of ± 8 kJ mol^{-1} in ΔH_v and ± 5 J mol^{-1} K^{-1} in ΔS_v.

It would be possible to eliminate many of the sources of error, but we are interested here in assessing the method for measuring equilibrium constants for reactions which are far less well characterised than the vaporisation of lead. The results of one such investigation are reported in the next paper.

6. CONCLUSIONS

The modification of the entrainment method, described in this paper, has been discussed theoretically on the basis of a one-dimensional model, and tested on the evaporation of water and of lead. The results obtained are in good agreement with literature values, and demonstrate that the method is reliable.

While little effort was made to refine the apparatus, and various sources of random and systematic errors certainly exist, the accuracy obtained is adequate for our present purpose. With some sophistication of the technique, the precision could be improved considerably.

Acknowledgement is made to the Director of Research of the Post Office for permission to publish this paper.

[1] A. N. Nesmeyanov, *Vapour Pressure of the Elements* (Infosearch, 1963).
[2] O. Kubaschewski, E. Ll. Evans and C. B. Alcock, *Metallurgical Thermochemistry* (Pergamon, New York, 1967).
[3] M. M. Faktor and J. I. Carasso, *J. Electrochem. Soc.*, 1965, **112**, 817.
[4] J. L. Margrave, *Characterisation of High Temperature Vapours* (Wiley, New York, 1967).
[5] D. A. Frank-Kamenetskii, *Diffusion and Heat Transfer in Chemical Kinetics* (Plenum, New York, 1969).
[6] M. M. Faktor, R. Heckingbottom and I. Garrett, *J. Chem. Soc. A*, 1970, 2657.
[7] M. M. Faktor, R. Heckingbottom and I. Garrett, *J. Chem. Soc. A*, 1971, 1.
[8] S. Chapman and T. G. Cowling, *The Mathematical Theory of Non-Uniform Gases* (Cambridge, 1960).
[9] D. Battat, to be published.
[10] H. Fujita, *Kagaku Kikai*, 1951, **15**, 234.
[11] C. R. Wilke, *Chem. Eng. Progr.*, 1950, 46, 95.
[12] *International Critical Tables*, 1929, **5**, 62.
[13] *Handbook of Heat Transfer*, ed. W. M. Rohsenow and J. P. Hartnett (McGraw-Hill, New York, 1973).
[14] W. H. Shepherd, *J. Electrochem. Soc.*, 1965, **112**, 988.
[15] F. A. Schwertz and J. E. Brow, *J. Chem. Phys.*, 1951, **19**, 640.
[16] A. M. Kuethe and J. D. Schetzer, *Foundations of Aerodynamics* (Wiley, New York, 1950).
[17] G. W. C. Kaye and T. H. Laby, *Physical and Chemical Constants* (Longman, London, 1959).
[18] D. Ambrose and I. J. Lawrenson, *J. Chem. Thermodynamics*, 1972, **4**, 755.
[19] A. C. Egerton, *Proc. Roy. Soc. A*, 1923, **103**, 469.
[20] J. Fischer, *Festsch. Tech. Hochschule*, 1935, 172.
[21] P. Gross, C. S. Campbell, P. J. C. Kent and D. L. Levi, *Disc. Faraday Soc.*, 1948, **4**, 206.
[22] D. R. Stull and G. C. Sinke, *Thermodynamic Properties of the Elements* (Amer. Chem. Soc., Washington, 1956).

Journal of The Chemical Society, Faraday Transactions 1, 1974, Volume 70, pp 2280–2292

Modified Entrainment Method for Measuring Vapour Pressures and Heterogeneous Equilibrium Constants

Part 2.—Equilibria in the Water/Gallium System

BY DAVID BATTAT, MARC M. FAKTOR,* IAN GARRETT AND RODNEY H. MOSS

Post Office Research Department, Dollis Hill, London NW2 7DT

Received 27th March, 1974

The modified entrainment method is applied to the study of a heterogeneous equilibrium: water vapour/liquid gallium, in the temperature range 1200-1400 K. Two gaseous gallium species, Ga_2O and GaOH, were observed. The theory of the modified entrainment method is extended to this more complex case involving two simultaneous reactions.

The entropies and enthalpies of formation are:

	ΔH°_{298}/kJ mol^{-1}	S°_{298}/J mol^{-1} K^{-1}
Ga_2O	-90.8 ± 8	287 ± 6
GaOH	-148 ± 15	248 ± 12.

1. INTRODUCTION

The gallium/water equilibrium at high temperature is of interest for several reasons. Under suitable conditions of temperature and water/hydrogen ratio, volatile gallium species are evolved [1, 2] at appreciable partial pressures. The system can therefore be used for chemical vapour transport of gallium compounds, as has been done by several workers.[3-5] Water vapour is an attractive reagent for such a process.

It appeared that the gallium/water system was well characterised,[1, 2] and would be a useful and interesting reactive system for testing our modified entrainment method described in Part 1.[6] Previous workers [3-5, 7, 8] have assumed that the volatile gallium species is the sub-oxide, formed by the reaction:

$$2Ga(l) + H_2O(g) \rightleftharpoons Ga_2O(g) + H_2(g). \quad (1)$$

The enthalpy of formation of $Ga_2O(g)$ was reported by Frosch and Thurmond,[1] and by Cochran and Foster,[2] as the result of measurements of the equilibria between gallium and the oxides SiO_2 and MgO, and Ga_2O_3.

Our work shows that in addition to the suboxide, a volatile mono-hydroxide is formed in the presence of hydrogen:

$$Ga(l) + H_2O(g) \rightleftharpoons GaOH(g) + \tfrac{1}{2}H_2(g). \quad (2)$$

This reaction is important under the conditions that have been used for vapour transport of gallium compounds in water vapour/hydrogen mixtures.[3-5, 7, 8] The equilibrium constant for the reaction:

$$2GaOH(g) \rightleftharpoons Ga_2O(g) + H_2O(g) \quad (3)$$

is unity at about 1000 K.

This paper describes the application of our method for studying heterogeneous equilibria [6] to the gallium/water vapour system in the temperature range 1200-1400 K,

and we report second-law and third-law enthalpies and entropies of formation for gallium suboxide and gallium monohydroxide.

A third reaction may occur in the system:

$$2Ga(l)+3H_2O(g)\rightarrow Ga_2O_3(s)+3H_2(g). \quad (4)$$

Gallium sesquioxide forms as a crust on the liquid gallium, and hinders reactions (1) and (2). We designed our experiment so as to avoid formation of the sesquioxide.

2. EXPERIMENTAL

In Part 1 of this series [6] we described the method and its application to measurement of vapour pressures. Briefly, a small silica bottle with a long narrow neck of known dimensions is suspended in a furnace from a recording microbalance. The condensed phase sample (gallium in the present instance) is contained in the bottle, and a suitable atmosphere (water vapour/hydrogen mixture) flows round the bottle. The reactant gases enter the bottle via the neck, and the products leave by the same route. Changes in gas composition are confined essentially to the neck of the bottle, and may be accurately described using a simple theory of gas transport.[6, 9]

Fig. 1 is a schematic illustration of the apparatus. The temperature of the bottle is measured with a Pt/Pt-10 % Rh thermocouple, positioned on the outside of the furnace tube level with the reaction bottle. The vapour pressure measurements reported in Part 1 indicate that our temperature measurements were about 1 % too low, and we have corrected the temperatures accordingly.

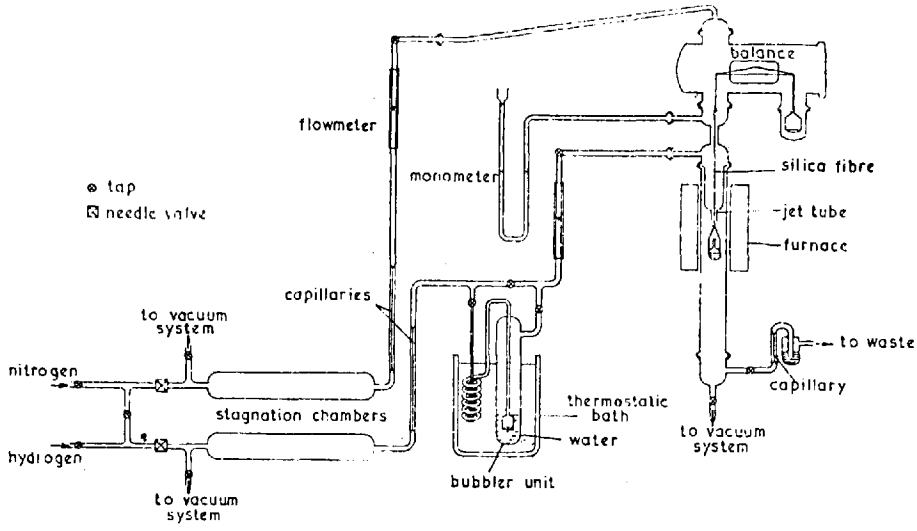

FIG. 1.—Experimental arrangement. ⊗, tap; ⊠, needle valve.

The primary hydrogen stream passes through a fine sintered frit bubbler containing deionized, double quartz distilled water. The bubbler stands in a thermos flask, and thermostatted kerosene is passed round it continuously to control its temperature. The coil preceding the bubbler allows the hydrogen to reach the temperature of the water. A secondary hydrogen stream enters the system through the balance chamber, thus keeping it free of reactive gases. The hydrogen was purified using a palladium diffuser. The secondary flow was replaced by dry nitrogen for the second experiment, for reasons discussed in section 4. Flow rates were measured with Meterate flow meters, and controlled with needle valves.

Successful operation of the balance requires smooth gas flow, which was achieved by using stagnation chambers and capillaries in the equivalent of a capacitor-resistor network (fig. 1).

The practical limits of temperature and water vapour/hydrogen ratio that can be used in this experiment are shown in fig. 2, in which an " operating window " is delineated. The upper bound of temperature is set by the furnace elements and by the silica furnace tube. At a given temperature, there is a water vapour/hydrogen ratio at which gallium sesqui-oxide becomes stable, and this ratio is the upper bound for that dimension of the " window ". The lower bounds of the " window " are determined by the sensitivity of the balance to small rates of weight loss. In calculating the bounds in fig. 2, we have used literature data for the formation of Ga_2O_3 [10] and Ga_2O.[1, 2]

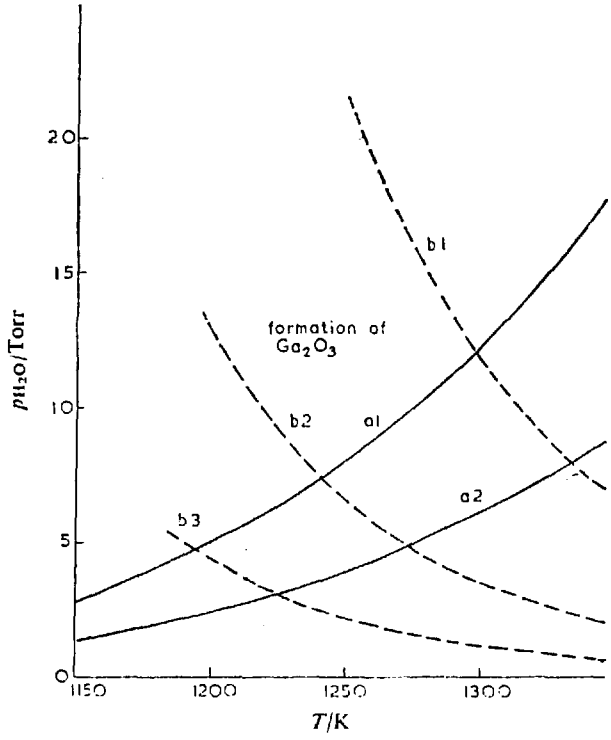

FIG. 2.—Bounds of the experimental "window". (a1) $p_{H_2}/P = 1$, (a2) $p_{H_2}/P = 0.5$; required sensitivity of the balance (b1) 1.0 μg s^{-1}, (b2) 0.3 μg s^{-1}, (b3) 0.1 μg s^{-1}.

3. RESULTS

Two sets of experiments were performed. In the first, experiment (*a*), a ratio of partial pressures of water vapour to hydrogen of 0.003 25 was used. The rates of loss of weight at the experimental temperatures are given in table 1.

A linear least squares fit yields the representation:

$$\ln \dot{W}_a = -9793.7\ \mathrm{K}/T + 7.094 \qquad (5)$$

with an index of determination of -0.991.

In the second experiment, experiment (*b*), the secondary hydrogen flow was replaced by dry nitrogen. The water vapour partial pressure was 0.001 63 atm, and the hydrogen partial pressure was 0.223 atm. The results of the second experiment are given in table 1(*b*).

A least squares fit yields the representation

$$\ln \dot{W}_b = -8680.7\ \mathrm{K}/T + 5.236 \qquad (6)$$

with an index of determination of -0.97.

Throughout the discussion which follows, we use subscripts a and b to distinguish quantities referring to experiments (a) and (b), and subscripts 1 and 2 to distinguish quantities referring to reactions (1) and (2).

TABLE 1.—SAMPLE WEIGHT LOSS AT VARIOUS TEMPERATURES

experiment (a)		experiment (b)	
T/K	$\dot{W}$/mg h^{-1}	T/K	$\dot{W}$/mg h^{-1}
1186	0.299	1217	0.157
1215	0.400	1262	0.181
1243	0.464	1292	0.220
1268	0.532	1324	0.281
1291	0.584		
1291	0.636		
1303	0.646		

4. DISCUSSION

4.1 GENERAL REMARKS

To convert the experimental data into equilibrium constants, we apply the theory developed in Part 1.[6] In the next subsection, we take the simplest approach and assume that one reaction dominates over the experimental temperature range. We then adduce evidence to show that this assumption is not consistent with all our experimental results. In subsection 4.3, we extend the theory given in Part 1, to cover simultaneous equilibria, and we obtain second law entropies and enthalpies for reactions (1) and (2). The calculation of third law data is described in subsection 4.4, and the two sets of results compared. Our results are compared with previously published results in subsection 4.5.

4.2 ONE DOMINANT REACTION

We assume that either reaction (1) or reaction (2) accounts for the observed loss of weight. For these reactions, the equilibrium constants are:

$$K_1 = \frac{p^{(\circ)}_{Ga_2O} p^{(\circ)}_{H_2}}{p^{(\circ)}_{H_2O}} \tag{7}$$

and

$$K_2 = \frac{p^{(\circ)}_{GaOH} [p^{(\circ)}_{H_2}]^{\frac{1}{2}}}{p^{(\circ)}_{H_2O}}. \tag{8}$$

Using the analysis in Part 1, and the approximations of Case (2) which are appropriate here; we can write the equilibrium constants as:

$$K_1 = \frac{YP\xi_{Ga_2O}}{\varepsilon - \xi_{H_2O}} \tag{9}$$

and

$$K_2 = \frac{2\sqrt{PY} \times \xi_{GaOH}}{\varepsilon - 2\xi_{H_2O}} \tag{10}$$

where Y is p_{H_2}/P, ≈ 1 in experiment (a) and 0.223 in experiment (b), $\varepsilon = p_{H_2O}/P$ in the gas stream flowing through the furnace, and ξ_i is the transport function of species i, defined by:

$$\xi_i = \frac{\dot{W}}{2CM_{Ga}} \times \frac{RTl}{PD_i(T)}.$$

D_i is the binary diffusion coefficient for species i in hydrogen, C and l are the cross-sectional area and the length of the neck of the bottle, M_{Ga} is the atomic weight of gallium, P, T, and R are the total pressure, temperature and gas constant.

The diffusion coefficients for the minority species in hydrogen were obtained as follows: the diffusivities at 0°C were obtained in terms of the critical temperature and pressure [11] in the case of water, using the relationship proposed by Arnold [12] and Fujita,[13] and in terms of the molecular weights for the volatile gallium species, using Shepherd's [14] empirical curve. The diffusion coefficients at high temperature were then calculated from the equation [15]:

$$D(T) = D_0(T/273\ \mathrm{K})^{1+s}$$

where s was taken as 0.833 for the diffusion of water in hydrogen,[13] and 0.75 for the other species.[15] The values of D_0 are given in table 2.

TABLE 2.—BINARY DIFFUSION COEFFICIENTS AT 0°C

species	D_{i,H_2}/cm^2 s^{-1}	D_{i,N_2}/cm^2 s^{-1}	D_i'/cm^2 s^{-1}	s
H_2O	0.686	0.231	0.271	0.833
Ga_2O	0.18	0.0605	0.0711	0.75
GaOH	0.275	0.0925	0.109	0.75

To estimate the effective diffusion coefficients of the minority species in a hydrogen + nitrogen mixture, we first estimate the diffusion coefficients in nitrogen alone. We assume that the ratio of the diffusion coefficient of species i in hydrogen to that in nitrogen is independent of species i. This assumption holds good for most permanent gases [16] and a large number of organic vapours.[17] We calculate the diffusion coefficient of water in nitrogen, using the critical data [11] and Fujita's equation,[13] and hence estimate the diffusion coefficients of the gallium species in nitrogen. The diffusion coefficient D_i' for species i in a mixture of hydrogen and nitrogen is given by :[18]

$$D_{i,H_2}'/D_i' = Y+(1-Y)(D_{i,H_2}/D_{i,N_2}) \qquad (11)$$

where Y is p_{H_2}/P in the mixture, and D_{i,H_2} and D_{i,N_2} are the diffusion coefficients of species i in hydrogen and in nitrogen. The values for D_{i,H_2}, D_{i,H_2}, and D_i' are given in table 2.

It is now possible to calculate the values of the equilibrium constants K_1 and K_2, using the eqn (9) and (10). As ξ is of the order 10^{-3}, these approximate formulae are quite adequate. The results are plotted in fig. 3. The corresponding second-law enthalpy and entropy changes for reactions (1) and (2) are given in table 4.

If either reaction were dominant over our temperature range, we would expect the values of the equilibrium constant for that reaction yielded by the two experiments to be the same. In table 3, we give the ratio of values of the two equilibrium constants determined from the two experiments. We have used the least-squares fit to the experimental points, as given by eqn (5) and (6), to determine values of the equilibrium constants at several temperatures, because different temperatures were used in the two experiments. The ratios in table 3 depart appreciably from unity, and vary considerably with temperature. Although the experimental data from experiment (*b*) are scattered because the operational "window" is very small, it is clear that neither reaction is dominant over our experimental temperature range.

Two other pieces of evidence support this conclusion.

(1) We have investigated the composition of the vapour in a capsule loaded with liquid gallium and wet hydrogen and heated to 1000°C, using a VG Micromass 12 mass

spectrometer. Peaks were observed at mass numbers 154, 156, 158 (corresponding to the molecules $^{69}Ga_2{}^{16}O$, $^{69}Ga^{71}Ga^{16}O$, $^{71}Ga_2{}^{16}O$) and 86 and 88 (corresponding to $^{69}Ga^{16}O^1H$ and $^{71}Ga^{16}O^1H$), with heights in roughly the ratios expected from the

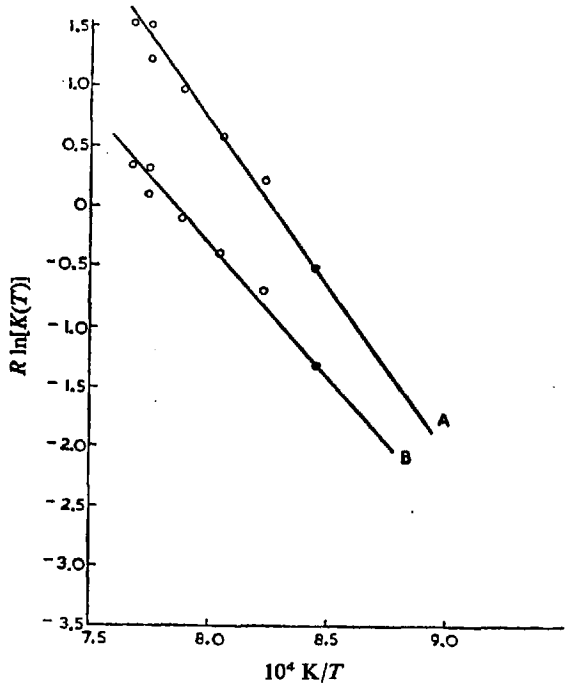

FIG. 3.—Variation of equilibrium constant with temperature assuming a dominant reaction. (A) GaOH: $\Delta H = 114$ kJ mol^{-1}, $\Delta S = 94$ J mol^{-1} K^{-1}; (B) Ga_2O: $\Delta H = 93$ kJ mol^{-1}, $\Delta S = 73$ J mol^{-1} K^{-1}.

relative abundance of the gallium isotopes. The peaks were only a few times the background in height, however, and we were unable to carry out diagnostic tests (e.g. plotting ionization efficiency curves) that would result in unambiguous identification of the species giving rise to these peaks.

TABLE 3.—EQUILIBRIUM CONSTANTS DETERMINED FROM THE TWO EXPERIMENTS

T/K	$K_{1,a}/K_{1,b}$	$K_{2,a}/K_{2,b}$
1200	1.66	0.57
1225	1.63	0.50
1250	1.61	0.43
1275	1.57	0.33
1300	1.52	0.19

(2) We have estimated the enthalpy of formation of GaOH from the dissociation energy of the Ga—OH bond,[19] 427±20 kJ mol^{-1}, and other bond energy data.[20, 21] We find it to be 125±20 kJ mol^{-1}, which gives the enthalpy change for reaction (2) as around 116 kJ mol^{-1} at room temperature. The entropy of GaOH (gas) we estimate as 248±8 J mol^{-1} K^{-1} at room temperature (see section 4.4 below), so that the entropy change for reaction (2) at room temperature is around 84 J mol^{-1} K^{-1}. The free energy change for the reaction is zero at 1300-1400 K, so that we expect the partial

pressure of GaOH to be appreciable in this temperature range. For gallium suboxide, an enthalpy of formation of -84 kJ mol^{-1} has been reported,[1, 2] and we estimate the entropy to be 287 ± 8 J mol^{-1} K^{-1} (see section 4.4). The enthalpy and entropy changes for the reaction (1) are therefore 159 kJ mol^{-1} and 151 J mol^{-1} K^{-1} at room temperature, so that the free energy change is zero at 1000-1100 K. In these rough calculations we have ignored the specific heat corrections, but clearly the partial pressures of GaOH and Ga_2O are comparable in our experimental temperature range.*

4.3 THEORETICAL TREATMENT FOR TWO SIMULTANEOUS REACTIONS

It is not difficult to show, by extending the treatment given in Part 1,[6] that:

$$K_1 = \frac{D_{H_2O,T}}{D_{Ga_2O,T}} Y_b^{\frac{1}{2}} \frac{x(\frac{1}{2}-y)-Y_b^{\frac{1}{2}}y(\frac{1}{2}-x)}{Y_b^{\frac{1}{2}}(\frac{1}{2}-y)(1-x)-(1-y)(\frac{1}{2}-x)} \tag{12}$$

$$K_2 = \frac{D_{H_2O,T}}{D_{GaOH,T}} \frac{Y_by(1-x)-x(1-y)}{Y_b^{\frac{1}{2}}(\frac{1}{2}-y)(1-x)-(1-y)(\frac{1}{2}-x)} \tag{13}$$

where $Y_b = p_{H_2}/P$ in experiment (b) ($= 0.223$) and x and y are variables or coordinates which are related to the position of the reaction equilibrium, and are defined by:

$$x = \frac{\xi_{H_2O,a}}{\varepsilon_a} = \frac{\dot{W}_a}{2CM_{Ga}} \times \frac{RTl}{PD_{H_2O,T}} \tag{14}$$

$$y = \frac{\xi_{H_2O,b}}{\varepsilon_b} = \frac{\dot{W}_b}{2CM_{Ga}} \times \frac{RTl}{PD_{H_2O,T}} \tag{15}$$

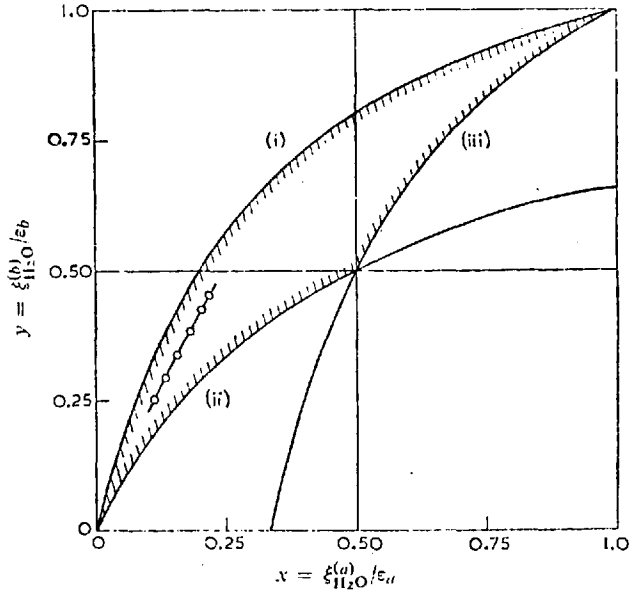

FIG. 4.—Reaction domain for the formation of Ga_2O and GaOH ($Y = 0.25$). (i) Locus of $K_2 = 0$, $y = 4x/1+3x$; (ii) locus of $K_1 = 0$, $y = x/\frac{1}{2}+x$; (iii) locus of $\Delta = 0$, $y = 3x-1/2x$; —○—○—, experimental data.

* We are indebted to a referee for drawing our attention to the following data in the literature [31]: for GaOH(g), $\Delta H^\circ_{f298} = -124\pm21$ kJ mol^{-1}, $S^\circ_{298} = 239\pm3$ J mol^{-1} K^{-1}, and for Ga_2O, $\Delta H^\circ_{f298} = -86\pm6$ kJ mol^{-1}, $S^\circ_{298} = 284\pm2$ J mol^{-1} K^{-1}.

where ε is again p_{H_2O}/P in the gas stream, and $\dot{W}_a$ and $\dot{W}_b$ are the measured rates of weight loss in experiments (*a*) and (*b*) at one specific temperature. In deriving eqn (12) and (13) we have made the assumptions about the diffusion coefficients which we discussed earlier, and we also take $\varepsilon \ll 1$.

Note that if either K_1 or K_2 is very small, the expression for the other equilibrium constant reduces to eqn (9) or (10).

We examine eqn (12) and (13) on a plot of x against y in the range which is physically meaningful, i.e. $0 \leqslant x, y, \leqslant 1$ (fig. 4). Physically acceptable solutions lie between the lines $K_1 = 0$ and $K_2 = 0$, and above the line marked $\Delta = 0$, Δ being the denominator in eqn (12) and (13).

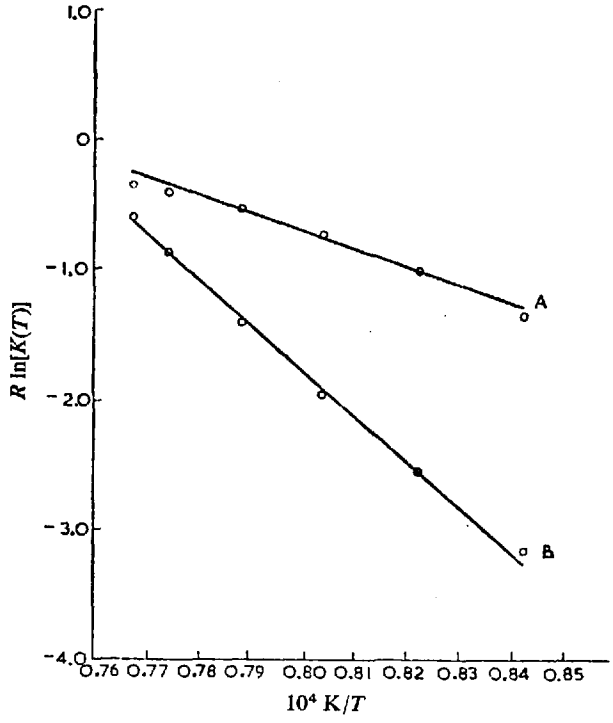

FIG. 5.—Variation of equilibrium constant with temperature. (A) GaOH: $\Delta H = 55.6$ kJ mol^{-1}, $\Delta S = 41.4$ J mol^{-1} K^{-1}, index of determination -0.993; (B) Ga_2O: $\Delta H = 142$ kJ mol^{-1}, $\Delta S = 10.6$ J mol^{-1} K^{-1}, index of determination -0.999.

Using the linear representations for ln $\dot{W}$ in terms of $1/T$, eqn (5) and (6), we can calculate values of x and y over our experimental temperature range, and plot our experimental results on fig. 4. The values of x and y are subject to uncertainties arising from errors in the experimental values of $\dot{W}$ and T, and uncertainties in the binary diffusion coefficients of water in hydrogen and in the hydrogen + nitrogen mixture.

Calculations using eqn (12) and (13) show that the equilibrium constants are particularly sensitive to experimental errors, and that both random and systematic errors influence the results. The measurements of ε and Y are significant sources of errors, but the scatter in $\dot{W}_b$ (see fit of linear representation) is much more important. Because reactions (1) and (2) are of about equal importance in the short temperature

range studied, the experimental results contain information about K_1 and K_2 simultaneously. The requirement that ln K should be linear in $1/T$ for both reactions imposes a limit on the range of uncertainties in the experimental data.

For instance, an uncertainty in the slopes of $W_a(T)$ and $W_b(T)$ greater than 10 % would lead to a nonlinear dependence of one equilibrium constant with temperature. The raw experimental data lead to plots of R ln K against $1/T$ as shown in fig. 5, but in table 4 we give the ranges for the second law values, which were obtained from considerations of simultaneous linearity of ln K against $1/T$.

4.4 THIRD LAW CALCULATIONS

We have carried out calculations of the thermodynamic functions of Ga_2O and GaOH, using the rigid rotator approximation.[22] We took the Ga—O bond length to be 1.86 Å, and the bond angle to be 143°, as reported by Hinchcliffe and Ogden.[24] The product of the moments of inertia is then 4360×10^{-117} g^3 cm^6. The vibrational frequencies ν_1 and ν_3 have been reported [25] as 472 cm^{-1} and 809.4 cm^{-1}. We estimated ν_2 as 137 cm^{-1} using the valence force theory.[26] This estimation is subject to an error due to the uncertainty of $\pm 5°$ in the Ga—O—Ga bond angle.[24] We obtain a room temperature entropy of 287 J mol^{-1} K^{-1}, a little lower than the value of 318 J mol^{-1} K^{-1} given by the empirical formula of Dasent [27] for a polyatomic molecule. This is acceptable, since the Ga_2O molecule has a small moment of inertia about one axis. The results of the calculations are given in table 5 (1).

For GaOH, we assumed a linear structure as for NaOH,[28] RbOH,[28] and CsOH [29] in accordance with Walsh's prediction,[30] with a Ga—O bond length of 1.95 Å (0.5 Å less than the sum of the covalent radii,[23] as in AlOH) [20] and the O—H bond length as 0.96 Å as in H_2O.[20] The rotational constant B is then 0.301. The O—H stretch frequency ν_3 was taken as 3600 cm^{-1} as in other hydroxides [20, 28, 29] and in water.[20] The Ga—O stretch, ν_1, and the bending frequency ν_2 were estimated, on the basis of the weight of the metal atom, to lie part way between those of NaOH and RbOH,[28] and we took the values 374 and 316 cm^{-1}. The results of the calculations are given in table 5 (2). We have used these calculated data to obtain third law enthalpy and entropy changes for reactions (1) and (2) and to find the entropy and enthalpy of formation of Ga_2O and GaOH, using values of the equilibrium constant for reactions (1) and (2) calculated from our second law results described in the previous section. It makes very little difference which extreme pairs of values of ΔH and ΔS one takes for the reactions. The third law results are given in table 4. Free energy functions and entropies for gallium and hydrogen were taken from Stull and Sinke,[21] and for water from the *JANAF Tables*.[20]

The sources of error in the third-law calculations lie (1) in the parameters used for the calculations and (2) in the values of the equilibrium constants calculated from our second-law results. Uncertainties in the parameters yield an error which we estimate as ± 6 J mol^{-1} K^{-1} for Ga_2O and 12 J mol^{-1} K^{-1} for GaOH (± 8 kJ mol^{-1} and ± 17 kJ mol^{-1} in the enthalpies of formation). The errors from the second source are surprisingly small, since our extreme pairs of values ($\Delta H°$, $\Delta S°$) for the reactions yield very similar equilibrium constants [0.32-0.28 for reaction (1), 0.7-0.9 for reaction (2) at 1250 K]. We estimate the errors from this source as ± 4 kJ mol^{-1} and ± 3 J mol^{-1} K^{-1} in all the enthalpies and entropies.

Agreement between the third-law and second-law values (derived from the analysis in section 4.3 for simultaneous reactions) is within the estimated error limits, and is quite good for gallium suboxide.

4.5 COMPARISON WITH LITERATURE VALUES

The enthalpy of formation of gallium suboxide has been reported by Frosch and Thurmond [1] as 86.6 ± 10 kJ mol^{-1}, and by Cochran and Foster [2] as 82.4 ± 3 kJ mol^{-1}. Our third-law value of 90.8 ± 8 kJ mol^{-1} is in good agreement with these data. Cochran and Foster [2] used a value of 291 J mol^{-1} K^{-1} for the entropy of gallium suboxide, based on data for the heat capacity of CTeSe and other triatomic molecules of the same molecular weight. The uncertainty in their value is ± 8 J mol^{-1} K^{-1} and it compares well with our value of 287 ± 6 J mol^{-1} K^{-1}.

TABLE 4.—THERMODYNAMIC DATA FOR REACTIONS (1) AND (2)

	reaction (1)		reaction (2)		Ga_2O		GaOH	
method	ΔH°_{298}/ kJ mol^{-1}	ΔS°_{298}/ J mol^{-1} K^{-1}	ΔH°_{298}/ kJ mol^{-1}	ΔS°_{298}/ J mol^{-1} K^{-1}	ΔH_{f298}/ kJ mol^{-1}	S°_{298}/ J mol^{-1} K^{-1}	ΔH_{f298}/ kJ mol^{-1}	S°_{298}/ J mol^{-1} K^{-1}
dominant reaction 2nd law	120	126	117	109	−121	266	−125	273
simultaneous reactions	161	160	59	56	−80	300	−183	221
↓	↓	↓	↓	↓	↓	↓	↓	↓
2nd law	172	165	79	74	−70	305	−163	239
third law	151	147	94	84	−90.8 ±8	287±6	−148± 17	248±12
estimated			117±20				−125 ± 20	
literature	159				−84			

We are not aware of any measurements or calculations of the enthalpy of formation or entropy of gallium hydroxide.* The Ga—OH bond dissociation energy is given as 427 ± 20 kJ mol^{-1}, from which we deduce an enthalpy of formation of 125 ± 20 kJ mol^{-1}, which is not in conflict with our third-law value of 148 ± 15 kJ mol^{-1}. The Ga—O bond energy in Ga_2O may be calculated from the enthalpies of formation of Ga_2O, of sublimation of gallium, and of dissociation of oxygen. We obtain 437 ± 4 kJ mol^{-1}. This value is very similar to the energy of the Ga—OH bond, as we would expect.

5. CONCLUSIONS

The thermodynamic parameters resulting from this work are given in tables 4, 5 (1) and 5 (2). The enthalpies of formation of gallium suboxide measured by previous workers [1, 2] and by us agree in the range −82.8 to −96.6 kJ mol^{-1}, lending support to the value reported by Cochran and Foster. For the enthalpy of formation of GaOH, and for the entropies of Ga_2O and GaOH, we recommend the third-law results in table 4.

Gallium hydroxide is an important volatile product of the reaction between gallium and water vapour+hydrogen mixtures at high temperatures. We believe that this is the first time that thermodynamic data for this species have been reported.

* But see footnote on p. 2286

TABLE 5.—THERMODYNAMIC FUNCTIONS OF (1) GALLIUM SUBOXIDE AND (2) GALLIUM HYDROXIDE

T/K	C_p°/J mol^{-1} K^{-1}	S_T°/J mol^{-1} K^{-1}	$(H_T^\circ - H_{298}^\circ)$/ kJ mol^{-1}	$[(G_T - H_{298}^\circ)/T]$/ J mol^{-1} K^{-1}
		(1) Ga_2O		
100	39.773	239.375	−8.911	328.487
200	45.209	268.649	−4.657	291.932
273	48.497	283.248	−1.224	287.730
298	49.423	287.536	0.000	287.536
300	49.488	287.842	0.091	287.537
400	52.263	302.491	5.190	289.515
500	54.002	314.355	10.510	293.334
600	55.109	324.306	15.970	297.689
700	55.844	332.860	21.520	302.117
800	56.352	340.352	27.131	306.438
900	56.714	347.011	32.785	310.583
1000	56.982	353.001	38.471	314.530
1100	57.184	358.442	44.180	318.279
1200	57.340	363.424	49.906	321.836
1300	57.463	368.019	55.646	325.214
1400	57.562	372.281	61.398	328.426
1500	57.642	376.256	67.158	331.483
1600	57.708	379.978	72.926	334.399
1700	57.763	383.478	78.700	337.184
1800	57.810	386.781	84.478	339.849
1900	57.849	389.908	90.261	342.402
2000	57.883	392.876	96.048	344.852
		(2) GaOH		
100	33.94	196.48	−8.65	282.97
200	44.80	223.77	−4.65	247.01
273	48.45	238.34	−1.22	242.81
298	49.23	242.62	0.00	242.62
300	49.28	242.92	0.09	242.62
400	51.22	257.40	5.13	244.58
500	52.21	268.95	10.31	248.34
600	52.84	278.52	15.56	252.59
700	53.35	286.71	20.87	256.89
800	53.84	293.87	26.23	261.08
900	54.33	300.23	31.64	265.08
1000	54.83	305.98	37.10	268.89
1100	55.34	311.23	42.61	272.50
1200	55.83	316.07	48.17	275.93
1300	56.31	320.56	53.77	279.19
1400	56.75	324.75	59.43	282.30
1500	57.17	328.68	65.12	285.26
1600	57.56	332.38	70.86	288.09
1700	57.92	335.88	76.64	290.80
1800	53.24	339.20	82.44	293.40
1900	58.54	342.36	88.28	295.89
2000	58.81	345.37	94.15	298.29

The ratio α of partial pressures of gallium suboxide to gallium hydroxide is given by:

$$\alpha = \frac{K_1}{K_2}\frac{1}{p_{H_2}^{\frac{1}{2}}} \tag{16}$$

and

$$\frac{K_1}{K_2} = \exp\left\{-\frac{86\,190\ \text{J mol}^{-1}}{RT} + \frac{64.9\ \text{J mol}^{-1}\ \text{K}^{-1}}{R}\right\}$$

on the basis of the two-reaction calculations (see fig. 6). The suboxide becomes relatively more important at high temperature, while the reverse condition favours the hydroxide. This conclusion also holds for the vapour products of reactions between

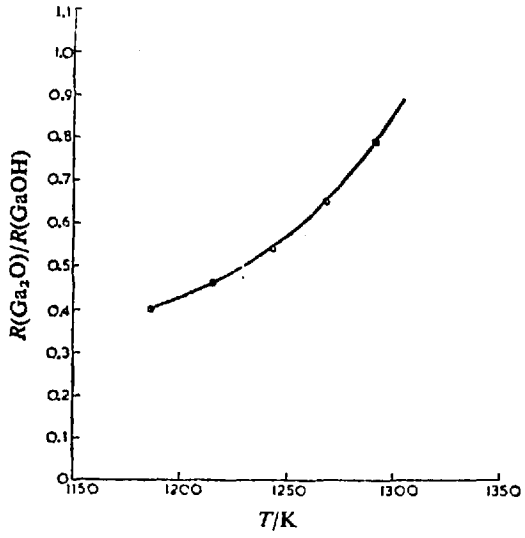

FIG. 6.—Variation of ratio of equilibrium constants with temperature.

water+hydrogen mixtures and gallium compounds. It thus seems likely that the vapour species responsible for the chemical vapour transport of gallium arsenide in water+hydrogen mixtures is the hydroxide, not the suboxide as has been assumed previously.[3-5, 7, 8] This could well account for the appreciable, systematic discrepancy between the experimental results of Michelitsch *et al.*[3] and the equilibrium constant for reaction (1).

Reaction (3), that is:

$$2GaOH(g) \rightleftharpoons Ga_2O(g) + H_2O(g)$$

cannot result in a large change in free energy since on each side of the reaction there are two vapour molecules (i.e. ΔS° is small), two Ga—O bonds and two O—H bonds (i.e. ΔH° is small). In general, we would expect the same to apply to all metals with a lower valency of one. The corresponding reaction for an element with a lower valency of two, e.g.:

$$SiO(g) + H_2O(g) \rightleftharpoons Si(OH)_2(g)$$

results in a decrease in the number of vapour molecules, and hence in entropy, in forming the hydroxide. There would seem to be no compensating enthalpy change.

While our modified entrainment method [6] is capable of yielding accurate thermodynamic data for heterogeneous equilibria, the accuracy of our results for this system is low because of the restricted " window " available in this system. We have demonstrated, however, that the method is applicable to a system in which two reactions of comparable importance are taking place.

Acknowledgement is made to the Director of Research of the Post Office for permission to publish this paper.

[1] C. F. J. Frosch and C. D. Thurmond, *J. Phys. Chem.*, 1962, **66**, 877.
[2] C. N. Cochran and L. M. Foster, *J. Electrochem. Soc.*, 1962, **109**, 144.
[3] M. Michelitsch, W. Kappallo and G. Hellbardt, *J. Electrochem. Soc.*, 1964, **111**, 1248.
[4] K. L. Lawley, *J. Electrochem. Soc.*, 1966, **113**, 240.
[5] C. Lin, L. Chow and K. J. Miller, *J. Electrochem. Soc.*, 1970, **117**, 407.
[6] D. Battat, M. M. Faktor, I. Garrett and R. H. Moss, *J.C.S. Faraday I*, 1974, **70**, 2267
[7] P. H. Robinson, *R.C.A. Rev.*, 1963, **24**, 574.
[8] G. E. Gottlieb and J. F. Corboy, *R.C.A. Rev.*, 1963, **24**, 585.
[9] M. M. Faktor, R. Heckingbottom and I. Garrett, *J. Chem. Soc. A*, 1970, 2657.
[10] A. D. Mah, *U.S. Bur. Mines Rep. Invest.*, 1962, no. 5965.
[11] G. W. C. Kaye and T. H. Laby, *Physical and Chemical Constants* (Longman, London, 1959).
[12] J. H. Arnold, *Ind. Eng. Chem.*, 1930, **22**, 1091.
[13] J. Fujita, *Kagaku Kikai*, 1951, **15**, 234.
[14] W. H. Shepherd, *J. Electrochem. Soc.*, 1965, **112**, 988.
[15] J. Jeans, *Kinetic Theory of Gases* (Cambridge, 1962).
[16] *Handbook of Heat Transfer*, ed. W. M. Rohsenow and J. P. Hartnett (McGraw-Hill, New York, 1973).
[17] *Int. Critical Tables*, 1929, **5**, 62.
[18] D. Battat unpublished work.
[19] V. I. Vedeneyev, L. V. Gurvich, V. N. Kondrat'yev, V. A. Medvedev and Ye. L. Frankevich, *Bond Energies, Ionization Potentials and Electron Affinities* (Arnold, London, 1966).
[20] *J.A.N.A.F. Thermochemical Tables*, NSRDS-NBS 37 (Nat. Bur. Stand., 2nd edn., 1971).
[21] D. R. Stull and G. C. Sinke, *Thermodynamic Properties of the Elements* (Amer. Chem. Soc., Washington, 1956).
[22] J. D. Fast, *Entropy*, (Philips Technical Library, 1962)
[23] from a table of Periodic Properties of the Elements, *J. Chem. Educ.*, 1971, **48**.
[24] A. J. Hinchcliffe and J. S. Odgen, *J. Phys. Chem.*, 1973, **77**, 2537.
[25] A. J. Hinchcliffe and J. S. Ogden, *J. Phys. Chem.*, 1971, **75**, 3908.
[26] G. Herzberg, *Molecular Spectra and Molecular Structure, Part II* (Van Nostrand, New York, 1947).
[27] W. E. Dasent, *Inorganic Energetics* (Penguin, London, 1970).
[28] N. Acquista and S. Abramowitz, *J. Chem. Phys.*, 1969, **51**, 2911.
[29] N. Acquista, S. Abramowitz and D. R. Lide, *J. Chem. Phys.*, 1968, **49**, 780.
[30] A. D. Walsh, *J. Chem. Soc.*, 1953, 2288.
[31] *Termicheskie Konstanty Veschestv* (*Thermodynamic constants of Substances*) (Academy of Science, Moscow, 1971), vol. 5.

Journal of The Chemical Society, Faraday Transactions I, 1974, Volume 70, pp 2293–2301

Modified Entrainment Method for Measuring Vapour Pressures and Heterogeneous Equilibrium Constants

Part 3.—Measurement of Diffusivity of Hydrogen Chloride in Hydrogen and Extension of the Method to Multicomponent Diffusion at 700-1300 K

BY DAVID BATTAT, MARC M. FAKTOR,* IAN GARRETT AND RODNEY H. MOSS

Post Office Research Department, Brook Road, Dollis Hill, London NW2 7DT

Received 27th March, 1974

The binary diffusion coefficient of HCl in H_2 may be represented by $0.54(T/273\ \mathrm{K})^{1.85}\ \mathrm{cm^2\ s^{-1}}$ over the temperature range 700-1300 K. We present a useful second-order approximation to multicomponent diffusion, which permits calculation of effective diffusion coefficients in multicomponent gas mixtures.

1. INTRODUCTION

Mixtures of hydrogen chloride and hydrogen gases are used in the chemical vapour transport of many semiconductor materials, such as the Group III-V compounds.[1, 2] The increasing need for better control over the chemical vapour transport systems used in the electronics industry has led to the construction of a useful theory of vapour transport [3-6] and to the development of a versatile method [7-9] for measuring the chemical thermodynamic and kinetic parameters required to apply the theory. The rate of diffusion of hydrogen chloride in a gas consisting largely of hydrogen, but containing also the products of the transport reaction, is one of the factors which determine the rate of transport[6] of the solid material. We used a chemical vapour transport reaction to study the diffusion of hydrogen chloride in such a multicomponent gas. We have developed also a useful second-order approximation to the theory of multi-component diffusion, which allows us to obtain the binary diffusion coefficient of hydrogen chloride in hydrogen from experimental transport rates. We are thus able to predict effective diffusion coefficients for multi-component gas mixtures used in chemical vapour transport.

The modified entrainment method described earlier [7, 8] was shown to be useful for measuring equilibrium constants provided they are not extreme (less than about 10). The uncertainties in diffusion coefficients then lead to acceptably small errors. On the other hand, when the equilibrium constant is large, the method becomes suitable for investigating gaseous interdiffusion, since the reaction then acts as effective sink for the reactant. In this investigation reaction (1) was used:

$$\mathrm{Ga(liquid) + HCl(gas) \rightleftharpoons GaCl(gas) + \tfrac{1}{2}H_2(gas).} \qquad (1)$$

Existing data [10-14] suggest that in the temperature range 700-1300 K the enthalpy change for this reaction ΔH° is $+12 \pm 8$ kJ mol^{-1}, and the entropy change ΔS° is $+65.6 \pm 4$ J mol^{-1} K^{-1}. The equilibrium is thus well to the right, and the partial pressure of hydrogen chloride over the gallium is very nearly zero.

We have considered the possible formation of other gaseous chlorides [9, 15] of gallium, and we conclude that under our experimental conditions their partial pressures are negligibly small.

2. EXPERIMENTAL

The apparatus has been described in detail elsewhere.[7]

The gallium was 99.9999 %, supplied by Mining and Chemical Products Ltd. The hydrogen was British Oxygen Company electronic grade, and was passed through a palladium diffuser. The hydrogen chloride was Air Products electronic grade, of quoted purity 99.99 %. The flow of hydrogen chloride was controlled by a Drovewood automatic flow controller. Flow rates of hydrogen chloride and of hydrogen were measured with Meterate flow meters. The hydrogen chloride flow meter was calibrated by determining the HCl content of the $HCl+H_2$ gas mixture by titration against NaOH. The temperature was measured with a Pt/Pt–13 % Rh thermocouple running up the centre of the furnace tube to within 3 mm of the sample bottle.

The rate of weight loss from the sample bottle, $\dot{W}$, was measured as a function of temperature, using three ratios ε of HCl to H_2 in the gas stream: $p_{HCl}/P = 0.018$, 0.060 and 0.10, where p_{HCl} is the partial pressure of HCl and P is the total pressure.

3. RESULTS

The results from the three runs are given in table 1.

TABLE 1

$\varepsilon = 0.018$		$\varepsilon = 0.060$		$\varepsilon = 0.10$	
T/K	$\dot{W}$/mg h^{-1}	T/K	$\dot{W}$/mg h^{-1}	T/K	$\dot{W}$/mg h^{-1}
1290	1.638	1271	3.570	1248	4.976
1290	1.542	1271	3.449	1248	4.997
1290	1.542	1271	3.592	1019	4.450
1239	1.357	1225	3.271	1019	4.406
1239	1.287	1225	3.438	832	3.644
1239	1.386	1225	3.367	832	3.676
1184	1.350	1183	3.445	832	3.704
1184	1.269	1183	3.281	779	3.463
1184	1.255	1183	3.319	779	3.526
1136	1.366	1129	3.206	779	3.512
1135	1.341	1129	3.151	786	3.512
1135	1.233	1129	3.104	1274	5.268
1082	1.170			1274	5.250
1082	1.136			891	3.836
1082	1.140			891	3.814
1036	1.061			891	3.884
1036	1.031				
1035	1.184				
1035	1.241				
1035	1.151				
984	1.100				
984	1.072				
984	1.084				
935	1.008				
935	0.989				
888	0.937				
888	0.936				

4. ANALYSIS OF RESULTS

Following the lines of argument [7, 8] given previously, we assume that the vapour in the bottle is in equilibrium with the liquid gallium, and that at the outlet from the

neck of the bottle the vapour composition is the same as that in the main stream, i.e., the reaction products are rapidly diluted and swept away. The partial pressures inside the bottle are given by:

$$p_{GaCl}(0) = [p_{GaCl}(l) - 2P]\exp(-\xi_{GaCl}) + 2P \sim 2\xi_{GaCl}P \quad (2)$$

since $p_{GaCl}(l)$ is taken as zero and $\xi_{GaCl} \ll 1$;

$$p_{HCl}(0) = P[\varepsilon + 2]\exp(-\xi_{HCl}) - 2P \sim P[\varepsilon - 2\xi_{HCl}] \quad (3)$$

$$p_{H_2}(0) = P - p_{GaCl}(0) - p_{HCl}(0). \quad (4)$$

In these equations, partial pressures in the bottle are denoted by (0), and ξ_i is the transport function for species i, defined in eqn (5).

$$\xi_i = \dot{W}RTl/2D_{i,m}PMA. \quad (5)$$

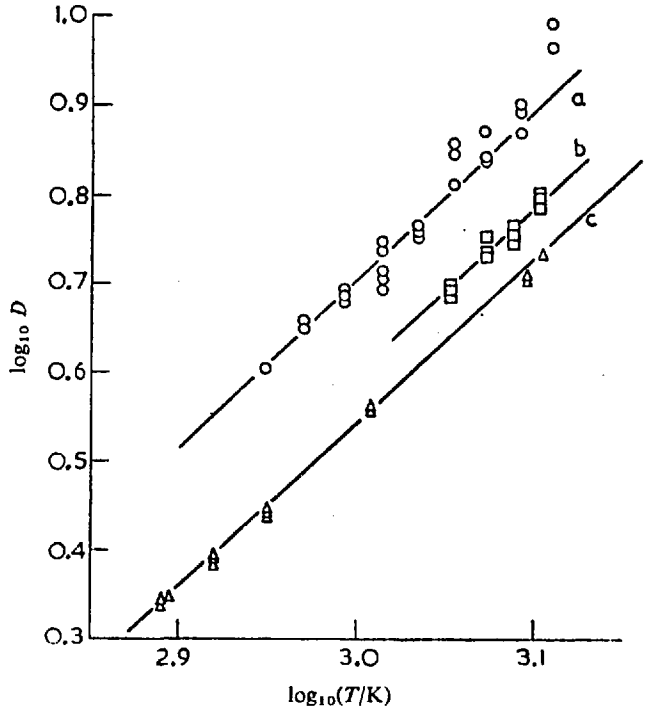

FIG. 1.—Variation of D_{HCl,H_2} with temperature: diffusion coefficients independent of concentration. ○, $\varepsilon = 0.018$; □, $\varepsilon = 0.06$; △, $\varepsilon = 0.10$.

Here R is the gas constant, l is the length and A the cross-sectional area of the neck of the bottle, M is the atomic weight of gallium, and $D_{i,m}$ is the effective diffusion coefficient of species i in the multicomponent gas mixture. The equilibrium constant for reaction (1) can now be expressed as:

$$K_p = \frac{2\xi_{GaCl}\sqrt{P}}{\varepsilon - 2\xi_{HCl}}. \quad (6)$$

In the present experiment, $P = 1$ atm, so that

$$\varepsilon = 2\xi_{HCl}\left(1 + \frac{D_{HCl,m}}{D_{GaCl,m}}\frac{1}{K_p}\right). \quad (7)$$

We note that if K_p is large, we can neglect $D_{HCl,m}/(D_{GaCl,m}K_p)$ in comparison with unity. Now our expression for the diffusion coefficient of the reactant HCl in the gas mixture is simply:

$$D = WRTl/PM\varepsilon A.$$

In effect we have equated $p_{HCl}(0)$ (over the gallium), to zero. The fractional error in so doing is $\sim 1/K_p$.

Using this simple formula, we calculate a value of D for each experimental point. The results are plotted as $\log_{10} D$ against $\log_{10} T$ in fig. 1. The scatter of points is greatest for the run with $\varepsilon = 0.018$, where the rate of loss of weight was very small and is subject to the largest error. The points from each run can be fitted by the well-known expression [16] of the kinetic theory:

$$D(T) = D^\circ(T/273\ \mathrm{K})^{1+s} \qquad (9)$$

where D° is a constant (the diffusivity at 0°C) and s is around 0.8-0.9. The value of s is the same for each run, within experimental error, but the calculated value of D° increases as ε decreases. This is significant.

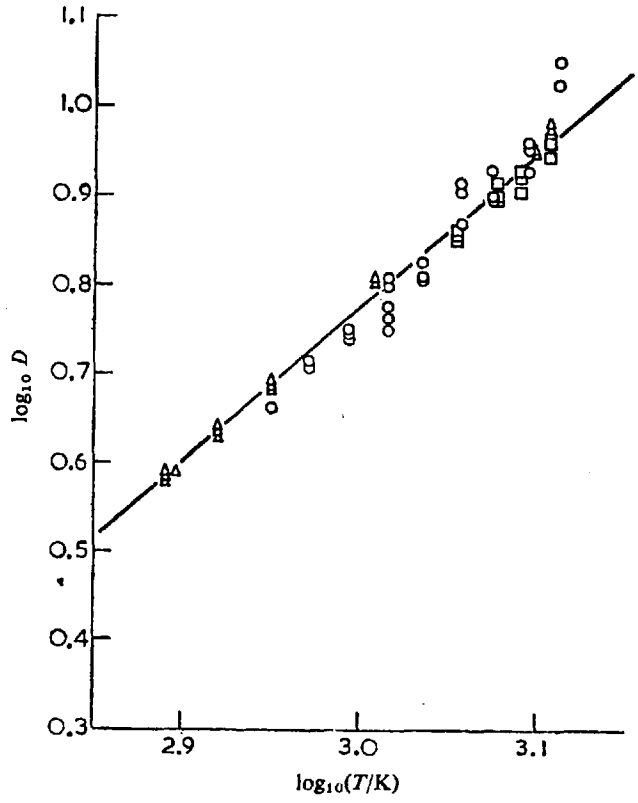

FIG. 2.—Variation of D_{HCl,H_2} with temperature: diffusion coefficients dependent on concentration. ○, $\varepsilon = 0.018$; □, $\varepsilon = 0.06$; △, $\varepsilon = 0.10$. $a = 6.5$; $b = 3.0$.

In the analysis presented [8] previously, it was assumed that the partial pressures of the minority components (GaCl and HCl in this case) are so small that the diffusion may be described as two independent binary systems (GaCl in H_2 and HCl in H_2).

This first-order or very dilute solution approximation becomes increasingly inaccurate as ε is made larger. Our experimental range of ε is sufficient to introduce an inaccuraey of up to a factor of two. In the Appendix we present a second-order approximation to multi-component diffusion, and we show that the diffusion coefficient $D_{\mathrm{HCl,m}}$ in eqn (5) is replaced by the binary eoefficient $D_{\mathrm{HCl,H_2}}$ divided by a composition-dependent factor γ_{HCl}:

$$\gamma_{\mathrm{HCl}} = 1 + a_{\mathrm{HCl}}\varepsilon + b_{\mathrm{HCl}}\xi_{\mathrm{HCl}}. \tag{10}$$

We may regard the coefficients a_{HCl} and b_{HCl} as empirical quantities to be obtained from the experiment, or as quantities whose values may be calculated using the theoretical expressions in the Appendix, eqn (A12) and (A13). We have used both approaches, and find adequate agreement.

Eqn (8) can now be re-written as:

$$D_{\mathrm{HCl,H_2}} = \frac{\dot{W}RTl}{PMA}\left\{\frac{b_{\mathrm{HCl}}}{-(1+a_{\mathrm{HCl}}\varepsilon)+\sqrt{(1+a_{\mathrm{HCl}}\varepsilon)^2+2b_{\mathrm{HCl}}\varepsilon}}\right\} = D^\circ\left(\frac{T}{273K}\right)^{1+s}.$$

A least-squares fit to our experimental results yields $a_{\mathrm{HCl}} = 6.5\pm1$, $b_{\mathrm{HCl}} = 3\pm1$, $D^\circ_{\mathrm{HCl,H_2}} = 0.54\pm0.07\ \mathrm{cm^2\ s^{-1}}$, $s = 0.853\pm0.022$.

5. DISCUSSION

There are several sourees of experimental error, whieh are diseussed below. The error introduced by ignoring $1/K_p$ in comparison with unity is expected to be no greater than 0.3 % at 700 K and 0.1 % at 1300 K. It is much smaller than the experimental error in ε, the fractional HCl coneentration in the gas stream.

l AND *A*.—The dimensions of the neck of the bottle were measured with a catheto-meter to 1 % or better. We estimate that end effeets introduee an error in *l* of about 1 %.

T AND $\dot{W}$.—The error in *T* is unlikely to be more than 10 K, and would probably be systematie. The error introduced in *D* is therefore less than 2 %. The fractional error in $\dot{W}$ increases as $\dot{W}$ decreases, as evidenced by the seatter in experimental results for low ε. This scatter is reflected in the standard deviation of ±0.022 in *s* and $\pm0.07\ \mathrm{cm^2\ s^{-1}}$ in $D^\circ_{\mathrm{HCl,H_2}}$ obtained from the least-squares fit.

ε.—The principal source of error in ε is the uncertainty in reading the flow meters. Although we took preeautions to obtain a steady flow, there was a slow drift in flow rate during a run, possibly caused by a change in laboratory temperature. We estimate the uncertainty in ε to be ±5 %.

a_{HCl} AND b_{HCl}.—These coefficients depend quite sensitively on the ratios of binary diffusion eoeffieients, in partieular, on the ratio $D_{\mathrm{H_2,HCl}}/D_{\mathrm{GaCl,HCl}}$ [see eqn (A12)]. Because of the scatter of experimental points, varying a_{HCl} between 5.5 and 7.5, and varying b_{HCl} between 2 and 4, makes very little difference to the standard deviations in *s* and $D^\circ_{\mathrm{HCl,H_2}}$ obtained from the least-squares fit.

We find, then, that by far the largest source of uncertainty arises from the scatter of experimental points. Our final values for the diffusivity of HCl in H_2, and for *s*, are thus:

$$D^\circ_{\mathrm{HCl,H_2}} = 0.54\pm0.07\ \mathrm{cm^2\ s^{-1}}$$
$$s = 0.85\pm0.022.$$

We have applied the second-order approximation to multieomponent diffusion for ε up to 0.1. With the wide disparity in molecular weights and binary diffusivities among the vapour species in our present experiment, it is not elear *a priori* that the theory is

valid for such large values of ε. We observe that there is adequate agreement between empirical and estimated values for a_{HCl} and b_{HCl}, however. Furthermore, we can argue loosely that as ε is increased towards unity, the apparent diffusion coefficient of HCl in the gas mixture must approach the binary diffusion coefficient of HCl in GaCl, which we estimate to be about 0.075 $cm^2\ s^{-1}$, using Graham's law.[17] Thus either the apparent diffusion coefficient varies roughly linearly with γ, in which case a value of $a_{HCl} = 6$ is reasonable, or else some specific chemical interaction between the diffusing species causes a departure from linearity (e.g. short-lived molecular complexes). Our experiment suggests that such interactions are insignificant for $\varepsilon \leqslant 0.1$.

6. CONCLUSION

The modified entrainment method which we have developed for investigating heterogeneous equilibria can be used to measure binary diffusion coefficients over a wide range of temperature in reactive gas mixtures. The second-order approximation to multi-component diffusion provides an adequate description for systems containing 90 % of one component, although the first-order approximation is not valid here. In systems not containing highly diffusive gases (H_2 or He) we expect the approximation to hold for considerably more concentrated mixtures.

The empirical approach gives values for a and b, and a value for s which is independent of composition. It is gratifying to find that the theory predicts values of a and b close to the empirical ones, and confirms that s is independent of ε, the fractional HCl concentration in the gas stream.

APPENDIX

ONE-DIMENSIONAL TERNARY DIFFUSION WITH ONE MAJORITY COMPONENT

In a non-uniform gas, each species i may be thought of as moving with a velocity u_i, which is the average over all molecules of species i, and in general different from the average velocities of all other species. The average velocity of the gas mixture can be defined in terms of the u_i values in any way we choose. A common choice [18, 19] is to weight each u_i according to the mass fraction c_i, to obtain the *mass-average* velocity:

$$u = \sum_i c_i u_i. \tag{A1}$$

The diffusion speed σ_i of species i is then defined as:

$$\sigma_i = u_i - u. \tag{A2}$$

It follows that the sum of the diffusion fluxes, $\Sigma_i c_i \sigma_i$, is identically zero.

For many chemical problems, the *mole-average* velocity [18] defined by eqn (A3) is more useful

$$U = \sum_i y_i u_i \tag{A3}$$

where y_i is the mole fraction of species i in the gas. From eqn (A2) and (A3) we obtain:

$$U = u + \sum_i y_i \sigma_i. \tag{A4}$$

The kinetic theory of gases [19, 20] gives an expression for σ_i. For diffusion due to concentration gradients alone it is:

$$\sigma_i = \frac{n}{\rho y_i} \sum_j M_j \mathscr{D}_{ij} \frac{dy_j}{dx} \tag{A5}$$

where n is the total mole density, ρ is the mass density, M_j is the molar weight of species j, and $\mathscr{D}_{ij}$ is the multi-component diffusion coefficient for the flux of species i due to a concentra-

tion gradient in species j. For a ternary mixture, $\mathscr{D}_{ij}$ is related [20] to the binary coefficient D_{ij} by:

$$\mathscr{D}_{ij} = D_{ij}\left[1 + \frac{n_k\{(M_k/M_j)D_{ik} - D_{ij}\}}{n_iD_{jk} + n_jD_{ki} + n_kD_{ij}}\right], \qquad i \neq j \neq k \tag{A6}$$

and $\mathscr{D}_{ii} \equiv 0$.

If we take n as constant, we can rewrite eqn (A4), using eqn (A5), as:

$$\rho(U-u) = M_1(\mathscr{D}_{21}+\mathscr{D}_{31})\frac{dn_1}{dx} + M_2(\mathscr{D}_{32}+\mathscr{D}_{12})\frac{dn_2}{dx} + M_3(\mathscr{D}_{13}+\mathscr{D}_{23})\frac{dn_3}{dx}. \tag{A7}$$

The total flux of species i is:

$$J_i = n_iu_i = \frac{\rho c_iu_i}{M_i}. \tag{A8}$$

We confine our analysis to the case where one component is predominant, i.e. $n_1, n_2 \ll n_3$. Using eqn (A2), (A5) and (A7) we can express the flux J_1 in terms of the mole-average velocity U and the ternary diffusion coefficients $\mathscr{D}_{ij}$ as follows:

$$J_1 = n_1U - \frac{n_1}{\rho}\left[M_1(D_{21}+D_{31})\frac{dn_1}{dx} + M_2(D_{12}+D_{32})\frac{dn_2}{dx} + M_3(D_{13}+D_{23})\frac{dn_3}{dx}\right] + \frac{n}{\rho}\left[M_2D_{12}\frac{dn_2}{dx} + M_3D_{13}\frac{dn_3}{dx}\right]. \tag{A9}$$

Eqn (A6) can be expanded for $n_1, n_2 \ll n_3$, and the resulting approximate expressions substituted in (A9). We retain terms in $n_i(dn_j/dx)$ $(i = 1, 2;\ j = 1, 2, 3)$ but ignore higher-order terms. Note that dn_j/dx is of the same order as n_1, n_2, and that n, the total mole concentration, is essentially independent of x. We obtain eqn (A10) for J_1:

$$J_1 = n_1U - D_{13}\frac{dn_1}{dx} + \frac{nM_3}{\rho}\left(\frac{D_{13}}{D_{12}} - 1\right)\left[\frac{n_2}{n}D_{13}\frac{dn_1}{dx} - \frac{n_1}{n}D_{23}\frac{dn_2}{dx}\right]. \tag{A10}$$

The corresponding expression for J_2 has 2 substituted for 1 throughout. In deriving (A10), we have neglected all terms which are third order in n_1, n_2, irrespective of their coefficients. Because of the large ratios of molecular weights in our system, some of these coefficients are not of order unity. We have therefore inspected the third order correction, and find that the only effect is to multiply the last term in (A10) by the quantity:

$$1 - \left(\frac{D_{23}}{D_{12}} - 1\right)\frac{n_1}{n} - \left(\frac{D_{13}}{D_{12}} - 1\right)\frac{n_2}{n}.$$

Clearly we may neglect the third-order terms if $n_1, n_2 \ll n$.

Eqn (A10) expresses J_1 as a sum of three terms. The first is the Stefan flow,[18] the second is binary diffusion of species 1 in the majority species 3, and the third term represents a correction caused by the presence of a significant concentration of species 2.

To solve eqn (A10) with the boundary conditions imposed by our experimental conditions $[n_1(l)/n = \varepsilon,\ n_2(l) = 0]$, we assume power series solutions of the form:

$$n_i(x)/n = f_i(x)\varepsilon + g_i(x)\varepsilon^2, \qquad i = 1, 2. \tag{A11}$$

We insert this solution into (A10) and the corresponding equation for J_2. The fluxes J_i are related by the stoichiometry of the reaction:

$$J_{Ga} = -J_1 = J_2 = 2J_3.$$

We equate terms in like powers of ε, and thus determine the functions $f_i(x)$ and $g_i(x)$. We are now able to express each of the mole concentrations n_i as a function of x. In particular, we find that for HCl:

$$n_{HCl}(0)/n = p_{HCl}(0)/P = \varepsilon - 2\gamma_{HCl}\zeta_{HCl}$$

where

$$\gamma_{HCl} = 1 + a_{HCl}\varepsilon + b_{HCl}\xi_{HCl}$$

and

$$a_{HCl} = \frac{D_{HCl,H_2}}{D_{HCl,GaCl}} - \tfrac{1}{2} \tag{A12}$$

$$b_{HCl} = \left(\frac{D_{HCl,H_2}}{D_{HCl,GaCl}} - 1\right)\left(\frac{D_{H_2,HCl}}{D_{H_2,GaCl}} - 1\right) - \tfrac{1}{2}. \tag{A13}$$

To estimate the ratios of diffusion coefficients appearing in a_{HCl} and b_{HCl}, we have compared the results of two approaches; Graham's law,[17] and the hard-sphere model [19, 20] of kinetic theory. For Graham's law,

$$D_{ij}/D_{ik} = \sqrt{M_k/M_j}$$

and we obtain $a_{HCl} = 6.75$, $b_{HCl} = 3.92$.

For the hard-sphere model,

$$\frac{D_{ij}}{D_{ik}} = \left(\frac{\sigma_{ik}}{\sigma_{ij}}\right)^2\left[\frac{M_i^{-1} + M_j^{-1}}{M_i^{-1} + M_k^{-1}}\right]^{\frac{1}{2}}$$

where σ_{ij} is the hard sphere collision diameter. Using the semi-empirical method of Jona and Mandel,[21] we obtain $a_{HCl} = 8.32$ and $b_{HCl} = 5.28$. These estimated values of a_{HCl} and b_{HCl} are acceptably close to our empirical values, bearing in mind that both HCl and GaCl molecules are polar, so that their dynamics of motion and collision are unlikely to be well described by the above results of the kinetic theory.[22]

Finally, we have used our empirical values of a_{HCl} and b_{HCl} and our value for D°_{HCl,H_2}, to calculate $D^\circ_{HCl,GaCl}$ and D°_{GaCl,H_2} from eqn (A12) and (A13). The results are given in table 2. with the corresponding values obtained from Graham's law and from the hard-sphere model for comparison. The agreement is well within the large error limits which arise from the uncertainties in a_{HCl} and b_{HCl}.

TABLE 2

binary diffusivity	Graham's law	hard sphere	empirical: this work
$D^\circ_{HCl,GaCl}/cm^2\ s^{-1}$	0.075	0.061	0.077 ± 0.024
$D^\circ_{GaCl,H_2}/cm^2\ s^{-1}$	0.32	0.31	0.34 ± 0.05

The authors thank the Director of Research of the Post Office for permission to publish this paper.

[1] J. J. Tietjen, R. E. Enstrom and D. Richman, *R.C.A. Rev.*, 1970, **31**, 635.
[2] H. T. Minden, *Solid State Tech.*, 1973, 31.
[3] M. M. Faktor, R. Heckingbottom and I. Garrett, *J. Chem. Soc. A*, 1970, 2657.
[4] M. M. Faktor, R. Heckingbottom and I. Garrett, *J. Chem. Soc. A*, 1971, 1.
[5] M. M. Faktor and I. Garrett, *J. Chem. Soc. A*, 1971, 934.
[6] M. M. Faktor, I. Garrett and R. H. Moss, *J.C.S. Faraday I*, 1973, **69**, 1915.
[7] D. Battat, M. M. Faktor, I. Garrett and R. H. Moss, *J.C.S. Faraday I*, 1974, **70**, 2267.
[8] D. Battat, M. M. Faktor, I. Garrett and R. H. Moss, *J.C.S. Faraday I*, 1974, **70**, 2280.
[9] D. Battat, M. M. Faktor, I. Garrett and R. H. Moss, *J.C.S. Faraday I*, 1974, **70**, 2302.
[10] D. J. Kirwan, *J. Electrochem. Soc.*, 1970, **117**, 1572.
[11] G. F. Day, *Heterojunction Device Concepts*, Varian Report No. 324-6Q, Air Force Contract No. AF 33 (615)-1988 (Varian Associates, Palo Alto, California).

[12] R. Hultgren, R. L. Orr and K. K. Kelley, *Supplements to Selected Values of Thermodynamic Properties of Metals and Alloys*, University of California (up to 1972).
[13] J. B. Mullin and D. T. J. Hurle, *J. Luminescence*, 1973, **7**, 176.
[14] Yu. Kh. Shaulov and A. M. Mosin, *Zhur. fiz. Khim.*, 1973, **47**, 1131.
[15] O. Kubaschewski, E. LL. Evans and C. B. Alcock, *Metallurgical Thermochemistry* (Pergamon, New York, 4th edn., 1967).
[16] J. Jeans, *Introduction to the Kinetic Theory of Gases* (University Press, Cambridge, 1962).
[17] T. Graham, *Phil. Trans. Roy. Soc.*, 1846, **136**, 573.
[18] D. A. Frank-Kamenetski, *Diffusion and Heat Transfer in Chemical Kinetics*, trans. J. P. Appleton (Plenum, New York, 1969).
[19] S. Chapman and T. Cowling, *The Mathematical Theory of Non-uniform Gases* (University Press, Cambridge, 1960).
[20] W. Dorrance, *Viscous Hypersonic Flow* (McGraw-Hill, New York, 1962).
[21] F. Jona and G. Mandel, *J. Chem. Phys.*, 1963, **38**, 346.
[22] J. O. Hirschfelder, C. F. Curtiss and R. B. Bird, *Molecular Theory of Gases and Liquids* (Wiley, London, 1964).

P50
Journal of The Chemical Society, Faraday Transactions I, 1974, Volume 70, pp 2302–2312

Modified Entrainment Method for Measuring Vapour Pressures and Heterogeneous Equilibrium Constants

Part 4.—The Gallium Arsenide/Hydrogen Chloride System

By David Battat, Marc M. Faktor,* Ian Garrett and Rodney H. Moss

Post Office Research Department, Brook Road, Dollis Hill, London NW2 7DT

Received 27th March, 1974

The modified entrainment method described earlier has been used to study the GaAs/HCl system. Above about 900 K, the principal gallium vapour species is the monochloride, for which $\Delta Hf^{\circ}_{298} = -63.2 \pm 3$ kJ mol^{-1} and $S^{\circ}_{298} = 247 \pm 2$ J mol^{-1} K^{-1}. Below this temperature, another gallium species thought to be $GaCl_2$ becomes important.

1. INTRODUCTION

The reactions between the Group IIIB—VB compounds and the hydrogen halides are widely used in the electronics industry for depositing thin films of these compounds by chemical vapour transport.[1-4] The reaction of gallium arsenide with hydrogen chloride, the most exploited of these systems so far, has been the subject of various thermodynamic [5-8] and mass spectrometric [9, 10] studies, usually in parallel with crystal growth experiments. Although it is now generally agreed that the dominant reaction is:

$$GaAs(solid) + HCl(gas) \rightleftharpoons GaCl(gas) + \tfrac{1}{4}As_4(gas) + \tfrac{1}{2}H_2(gas) \qquad (1)$$

the enthalpy of formation of gallium monochloride is not accurately known. Furthermore, recent investigations of the dissociation of the tetrameric arsenic molecule [11, 12] have suggested a value of 227 kJ mol^{-1} for ΔH°_{298} for the reaction:

$$As_4(gas) \rightleftharpoons 2As_2(gas)$$

instead of 280 kJ mol^{-1} as suggested earlier,[13] so that the conventional vapour transport system may contain a significant partial pressure of As_2 at the usual operating temperature of 1000-1050 K.

We used the modified entrainment method described previously [14, 15] to study the gallium arsenide/hydrogen chloride system. This method, in addition to permitting us to calculate thermodynamic parameters for the transport reactions, provides a rapid, definitive, and inexpensive test of chemical vapour transport systems.

EXPERIMENTAL

The apparatus has been described in detail previously.[14, 15]

Gallium arsenide was nominally undoped material supplied by Mining and Chemical Products, hydrogen was purified by passing through a palladium diffuser, and hydrogen chloride was electronic grade, supplied by Air Products Ltd., with a quoted purity of 99.99 %. The flow of hydrogen chloride was controlled by two stainless steel needle valves in series, using the gas cylinder as an effectively constant pressure source. The hydrogen flow was controlled with a needle valve and smoothed with a simple network of capillaries and a ballast tank. Flow rates were measured with Meterate flow meters.

The hydrogen chloride flow meter was calibrated initially by determining the HCl content of the HCl+H_2 gas mixture by titration against aqueous NaOH. The temperature of the bottle was measured with a Pt/Pt–13 % Rh thermocouple, the bead being about 3 mm below the bottle.

The rate of weight loss from the sample bottle, $\dot{W}$, was measured as a function of temperature, using two ratios of HCl to H_2 in the gas stream: $p_{HCl}/P(=\varepsilon)\approx 0.083$ and 0.051, where p_{HCl} is the partial pressure of HCl and P is the total pressure ($p_{HCl}+p_{H_2}$).

3. RESULTS

The experimental results of the two runs are given in table 1. In fig. 1 is plotted ln $\dot{W}$ as a function of reciprocal temperature for the two runs.

TABLE 1.—THE EXPERIMENTAL RESULTS

ε = 0.083				ε = 0.051			
T/K	$\dot{W}$/mg h^{-1}	T/K	$\dot{W}$/mg h^{-1}	T/K	$\dot{W}$/mg h^{-1}	T/K	$\dot{W}$/mg h^{-1}
713	0.248	1003	6.295	742	0.183	1200	13.125
763	0.419	1003	6.343	764	0.246	1200	13.170
763	0.430	1003	6.312	788	0.288	1249	14.205
808	0.628	1048	9.696	813	0.369	1249	13.935
808	0.646	1048	9.552	836	0.471	1151	11.244
859	1.049	1048	9.492	840	0.477	1151	11.364
859	0.992	1096	13.080	908	1.220	865	0.651
904	1.916	1096	12.915	908	1.299	865	0.663
904	1.922	1147	15.76	1008	4.507	1054	6.480
904	1.916	1147	15.72	1008	4.555	1054	6.544
950	3.588	1193	18.07	1103	9.180	952	2.408
950	3.708	1193	18.07	1103	9.430	952	2.400
950	3.633	1244	19.78	1200	13.065		
		1244	19.46				

4. ANALYSIS OF RESULTS

Each of the curves in fig. 1 shows three regions: a straight section at low temperatures, (I), a second straight section at intermediate temperatures, (II), and a curving off at the highest temperatures (III). The two straight sections represent the effect of two transport reactions, one of which is dominant at the low temperatures, and the other at the high temperatures. The curving off in region III is a result of the equilibrium constant for the dominant reaction becoming large. We previously derived [14] a general expression for the equilibrium constant in a system with one dominant reaction:

$$K_p = \xi/(\varepsilon-\xi)$$

where ε is the fractional concentration of reactant in the gas stream (p_{HCl}/P in the present experiment) and ξ is the transport function, defined as:

$$\xi = RTl\dot{W}/MPAD.$$

Here l is the length and A the cross-sectional area of the neck of the bottle, M is the molecular weight of the condensed phase, and D is the diffusion coefficient (an average over all the species may be used in an approximate simple treatment. We will use a refined treatment [16] below). Hence:

$$\dot{W} = \frac{MPAD}{RTl}\left(\frac{K_p\varepsilon}{1+K_p}\right).$$

Thus as K_p becomes large, $\dot{W}$ varies with temperature only inasmuch as D/T varies, i.e. the term in the brackets is close to ε.

As regards the relative positions of the two curves in fig. 1, we note that the vertical distance between them is constant, within experimental error, over regions II and III, and takes a larger, not quite constant, value over region I. It is possible to explain this observation only if the reaction which is dominant at low temperatures results in a volatile gallium species with a different ratio of gallium to chlorine than that of the gallium species formed by the high temperature reaction. Thus the reason for the change in slope between regions I and II cannot be due merely to the dissociation of As_4 or polymeric gallium chloride (though both these processes may occur as well). Furthermore the sign of the slope in region I indicates that the reaction is endothermic, thus ruling out [17] gallium trichloride as the volatile species in this region.

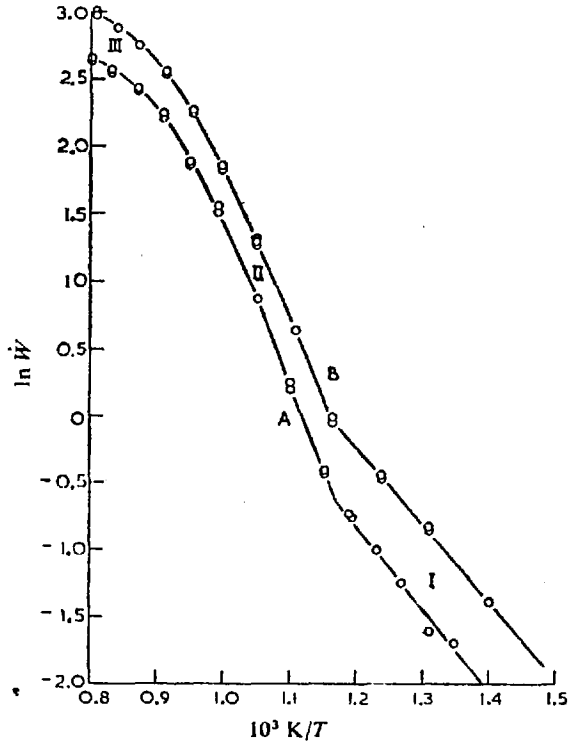

FIG. 1.—Plot of experimental data for GaAs/HCl.

There are two other gallium chlorides for which some data are available in the literature: $GaCl_2$ [ref. (18) and (19)] and $Ga(GaCl_4)$ [ref. (20) and (21)]. We therefore have two possibilities to consider for the reaction in region (I):

$$GaAs(solid)+2HCl(gas)\rightleftharpoons GaCl_2(gas)+\tfrac{1}{4}As_4(gas)+H_2(gas) \quad (2)$$

$$GaAs(solid)+2HCl(gas)\rightleftharpoons \tfrac{1}{2}Ga(GaCl_4)(gas)+\tfrac{1}{4}As_4(gas)+H_2(gas). \quad (3)$$

In addition, recent data [11, 12] indicate that the dissociation of As_4 occurs to a significant extent in our experimental temperature range (700-1250 K):

$$As_4\rightleftharpoons 2As_2. \quad (4)$$

We therefore have two schemes of simultaneous reactions to consider, namely: (1), (2) and (4) or (1), (3) and (4).

SCHEME 1

By applying the one-dimensional transport equations [14, 15] to the flow in the neck of the bottle, and solving them for the boundary conditions appropriate in this experiment,[15] we obtain a master equation relating the rate of loss of weight $\dot{W}$ to the equilibrium constants K_1, K_2 and K_4 for reactions (1), (2) and (4):

$$\frac{K_2}{K_2^{(\circ)}} = \left(1 - \frac{K_1}{K_1^{(\circ)}}\right)\left(1 - \frac{\gamma\xi'}{1-\gamma\xi'}\frac{K_1}{K_1^{(\circ)}}\right) \tag{5}$$

The derivation of this equation is given in the Appendix, where the quantities $K_1^{(\circ)}$ and $K_2^{(\circ)}$ are defined. The quantity ξ' is related to the transport function:

$$\xi' = \xi_{HCl}/\varepsilon = WRTl/MPA\varepsilon\, D_{HCl,H_2}$$

where D_{HCl,H_2} is the binary diffusion coefficient for HCl in hydrogen (the majority species in our experiment), and γ is the second-order correction [16] for multi-component diffusion. The quantities $K_1^{(\circ)}$ and $K_2^{(\circ)}$ are both functions of K_4.

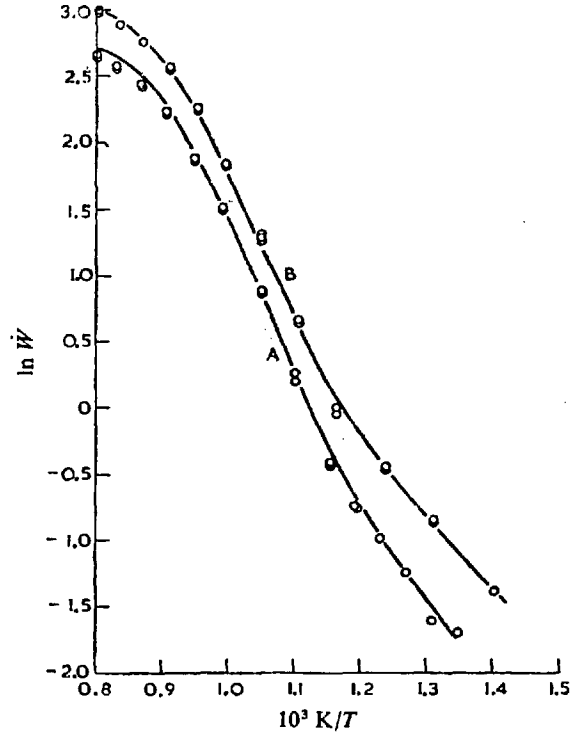

FIG. 2.—Scheme 1 for GaAs/HCl: O, experiment; —, theory.

In solving eqn (5), we have taken the value for K_4 given by Murray *et al.*[11, 12] Eqn (5) now contains four unknowns, i.e. the enthalpy and entropy changes ΔH_1, ΔH_2, ΔS_1, ΔS_2 for reactions (1) and (2). For any set of values of these four quantities, eqn (5) may be solved, and the expected rate of weight loss calculated as a function of

temperature. The problem now reduces to finding that set of values which gives the best fit to our experimental data. The criterion for the best fit was taken to be that

$$\sigma^2 = \sum\left(\ln \frac{\dot{W}_{obs}}{\dot{W}_{calc}}\right)^2 \tag{6}$$

should be a minimum, the summation being over all experimental points. Because of the slight scatter in the experimental data, the minimum of this function is about 4 kJ wide in the ΔH_1 and ΔH_2 dimensions, and about 2 J K^{-1} wide in the ΔS_1 and ΔS_2 dimensions. The values thus derived, appropriate to our mean experimental temperature of 950 K, are given in table 2 below. Fig. 2 shows the calculated variation of $\dot{W}$ with temperature, with our experimental points for comparison.

TABLE 2.—SECOND LAW ENTHALPY AND ENTROPY CHANGES FOR REACTION AT OUR MEAN TEMPERATURE OF 950 K

	(*a*) scheme 1		(*b*) scheme 2
ΔH_1	·157±3 kJ mol^{-1}	ΔH_1	159±5 kJ mol^{-1}
ΔS_1	134.5±1.5 J mol^{-1} K^{-1}	ΔS_1	141±4 J mol^{-1} K^{-1}
ΔH_2	44±3 kJ mol^{-1}	ΔH_3	67±5 kJ mol^{-1}
ΔS_2	35.3±1.5 J mol^{-1} K^{-1}	ΔS_3	91±4 J mol^{-1} K^{-1}

SCHEME 2

The master equation for this case is:

$$\left(\frac{K_3}{K_3^{(o)}}\right)^2 = \left(1 - \frac{K_1}{K_1^{(o)}}\right)\left(1 - \frac{\gamma\xi'}{1-\xi'\gamma}\frac{K_1}{K_1^{(o)}}\right)^3 \tag{5a}$$

where the quantities $K_1^{(o)}$ and $K_3^{(o)}$ are explained in the Appendix, and ξ' has the same meaning as before. We find that this equation does not fit our experimental data nearly as well as does eqn (5). Fig. 3 shows the calculated variation of W with temperature, in comparison with our experimental data. The parameter values which result in the best fit are given in table 2. The uncertainties in these values indicate the width of the minimum in the function σ^2 in the four dimensions. The minimum value of σ^2 is rather larger than for scheme 1. The values are: scheme 1, 0.1924; scheme 2, 0.9484.

While it is possible to obtain a good fit to each of the curves in fig. 1 separately, it is not possible to fit the two experimental curves simultaneously.

5. DISCUSSION

While it is obviously possible to obtain values of the entropy and enthalpy changes for transport reactions using the method we have described, the curves in fig. 1 have a more immediately obvious and valuable message to the preparer of materials. If one wishes to transport a material by chemical vapour transport in a temperature gradient, one can use experimental curves such as those in fig. 1 to determine the temperature range in which to operate. Thus we can say that below about 900 K and above 1200 K very little transport in a temperature gradient can be achieved, while the temperature range which will produce the fastest rate of transport is at the upper end of region II. It is interesting to note that our experiment has confirmed, in a matter of days, the knowledge gained empirically over several years for the gallium arsenide/hydrogen chloride system. As a method for providing a rapid, cheap, and *revealing* test of a transport system, this type of experiment has much to offer. The more

familiar method,[22] of putting the solid to be transported into a sealed capsule with some transporting agent, placing the capsule in a furnace, and awaiting developments (sometimes for several months) is frequently unproductive and uninstructive.

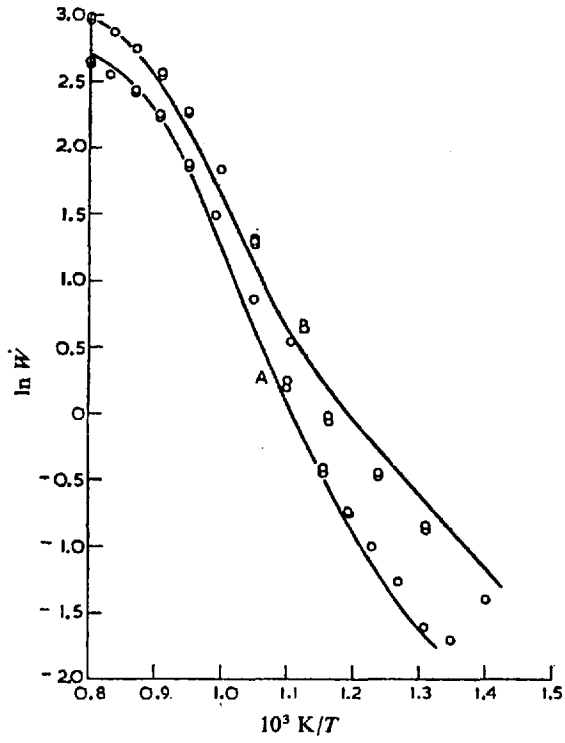

FIG. 3.—Scheme 2 for GaAs/HCl: O, experiment; —, theory.

From the enthalpy and entropy changes for reactions listed in table 2, we have calculated enthalpies of formation and entropies of the species GaCl, $GaCl_2$ and $Ga(GaCl_4)$. For the first two, specific heat data have been estimated by Shaulov and Mosin,[18] and we have corrected our values to room temperature. Very few data concerning $Ga(GaCl_4)$ as a vapour molecule are available in the literature, and we have been unable to estimate its specific heat or entropy with any confidence. The results are given in table 3 with values from the literature for comparison.

The enthalpy of formation of gallium monochloride has been reported as -67.6 kJ mol^{-1} by Fergusson and Gabor [23] (modified by Day [6]), as -84 ± 20 kJ mol^{-1} by Shaulov and Mosin [18] using bond energy data, and as -80 kJ mol^{-1} by Hurle and Mullin,[4] who fitted computed growth rates and compositions of Group III-V alloys to experimental data. In their computations, they used Arthur's [13] value of 266 kJ mol^{-1} for the dissociation enthalpy of As_4 to $2As_2$. We have used the value reported recently by Murray *et al.*[11, 12] (228 ± 6 kJ mol^{-1}), who employed a much-improved experimental technique. For comparison, we have also used Arthur's value for K_4 in eqn (5), and we do indeed obtain an enthalpy of formation of gallium monochloride close to that reported by Hurle and Mullin (-75.7 ± 4 kJ mol^{-1}), which we therefore consider to be in error because of the inaccurate dissociation enthalpy of As_4 used by them.

The entropy of gallium monochloride was reported as 236 J mol^{-1} K^{-1} by Fergusson and Gabor [23] (modified by Day [6]), and as 240 J mol^{-1} K^{-1} by Hurle and Mullin.[4] Shaulov and Mosin [18] calculated the entropy as 240 J mol^{-1} K^{-1}. Our second law value is acceptably close to these values. We have used the calculated thermodynamic functions of Shaulov and Mosin to correct our data to room temperature.

TABLE 3.—ENTHALPIES OF FORMATION AND ENTROPIES OF GALLIUM CHLORIDES

(*a*) scheme 1

GaCl		GaCl$_2$		
ΔH_{f298}°/ kJ mol^{-1}	S_{298}°/ J mol^{-1} K^{-1}	ΔH_{f298}°/ kJ mol^{-1}	S_{298}°/J mol^{-1} K^{-1}	references
−63.2±3	247±2	−267±3	265±2	this work, 2nd law
−67.6	236			23
−84±20	240	−260±25	302	18
−80	240			4
		−270±10		combination of (19) and (21)
			279, 290±10	estimates (see text)

(*b*) scheme 2

GaCl		Ga(GaCl$_4$)		
−60±5	250±4	−117±5	161±4	this work, 2nd law

We are not able to calculate values of K_1 and K_2 from each of our experimental points individually, so that a third law calculation for enthalpies of formation is not possible in the normal way. The good agreement betwen our second-law entropy and the calculated entropy indicates that our second-law enthalpy is reliable, however.

For gallium dichloride, the enthalpy of formation was estimated by Shaulov and Mosin as −260±25 kJ mol^{-1} using bond energies. The enthalpy of formation of $GaCl_2$ liquid [21] is −341 kJ mol^{-1}. The vapour pressure over the liquid was measured by Laubengayer and Schirmer,[19] whose data indicate an enthalpy of evaporation of 70±8 kJ mol^{-1}. The enthalpy of formation of $GaCl_2$ vapour is thus −270±10 kJ mol^{-1}, in good agreement with our second law value. The entropy of $GaCl_2$ has been calculated (S_{298}° = 302 J mol^{-1} K^{-1}) by Shaulov and Mosin, assuming a bent molecule with a Cl—Ga—Cl bond angle of 120°, and fundamental frequencies estimated by comparison with the chlorides of boron and aluminium.

While their calculated value is subject to the errors inevitable in such an estimation, the disagreement with our second law value is disturbing. We have calculated the entropy using the same frequencies, but assuming a linear structure for the molecule. The result [table 2(*a*)] is closer to our second law experimental value but still 18 J mol^{-1} K^{-1} larger. Comparing $GaCl_2$ with linear dichlorides [24] (of Mg, Ca, Si, Ti, Fe, Zr, W, Hg and Pb), on the basis of atomic weight of the metal atom, we estimate a value of 290±10 J mol^{-1} K^{-1} for S_{298}°. We discuss the low temperature region below.

The enthalpy of formation and entropy of gallium tetrachlorogallate, obtained by scheme 2, are shown in table 3. Note that these values are appropriate to our mean experimental temperature of 960 K. No thermodynamic functions for this vapour molecule appear in the literature, although the solid is well characterised.[20] We would expect the structure to be similar to $NaAlF_4$,[24] $KAlF_4$,[24] and $TlAlF_4$.[25] Empirical formulae [17, 26] for entropies of vapour molecules are seriously in error for these complex molecules.

Earlier we showed [14] that for a system with only a single transport reaction, the

rate of weight loss $\dot{W}$ is proportional to the equilibrium constant K_p so long as K_p is not too large (<5, say). Thus a plot of ln $\dot{W}$ against $1/T$ has a slope of $-\Delta H/R$. In this system we have at least three reactions occurring simultaneously over much of our temperature range, and we note that the straight-line sections in regions I and II on fig. 1 have slopes corresponding to roughly 48 and 95 kJ mol^{-1} K^{-1} respectively. While the slope of region I is near to the enthalpy change of reaction (2), the slope in region II is very different from the enthalpy change of reaction (1). This difference is due to the dissociation of As_4 being significant in region II, and to the equilibrium constants becoming sufficiently large as to make the rate of transport less temperature sensitive. Michelitsch *et al.*[7] have measured the rate of etching of a gallium arsenide wafer in a $HCl+H_2$ gas mixture as a function of temperature, and have obtained an enthalpy of 104 ± 12 kJ mol^{-1} K^{-1} from their plot of logarithm of the rate of weight loss against reciprocal temperature. This they interpret as being the enthalpy change for reaction (1), an interpretation which this work shows to be erroneous. By working over an extended temperature range, we have been able to study the regions (i.e. regions I and III) either side of the temperature range investigated by Michelitsch *et al.*, which is the temperature range in which most chemical vapour transport experiments are carried out in this system. The effects which predominate in regions I and III have some influence in region II. Thus the slope of the ln $\dot{W}$ against $1/T$ plot does not give the enthalpy change for reaction (1) simply.

6. CONCLUSIONS

The method described in this paper provides a rapid, cheap, and revealing test of potential chemical vapour transport systems. In addition, it yields thermodynamic data for the transport reactions.

In the GaAs/HCl system, at least two volatile gallium species are formed. At high temperature and low chlorine potential, the monochloride predominates. Its enthalpy of formation ΔH_{f298}° is -63 ± 3 kJ mol^{-1}, and its entropy S_{298}° is 247 ± 2 J mol^{-1} K^{-1} (second law results). At low temperature and higher chlorine potential, another gallium species is formed. Our experiment lends tentative support to the dichloride since for this molecule we get a good fit to our experimental data using eqn (5), and our second law enthalpy of formation ($\Delta H_{f298}^{\circ} = -267\pm3$ kJ mol^{-1}), is in good agreement with literature values. The second-law entropy ($S_{298}^{\circ} = 265$ J mol^{-1} K^{-1}) is unaccountably low in comparison with reasonable estimates.

Our value for the enthalpy change for reaction (1) is larger than the values reported previously in the literature. We conclude that this discrepancy is a result of previous workers using a smaller temperature range, and thus being precluded from studying the low and high temperature regions (regions I and III). The effects which dominate in these regions also influence region II. the mid-range of temperature, leading to a smaller " apparent " enthalpy change.

APPENDIX

Here we derive the master equation (5) relating the rate of weight loss $\dot{W}$ to the equilibrium constant K_1, K_2, and K_4 for reactions (1), (2) and (4) considered in scheme 1. The master equation (5*a*) for scheme 2 may be derived in a similar manner, as may the corresponding equations for schemes of reactions involving $GaCl_3$ or $(GaCl)_n$ vapour species. We will not derive these here, as the method is very similar for all schemes.

For a vapour mixture containing one component (hydrogen in our case) in substantial majority, the one-dimensional transport equations for the minority species [14-16] are:

$$J_i = n_i U - D_i(\mathrm{d}n_i/\mathrm{d}x) \qquad \text{(A1)}$$

where J_i is the flux (in molar units) of species i, U is the mole-average Stefan velocity,[27] n_i is the molar concentration of species i, and D_i is the binary diffusion coefficient of species i in the majority species. Integration of the transport equations for the minority species yields the solutions:

$$\frac{p_i(0)}{P} = \frac{J_i}{J} + \left[\frac{p_i(l)}{P} - \frac{J_i}{J}\right]\exp(-\xi_i) \tag{A2}$$

where P is the total pressure $\Sigma_i p_i$, J is $\Sigma_i J_i$, (0) and (l) denote partial pressures in the reaction bottle and at the open end of the neck (i.e. in the furnace gas stream), and ξ_i is the transport function, defined as

$$\xi_i = JRTl/PD_i. \tag{A3}$$

The symbols were defined earlier in the text. Since ξ_i is at most of the order of ε the fractional HCl concentration in the gas stream, and consequently small compared with unity, we may express the partial pressures inside the reaction bottle as:

$$p_i(0)/P = p_i(l)/P + J_i\xi_i/J. \tag{A4}$$

The quantities $p_i(l)/P$ are known boundary conditions. If there is a single reaction occurring,[14] the J_i values are related by stoichiometric coefficients and may be related simply to the rate of weight loss. Here we are considering three simultaneous reactions, and the relationships between the J_i values become temperature dependent. We define:

$$\alpha = J_{As_2}/J_{As_4} \tag{A5}$$

and

$$\theta = J_{GaCl}/J_{GaCl_2}. \tag{A6}$$

It can now be shown that the partial pressures inside the reaction bottle are given by:

$$p_{GaCl}(0)/P = \frac{\theta}{1+\theta}\bar{\xi}_{GaCl} \tag{A7}$$

$$p_{GaCl_2}(0)/P = \frac{1}{1+\theta}\bar{\xi}_{GaCl_2} \tag{A8}$$

$$p_{As_4}(0)/P = \frac{1}{4+2\alpha}\bar{\xi}_{As_4} \tag{A9}$$

$$p_{As_2}(0)/P = \frac{\alpha}{4+2\alpha}\bar{\xi}_{As_2} \tag{A10}$$

$$p_{HCl}(0)/P = \varepsilon - \frac{2+\theta}{1+\theta}\bar{\xi}_{HCl} \tag{A11}$$

where $\bar{\xi}_i$ is the reduced transport function:

$$\bar{\xi}_i = WRTl/AMPD_i. \tag{A12}$$

Note that if there is a single reaction, $\zeta_i \propto \bar{\xi}_i$ and $J \propto W/AM$. With more than one reaction, the relation between J and W depends on quantities such as α and θ.

We can express α and θ in terms of the equilibrium constants, and we obtain:

$$\alpha = \frac{1+\sqrt{1+4A}}{A} \tag{A13}$$

where

$$A = \frac{D_{As_4}}{D_{As_2}}\frac{\bar{\xi}_{As_2}}{K_4} \tag{A14}$$

and

$$\theta = -1+\frac{(1+\theta')+[(1-2\xi')^2+\theta'^2+2\theta']^{\frac{1}{2}}}{2(1-\xi')} \tag{A15}$$

where

$$\theta' = \frac{K_1}{K_2}\frac{1}{\varepsilon}\frac{D_{GaCl}}{D_{GaCl_2}} \tag{A16}$$

which is the value of θ at the open end of the neck of the bottle, and

$$\xi' = \bar{\xi}_{HCl}/\varepsilon \tag{A17}$$

which approaches unity as K_1 becomes very large, i.e. ξ' is a measure of the extent of reaction. We now define the parameters:

$$K_1^{(\circ)} = \frac{\bar{\xi}_{GaCl}}{\varepsilon-\bar{\xi}_{HCl}}\left(\frac{\bar{\xi}_{As_4}}{4+2\alpha}\right)^{\frac{1}{4}} \tag{A18}$$

and

$$K_2^{(\circ)} = \frac{\bar{\xi}_{GaCl_2}}{(\varepsilon-2\bar{\xi}_{HCl})^2}\left(\frac{\bar{\xi}_{As_4}}{4+2\alpha}\right)^{\frac{1}{4}}. \tag{A19}$$

Note that if reaction (2) did not exist, K_1 would be $K_1^{(\circ)}$ (i.e. if $\theta\to\infty$). Similarly, if reaction (1) did not exist ($\theta\to 0$), K_2 would be $K_2^{(\circ)}$.

We can now substitute for α and θ in eqn (A7)-(A11), and substitute the resulting equations into the expression for K_1:

$$K_1 = \frac{p_{GaCl}(0)\sqrt{p_{H_2}(0)}[p_{As_4}(0)]^{\frac{1}{4}}}{p_{HCl}(0)} \tag{A20}$$

Using the parameters $K_1^{(\circ)}$ and $K_2^{(\circ)}$, we obtain the master equation:

$$\frac{K_2}{K_2^{(\circ)}} = \left(1-\frac{K_1}{K_1^{(\circ)}}\right)\left(1-\frac{\xi'}{1-\xi'}\frac{K_1}{K_1^{(\circ)}}\right). \tag{A21}$$

In our experimental temperature range, the second term on the right of eqn (A21) is not very far from unity. Thus we find, approximately:

$$\frac{K_2}{K_2^{(\circ)}}+\frac{K_1}{K_1^{(\circ)}} \approx 1.$$

We have included also the second-order approximation [16] to multicomponent diffusion. This has the effect of multiplying each ξ_i by factors γ_i which are functions of the binary diffusion coefficients for all pairs of species in the system. To the accuracy of our second-order correction,

$$\gamma_{GaCl} = \gamma_{GaCl_2} = \gamma_{As_4} = \gamma_{As_2} = 1+3.2\varepsilon$$
$$\gamma_{HCl} = 1+10\varepsilon+4\bar{\xi}_{HCl}.$$

We have used Graham's law [28] to estimate ratios of binary diffusion coefficients. The best fit of eqn (5) to our experimental data is obtained if we take D_{HCl} (273 K) to be 0.4 cm^2 s^{-1}, with a temperature dependence of $T^{0.8}$. This is not in agreement with our previous measurement [16] of D_{HCl} (273 K) of 0.54 cm^2 s^{-1} with a temperature dependence of $T^{0.853}$. In view of the uncertainty in the coefficients of ε and $\bar{\xi}_{HCl}$ in γ_{HCl}, which have been estimated using Graham's law, this discrepancy is not considered to be serious. If we accept that D_{HCl}/γ_{HCl} must have such a value as to produce a good fit to our experimental data in region III, then the uncertainties in D_{HCl} and γ_{HCl} do not affect our best fit values for ΔH_1° and ΔS_1°.

We have considered also the effect of reactions in the gas phase within the neck of the bottle. It can be shown that the master equations (5) and (5*a*) remain valid. This work will be reported in a future communication.

We thank the Director of Research of the Post Office for permission to publish this paper.

[1] J. R. Knight, D. Effer and P. R. Evans, *Solid State Electronics*, 1965, **8**, 178.
[2] H. T. Minden, *J. Electrochem. Soc.*, 1965, **112**, 300.
[3] J. J. Tietjen, R. E. Enstrom and D. Richman, *R.C.A. Rev.*, 1970, **31**, 635; *Solid State Tech.*, 1972, 42.
[4] J. B. Mullin and D. T. J. Hurle, *J. Luminescence*, 1973, **7**, 176; D. T. J. Hurle, J. B. Mullin, *J. Phys. Chem. Solids*, Suppl. No. 1, 1967, 241.
[5] D. J. Kirwan, *J. Electrochem. Soc.*, 1970, **117**, 1572.
[6] G. F. Day, *Heterojunction Device Concepts*, Varian Report No. 324-6Q, Air Force Contract No. AF 33 (615)-1988 (Varian Associates, Palo Alto, California).
[7] M. Michelitsch, W. Kappallo and G. Hellbardt, *J. Electrochem. Soc.*, 1964, **111**, 1248.
[8] A. Boucher and L. Hollan, *J. Electrochem. Soc.*, 1970, **117**, 932.
[9] V. S. Ban, *J. Electrochem. Soc.*, 1971, **118**, 1473.
[10] V. S. Ban, *J. Electrochem. Soc.*, 1972, **119**, 761.
[11] J. J. Murray, C. Pupp and R. F. Pottie, *J. Chem. Phys.*, 1973, **58**, 2569.
[12] C. Pupp, J. J. Murray and R. F. Pottie, *J. Chem. Thermodynamics*, 1974, **6**, 123.
[13] J. R. Arthur, *J. Phys. Chem. Solids*, 1967, **28**, 2257.
[14] D. Battat, M. M. Faktor, I. Garrett and R. H. Moss, *J.C.S. Faraday I*, 1974, **70**, 2267.
[15] D. Battat, M. M. Faktor, I. Garrett and R. H. Moss, *J.C.S. Faraday I*, 1974, **70**, 2280.
[16] D. Battat, M. M. Faktor, I. Garrett and R. H. Moss, *J.C.S. Faraday I*, 1974, **70**, 2293.
[17] O. Kubaschewski, E. Ll. Evans and C. B. Alcock, *Metallurgical Thermochemistry* (Pergamon, New York, 4th edn., 1967).
[18] Yu. Kh. Shaulov and A. M. Musin, *Zhur. fiz. Khim.*, 1973, **47**, 1131.
[19] A. W. Laubengayer and F. B. Schirmer, *J. Amer. Chem. Soc.*, 1940, **62**, 1578.
[20] J. D. Beck, R. H. Wood and N. N. Greenwood, *Inorg. Chem.*, 1970, **9**, 86.
[21] P. I. Fedorov and G. A. Lovetskaya, *Zhur. neorg. Khim.*, 1968, **13**, 3357.
[22] see, for example, the references cited in H. Schäfer, *Chemical Transport Reactions* (Academic Press, London, 1964).
[23] R. R. Fergusson and T. Gabor, *J. Electrochem. Soc.*, 1964, **111**, 585.
[24] *J.A.N.A.F. Thermochemical Tables* (U.S. Department of Commerce, Nat. Bur. Stand., Washington, 2nd edn., 1971).
[25] D. H. Feather and A. Büchler, *J. Phys. Chem.*, 1973, **77**, 1599.
[26] W. E. Dasent, *Inorganic Energetics* (Penguin, London, 1971).
[27] D. A. Frank-Kamenetskii, *Diffusion and Heat Transfer in Chemical Kinetics*, trans. J. P. Appleton (Plenum, New York, 1969).
[28] T. Graham, *Phil. Trans. Roy. Soc.*, 1846, **136**, 573.